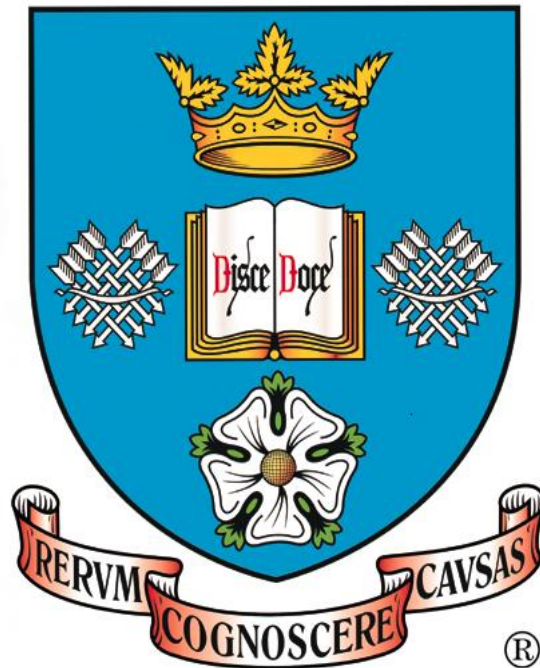


An Experimental Investigation and Improvement of Insulated Rail Joints (IRJs) End Post Performance.



A thesis submitted for the degree of Doctor of Philosophy in the Faculty of Engineering of the University of Sheffield

by
Fathi A. Elshukri

Department of Mechanical Engineering
The University of Sheffield

January 2016

Abstract

Insulated rail joints are a safety valve in railways that are used as part of the signalling system to determine the position of a train. Insulated rail joints are the weakest part of the railroad, where their life ranges between a third and half of the life of rails.

One of the most significant issues in insulated rail joints is metal flow, and damage and loss of the end post. Major causes of these issues include sliding wear, impact wear, wear due to rolling/sliding contact, and wear due to rail compression and plastic flow of rail material. In this study experimental investigations have been applied to improve insulated rail joints. The aim of this work was to experimentally determine the resistance to sliding wear, impact wear, rolling/sliding contact wear, compression wear of five specimens of end post materials with different properties against train wheel material (steel), and the influence of tests parameters and lubrication on these materials. The end post materials were classified into thermoplastic materials such as Nylon 12, Nylon 66 and Nylon66a materials and thermosetting materials such as Epoxy Glass and Phenolic Resin Bonded Fabric materials according to melting point temperature. A Block-on-Ring apparatus has been used to achieve sliding wear tests and 100% slip ratio lipping tests; a Ball-on-Plate Impact device has been used to implement impact wear tests; a Twin-Disc Machine has been employed to carry out partial slip ratio (1%) lipping tests and rolling/sliding contact wear tests and a Tinius Olsen-H25ks compression/tension machine has been used to conduct compression tests. The contact scenarios of wheel/rail and IRJ were identified, and the material wear resistance of studied end post materials was determined via experimental studies. The wear mechanism of the end post materials is explained. It was found that excessive loads caused the materials to yield which then caused plastic deformation and rupture and rise in temperature (from friction in sliding) caused the thermoplastic materials to melt. The thermosetting materials were not affected by increases in temperature.

From the studies of the different scenarios of contact between wheel and IRJ (end post). It was shown that the performance of the insulated rail joints can be improved with selection of the optimum end post material.

Table of Contents

| | |
|--|------|
| Abstract..... | i |
| Table of Contents..... | ii |
| List of Figures..... | vii |
| List of Tables..... | xiii |
| Acknowledgements..... | xiv |
| Chapter 1- Introduction..... | 1 |
| 1.1- Rail Transport Importance..... | 1 |
| 1.2- Rail Transport Maintenance..... | 1 |
| 1.2.1- Rail Transport Maintenance Costs..... | 1 |
| 1.2.1.1- Direct Maintenance Costs..... | 2 |
| 1.2.1.2- Indirect Maintenance Costs..... | 2 |
| 1.3- Structure of the Railway Track..... | 2 |
| 1.3.1- Rail..... | 2 |
| 1.3.2- Sleepers..... | 3 |
| 1.3.3- Gauges..... | 4 |
| 1.3.4- Ballast..... | 5 |
| 1.4- Rail Joints..... | 5 |
| 1.4.1- Standard Rail Joints..... | 6 |
| 1.4.2- Compromise Rail Joints..... | 6 |
| 1.4.3- Insulated Rail Joint (IRJs)..... | 7 |
| 1.4.3.1- End Post..... | 8 |
| 1.5- Insulated Rail Joint Design..... | 9 |
| 1.6- Importance of IRJs..... | 11 |
| 1.7- Insulated Rail Joints Failures..... | 11 |
| 1.7.1- Wheel-Rail Contact..... | 12 |
| 1.7.2- Insulated Rail Joints Failures Types..... | 12 |
| 1.8- Aims and Objectives..... | 15 |
| 1.9- Thesis Outline..... | 16 |
| Chapter 2- Literature Review..... | 17 |
| 2.1- Experimental Investigations of Insulated Rail Joints..... | 17 |
| 2.2- Investigation of Insulated Rail Joints Using Finite Element Analysis..... | 17 |

| | |
|---|----|
| 2.3- Failure Analysis..... | 18 |
| 2.4- Investigation of Polymer Wear..... | 19 |
| 2.4.1- Investigation of Polymer Sliding Wear..... | 19 |
| 2.4.2- Investigation of Polymer Impact Wear..... | 22 |
| 2.4.3- Investigation of Polymer Wear in Rolling-Sliding Contacts..... | 22 |
| 2.4.4- Investigation of Polymer Static Compression Failures..... | 24 |
| 2.5- Comparison between Previous Studies and Current Study..... | 25 |
| 2.6- Summary..... | 28 |
| 2.6.1- IRJs..... | 28 |
| 2.6.2- Polymers..... | 28 |
| 2.7- Novelty in Methods..... | 28 |
| Chapter 3- Test Method and Materials..... | 30 |
| 3.1- Introduction..... | 30 |
| 3.2- Test Apparatus..... | 30 |
| 3.2.1- Block-on-Ring Rig..... | 33 |
| 3.2.2- Twin-Disc Machine..... | 33 |
| 3.2.3- Pneumatic Ball-on-Plate Impact Rig..... | 34 |
| 3.2.4- Tinius Olsen-H25ks Machine..... | 36 |
| 3.3- Specimens and Material Properties | 36 |
| 3.3.1- Melting Point Test..... | 37 |
| 3.4- Testing..... | 39 |
| 3.5- Test Methods..... | 40 |
| 3.5.1- Dry and Wet Sliding Wear Test (Block-on-Ring)..... | 40 |
| 3.5.1.1- Coefficient of Friction Test..... | 43 |
| 3.5.1.2- Hardness Test..... | 44 |
| 3.5.2- Lipping Test..... | 44 |
| 3.5.2.1- 100% Slip Ratio Lipping Test (Block-on-Ring)..... | 45 |
| 3.5.2.2- Partial Slip Ratio Lipping Test..... | 46 |
| 3.5.2.2.1- End Post Specimen Thickness Determination..... | 46 |
| 3.5.3- Dry and Wet Rolling/Sliding Wear Test..... | 49 |
| 3.5.4- Dry and Wet Impact Test..... | 51 |
| 3.5.5- Static Compression Test..... | 53 |

| | |
|--|----|
| Chapter 4- Block-on-Ring Sliding Tests..... | 55 |
| 4.1- Introduction..... | 55 |
| 4.2- Results..... | 55 |
| 4.2.1- Volume Loss Data | 55 |
| 4.2.2- Specimens Wear Resistance..... | 59 |
| 4.2.3- Specimens Surface Roughness..... | 62 |
| 4.2.4- Specimens Friction Coefficient..... | 64 |
| 4.2.5- Worn Contact Surfaces of Specimens..... | 66 |
| 4.3- Discussion..... | 71 |
| 4.3.1- Thermoplastic Materials..... | 71 |
| 4.3.1.1- Nylon 12 Material (N12)..... | 71 |
| 4.3.1.2- Nylon 66 Material (N66)..... | 72 |
| 4.3.1.3- Nylon 66a Material (N66a)..... | 73 |
| 4.3.2- Thermosetting Materials..... | 74 |
| 4.3.2.1- Epoxy Glass Material (EG)..... | 74 |
| 4.3.2.2- Phenolic Resin Bonded Fabric Material (PRBF)..... | 75 |
| 4.4- Summary..... | 76 |
| Chapter 5- Impact Tests..... | 77 |
| 5.1- Introduction..... | 77 |
| 5.2- Results..... | 77 |
| 5.2.1- Crater Dimensions..... | 77 |
| 5.2.2- Wear Images..... | 85 |
| 5.3- Discussion..... | 90 |
| 5.3.1- Thermoplastic Materials..... | 90 |
| 5.3.1.1- Nylon 12 Material..... | 90 |
| 5.3.1.2- Nylon 66 Material..... | 90 |
| 5.3.1.3- Nylon 66a Material..... | 91 |
| 5.3.2- Thermosetting Materials..... | 91 |
| 5.3.2.1- Epoxy Glass Material..... | 91 |
| 5.3.2.2- Phenolic Resin Bonded Fabric Material | 91 |
| 5.4- Summary..... | 92 |
| Chapter 6- Lipping Tests..... | 94 |

| | |
|---|-----|
| 6.1- Introduction..... | 94 |
| 6.2- Specimens..... | 94 |
| 6.2.1- 100% Slip..... | 94 |
| 6.2.2- Partial Slip..... | 95 |
| 6.3- Results..... | 95 |
| 6.3.1- 100% Slip Ratio Lipping Test..... | 95 |
| 6.3.2- 100% Slip Ratio Lipping Test Images..... | 96 |
| 6.3.3- Partial Slip Ratio (1%) Lipping Test..... | 97 |
| 6.3.4- Partial Slip Ratio (1%) Lipping Test Images..... | 97 |
| 6.4- Discussion..... | 99 |
| 6.4.1- 100% Sliding SlipTest..... | 99 |
| 6.4.2- Partial Slip (1%) Test..... | 99 |
| 6.4.2.1- End Post Width of 0.5 mm..... | 99 |
| 6.4.2.2- End Post Width of 1 mm..... | 100 |
| 6.5- Summary..... | 101 |
| Chapter 7- Rolling/Sliding Tests..... | 102 |
| 7.1- Introduction..... | 102 |
| 7.2- Specimens..... | 102 |
| 7.3- Results..... | 102 |
| 7.3.1- Worn Surface Images..... | 102 |
| 7.4- Discussion..... | 104 |
| 7.4.1- Thermoplastic Materials..... | 104 |
| 7.4.1.1- Nylon 12, 66 and 66a Materials..... | 105 |
| 7.4.2- Thermosetting Materials..... | 105 |
| 7.4.2.1- Epoxy Glass Material..... | 105 |
| 7.4.2.2- Phenolic Resin Bonded Fabric Material..... | 105 |
| 7.5- Summary..... | 105 |
| Chapter 8- Static Compression Test..... | 107 |
| 8.1- Introduction..... | 107 |
| 8.2- Specimens..... | 108 |
| 8.3- Results..... | 109 |
| 8.3.1- Failure Behaviour..... | 109 |

| | |
|--|-----|
| 8.3.1.1- Stress Strain Curves Analysis..... | 109 |
| 8.4- Discussion..... | 114 |
| 8.4.1- Thermoplastic Materials..... | 114 |
| 8.4.1.1- Nylon 12..... | 114 |
| 8.4.1.2- Nylon 66..... | 115 |
| 8.4.2- Thermosetting Materials..... | 115 |
| 8.4.2.1- Epoxy Glass..... | 115 |
| 8.4.2.2- Phenolic Resin Bonded Fabric..... | 115 |
| 8.5- Summary..... | 116 |
| Chapter 9- Conclusions and Recommendations..... | 117 |
| 9.1- Conclusions..... | 117 |
| 9.1.1- Block-on-Ring Sliding Wear Tests..... | 117 |
| 9.1.1.1- Dry Test Condition..... | 117 |
| 9.1.1.2- Wet Test Condition..... | 117 |
| 9.1.2- Impact Tests..... | 118 |
| 9.1.3- Lipping Tests..... | 118 |
| 9.1.3.1- 100% Slip Ratio Lipping Test..... | 119 |
| 9.1.3.2- Partial Slip Ratio (1%) Lipping Test..... | 119 |
| 9.1.4- Rolling/Sliding Contact Wear Tests..... | 119 |
| 9.1.5- Static Compression Tests..... | 119 |
| 9.2- Recommendations for Future Work..... | 121 |
| References..... | 122 |
| Published Work..... | 130 |
| Appendix A..... | 131 |
| Appendix B..... | 134 |

List of Figures

| | |
|--|----|
| Figure 1:1- Railway Track Cross-Section | 2 |
| Figure 1:2- Flat-Footed Rail Section [13]..... | 3 |
| Figure 1:3- Rail Types Cross- Sections [8]..... | 3 |
| Figure 1:4- Wooden Sleeper [8, 14, 15]..... | 4 |
| Figure 1:5- Metal Sleeper [8, 14, 15]..... | 4 |
| Figure 1:6- Concrete Sleeper [8, 14, 15]..... | 4 |
| Figure 1:7- 4 Bolt Rail Joint “fish plates” [18]..... | 5 |
| Figure 1:8- Standard Joint Bar [19]..... | 6 |
| Figure 1:9- Compromise Joint Bar [19]..... | 6 |
| Figure 1:10- Clear Track Circuit [20]..... | 7 |
| Figure 1:11- Occupied Track Circuit [20]..... | 7 |
| Figure 1:12- Cross-Section of an Insulated Joint [21, 22]..... | 8 |
| Figure 1:13- End Post Shape..... | 9 |
| Figure 1:14- Square Joint [24, 25]..... | 9 |
| Figure 1:15- Inclined Joint (Top View) [24, 25]..... | 9 |
| Figure 1:16- Suspended IRJs [26]..... | 10 |
| Figure 1:17- Continuous Insulated Rail Joints [14]..... | 10 |
| Figure 1:18- Non-Continuous Supported IRJs [28]..... | 11 |
| Figure 1:19- Cracked Joint Bar [31]..... | 12 |
| Figure 1:20- Rail End Battering [32]..... | 12 |
| Figure 1:21- Rail End Metal Flow [27]..... | 13 |
| Figure 1:22- Schematic Diagram of Rail End Metal Flow..... | 13 |
| Figure 1:23- Rail Head Metal Spalling in the Gap between Adjoining Rail at IRJs [27]..... | 14 |
| Figure 1:24- IRJ with End Post Crushed [27]..... | 14 |
| Figure 1:25- Plastic Deformation of Rail End with Deterioration of End Post [33] | 14 |
| Figure 1:26- Percentage Split of IRJ Failures (Data from [11])..... | 15 |
| Figure 3:1- Schematic Diagram of Block-on-Ring Test Rig..... | 33 |
| Figure 3:2- Twin-Disc Test Machine Schematic | 34 |

| | |
|---|----|
| Figure 3:3- Schematic Diagram of End Post Material Disc and Train Wheel Disc Contact in a Twin-Disc Machine..... | 34 |
| Figure 3:4- Schematic of the Pneumatic Ball-on-Plate Tester..... | 35 |
| Figure 3:5- Schematic of the Movement of the Pneumatic Actuator..... | 35 |
| Figure 3:6 - Schematic of Tinius Olsen-H25ks..... | 36 |
| Figure 3:7- Melting Point of Nylon 66 (N66) End Post Material..... | 38 |
| Figure 3:8- Melting Point of Nylon 66a (N66a) End Post Material..... | 38 |
| Figure 3:9- Epoxy Glass (EG) End Post Material Showing no Melting Point..... | 39 |
| Figure 3:10- Phenolic Resin Bonded Fabric (PRBF) End Post Material Showing an Endo-Thermic Transition..... | 39 |
| Figure 3:11- Schematic of End Post Specimen..... | 41 |
| Figure 3:12- Schematic of Steel Ring..... | 41 |
| Figure 3:13- Block-on-Ring Test..... | 41 |
| Figure 3:14- Data for NRC Modelling of Wheel/Rail Contact Using Multi Body Dynamics Software [Informal Communication with Eric Magel, NRC, Canada]..... | 42 |
| Figure 3:15- CETR Machine..... | 43 |
| Figure 3:16- Schematic for Pin and Disc..... | 43 |
| Figure 3:17- Schematic of the Lipping Test Set-up..... | 45 |
| Figure 3:18- Schematic of the 100% Slip Lipping Test Specimen Set-up..... | 45 |
| Figure 3:19- Two Different Radii Bodies in Contact [95]..... | 46 |
| Figure 3:20- Schematic of Actual End Post Thickness..... | 48 |
| Figure 3:21- Schematic of End Post Specimen Thickness..... | 48 |
| Figure 3:22- Schematic of 1% Partial Slip Specimens..... | 49 |
| Figure 3:23- Twin-Disc Machine End Post Specimen Holder..... | 50 |
| Figure 3:24- Twin-Disc Test Specimens Set-up | 51 |
| Figure 3:25- Schematic of Steel Disc and End Post Disc Contact..... | 51 |
| Figure 3:26- Contact Pressure Distribution on Rail and End Post [96]..... | 51 |
| Figure 3:27- Pneumatic Ball-on-Plate Apparatus..... | 51 |
| Figure 3:28- Schematic Diagram of the End Post Specimen..... | 52 |
| Figure 3:29- Profilometer Diagram..... | 53 |
| Figure 3:30- Microscope Image..... | 53 |

| | |
|--|----|
| Figure 3:31 - Tinius Olsen-H25ks Machine..... | 54 |
| Figure 3:32- Schematic of Specimen..... | 54 |
| Figure 4:1- Volume Loss of End Post Materials in Dry and Wet Sliding Tests..... | 59 |
| Figure 4:2- Sliding Tests for All Studied End Post Materials in Dry and Wet Test Conditions at an Applied Load of 10 N and Sliding Speeds of 1.5 m/sec, 3.3 m/sec and 7.2 m/sec..... | 59 |
| Figure 4:3- Sliding Tests for All End Post Materials in Dry and Wet Test Conditions at an Applied Load of 30 N and Sliding Speeds of 1.5 m/sec, 3.3 m/sec and 7.2 m/se..... | 60 |
| Figure 4:4- Sliding Test for All Studied End Post Materials in Dry and Wet Test Conditions at an Applied Load of 50 N and Sliding Speeds of 1.5 m/sec, 3.3 m/sec and 7.2 m/sec..... | 60 |
| Figure 4:5- Surface Roughness (R_a) Changes of End Post Materials Under Study after Dry and Wet Sliding Wear Tests..... | 62 |
| Figure 4:6- Coefficient of Friction of (N12) at Sliding Velocities of 1.5 m/sec., 3.3 m/sec., and 7.2 m/sec. and Applied Loads of 10 N, 30 N, 50 N.... | 64 |
| Figure 4:7- Coefficient of Friction of (N66) at Sliding Velocities of 1.5 m/sec., 3.3 m/sec., and 7.2 m/sec. and Applied Loads of 10 N, 30 N, 50 N.... | 64 |
| Figure 4:8- Coefficient of Friction of (N66a) at Sliding Velocities of 1.5 m/sec., 3.3 m/sec., and 7.2 m/sec. and Applied Loads of 10 N, 30 N, 50 N.... | 65 |
| Figure 4:9- Coefficient of Friction of (EG) at Sliding Velocities of 1.5 m/sec., 3.3 m/sec., and 7.2 m/sec. and Applied Loads of 10 N, 30 N, 50 N..... | 65 |
| Figure 4:10- Coefficient of Friction of (PRBF) at Sliding Velocities of 1.5 m/sec., 3.3 m/sec., and 7.2 m/sec. and Applied Loads of 10 N, 30 N, 50 N..... | 65 |
| Figure 4:11- Contact Surface of End Post Material in Both Dry and Wet Test Conditions..... | 70 |
| Figure 4:12- Schematic Diagram of Wear Mechanism..... | 70 |
| Figure 4:13- Photos of Melted Materials of (a) Nylon 12, (b) Nylon 66 and (c) Nylon 66a..... | 74 |
| Figure 5:1- Crater Diameter of End Post Materials in Dry and Wet Impact Tests... | 79 |

| | |
|---|----|
| Figure 5:2- Impact Test for All End Post Materials in Dry and Wet Conditions at an Applied Load of 100 N and 1000 Cycles, 5000 Cycles and 10000 Cycles..... | 80 |
| Figure 5:3- Impact Test for All End Post Materials in Dry and Wet Conditions at an Applied Load of 300 N and 1000 Cycles, 5000 Cycles and 10000 Cycles..... | 80 |
| Figure 5:4- Impact Test for All End Post Materials in Dry and Wet Conditions at an Applied Load of 500 N and 1000 Cycles, 5000 Cycles and 10000 Cycles..... | 81 |
| Figure 5:5- Crater Depth of End Post Materials in Dry and Wet Impact Tests..... | 83 |
| Figure 5:6- Impact Test for All End Post Materials in Dry and Wet Conditions at an Applied Load of 100 N and 1000 Cycles, 5000 Cycles and 10000 Cycles..... | 83 |
| Figure 5:7- Impact Test for All End Post Materials in Dry and Wet Conditions at an Applied Load of 300 N and 1000 Cycles, 5000 Cycles and 10000 Cycles..... | 84 |
| Figure 5:8- Impact Test for All End Post Materials in Dry and Wet Conditions at an Applied Load of 500 N and 1000 Cycles, 5000 Cycles and 10000 Cycles..... | 84 |
| Figure 5:9- Wear Images of Nylon 66 Material at Forces of 100 N, 300 N and 500 N and 1000 Cycles, 5000 Cycles and 10000 Cycles in both Dry and Wet Conditions..... | 86 |
| Figure 5:10- Wear Images of Epoxy Glass Material at Forces of 100 N, 300 N and 500 N and 1000 Cycles, 5000 Cycles and 10000 Cycles in both Dry and Wet Conditions..... | 88 |
| Figure 5:11- Wear Images of Phenolic Resin Bonded Fabric Material at Forces of 100 N, 300 N and 500 N and 1000 Cycles, 5000 Cycles and 10000 Cycles in both Dry and Wet Conditions..... | 90 |
| Figure 5:12- Schematic of N 66 Material Wear Mechanisms..... | 91 |
| Figure 5:13- Schematic of EG Material Wear Mechanisms..... | 91 |
| Figure 5:14- Schematic of PRBF Material Wear Mechanisms..... | 92 |
| Figure 6:1- Rail Steel Disc and Epoxy Glass End Post Materials (R1, R2 and R3). | 95 |

| | |
|--|-----|
| Figure 6:2- End Post Thickness before and after the Test..... | 96 |
| Figure 6:3- Schematic Gap before Test..... | 96 |
| Figure 6:4- Schematic Gap after Test..... | 96 |
| Figure 6:5- Length of Gap Image after the Test..... | 96 |
| Figure 6:6- Gaps Length Images after the Test..... | 98 |
| Figure 6:7- Average Length of Lip (mm)..... | 99 |
| Figure 6:8- R3 Specimen Imitating Rail Head Deformation over the Insulating End Post (0.5 mm)..... | 101 |
| Figure 6:9- R3 Specimen Imitating Rail Head Deformation over the Insulating End Post (1 mm)..... | 101 |
| Figure 7:1- Disc Specimens of End Post and Steel Wheel..... | 102 |
| Figure 7:2- Specimens Tested Surface Images of Nylon 12, Nylon 66, Nylon 66a, Epoxy Glass and Phenolic Resin Bonded Fabric Materials..... | 104 |
| Figure 8:1- Rail End Bending..... | 107 |
| Figure 8:2- Static Compression Test Set-up..... | 108 |
| Figure 8:3- End Post Material Specimens (1) PRBF, (2) EG, (3) N12 and (4) N66 Materials..... | 109 |
| Figure 8:4- Nylon 12 Stress vs Strain..... | 110 |
| Figure 8:5- Nylon 66 Stress vs Strain..... | 111 |
| Figure 8:6- Epoxy Glass Stress vs Strain..... | 111 |
| Figure 8:7- Phenolic Resin Bonded Fabric Stress vs Strain..... | 112 |
| Figure 8:8- Nylon 12 Material Specimen after Test..... | 112 |
| Figure 8:9- Schematic Diagram of Nylon 12 (a) before Test (b) after Test..... | 112 |
| Figure 8:10- Nylon 66 Material Specimen after Test..... | 113 |
| Figure 8:11- Schematic Diagram of Nylon 66 (a) before Test (b) after Test..... | 113 |
| Figure 8:12- Epoxy Glass Material Specimen after Test..... | 113 |
| Figure 8:13- Epoxy Glass Specimen Fracture Surface Image..... | 113 |
| Figure 8:14- Schematic Diagram of Epoxy Glass (a) before Test (b) after Test..... | 113 |
| Figure 8:15- Phenolic Resin Bonded Fabric Material Specimen after Test..... | 114 |
| Figure 8:16- Phenolic Resin Bonded Fabric specimen Fracture Surface Image..... | 114 |

Figure 8:17- Schematic Diagram of Phenolic Resin Bonded Fabric (a) before
Test (b) after Test..... 114

List of Tables

| | |
|---|-----|
| Table 2:1- Comparison between Previous Studies and present Study..... | 25 |
| Table 3:1- Contact Scenarios - Wheel/Rail and IRJ..... | 30 |
| Table 3:2- Outline of Test Approaches Used to Replicate Contact Conditions..... | 32 |
| Table 3:3- End Post Material Properties [89-92]..... | 37 |
| Table 3:4- Shore D Hardness (D) Value of End Post Material..... | 44 |
| Table 3:5- Summarised Wheel and Rail Radii (Data from [14, 28])..... | 47 |
| Table 4:1- Test Conditions..... | 55 |
| Table 5:1- Test Conditions..... | 77 |
| Table 6:1- Partial Slip Ratio 1% Lipping Test Conditions..... | 94 |
| Table 7:1- Rolling/Sliding Test Conditions..... | 102 |

Acknowledgements

I would like to express my sincere appreciation thanks and gratitude to Almighty Allah, who helped and blessed me during the courses of my studies in general.

I would like also to express my sincere thanks and gratitude to my supervisor Prof. Roger Lewis for his sustained help, guide, support and advice during the preparation of this thesis.

I also would like to express my thanks to my colleagues Luke E Buckley-Johnstone for his help and advice in rolling/sliding contact tests, Oliver Burke for his help in coefficient of friction tests and Philip Beaty for his help in lipping tests.

Thanks to Mr. David Butcher from the mechanical engineering department's workshop for preparing the tests specimens.

The thesis was possible thanks to the scholarship awarded by the Ministry of higher education of my home country of Libya.

I would like also to extend my great thanks appreciation to my wife, sisters and brothers and all my family and friends for their support and help to finalize the thesis.

Last but not least I would like to extend my great special thanks and gratitude to my parents for their sustained advice and support in all stages of my education from primary school to my PhD.

FATHI A. ELSHUKRI

1- Introduction

1.1- Rail Transport Importance

Trains are the quickest, most comfortable and reliable transport choice compared with other land transport. They can carry huge numbers of individuals or extensive cargo loads at high speed in one unit, where the same number or burden would take numerous buses and considerably more lorries or cars. The train is far faster and more reliable than cars, buses and lorries [1]. Rail transport started in Greece during the 6th century. The railway was 6 km long in the beginning [2]. The railway reappeared in 1350 in Germany after the dark ages. The rail was made from wood and the line was operated by animal or human power [3, 4]. By the 17th century wooden rails were used in England and Wales for transporting coal. One of the oldest railways in the world, is the railway in Leeds that was built in 1758. In 1810, the first tramway was the Leiper Railroad. In 1768 wrought iron plate was placed on the top of wooden rail. In 1803 the length of rail extended to 4.6 m. In 1857 the rail was made with steel. In 1825 the first public steam railway began to operate in North East England. 1435 mm gauge began use in UK in 1830 and an electrical railway was working in 1838. High speed rail was introduced in Japan in 1964 [5-7]. After that the rail transport witnessed great development until the present day.

1.2- Rail Transport Maintenance

Railways require preventive and corrective maintenance to stay in good condition, particularly in the case of high speed trains [8].

1.2.1- Rail Transport Maintenance Costs

It is difficult to determine rail transport maintenance costs. They depend on many factors: track type, geological condition, electric traction, high humidity and typhoon immunity, high passenger capacity and high technology specifications trains ... etc. [9].

Rail transport maintenance costs are divided into two types [10]:

- i) Direct Maintenance Costs
- ii) Indirect Maintenance Costs

1.2.1.1- Direct Maintenance Costs

Direct maintenance costs are the costs of all activities directly used in railway maintenance, i.e., labour and materials.

1.2.1.2- Indirect Maintenance Costs

Indirect maintenance costs are the costs of all functions not directly involved in railway maintenance such as preparing material costs, staff training costs, transport to a maintenance site costs, inventory costs, material order costs, etc.

1.3- Structure of the Railway Track

Railway track consists of parallel lines of rails with their sleepers, fittings and fastenings, ballast, etc. (see Figure 1:1) to equip a path for the movement of trains for transportation [8]. The total length of track in the UK is 32,186 km [11].

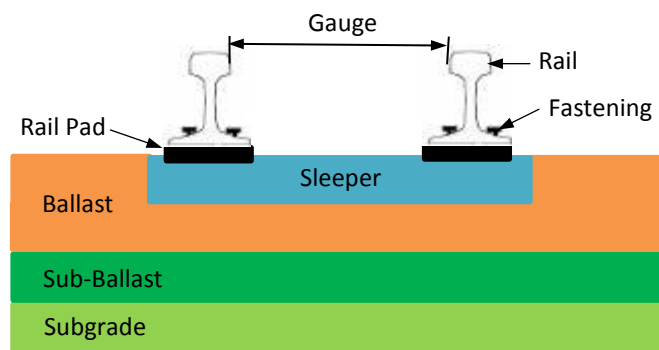


Fig. 1:1- Railway Track Cross-Section.

1.3.1- Rail

The rail is the main part of the track and is made of rolled steel (see Figure 1:2). The main function of the rail is to [12]:

- Distribute the weight of a train to the sleepers.
- Provide a suitable running surface and work with the wheels in steering the coaches in required directions.
- Carry reversion traction current and to transfer electric current for signalling objectives in track circuited regions.



Fig. 1:2- Flat-Footed Rail Section [13].

There are three different types of rail (see Figure 1:3) [8]:

i) Double-headed rail

This type of rail is not commonly used now. The head and foot of double headed rails is made in the same size (see Figure 1:3 (a)). Double headed rail can be inverted when the rail head is worn out, but craters can be found in the foot at the sleeper support points which do not provide smooth running for the trains.

ii) Bull-headed rail

The bull-headed rails head is made larger than its foot, as shown in Figure 1:3 (b).

iii) Flat-footed rail.

The shape of flat-footed rails is a “I” shape (see Figure 1:3 (c)). In the beginning, flat-footed rails were located immediately on the sleeper. After that steel bearing plates have been put between the rail foot and the sleepers due to the increase in loads.

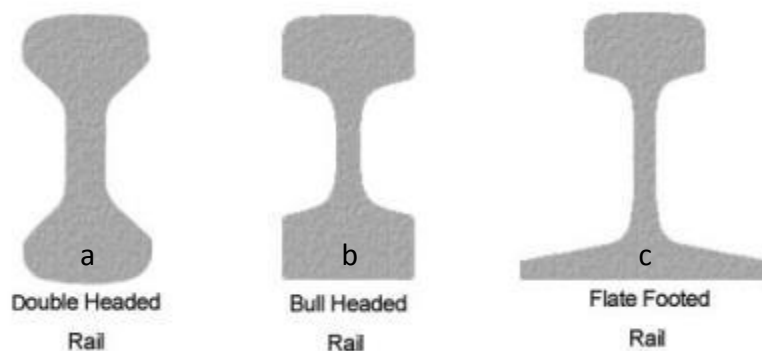


Fig. 1:3- Rail Types Cross- Sections [8].

1.3.2- Sleepers

Sleepers are used to transmit the oncoming loads to the track ballast and hold the track

and assist in maintaining the gauge. There are three types of sleepers now commonly used [8]:

- a) Wooden sleepers (see Figure 1:4).

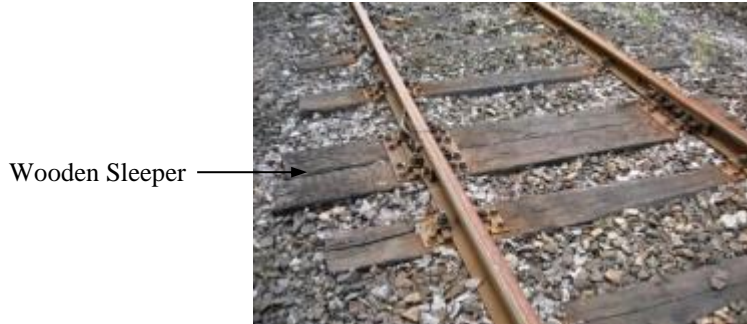


Fig. 1:4- Wooden Sleeper [8, 14, 15].

- b) Metal sleepers, divided into cast iron sleepers and steel sleepers (see Figure 1:5).



Fig. 1:5- Metal Sleeper [8, 14, 15].

- c) Concrete sleepers (see Figure 1:6).

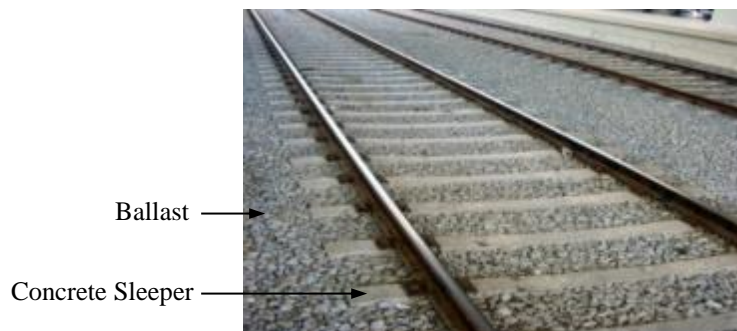


Fig. 1:6- Concrete Sleeper [8, 14, 15].

1.3.3- Gauges

The distance between the inner edges of the rail heads is called the “gauge”. It is equal to 1435 mm in the UK and measured at 16 mm below the top of the rail [8].

1.3.4- Ballast

One of the most important components in the track structure is ballast. With the increasing axle loads and train speeds, the importance of the ballast has risen. Different types of materials are used according to the availability, requirement and economic motives, such as rock aggregates, natural gravel, sand and shingle etc. The shape is angular or cubic.

The ballast layer performs major functions in a track system such as supporting the track against train forces, providing stability to the track, and allowing rain water drainage (see Figures 1:1 and 1:6) [16, 17].

1.4- Rail Joints

Rail joints are used to connect two rails end to end, so as to prevent the movement of the rail horizontally and vertically. They act as a bridge between the adjacent rails, as well as allowing longitudinal movement of rails when expanding and contracting as a result of temperature changes. Rail joints are the weakest part of the track, where their life ranges between a third or a half of the life of the rails.

Rail joints consist of two opposite bars called “fish plates” with four or six bolts and washers (see Figure 1:7). The joint bars are put in place by the action of bolt connections through rails.

There are three types of rail joints which are described in the following sections [8]:

- i) Standard rail joints.
- ii) Compromise rail joints.
- iii) Insulated rail joints.



Fig. 1:7- 4 Bolt Rail Joint “fish plates” [18].

1.4.1- Standard Rail Joints

Standard rail joints, as shown in Figure 1:8, are used to connect two rail ends of the same specification, such as weight section. Standard rail joints are divided into standard rail joints 24in in length with 4-bolt holes for small rail sections and 36in in length with 6-bolt holes for larger rail sections.

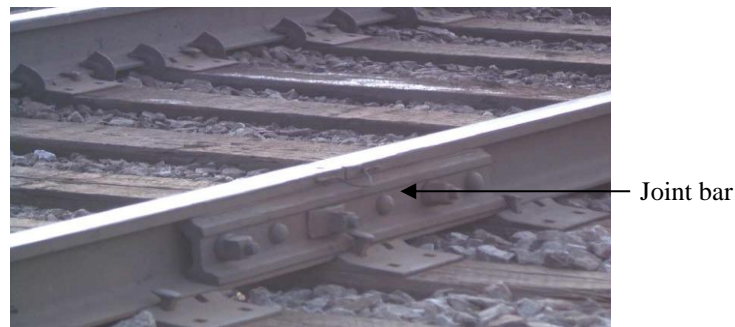


Fig. 1:8- Standard Joint Bar [19].

1.4.2- Compromise Rail Joints

Compromise rail joints are used to connect two rails of different specifications, such as weight and section (see Figure 1:9). There are two types of compromise rail joints, directional compromise rail joints and non-directional compromise rail joints.

The directional compromise rail joints (right and left hand) are employed where a difference in the width of the head between two sections means offsetting of the rails is required to align the gauge side of the rails.

The non-directional (gauge or field side) compromise joints are used where the contrast between sections is not more than 3.157 mm at the gauge point or where the contrast is in the height of the head.



Fig. 1:9- Compromise Joint Bar [19].

1.4.3- Insulated Rail Joint (IRJs)

Insulated Rail Joints (IRJs) are used in track as part of the signalling system. Track signalling is employed to ensure that the movement of trains is safe and smooth so as not to pause the trains. For the purpose of train detection the track is split into blocks, each of which form a circuit. A low-voltage electric current is fed from a battery to the rails at one end of the track section. At the other end of the track, a relay is attached to the rails. In an unoccupied circuit, as seen in Figure 1:10, the current is allowed to run through the relay keeping it switched to a position that allows a track signal to show that the track section is clear [20].

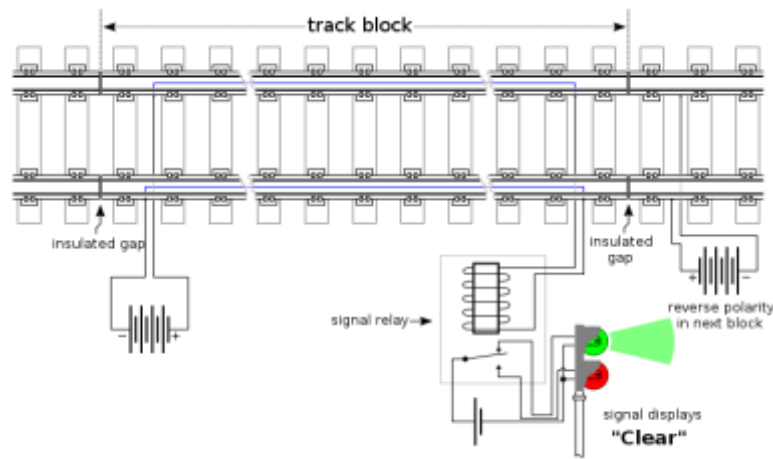


Fig. 1:10- Clear Track Circuit [20].

When a train enters the insulated track section, the wheels and axles short the circuit as shown in Figure 1:11.

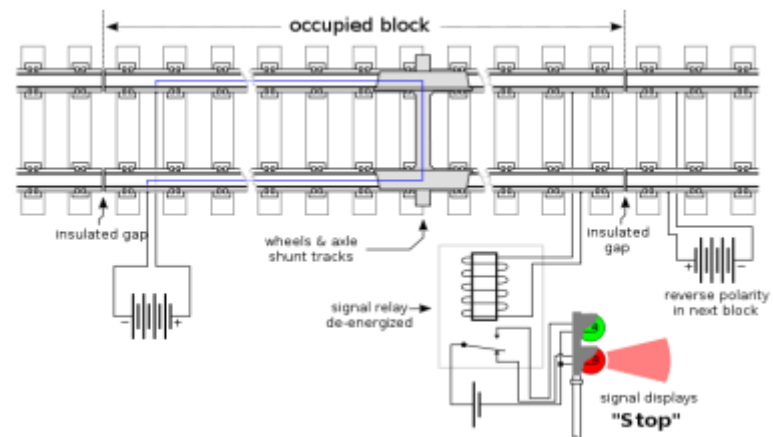


Fig. 1:11- Occupied Track Circuit [20].

The current is therefore diverted from the relay, causing the relay to switch to its other position which causes a track signal to show that a train is present in the block.

IRJs are used to connect adjoining rails and provide a smooth surface for passage of train wheels on the railways as well as make the rail network electrically isolated. They preclude electrical current transfer between adjoining rails, thereby dividing a track circuit into circuit sections. IRJs employ insulating material between the rail ends (end posts). Insulated joints completely isolate the rails by insulating material placed between the fishplate and the rails and around the bolts. IRJs consist of the following components, as shown in Figure 1:12 [21, 22].

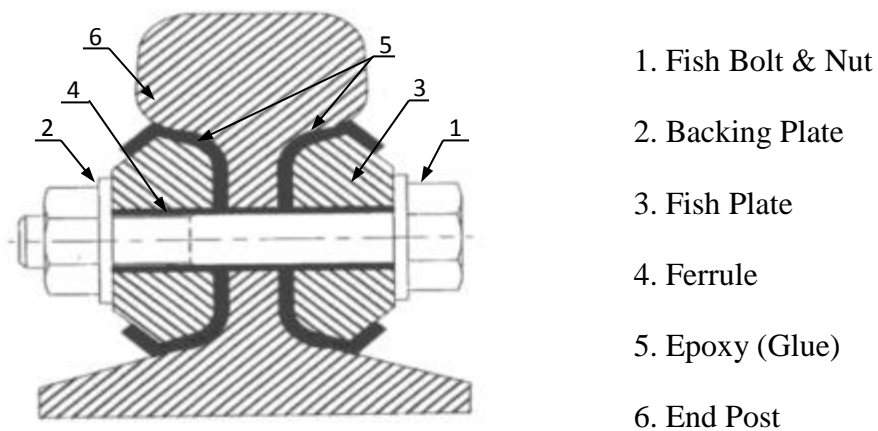


Fig. 1:12- Cross-Section of an Insulated Joint [21, 22].

There are two designs of IRJs:

- i) Non-glued (loose) IRJs
- ii) Glued IRJs

In non-glued IRJs, the end post is put in the gap between rails then fishplates are installed on the rails by the action of bolts, while in glued IRJs the end post is put firmly in place by the action of high strength glue between joint bars and rails and bolts connections through rails and joint bars to ensure that they are coherent as one piece to bear the excessive loads and frequent vibration. The focus in this work will be on Insulated Rail Joints (IRJs).

1.4.3.1- End Post

The end post is a buffer made from electrically non-conductive material such as Nylon or composite materials which is placed in the gap between the adjacent rails, so as not to

allow the passage of electrical current from one rail to the other. End posts take the same shape as the section of the rail and their thickness ranges from 6 mm to 15 mm (see Figure 1:13) [8, 23, 24].

End post material, properties and thickness are closely related to IRJ failures and dynamic action. The end post material may be placed in the gap between the rails perpendicular to the longitudinal rail axis, this layout is known as “square IRJs” (see Figure 1:14). In a different layout, end post material is put at a 15° inclination from the lateral rail axis, this arrangement is called an inclined IRJ (see Figure 1:15) [24].

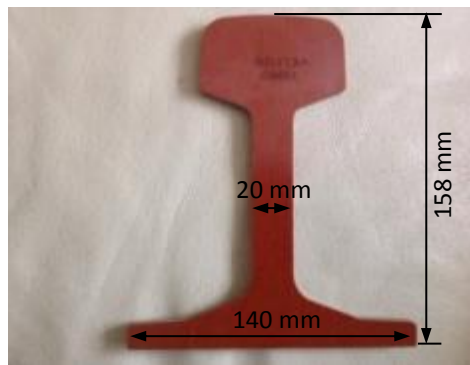


Fig. 1:13- End Post Shape.

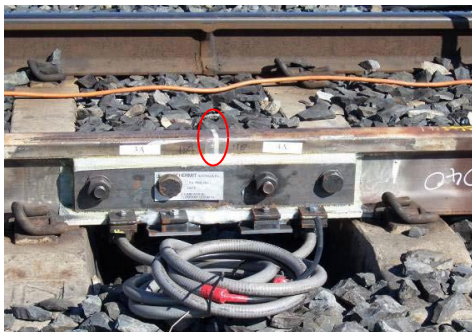


Fig. 1:14- Square Joint [24, 25].

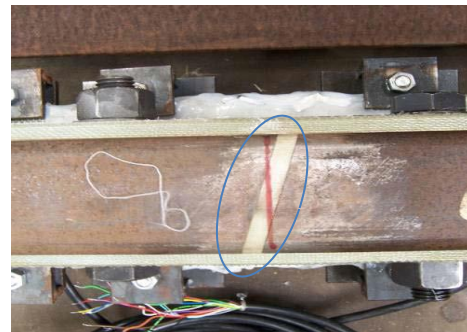


Fig. 1:15- Inclined Joint (Top View) [24, 25].

1.5- Insulated Rail Joint Design

IRJs consist of insulating material (end post) placed in the gap between adjoining rails, and two joint bars held by bolts or by adhesive and bolts which connect the rails. There are several types of design depending on the form of rail and its support system.

Two types of IRJ supporting systems are used [8, 24]:

- i) Supported IRJs

ii) Suspended IRJs

Figure 1:16 shows the presence of the sleepers in a symmetrical position to the end post for suspended IRJs. For the suspended IRJs, there is no support under the end post.

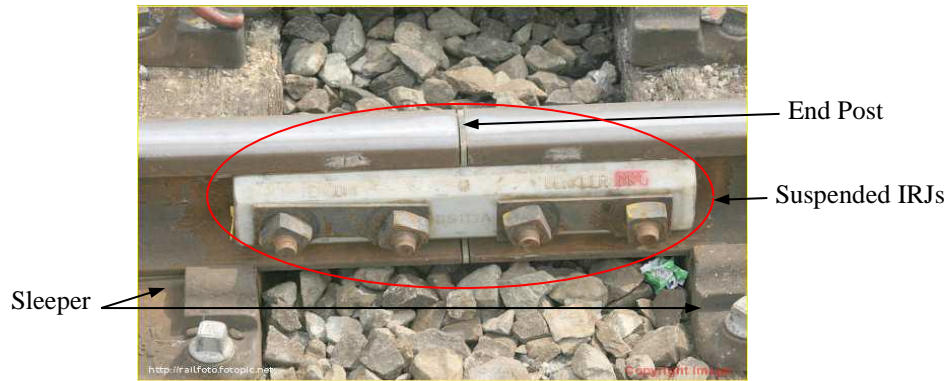


Fig. 1:16- Suspended IRJs [26].

In supported IRJs, the end post is fixed on the sleepers. There are two types of supported IRJs:

1- Continuous IRJs (see Figure 1:17)

They are called continuous because they continuously support base of the rail. No metal-to-metal contact occurs between the joint steel bars and the rails.



Fig. 1:17- Continuous Insulated Rail Joints [14].

2- Non-continuous IRJs

In the non-continuous supported IRJs the end post is fixed immediately above a sleeper, as shown in Figure 1:18, which reduces the dipping of the rails, and thus relieves compression on the end post and prevents its cracking and fragmentation [27].



Fig. 1:18- Non-Continuous Supported IRJs [28].

1.6- Importance of IRJs

IRJs are used to electrically isolate the rails and split the circuit into sections to achieve signal control. IRJs failure is a serious safety case and railways operators are very focused on the issue of their maintenance and conservation. IRJs are considered to be a weak spot in the rail track. The service life of IRJs is 1/3 to 1/2 of rail life [27]. There are approximately 96000 units in the UK network, with 4000 being replaced each year.

The annual cost to Network Rail for the replacement and maintenance of IRJs has been estimated to be £3.5 million in delay minutes and further £9 million in unit replacements per year [11]. Improvement of the present IRJs is therefore needed to solve this growing issue. Recently there have been some studies looking at the mechanism of failures of IRJs in order to develop and improve their performance.

1.7- Insulated Rail Joints Failures

Many industries face the problem of wear, especially in the moving parts. Practically the moving parts are subject to wear in contact region with other parts. Wearing parts need replacement and this process leads to an increase in costs and down time. The engineers working in this area need to find and design certain materials to resist this wear occurring to the moving parts to increase the part's life and reduce the replacement of the part. Failures in rail joints are driven largely by the wheel/rail contact [25].

1.7.1- Wheel-Rail Contact

The bulk material and surface in the contact region between rail and train wheel must be very strong to bear the vertical normal forces from heavy loads and dynamic action induced by wheel and track irregularities [29].

The area of contact between train wheel and rails (approximately 100 mm²) is small compared with the overall dimensions of the wheel and rail.

It is not easy to measure the contact zone between the rail and the railway wheel. One of the interesting methods for measuring the contact area between railway wheel and rail is ultrasonic reflection technique it was presented by Marshall et al. [30].

Another way for simulating the contact between bodies is with finite element methods.

1.7.2- Insulated Rail Joints Failures Types

The first type is mechanical failure; this type of failure affects steel parts, such as the rails, joint bars and bolts. All the steel parts in the track are subjected to static and dynamic loads and fatigue. The first type of mechanical failure is broken joint bar failure due to excessive load and high impact forces at the IRJs as shown in Figure 1:19.

The second type of mechanical failure is “battered” rail end. The influence of running wheels causes the rail end to be flow downwards and become flattened. These flattened rail ends are called “battered” or “crippled” rail ends. This happens when the gap between adjoining rails is excessive and fish plates do not fit snugly because of the lack of strong support at the ends of the rails (see Figure 1:20). It is measured by comparing the height of the rail at the rail end and at a point 300 mm away from the rail end. Rail end battering up to 2 mm is accepted and 3 mm is critical.

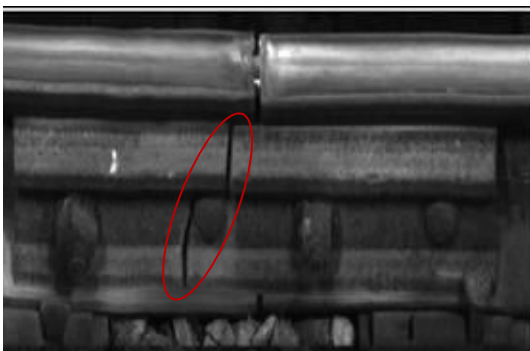


Fig. 1:19- Cracked Joint Bar [31].



Fig. 1:20- Rail End Battering [32].

High loads can also cause failures in the epoxy that is used to hold the joints together. The epoxy can crack or peel away from the joint bars and rail that it is attached to, which can significantly weaken the insulated joint. Once the epoxy is weakened, it can cause the insulated joint to fail.

The second type is electrical failure, which is a destruction of the insulated joints so that loss of the ability to isolate the electrical current in the rail network occurs. This leads to the transmission of electrical current between the adjacent rails. There are a few ways in which an electrical failure can occur in bonded insulated rail joints.

The first reason that leads to electrical failure in IRJs is “Lipping”, which is flow of rail head material due to high wheel loads and traction. When the train wheels pass over the rail head near the gap between adjoining rails at an IRJ, the steel of the rail can deform over time. After a period of time, the gap between rails will close and the adjoining rail comes into contact and an electrical short occurs (see Figures 1:21 and 1:22).



Fig. 1:21- Rail End Metal Flow [27].

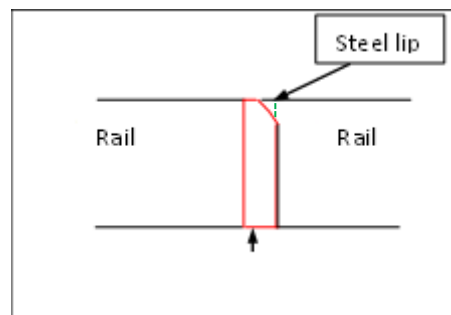


Fig. 1:22- Schematic Diagram of Rail End Metal Flow.

It can lead to the development of further damage such as spalling as shown in Figure 1:23. Key factors associated with this type of failure are rolling contact fatigue and the associated loading rate dependent metal plasticity as the wheel load exceeds the material yield point at the point of contact.



Fig. 1:23- Rail Head Metal Spalling in the Gap between Adjoining Rail at IRJs [27].

Electrical failure can also occur when bolts used to hold the joint bars together are permitted to touch the joint bars and the rail at the same time. This may happen when the insulation ferrules around the bolts fail due to high loads.

Another method of electrical failure is a failure of the insulating end post of the joint. The end post may crack and come out of the space between the rails in the joint which may allow the rails to touch when they are extended or when the joint is loaded this is due to thermal effects and higher impact forces at IRJs (see Figures 1:24 and 1:25). Damage or loss of the end post can allow water in the joint and thus allow the passage of electrical current.

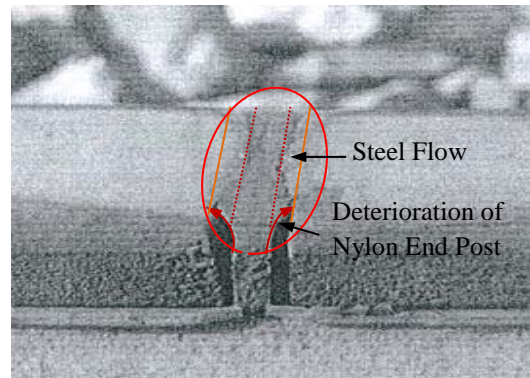
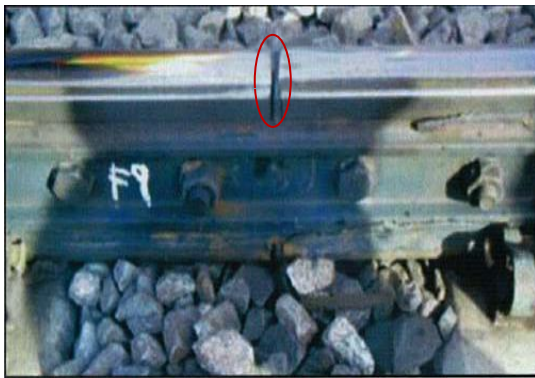


Fig. 1:24- IRJ with End Post Crushed [27]. Fig. 1:25- Plastic Deformation of Rail End with Deterioration of End Post [33].

To improve and develop IRJs, understanding of their failure mechanisms is firstly required. There are several types of insulated rail joint failures related to various design of IRJs. In the UK, the main failure mode as shown in Figure 1:26 is insulation failure 29%, fishplate

defect 23%, lipping 17%, swarf contamination 15%, rail failure 12%, bolt defect 3% and rail fracture 1% [11].

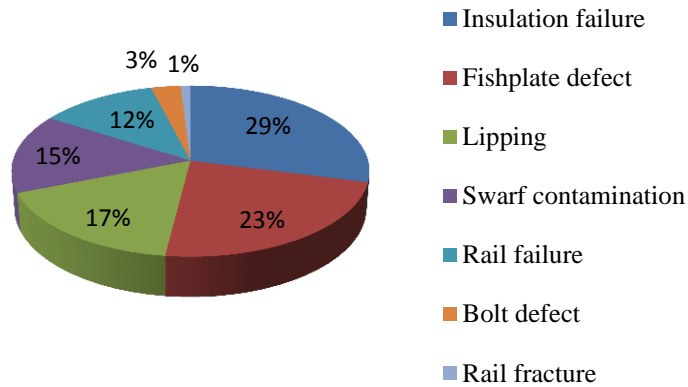


Fig. 1:26- Percentage Split of IRJ Failures (Data from [11]).

1.8- Aims and Objectives

The overall aim of this study was to use experimental investigations to understand end post and end of rail lipping failures and identify optimum end post materials.

The objectives can be stated as:

- i) Review the common types of damage that affect the performance of insulated rail joints.
- ii) Review the previous research/studies on insulated rail joints.
- iii) Test five types of end post materials that are widely used in the field.
- iv) Examine the effect of sliding on end post materials.
- v) Examine the effect of impact damage on end post materials.
- vi) Prove effect of rolling/sliding damage on end post materials.
- vii) Prove the influence of static compression loads on the end post materials.
- viii) Examine the effect of rail metal follow on end post materials.
- ix) Examine the effect of water on end post wear resistance.
- x) Select the best material that has higher wear resistance and good mechanical properties which will lead to improved design and performance of End Posts and Insulated Rail Joints (IRJs) when it put in service.

1.9- Thesis Outline

The Thesis is divided into nine chapters. The following is a brief overview of this thesis.

After the introductory chapter, chapter two contains a literature review consisting of four parts: investigation of insulated rail joints (IRJs) using finite element analysis, failure analysis, experimental investigation of insulated rail joints and polymer wear.

Chapter three describes the test rigs, materials, and tests methods used. Block-on-Ring tests for all five different types of end post materials in both dry and wet conditions are described in chapter four. The analysis of the experimental results is presented, together with discussion of the effect of operational parameters on wear resistance of each material. Impact tests for all five different types of end post materials in both dry and wet conditions are described in chapter five. The analysis of the experimental results is presented, together with discussion of the effect of operational test parameters on wear resistance of each material. The lipping tests (the effect of rail metal flow) are explained in chapter six. The analysis of the experimental results is exhibited, together with discussion of the effect of operational test parameters on wear resistance of each material. Rolling/sliding wear tests, in both dry and wet conditions are explained in chapter seven. The analysis of the experimental results is introduced, together with discussion of the effect of operational test parameters on wear resistance of each material. The effect of static compression is described in chapter eight. Finally, conclusions of this study are presented in chapter nine.

2- Literature Review

A literature search has been carried out to investigate work that has been done previously in the area of Insulated Rail Joints. The studies have been conducted using different methods to investigate the problem. Much work has been performed using modelling, and the other work has been implemented employing experimental techniques. The results of this review are displayed in the first half of the chapter. In the second part, the tribology of polymers is outlined to help inform testing of the end post materials and provide data for comparison.

2.1- Experimental Investigations of Insulated Rail Joints

Myville and Ronal [34] carried out analytical and experimental investigations to find the reason for a ridge characteristic seen on the fracture surface of a railroad rail-end bolt hole fatigue crack. The obtained results indicated that stress fluctuations resulting from thermal expansion of the rail were the main cause of the ridges.

Dhanasekar et al. [35, 36] presented field testing of dynamic impacts occurring at an IRJ due to wheel passages. Strain gauges were used in the throat and foot of the rail in square and inclined joints. Vertical, longitudinal and shear strains are reported in the study. An automated computer system powered by a solar system was used to collect strain data.

Changes of microstructure in the vicinity of end posts of insulated rail joints manufactured from surface uncoated and coated rail were examined by Rathod et al. [37]. Optical and scanning electron microscopy techniques were employed. A laser clad and reference angle cut, 6-bolt, insulated rail joints were taken from an Australian standard. Laser cladding was implemented by cutting a bathtub shape into the rail head and then using powder laser immersion to fill it with 431 martensitic stainless steel. Severe deformation in the head hardened area near the surface of the top rail appeared on the ends of the rail of the unclad specimen. Metal flow, cracking and spalling damage on the head hardened rail appeared. The laser clad IRJ suffered less defects compared with head hardened reference specimen.

2.2- Investigation of Insulated Rail Joints Using Finite Element Analysis

Work on modelling using Finite Element techniques has focused on:

- Effect of a free rail end on contact stress distribution [33].
- Impact forces affecting the end of the rail [38].

- The relationship between gap size and impact force [39].
- Rail mechanical behaviour due to the action of rolling wheel [40].
- Contact impact analysis of the rail joint region [41].
- The effect of an insulated rail joints on the rail/wheel contact stresses under condition of partial slip [42].
- The influence of the rail joint on generation of wheel-rail impact load and subsequent material deterioration of the joint [43].
- Quantifying railhead material and end post damage and plastic deformation of insulated rail joints [23].

Significant work has been implemented on insulated rail joints using finite element analysis. A number of researchers have conducted modelling methods to study end post damage and metal flow, but no experimental studies have been carried on end posts. The present work was focused on experimental investigation to improve the end post performance.

2.3- Failure Analysis

Mandal and Peach [44] carried out an engineering analysis of different designs and failure modes of the IRJ and 3D finite element modelling for analysing the stresses experienced by three different joint bar size. They used the ABAQUS/ CAE product in their study. The longitudinal stress at the bottom and top of the joint bar is determined considering bending moment caused by train wheel load on the insulated rail joint.

Rathod et. al. [37] investigated microstructural changes in the vicinity of the end post of insulated rail joints manufactured from uncoated and coated rail using scanning and optical electron microscopy techniques. Deteriorated insulated rail joints made from pearlitic head hardened rail steel was compared with head hardened rail steel laser coated with martensitic stainless steel. Service life of the laser coated steel was longer than the service life of the untreated rail. The problems related to the surface were identified and ways for developing IRJ's resistance to rolling contact fatigue proposed.

Sandstrom et al. [45] monitored several insulated rail joints in the track over three years to show degradation. The material was damaged in early stage after installation, even though the applied loads were low. The damage of all joints was the same pattern with

deformation on the same side. Several joints exhibited cavity-like damage on the off-station side. During the period of the study the joints degradation and dip rise was shown.

2.4- Investigation of Polymer Wear

The purpose of reviewing previous studies of polymer wear was to determine the effect of operating factors such as sliding speed, applied load and surface roughness on the wear rate of the polymers against steel, as well as to see the wear mechanisms that occur for comparison with the results obtained in this study. The review focused on materials similar to those used in end posts.

2.4.1- Investigation of Polymer Sliding Wear

Holmberg and Wickstrom [46] conducted experimental studies to measure wear rates and coefficients of friction for 22 types of polymer materials. A pin-on-disc friction tribometer with a flat steel counterpart with surface roughness of $R_a = 0.2 \mu\text{m}$ was used for friction coefficient measurement and a multi pin-on-cylinder wear tribometer with a steel shaft counterpart with surface roughness of $R_a = 0.2 \mu\text{m}$ was employed for the wear tests. Both tests were carried out at speeds of 0.1-1 m/sec and applied stresses of 0.1-1 MPa. The coefficient of friction was measured for 0.5-1 hr of running time and the wear tests were conducted over 1000 of hrs running time. Low friction and wear rate were measured for polytetrafluoroethylenes and polyethylenes. The tribological properties of polymers were not always improved as a result of adding of fibres such as graphite, MoS_2 , and glass.

Clarke and Allen [48] considered a wet sliding test to investigate the behaviour of sliding wear of five polymeric materials. The study was conducted on ultrahigh molecular weight polyethylene (UHMWPE), polyoxymethylene (POM), poly(ethylene terephthalate) ((PETP), molybdenum disulphide filled polyamide 6 ($\text{PA6}/\text{MoS}_2$), and graphite filled poly(amide-imide) (P(A-1)/GR). A pin-on-disc rig was employed at sliding speeds of 0.13-2.27 m/ sec. and applied pressures of 1.3-5 MPa on a hardened stainless steel counterface with surface roughness of 0.25-1 μm . The wear rate of all studied materials was increased due to an increase in surface roughness of the counterface. The wear rate of materials rose then decreased and then increased rapidly for all materials as sliding speed was increased. The wear resistance was decreased for all materials as load was increased except for UHMWPE at a counterface roughness of 1 μm . This was due to an increase of temperature.

Mens and Gee [48] performed two types of experiment on 18 types of polymers. These were polyamide 66 (PA66), polyoxymethylen (POM), polyphenyleneterephthalateb (PETP), polyetheretherketone (PEEK), polyphenylenesulphide (PPS), and polyetherimide, initially using unfilled materials, and then the same materials filled with polytetrafluoroethylene (PTFE) or (PTFE plus glass fibre). The first experiment was a measurement of coefficient of friction as a function of the contact temperature. The second experiment was measurement of wear and friction in a 20 h test. These experiments were conducted in air and in water. In air the experiments ran between the polymers and rings of ball-bearing steel (AISI 52100), but in water the experiments ran between the polymers against rings of stainless steel (AISI 316). The tests were performed at applied loads of 150 N and 500 N contact pressures of 1.5 MPa and 5 MPa respectively and speed of 0.1 m/sec and 0.25 m/sec. The addition of PTFE was generally beneficial in air, but it did not function in water and the addition of glass fibres produced unfavourable impacts in water and in air.

Bellow and Viswanath [49] performed an experimental programme to investigate the wear behaviour of some polymer materials against a steel counter face. Vertical and horizontal pin-on-disc machines were used in this study the tests were conducted at room temperature and humidity. Two different steel counterfaces with surface roughness of 0.05-0.4 μm were used. The tests were carried out at a surface speed of 0.5 m/sec and applied load of 88.96 N. No relationship between wear and friction was observed. The wear behaviour of polymers material was influenced by counterface roughness.

Unal et al. [50] undertook experimental studies to investigate the effect of sliding velocity and applied pressure on the wear behaviour and friction of polyamide 66 (PA66), polyoxymethylene (POM), ultrahigh molecular weight polyethylene (UHMWPE), 30% glass fibre reinforced polyphenylene-sulfide (pps=30% GFR) and aliphatic polyketone (APK) polymers. The wear and friction tests of polymers against steel were performed at dry conditions. A pin-on-disc rig was used. The test was carried out at ambient temperature and at sliding velocity of 0.3-2.0 m/sec and applied pressure of 0.3-1.05 MPa. Small sensitivity of wear rate due to applied pressure and sliding speed was observed and there was inverse relationship between friction coefficient and pressure.

Wang and Gu [51] carried out experimental studies to investigate wear and friction properties of polymers material. A block-on-ring rig was employed in dry and wet conditions at room temperature and at sliding velocity of 0.42 m/sec. and different applied loads (50 to 400 N). The tested materials were Nylon 1010 and carbon fibre (CF)-reinforced Nylon 1010 composites. The Nylon 1010 wear rate was increased in water, but the friction coefficient was decreased in water compared with wear rate and friction coefficients in dry conditions. The resistance of wear of CF- >Nylon rose due to CF reinforcement. The CF- nylon wear rate in a dry condition was more than eight times, and coefficient of friction was reduced to half value in comparison to that in a wet condition under a 200 N load.

Basavarajappa et al. [52] performed dry sliding tests to study the tribological behaviour of glass epoxy polymer composites with SiC and graphite particles as secondary filler using a pin-on-disc rig. The rotating counterface was En-32 steel with $R_a = 10 \mu\text{m}$. The test was performed at sliding speeds of 3, 4 and 5 m/sec, loads of 20, 40 and 60 N and sliding distances of 1000, 2000 and 3000 m. The effect of sliding velocity, applied load and sliding period and the percentage of secondary fillers on the resistance of wear were studied. A Taguchi technique was employed to obtain data. The effect of test parameters on the wear rate was studied by using an orthogonal array and analysis of variance (ANOVA). The wear rate was decreased due to the addition of filler materials of SiC and graphite composites of glass epoxy.

From the previous studies of polymers sliding wear, the following information is summarised:

- The wear rate of studied polymer materials was increased as a result of a counter face surface roughness increase, and the wear rate increased due to an increase in sliding speed and applied load.
- The coefficient of friction and wear resistance of Nylon materials were decreased in water compared with a dry condition. This happens because of the absorption of water by Nylon materials which caused different effects, such as:
 - A reduction in the strength of the Nylon and rise in the elongation at break.
 - Chemical corrosion wear increased.

- An inhibition of the formation of transfer films of Nylon material debris on the counter face.
- There was an inverse relationship between coefficient of friction and pressure.
- The wear rate was decreased as a result of addition of filler materials of SiC and graphite of glass epoxy composite.
- There was no information available on the end post materials but the above information may help in a comparison with the results obtained from the current study.

2.4.2- Investigation of Polymer Impact Wear

Bayer et al. [53] considered impact wear tests of different thin polymers. The tests used two pivotal hammer systems. The first hammer system with an impact velocity of 89 cm/s, gave an impact energy of 31×10^3 ergs and the second hammer system with the velocities of 51-380 cm/s, had an impact energies of $0.8-30 \times 10^3$ ergs. The wear process was influenced by heat during hammer contact or overstress. The major heat source was fretting motion through contact and the stress distribution was affected by the material plasticity.

In another study Bayer [54] performed impact experiments on several polymers and developed a polymer impact wear model and compared the model with the results of experiments. Two phases of polymer impact wear were observed. Phase one does not lead to loss of material. The other one leads to a loss in material due to increases of wear rate and cracks seen in the wear surface.

2.4.3- Investigation of Polymer Wear in Rolling-Sliding Contacts

Kukureka et al. [55] carried out twin-disc tests to investigate the influence of fibre reinforcement on the wear resistance and coefficient of friction of polyamide 66 in a rolling-sliding contact. The tests were performed at rotational speeds within a range of 500-1500 rpm, applied loads of 50-600 N and slip ratios between 0-30%. The tests examined short fibre aramid, carbon and glass with composites against identical materials. The coefficient of friction was reduced due to using of glass fibre reinforcement.

Chen et al. [56] considered a twin-disc test to investigate the influence of many metallic counter face materials and surface treatments on the wear resistance of polymers and polymers composite in a dry case. The polymers studied were unreinforced polyamide 66

and its composite Resorcinol Formaldehyde Latex (RFL4036). The metallic materials were brass, steel and aluminium and the surface treatments were tuffride treated and magnesium phosphate treated. The experiments were performed over a range of slip ratios, an applied load of 300 N and a rotational speed of 105 rad/sec. The wear rate and friction coefficient for the polyamide composite was less than the wear rate and coefficient of friction for the unreinforced polyamide 66 when run against aluminium and steel counter face. Whilst the polyamide 66 had a higher wear resistance than the composite when tested against a brass counter face. The steel surface treatment had a clear influence on the wear resistance, coefficient of friction and wear mechanism of the polyamide 66 composite. The features of the counter face metallic materials and the surface treatment control the wear mechanism of polyamide 66 and its composite.

Avanzini et al. [57] conducted experimental work on unfilled PEEK and on three PEEK short fibre reinforced composites against steel to investigate wear and rolling contact fatigue. A four roller test bench was used in this investigation. The rolling contact in dry conditions and pure rolling, applying a constant (Hertzian) contact theory to each roller were achieved. Various applied loads were used for each type of material, to draw a pressure life diagram. Contact pressure varied from 80 MPa to 160 MPa. Rotating velocity was 500 rev/min. for the unfilled PEEK and 800 rev/min for the filled PEEK. The number of cycles was 10,000,000 and cooling air flow was used. Wear damage was detected as micro-pitting for unfilled PEEK and as delamination for filled PEEK. Filled PEEK material presented a lower wear rate compared with neat PEEK material. Different rolling contact fatigue damage for neat PEEK and composite rollers resulted. Deep cracks showed in the neat PEEK materials.

Hoskins et al. [58] used a twin-disc configuration to examine the behaviour of rolling-sliding wear of two PEEK discs. The tests were carried out in dry conditions. The tests were conducted at a rotational speed of 1000 rpm, range of applied loads of 100, 200, 300 and 400 N and range of slip ratios of 3.92%, 14.29% and 28.57%. The specimen surface roughness was 5 μm . Contact fatigue and thermal wear were observed. The mechanisms of failure were due to structure of the contact surface.

2.4.4- Investigation of Polymer Static Compression Failures

Boll et al. [59] employed a polarized-light microscopy technique to study the compression manner of single carbon filaments embedded in epoxy polymer block. The test piece was placed in side supporting key ways with a clearance of 1.2×10^{-2} mm. Hydraulic load was applied. A microbuckling failure mode was not observed. The shear failure was the basic mechanism of failure.

Jelf and Fleck [60] have investigated the compressive failure of composite materials. The tests were carried out on rectangular specimens (width = 45 mm, thickness = 8 mm and height = 60-170 mm). The specimens were compressed between two plates at a strain rate of 0.02 mm/sec. Four different types of failures of composite materials were recognized (failure of fibres, failure of the matrix, permanent microbuckling and elastic microbuckling). Permanent microbuckling was the most common failure mechanism. The compressive failure of A54/PEEK composite material was described.

Chen and Zhou [61] conducted quasi-static experiments to produce stress-strain curves for epoxy, Epon 82 2/T-403. The experiments were conducted at strain rate of 1.1×10^{-1} to $5.2 \times 10^{-3} s^{-1}$. The results obtained showed that the epoxy compressive strength increased with an increasing rate of strain.

Roslan et al. [62] studied the compressive properties of carbon fibre reinforced plastic. Three axial compression tests were performed Quasi-static, low strain and drop hammer. Quasi-Static axial compression tests were carried out using an Instron Universal test in a machine at a rate of 0.5 mm/min. and low strain rate tests were performed using a servo hydraulic, Development and Production (RDP) machine at different rates. The transverse compressive properties were obtained. A degree of non-linearity appeared in the stress-strain curve. The compressive strength and ultimate stress rose with increasing rate of strain.

Brown et al. [63] conducted quasi-static tests on an Instron electro-mechanical universal test machine to investigate the influence of rate of strain on compression, tensile and shear behaviour of Epoxy-Glass/Polypropylene woven fabric material. The specimens were loaded between two flat plates at a crosshead speed of 5 mm/min. The results obtained illustrated that the modulus of elasticity in tension and compression and strength rose with increasing strain rate, but the shear modulus and strength decreased.

2.5- Comparison between Previous Studies and Current Study

Table 2:1- Comparison between Previous Studies and present Study

| Previous Studies | Current Study |
|---|---|
| <p>1- Finite element method was conducted to investigate metal strain, end post materials and end post thickness.</p> | <p>1- Instead of finite element analysis, current study implemented experimental work to examine the wear resistance of metal flow, end post materials and end post thickness.</p> |
| <p>2- Pin-on-Disc was used to examine the wear rate of some polymeric materials. The following results were obtained:</p> <ul style="list-style-type: none"> i) Wear rate increased due to increase in surface roughness [47]. ii) Wear rate increased when sliding speed increased [47]. iii) Wear rate rose when applied load increased due to increase in contact temperature [47]. iv) The wear rate was decreased due to addition of filler material of SiC and graphite of glass epoxy [48]. v) Wear behaviour of polymers was influenced by counter face roughness [49]. vi) Small sensitivity of wear rate due to applied load and sliding speed was observed [50]. | <p>2&3- Pin-on-Disc was not suitable method for simulating wear in the current study. Block-on-Ring was a suitable method in this field. It has not been used before to examine wear resistance for end post materials.</p> <p>The results obtained from this study were similar with the results obtained by [51].</p> |

| | |
|--|---|
| <p>vii) Addition of glass fibre produced an unfavourable impact in water and air [52].</p> <p>3- Block-on Ring was used to examine wear behaviour of polymers material [48]. The results obtained showed that Nylon wear were rate was increased in water decreased in water composite materials.</p> | |
| <p>4- Pin-on-Disc rig was employed to investigate the effect of sliding speed and load on the coefficient of friction of polymers material.</p> <p>The obtained results illustrated that:</p> <p>i) There was inverse relationship between friction coefficient and load [47].</p> <p>ii) The tribological properties of polymers were not always improved as a result of adding of fibres.</p> | <p>4- Pin-on-Disc was employed in current study to examine the effect of sliding speed and applied load on friction</p> |
| <p>5- Pivotal hammer system was used to consider impact wear test of different thin polymers [53].</p> <p>The wear process was effected by heat during heat during hammer contact or over stresses.</p> <p>6- Impact experiments were conducted on several polymers [54]. Two phases of impact damages were observed</p> <p>i) Damage did not lead to loss of material.</p> <p>ii) Damage lead to loss of material and</p> | <p>5&6- Ball-on-Plate was used in current study to investigate the end post materials impact wear resistance. The results showed that the impact damage was plastic deformation without material loss in nylon, and wear with material loss and cracks for composite materials.</p> |

| | |
|---|--|
| cracks seen in the wear surface. | |
| 7- Twin-Disc machine was employed to examine the behaviour of a rolling/sliding contact with PEEK, [58] The mechanisms of failure were due to structure of the counter surface | 7- Twin-Disc machine was used to investigate the effect of a rolling/sliding contact on end post materials. The damage was severe wear due to high load, temperature and effect of partial sliding and full rolling. |
| 8- Static compression test was used to examine the compression manner of polymers and composite materials. The results appeared that: i) The basic mechanism of failure of composite materials was shear failure [59]. ii) Four different types of failure of composite materials were recognized (failure of fibre, failure of matrix, plastic and elastic microbuckling) [61]. iii) Epoxy compressive strength increased with an increasing of strength rate strain [61-63]. | 8- Tinius Olsen-H25kN machine was used in this study to investigate the resistance of end post materials to static compressive. Nylon material had elastic and plastic deformation, while the composite materials had fibre and matrix failure, but failure mechanism was shear failure. |

In the past significant work has been carried out to study wear resistance of polymer materials. A number of researchers have conducted sliding tests such as (Pin-on-Disc and Block-on-Ring) and others employed rolling/sliding contact tests (twin-disc machine) and static compression test and a few researchers achieved impact tests, but the effect of sliding wear, impact wear, rolling/sliding contact wear and static compression test on the end post in field of railway network has not been investigated. The experimental work is more realistic than using other techniques such as finite elements analysis and the results are more reliable.

2.6- Summary

2.6.1- IRJs

There are a lot of reasons identified that lead to insulated rail joints failure including (in order of significance):

- 1- Cracking and loosening of the end post
- 2- Loss of epoxy
- 3- Curvature and breaking of joints bar due to excessive loads
- 4- Rail end metal flow
- 5- Bending, break and loss of bolts due to excessive loads

While end posts are critical and their failure can promote other issues such as rail dipping (leading to bar failure and fracture), rail metal flow and lipping etc., they have not been well investigated.

2.6.2- Polymers

The review of polymer tribology indicated that very little relevant data was available for end post materials. Virtually no impact work has been carried out at all.

Many projects are reported in the literature that were intended to develop the present design of insulated rail joints. Much work has been performed using finite element analysis method, but these studies did not deepen to find solutions to problems resulting from the failure of end posts, and few had relevant experiments to validate outcomes. A lot of difficulties that lead to the failure of insulated rail joints are due to end post failure. This is what prompted the topic of this PhD to try to study these defects and investigate them experimentally in order to contribute to the further development and improvement in the performance of insulated rail joints.

2.7- Novelty in Methods

This study provides the first use of four types of test apparatus to achieve five experiments in this field on these types of end post material. They were previously employed, but not in the field of investigation of insulated rail joints especially in end post materials.

- The first rig used in this study is a Block-on-Ring test apparatus. This rig is a new application in this field and for these materials.

- The second rig was a Pneumatic Ball-on-Plate impact tester and is not used before in this field and not used to test the impact wear for these types of material or similar.
- The third machine used in this research was a Twin-Disc Test machine. This machine has been used before to examine rolling/sliding wear for rail steel against train wheel steel, but it has not been used prior to investigate rolling/sliding wear for end post material against train wheel steel. The holder of specimens of end post material was designed and used for the first time in this experiment.
- The fourth device was employed to test the failure caused by static compression load was a Tinius Olsen-H25kN hydraulic test machine. It has been employed to examine the effect of static compression load on the end post materials. This machine first time used to investigate these end post materials.

3- Test Method and Materials

3.1-Introduction

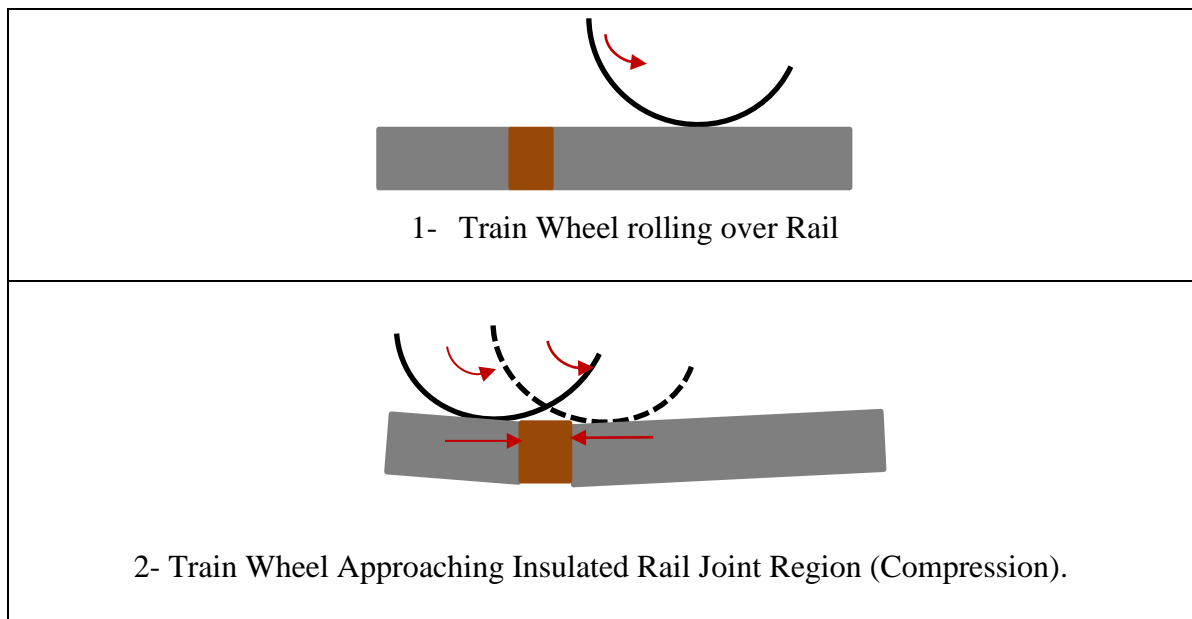
To study wear and deformation of the materials, the processes of wear must be simulated in a controlled manner that represents as accurately as possible what happens in the field and the effect on different specimens studied with the same test conditions. In this chapter the loading conditions existing in the rail and end posts are outlined and the tests chosen to replicate them are described. Table 3:1 outlines the contact scenarios and Table 3:2 the tests available to replicate these.

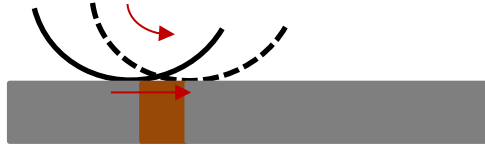
3.2- Test Apparatus

To achieve this study and investigate wear and damage of five different types of end post materials as a result of exposure to railway wheel loading; four different types of apparatus have been used as indicated in Table 3:2:

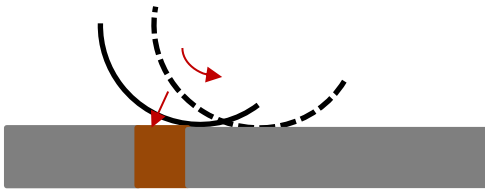
- Block-on-Ring Rig
- Twin- disc Machine
- Ball-on-Plate Impact device
- Tinius Olsen-H25ks

Table 3:1- Contact Scenarios - Wheel/Rail and IRJ.

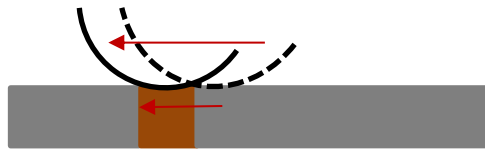




3- Train Wheel Rolling over Insulated Rail Joint Region (Rolling/Sliding Wear and Lipping).



4- Train Wheel Impacts End Post (Impact Wear).

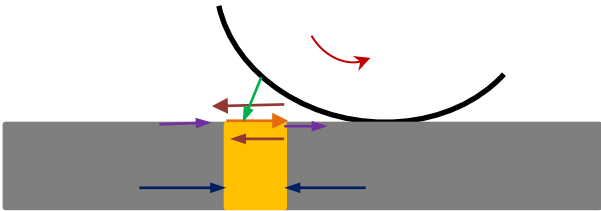

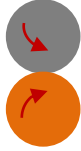
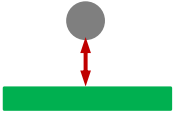
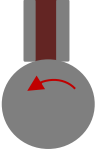
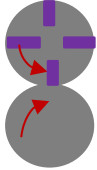
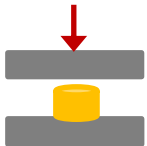


5- Train Wheel Sliding over Insulated Rail Joint Region (Sliding Wear and Lipping).



6- The Rails Extend and Compress the End Post

Table 3:2- Outline of Test Approaches Used to Replicate Contact Conditions.

| Loading that Occurs to End Post Material Due to Passage of Train Wheel | |
|--|---|
| (1)  | |
| Test Name (Contact Scenario) | Test Sketch |
| → Sliding Wear 100% Slip - - - Block-On-Ring Test (5) |  |
| → Rolling/Sliding Wear (Partial Slip) - - - Twin Disk Test (3) |  |
| → Impact Wear - - - Impact Test (4) |  |
| → Lipping Test 100% Slip - - - Block-On-Ring Test (5) |  |
| → Lipping Test (Partial Slip) - - - Twin Disk Test (3) |  |
| → Static Compression Test - - - Tinius Olsen-H25ks (6) |  |

3.2.1- Block-on-Ring Rig

One standard way to perform a wear test is with a Block-on-Ring approach. The rig has been employed extensively in the field of sliding wear [65-67].

The apparatus is a convenient way of simulating the sliding wear which is detected in end posts. The ring can represent the “wheel” and the “block” the end post. Figure 3:1 displays the Block-on-Ring rig utilized to carry out the testing. The maximum speed that can be used on the rig is 7.2 m/sec. and the minimum speed is 1.5 m/sec. and 50 N is the maximum load that can be used. An electrical motor provided the required velocity via a transmission belt and six different pulleys that allow nine different speeds to be achieved. The test block and ring are loaded together. The rig was driven at a controlled sliding velocity with a slip between the contacting steel ring and specimen block. This was used for dry and wet sliding wear tests (see Section 3.4.1) and the 100% slip ratio lipping tests (see Section 3.4.2).

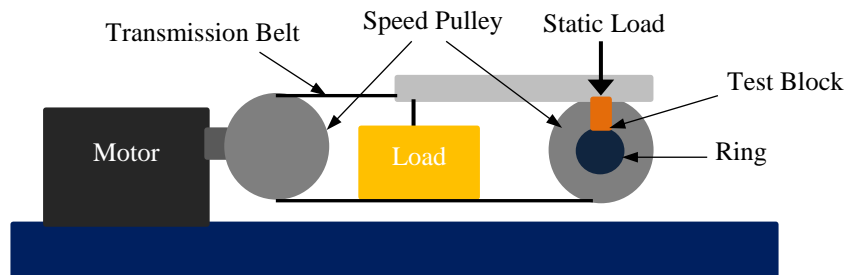


Fig. 3:1- Schematic Diagram of Block-on-Ring Test Rig.

3.2.2- Twin-Disc Machine

Many applications relating to the field of tribology are implemented by using a twin-disc machine [67]. The machine has been used in the field of lubricant development [68, 69] and plays a significant role in the field of research relating to railway development (rail-wheel contacts) [70, 73]. The twin-disc machine system is suitable for simulating the lipping and the rolling/sliding wear found in end posts, which can achieve the partial slip ratio (1%) between train wheels and end post. Figure 3:2 illustrates the twin-disc machine that was employed to achieve the testing. The basic developments that added to this machine and the other additional work that connected it with a computer control system have been discussed earlier [74, 75]. A hydraulic system is used to load the specimen test

discs together (see Figure 3:3) and they are driven at controlled speed by two separate electric motors with the relative slip ratio adjusted using the rotational speeds. A load cell is fixed below the hydraulic jack and a torque transducer is contained in one of the drive shaft. A PC is used to record all data and for load and speed control. This machine has been employed for rotating wear tests and the partial slip lipping test (see Sections 3.4.3 & 3.4.2.2).

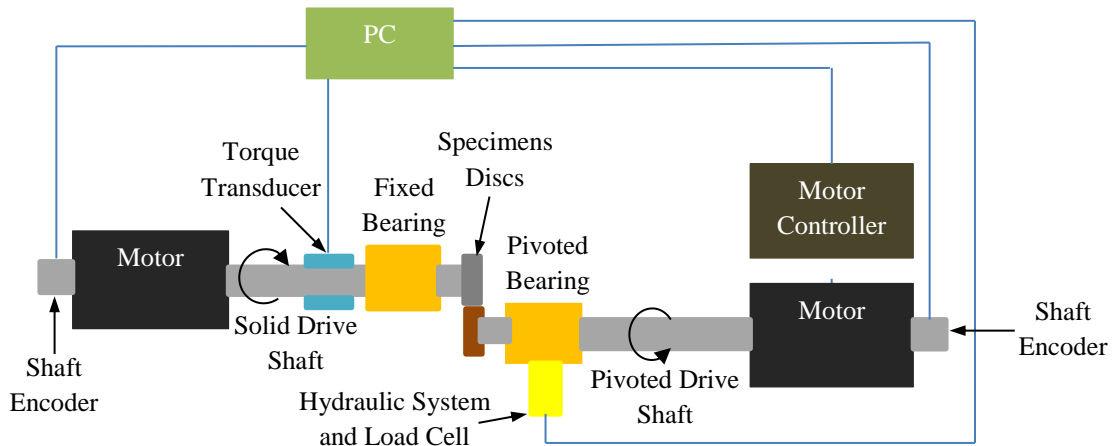


Fig. 3:2- Twin-Disc Test Machine Schematic.

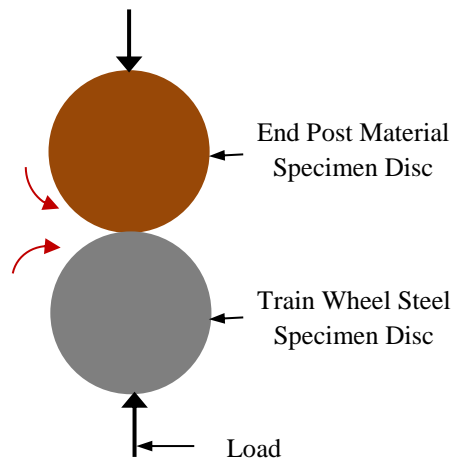


Fig. 3:3- Schematic Diagram of End Post Material Disc and Train Wheel Disc Contact in a Twin-Disc Machine.

3.2.3- Pneumatic Ball-on-Plate Impact Rig

No standard has been written for impact tests, so there are many types of impact test being achieved without any standardized method to compare the results obtained [76]. Many

applications relating to impact wear resistance and deformation of coatings are tested by ball-on-plate rigs [77-82]. The pneumatic ball-on-plate rig is an appropriate way of simulating the impact wear located in an end post. The test apparatus design was explained previously [76, 83, 84]. The pneumatic ball-on-plate rig, as shown in Figure 3:4, uses a pneumatic actuator to move an impact head assembly holding a 6mm diameter ball in a cyclic down and up motion against a specimen plate (see Figure 3:5) with an impact frequency of 8-10Hz. The load cell under the specimen plate is used to measure the impact load. The distance between the steel ball and specimen plate is 15 mm. 500N is the maximum impact load that can be used. The test duration is controlled by computer [85]. This was used for dry and wet impact wear tests (see Section 3.4.4).

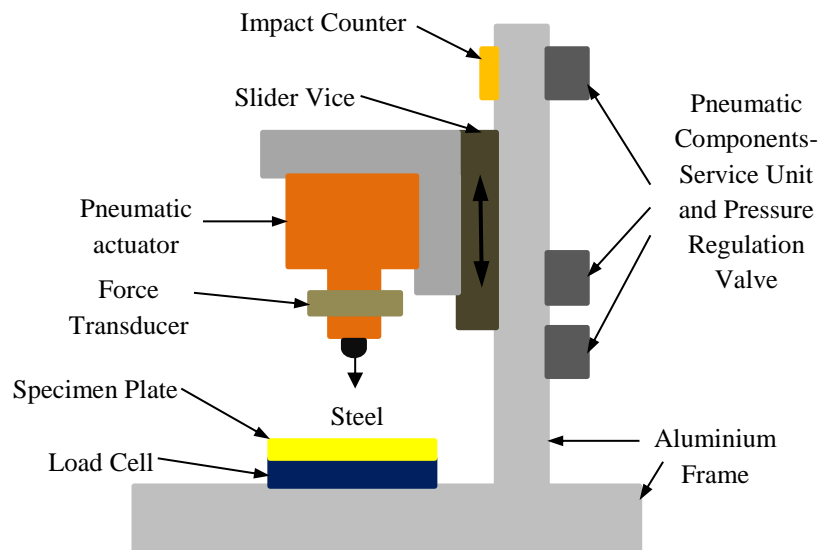


Fig. 3:4- Schematic of the Pneumatic Ball-on-Plate Tester.

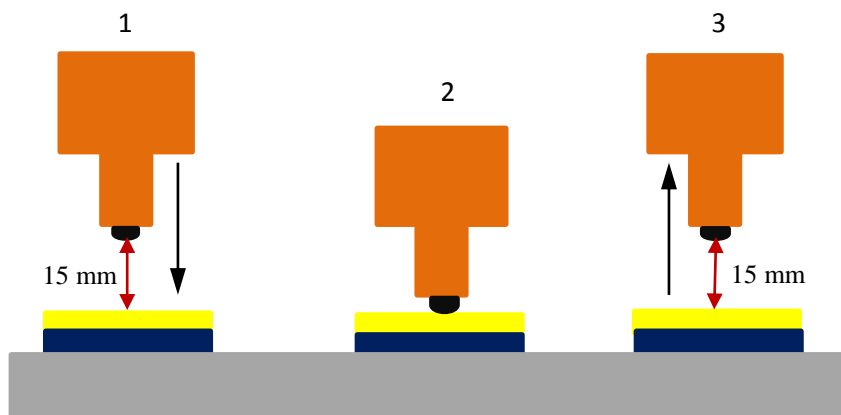


Fig. 3:5- Schematic of the Movement of the Pneumatic Actuator.

3.2.4- Tinius Olsen-H25ks Machine

One standard way to perform a compressive static load test is with a Tinius Olsen-H25kN machine (see Figure 3:6). The machine has been used widely in the field of static load compressive tests [85-87]. The Tinius Olsen-H25kN machine is an appropriate way of simulating damage caused by compressive static load located in the end post. The test machine specification was explained in [88]. Figure 3:6 shows the Tinius Olsen-H25kN machine. The maximum load that can be used on the machine is 25 kN.

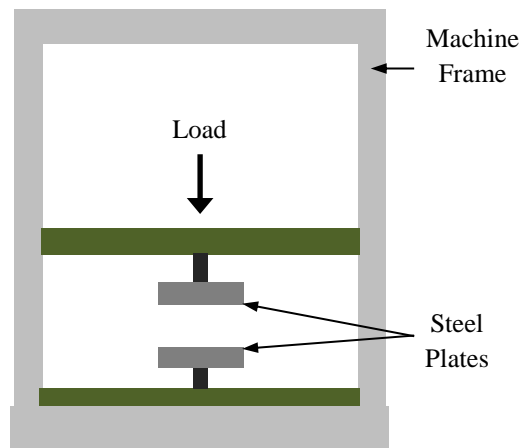


Fig. 3:6- Schematic of Tinius Olsen-H25kN

3.3- Specimens and Material Properties

Prospective end post materials for use in insulated joints need many special properties that are necessary for their successful function as an end post. They must possess a high electrical resistivity to effectively provide the electrical insulation required of insulated joints. They must also have mechanical properties that allow them to withstand the high loads facing them when the joint is in service. Insulated rail joints, along with heavy loads, are subjected to a rough service environment including oil, temperature changes, rain, snow, and other environmental effects. The end post materials used in track must be able to withstand this severe environment. Five different materials have been tested in this study: Nylon 12 (N12) with a surface roughness of $R_a \cong 1 \mu\text{m}$; Nylon 66 (N66) with a surface roughness of $R_a \cong 1 \mu\text{m}$; Nylon 66a (N66a) with a surface roughness of $R_a \cong 1 \mu\text{m}$; epoxy glass (EG) with a surface roughness of $R_a \cong 1.6 \mu\text{m}$; and phenolic resin bonded fabric material (PRBF) with a surface roughness of $R_a \cong 1.4 \mu\text{m}$; which is equal to the surface roughness of a real end post. Some of the important properties of these materials

are shown in Table 3:3. All are typically used on the UK rail network although at the moment Nylon 12 is being used to replace the most commonly used Nylon 66.

Table 3:3- End Post Material Properties [89-92].

| Materials | Max. Service Temp. (C ⁰) | Density (g/cm ³) | Modulus of Elasticity (MPa) | Compressive Strength (MPa) | Impact Strength (KJ/m ²) | Water Absorption (%) | Melting Point (C ⁰) |
|-----------|--------------------------------------|------------------------------|-----------------------------|----------------------------|--------------------------------------|----------------------|---------------------------------|
| N12 | 80 | 1.02 | 1800 | - | No break | 1.6 | 179 |
| N66 | 95 | 1.14 | 3100 | - | No break | 1.6 | 210 ¹ |
| N66a | 95 | 1.20 | 3100 | - | No break | 0.8 | 210 ² |
| EG | 130 | 1.92 | 240 | 300/420 | 55 | 0.05 | - |
| PRBFM | 130 | 1.35 | 240 | 200/350 | 8.8 | 1 | - |

¹ and ², theoretical onset melting point value that was measured using Differential Scanning Calorimeter (DSC) (see Section 3.3.1). All other values taken from material specifications provided by suppliers.

Thermosetting materials EG and PRBF never melt, unlike thermoplastic materials of N 12, N 66, and N 66a melt at a certain temperature. The thermoplastic materials have higher propriety to absorb water which led to becoming more effect with water. The thermosetting materials have lower modulus of elasticity which, making them less likely to fall into elastic and plastic deformation stages. The Nylon 66 material has greater propriety to absorb water than Nylon 66a, which led to it becoming soft and weak (see table 3:4).

3.3.1- Melting Point Test

Melting point tests were performed using a Differential Scanning Calorimeter (DSC). In this test [93]:

- i) The machine was set-up and the start temperature was selected (25 °C).
- ii) Small pieces of the specimens are taken.
- iii) Specimens were placed in the pan which was closed tightly and then put in the DSC.

iv) Temperature was increased gradually until the melting point was reached and measured.

The melting point values of Nylon 66 (N66) end post material, and Nylon 66a (N66a) were about 210 °C as shown in Figures 3:7 and 3:8. As shown in Figures 3:9 and 3:10, the Epoxy Glass (EG) end post material, and Phenolic Resin Bonded Fabric Material (PRBF) did not melt, but decomposed at high temperatures (almost 700 °C).

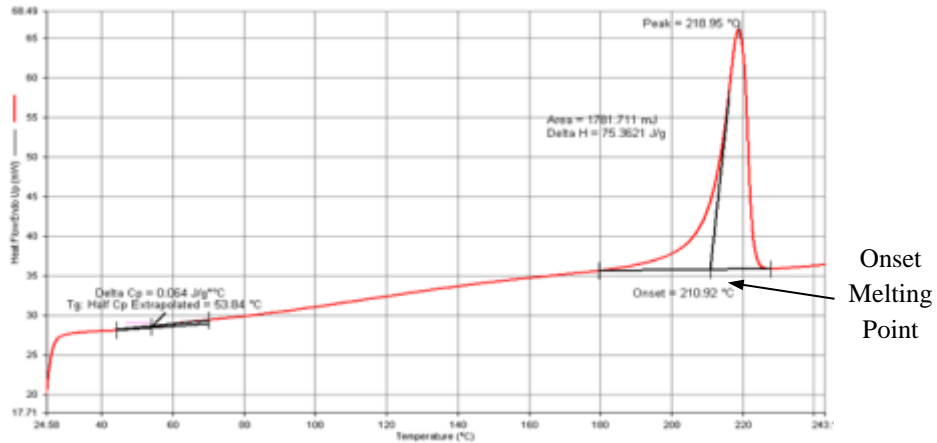


Fig. 3:7- Melting Point of Nylon 66 (N66) End Post Material.

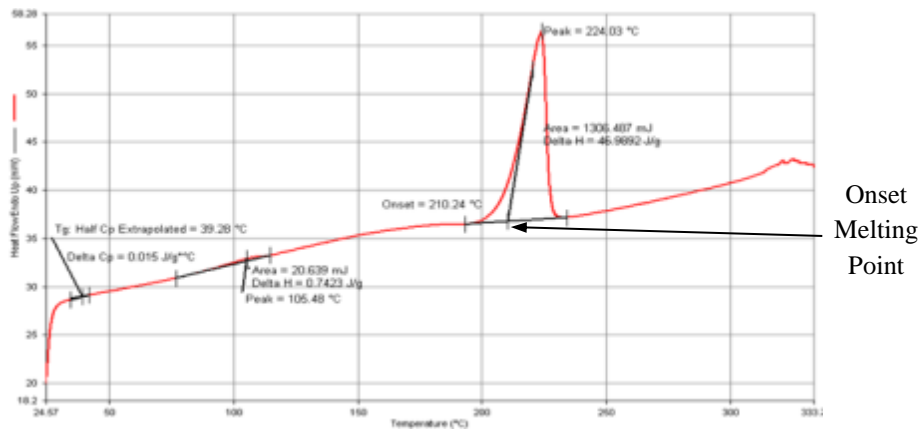


Fig. 3:8- Melting Point of Nylon 66a (N66a) End Post Material.

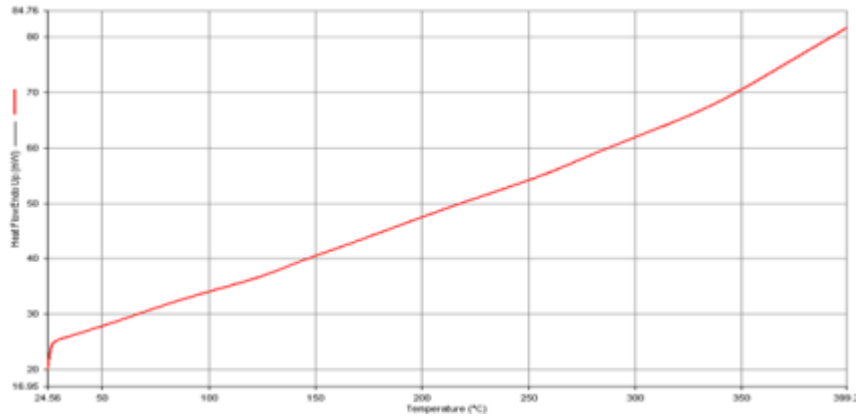


Fig. 3:9- Epoxy Glass (EG) End Post Material Showing no Melting Point.

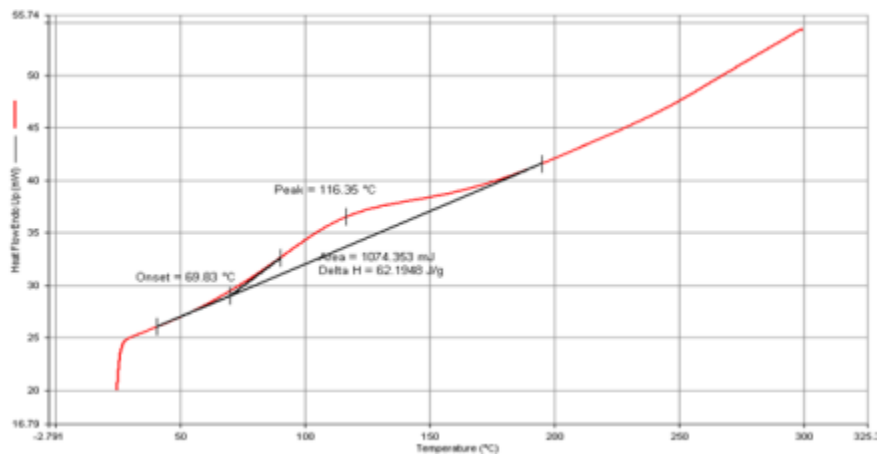


Fig. 3:10- Phenolic Resin Bonded Fabric (PRBF) End Post Material Showing an Endo-Thermic Transition.

3.4- Testing

The objective of the wear testing was to verify the wear resistance of end post materials in different operating conditions resulting from sliding of a train wheel, rolling/sliding of the train wheel, impact from a wheel, and compression from the rail movement due to the wheel load (see Tables 3:1 and 3:2). While the purpose of the lipping testing was investigation of the influences of metal flow occurring at the end post gap.

Different types of testing have been performed on five different types of end post material. A dry and wet sliding wear test has been performed on a Block-on-Ring rig and this test is described in Section 3.4.1. A friction test has been performed on a CETR tribometer and is described in Section 3.4.1.1. The lipping test has been done on the Block-on-Ring apparatus at a slip of 100% and on a twin disk machine with a partial slip of 1% and this

will be described in Section 3.4.2. A rotating wear test again with partial slip of 1% has been achieved on the Twin-Disk machine (wheel against end post) and this experiment will be explained in Section 3.4.3. An impact test has been implemented using a Pneumatic Ball-on-Plate Impact ring tester and is described in section 3.4.4. Finally, the compression cyclic test is described (see Section 3.4.5). It should be noted that some experimental parameters were used for reality and some only for ranking.

3.5- Test Methods

3.5.1- Dry and Wet Sliding Wear Test (Block-on-Ring)

This test method evaluated the performance of materials in a sliding contact. The Block-on-Ring test is generally employed as a comparative test in which controlled wear is implemented on the specimens to study. The material lost allows calculation of the wear rate of the material. When wear data are reported, the overall wear rate (WR) during sliding is often calculated by dividing the total measured wear volume, V_t , at the end of the test by the test time duration Tt or total sliding distance Xt : $WR = V_t/Xt$ or $WR = V_t/Tt$. This method assumes that the wear rate is constant and wear mechanisms are steady during the test and that the average wear rate is characteristic of the whole test. Since a similar action was carried out on all specimens, the wear rate can be employed as a quantitative comparative value for wear resistance. Wear resistance is not a characteristic material property, but depends on surface geometric features, material properties and wear process parameters such as sliding speed, temperature, load, test duration, and environment. In this test:

- i) Initially the measuring instruments used were calibrated.
- ii) The test specimens were machined into blocks 5mm x 5mm x 32mm, as shown in Figure 3:11.
- iii) The rings were machined into a cylindrical shape, 42mm diameter and 10mm length with surface roughness of $R_a \cong 1 \mu\text{m}$ as shown in Figure 3:12.
- iv) The specimens were carefully cleaned and dried then weighed.
- v) The surface roughness of the test surfaces were measured by profilometer for all specimens.
- vi) The contact surfaces of specimens were photographed using an optical microscope.

- vii) The test sheet was filled in with pre- test information.
- viii) The ring was fixed into a holder on the rig (see Figure 3:12).
- ix) The appropriate loads were selected and mounted into a holder.
- x) The appropriate sliding speeds were set.
- xi) The end post specimens were placed into a holder and placed into contact with the rotating steel ring, with a known force and speed, to create the wear.

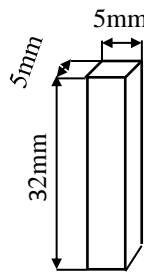


Fig. 3:11- Schematic of End Post Specimen.

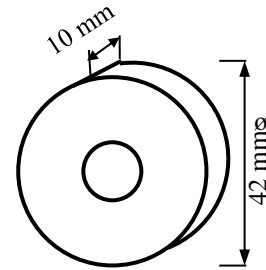


Fig. 3:12- Schematic of Steel Ring.

An overview photo of the test set-up can be seen in Figures 3:13.

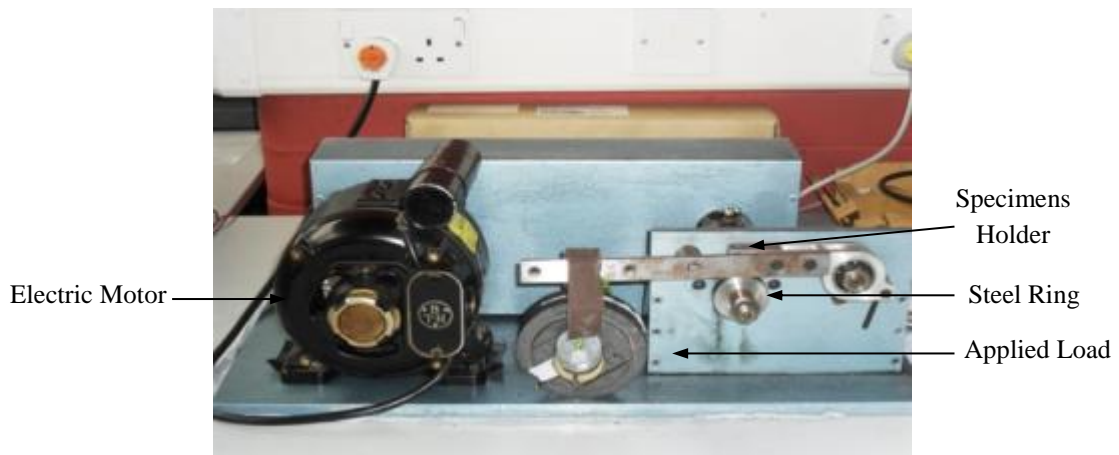


Fig. 3:13- Block-on-Ring Test.

With this type of test, conditions can be varied as there is control of sliding speed, the load applied, the duration of test and the material and geometry of the contact line. The tests were carried out at a sliding speed of 1.5 m/sec., 3.3 m/sec., and 7.2 m/sec. Under various constant loads of 10 N, 30 N, and 50 N and during a period of 60 minutes, with measurements of wear rate were taken at 5 minutes, 25 minutes, and 30 minutes. All tests were conducted at ambient temperature and humidity.

Specimens, in the case of a wet test, were dried at the start and end of the test to ensure accurate mass loss measurement.

- i) The specimens were weighted before the test.
- ii) The specimens were weighed after the test.
- iii) The specimens were placed in an oven at a certain temperature (lower than melting point temperature) for each material.
- iv) The weight was then measured using an electronic balance.
- v) The weighing process was repeated till the last three weight values become equal.

One way of comparing test conditions to those in the field is via the energy within the contact. In this case it can be calculated as $T\gamma$ (normal force x friction coefficient x slip in the contact) and scaled via the contact area (see Appendix A). For the Block-on-Ring $T\gamma/A$ values of 0.084 to 6.20 were calculated (using μ values from tests described in section 3.5.1.1). Typical field values for $T\gamma/A$ are shown in Figure 3:14; the Block-on-Ring tests are in the right regime. Because there is not a suitable reference for the energy within the contact for the UK network, energy within the contact of a Canadian rail network was used for comparison (see Figure 3:14). This shown that the $T\gamma/A$ for the Block-on-Ring tests was in the right regime.

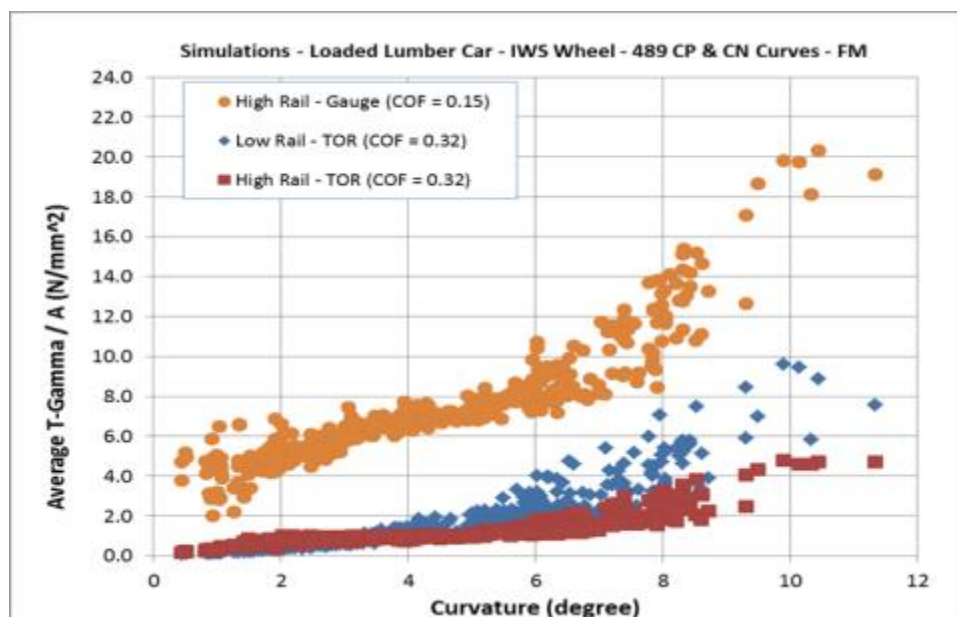


Fig. 3:14- Data for NRC Modelling of Wheel/Rail Contact Using Multi body Dynamics Software [Informal Communication with Eric Magel, NRC, Canada].

The volume loss is measured as follows:

$$\Delta V = V_0 - V_1 \tag{1}$$

$$V_0 = W_0/\rho \tag{2}$$

$$V_1 = W_1/\rho \tag{3}$$

where V_0 = volume of specimen prior to testing.

V_1 = volume of specimen after test.

W_0 = mass of specimen prior to testing.

W_1 = mass of specimen after test.

ρ = density of material.

3.5.1.1- Coefficient of Friction Test

The friction tests were carried out on a pin-on-disc rig (CETR) as shown in Figure 3:15 (this was used as the Block-on-Ring has no friction measurement capability). End post specimens were loaded against wheel steel discs in this set-up (see Figure 3:16).

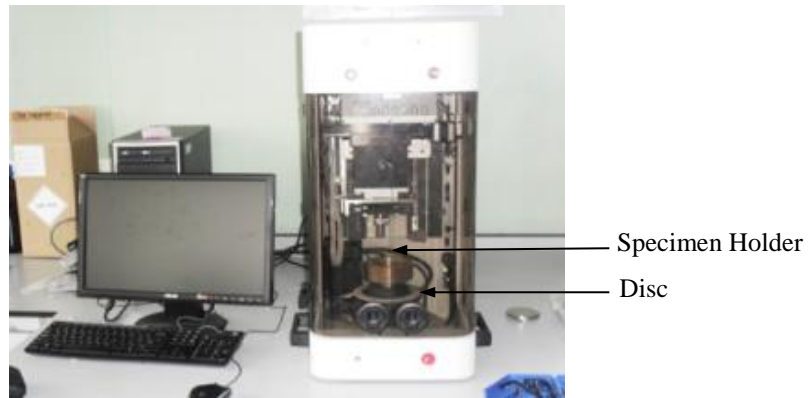


Fig. 3:15- CETR Machine.

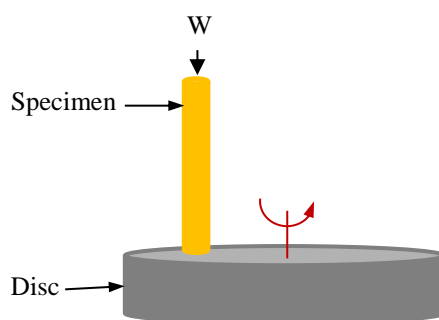


Fig. 3:16- Schematic for Pin and Disc.

In this test:

- i) The specimens were machined into cylinders with a 5mm diameter and 28mm length, then cleaned and dried.
- ii) The surface roughness of specimens was measured by profilometer.
- iii) The disc was mounted into a holder.
- iv) The software was set and the appropriate speeds and loads (those which were used in Block-on-Ring test) were selected.
- v) The end post specimens were fixed into a sample holder and brought into contact with the disc, with a known force and speed.
- vi) The tests were carried out at a rotational speed of 1.5 m/sec, 3.3 m/sec, and 7.2 m/sec at loads of 10 N, 30 N, and 50 N, and then the average coefficient of friction was calculated.

3.5.1.2- Hardness Test

The Shore (Durometer) hardness test was used in this study to measure the hardness of end post materials under study in dry and wet conditions. In this test the hardness of end post materials was measured in dry condition first and then the specimens were immersed in water for one hour and then hardness was remeasured. Table 3:4 shows the value of hardness of each end post material in dry and wet conditions.

Table 3:4- Shore D hardness Value of End Post Material.

| Shore Hardness (D) | | | | | |
|----------------------|--------|--------|--------|--------|--------|
| Condition | N12M | N66m | N66aM | EGM | PRBFM |
| Dry | 232.43 | 230.39 | 239.38 | 742.65 | 592.66 |
| Wet | 190.98 | 131.27 | 194.37 | 701.40 | 547.43 |
| % Change of Hardness | 18 | 43 | 18 | 5 | 7 |

3.5.2- Lipping Test

The End Post material used in this test was best material from the previous test (Epoxy Glass material).

3.5.2.1- 100% Slip Ratio Lipping Test (Block-on-Ring)

This test was carried out on the Block-on-Ring tester (see Figure 3:17). The samples under study here were steel (rail material) and end post materials against railway wheel steel.

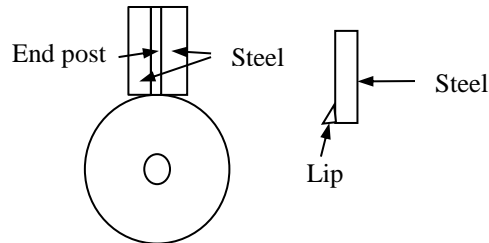


Fig. 3:17- Schematic of the Lipping Test Set-up.

- i) The rail steel material was machined into blocks 5mm x 5mm x 32mm with a surface roughness of $R_a \cong 1 \mu\text{m}$, then cleaned and arranged like an actual joint as shown in Figure 3:17
- ii) The end post material Epoxy Glass (EG) was machined into blocks 1mm x 5mm x 32mm in size, then cleaned and arranged like an actual joint as seen in Figure 3:17.
- iii) The surfaces roughness of the ring contact surface was measured by profilometer ($R_a \cong 1 \mu\text{m}$).
- iv) The rings were mounted into a holder.
- v) The end post specimens were placed between steel specimens then mounted into a sample holder and brought into contact with the ring as shown in Figure 3:18.
- vi) The tests were performed at a sliding speed of 7.2 m/sec., under a constant load of 50 N, and through 60 minutes.

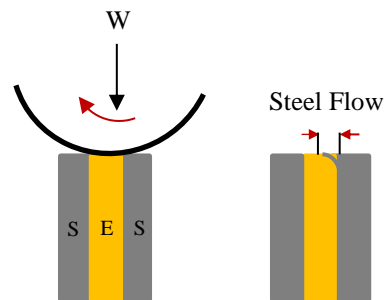


Fig. 3:18- Schematic of the 100% Slip Lipping Test Specimen Set-up.

3.5.2.2- Partial Slip Ratio Lipping Test

A (1%) partial slip ratio was used in this test [94]. This test was implemented on a Twin-Disc machine. The samples under study here were steel (rail material) and end post materials against railway wheel steel.

3.5.2.2.1- End Post Specimen Thickness Determination

The following section outlines the process used to select the end post thickness used in the twin-disc tests.

When two bodies with varying radii of curvature along x-y axes are in contact, the region of contact is approximately elliptical in form (see Figure 3:19).

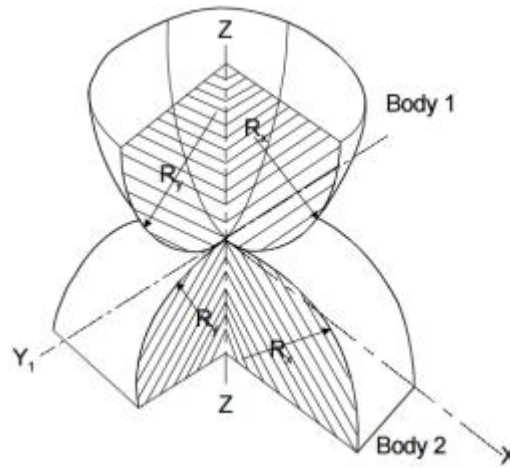


Fig. 3:19. Two Different Radii Bodies in Contact [95].

The dimensions of the area of contact can be calculated using the following expressions:

$$a = \sqrt[3]{\frac{3k^2 EPR}{\pi E^*}} \quad (4)$$

$$b = \sqrt[3]{\frac{3EPR}{\pi k E^*}} \quad (5)$$

$$\frac{1}{R_x} = \frac{1}{R_{1x}} = \frac{1}{R_{2x}} \quad (6)$$

$$\frac{1}{R_y} = \frac{1}{R_{1y}} = \frac{1}{R_{2y}} \quad (7)$$

$$\frac{1}{R} = \frac{1}{R_x} = \frac{1}{R_y} \quad (8)$$

where k is the ellipticity parameter = $a/b = 1.0339 \left(\frac{R_y}{R_x}\right)^{0.6360}$

E is an elliptical integral of the second kind = $[1.0003] + \frac{0.5968R_x}{R_y}$

An actual wheel/rail contact is approximately elliptical. Actual contact dimensions in a real contact are:

According to 54EN1 profile: $R(\text{rail})= 300$ mm and according to P8 profile: $R(\text{wheel})= 450$ mm.

Table 3:5- Summarised Wheel and Rail Radii (Data from [14, 28]).

| | R_x (mm) | R_y (mm) |
|-------|------------|------------|
| Wheel | 300 | 450 |
| Rail | 300 | ∞ |

For a typical contact pressure of 1500 MPa

$a = 3.95$ mm and $2a = 7.90$ mm, where a = semi contact length

$b = 5.51$ mm and $2b = 11.02$ mm, where b = semi contact width

Actual end post thickness in a real IRJ = 6-15 mm (see Figure 6:3).

The ratio of end post thickness to actual contact width is therefore:

i) In the case of an end post thickness of 6 mm: $\frac{6}{2b} = \frac{6}{11.02} = 0.544$

ii) In the case of an end post thickness of 15 mm: $\frac{15}{2b} = \frac{15}{11.02} = 1.36$

The contact in the twin-disc case is a line. Hertz line equations were used to calculate the end post specimens thickness at a contact pressure of 1500 MPa.

$$a = \sqrt{\frac{4PR}{\pi E^*}} \quad (9)$$

$$\frac{1}{R} = \frac{1}{R_1} + \frac{1}{R_2} \quad (10)$$

$$\frac{1}{E^*} = \frac{(1 - \nu_1^2)}{E_1} + \frac{(1 - \nu_2^2)}{E_2} \quad (11)$$

where a = contact half width,

P = load per unit width,

E_1, ν_1, E_2 and ν_2 = Material properties,

R_1 , and R_2 = contact radii.

These calculations give: $a = 0.3 \text{ mm}$ and $2a = 0.6 \text{ mm}$

The end post thickness in the test was therefore scaled as follows (see Figure 3:20):

- i) The ratio of low end post thickness to line contact width = $\frac{x_1}{2a} = \frac{x_1}{0.6} = 0.544$

$x_1 = 0.33 \text{ mm}$ (it was rounded up to 0.5 mm), where x_1 = lower end post thickness in the test.

x_1 represents the lower end post thickness of 6 mm in a real joint.

- ii) The ratio of high end post thickness to line contact width = $\frac{x_2}{2a} = \frac{x_2}{0.6} = 1.36$

$x_2 = 0.82 \text{ mm}$ (it was rounded up to 1 mm), where x_2 = higher end post thickness in the test.

x_2 represents the higher end post thickness of 15 mm in a real joint.

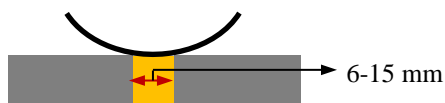


Fig. 3:20- Schematic of Actual End Post Thickness

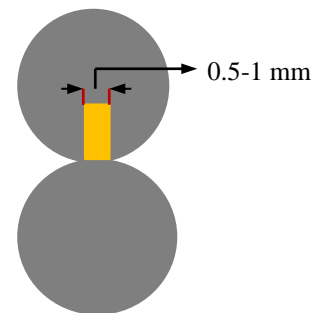


Fig. 3:21- Schematic of End Post Specimen Thickness

In this test:

- i) The rail steel material was machined into a disc with a 46 mm diameter and 10mm thickness with surface roughness of $R_a \cong 1 \mu\text{m}$.

- ii) The disc was machined with 3 grooves, 0.5mm x 10mm x 3mm, and 3 grooves, 1mm x 10mm x 3mm.
- iii) The end post material Epoxy Glass (EG) was cut into blocks 1mm x 10mm x 3mm, and 0.5mm x 10mm x 3mm in size and then glued in the grooves, then cleaned and dried.
- iv) The wheel steel disc was machined into a cylindrical shape with 46 mm diameter and 10mm thickness with surface roughness of $R_a \cong 1 \mu\text{m}$.
- v) The disc specimens were cleaned and mounted into a holder.
- vi) The tests were performed at rotating speeds of 400 rpm [97] slip 1%, contact pressures of 900 MPa, and 1500 MPa (typical actual contact pressure) [96], and for 2000 and 20000 cycles (see Figure 3:22).

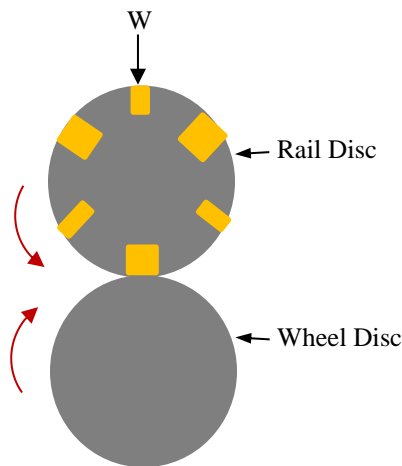


Fig. 3:22- Schematic of 1% Partial Slip Specimens.

3.5.3- Dry and Wet Rolling/Sliding Wear Test

One way to perform a wear test is with a twin disc set-up. This test method evaluates the performance of materials in a rolling/sliding test. The twin disc test is usually employed as a comparative test in which controlled wear is implemented on the specimens under study. The wear resistance of five types of end post material against wheel steel and the influence of load, rotating speed, and time on the wear resistance of these end post materials will be determined. In this test:

- i) The specimen holder was designed and manufactured in the Mechanical Engineering department workshop (see Figure 3:23).

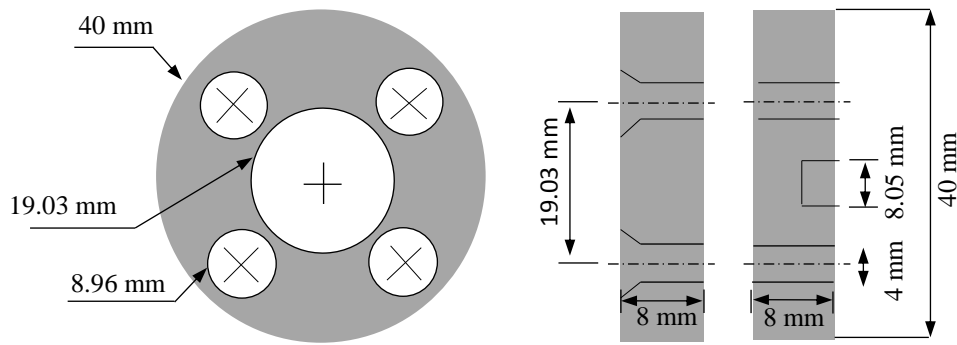


Fig. 3:23- Twin-Disc Machine End Post Specimen Holder.

- ii) The disc specimens were cut from end post materials and wheel steel sections into a disc, 47 mm in diameter and with a contact width of 6 mm and 10 mm respectively.
- iii) The specimens were carefully cleaned and dried then weighed.
- iv) The surface roughness of test surfaces was measured by profilometer.
- v) The contact surfaces of specimens were photographed by an optical microscope.
- vi) The specimens were placed into the holder on the rig and brought into contact with each other, with a known force, speed, and slip to create the wear as shown in Figure 3:24.

The tests were achieved employing the end post disc as the breaking disc and the steel wheel disc as the driving disc (see Figures 3:24 and 3:25). The tube at the top of the machine was used to drip in the water in the case of the wet test condition. The tests were carried out at a rotational speed of 400 rpm, a slip of 1% and a contact pressure of 200 MPa (see Figure 3:26) which is similar to the real wheel/end post contact [96]. Contact calculations are shown in Appendix A. The tests were first run dry, then wet with water (rain water was used). The water was applied at two drops per second (that is enough to make the disc specimens completely wet through the period of testing) [97]. Air cooling was used in this test.

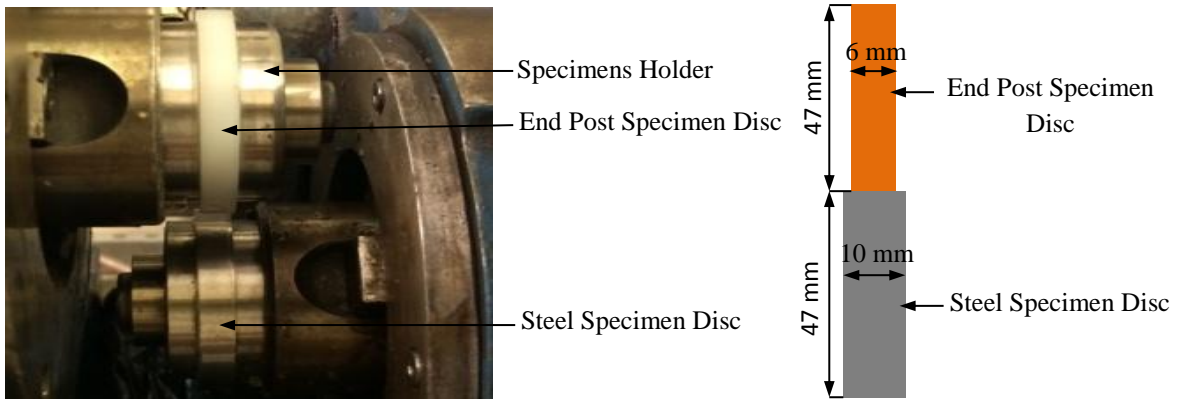


Fig. 3:24- Twin-Disc Test Specimens Set-up Fig. 3:25- Schematic of Steel Disc and End Post Disc Contact.

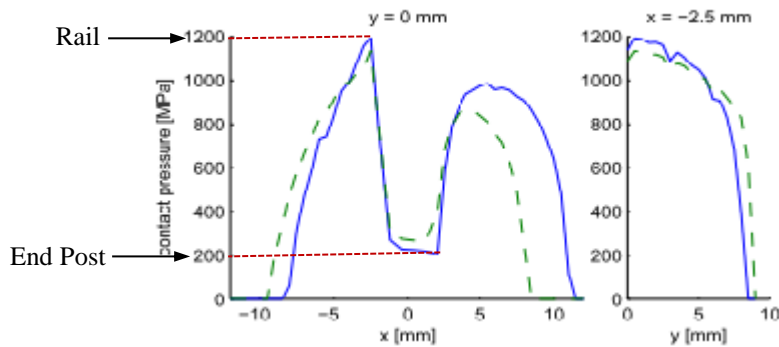


Fig. 3:26- Contact Pressure Distribution on Rail and End Post [96].

3.5.4- Dry and Wet Impact Test

One of the ways that can be used to test the wear caused by impact is a “Pneumatic Ball-on-Plate Impact Tester” (see Figure 3:27). This test technique characterises the behaviour of materials when subjected to cyclic impacts.

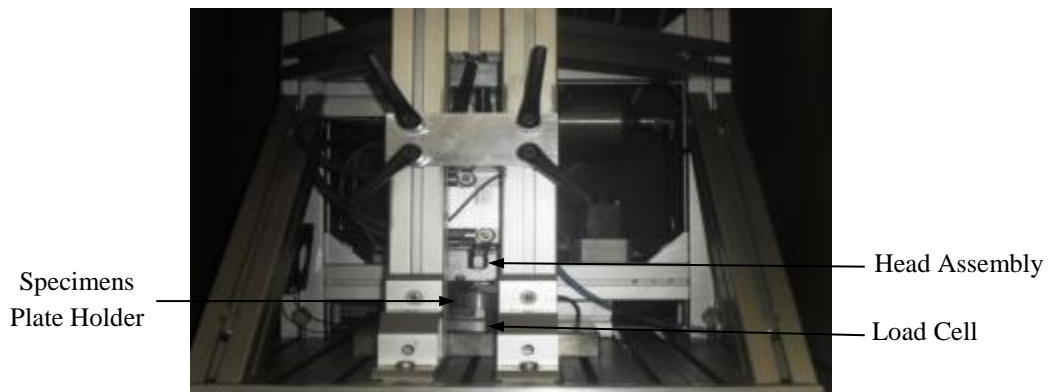


Fig. 3:27- Pneumatic Ball-on-Plate Apparatus.

There was no standard test for the wear due to impact, so the Pneumatic Ball-on-Plate impact test was used as a ranking test in which controlled wear is implemented on the samples to study. The diameter and depth of plastic deformation and/ or material removal which forms as a result of impacts allows observations of the wear of the material. When the work implemented on all specimens of the end post materials under study is similar, the wear can be employed as a comparative factor for wear resistance. The direction of impact was the direction in real use. The orientation of fibre has an important effect on the properties of specimens, which has to be born in mind in case the results are employed to analyse the action of other materials specimens. Resistance to wear depends on properties of a material and surface features and on variables of the wear system such as force and number of cycles as well. The tests were carried out in wet and dry conditions. The test specimens were machined into blocks 20mmx 40mmx 6mm in size as shown in Figure 3:28.

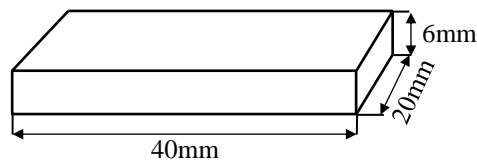


Fig. 3:28- Schematic Diagram of the End Post Impact Specimen.

The test procedure was as follows:

- i) The specimens were carefully cleaned and dried then weighed.
- ii) The steel balls and holder were carefully cleaned and dried.
- iii) The ball was placed into a holder on the rig and screwed on hand tight with a spanner used to tighten the holder to assembly.
- iv) The cylinder was pushed up to end of travel.
- v) The specimens were securely fastened to the base plate, ideally with rigid clamp and come into contact with the steel ball.
- vi) The steel ball and holder assembly was checked to make sure that it could not hit the specimen clamps during the impact strokes.
- vii) The forces were selected within the control software.
- viii) The number of cycles was set within the software as well.
- ix) Desired force (N) was inputted.
- x) The tests were run with a known force and cycles, to create the wear.

The tests were carried out at three different numbers of strokes: 1000 cycles, 5000 cycles, and 10000 cycles. Under impact forces levels of 100 N, 300 N, and 500 N. All tests were conducted at ambient temperature and humidity. Wear formed due to the impact of steel ball with specimen plates in the form of craters that were measured by diameter and depth.

The crater diameters and depths were determined as follows

- i) Crater depths were measured by profilometer as illustrated in Figure 3:29 (for more profilometer graphs see Appendix B).
- ii) Crater diameters were measured by profilometer as can be seen in Figure 3:29 and/or by optical microscope as shown in Figure 3:30.

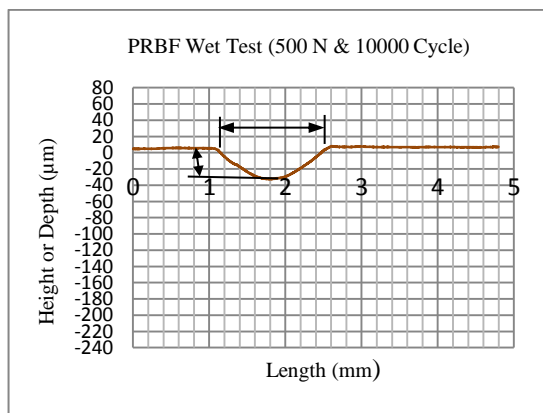


Fig. 3:29- Profilometer Diagram.

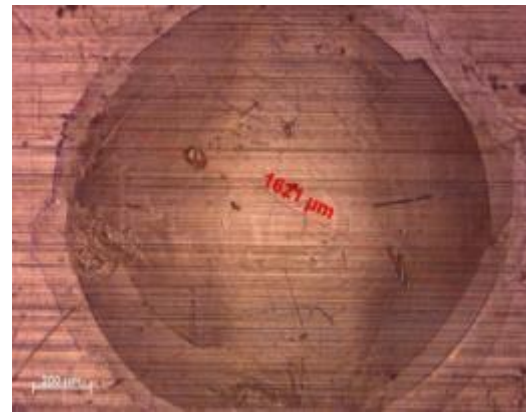


Fig. 3:30- Microscope Image.

The procedure for the wet tests condition was the same as that for the dry tests, but before the test was started, the specimens were weighed then immersed in water for an hour, then weighed again and then tested as when they were dry. The set-up can be seen in Figure 3:27.

3.5.5- Static Compression Test

This test was conducted on a Tinius Olsen-H25ks machine (see Figure 3:31). The specimens of Nylon 12, Nylon 66, Epoxy Glass and Phenolic Resin Bonded Fabric materials were cut out from real end posts into cylindrical shapes, 8 mm in diameter and 6 mm in thick (see Figure 6:32). The specimens were tested under compressive load test to determine their yield strength and determine the strongest material.

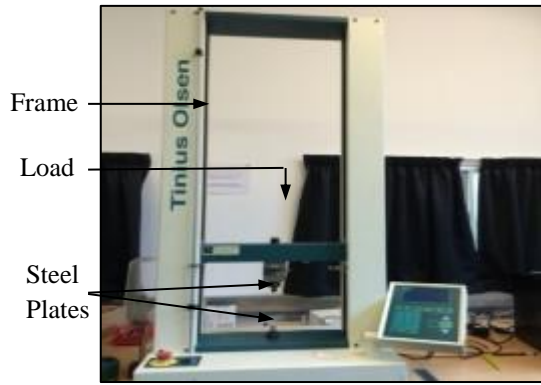


Fig. 3:31- Tinius Olsen-H25kN Machine.

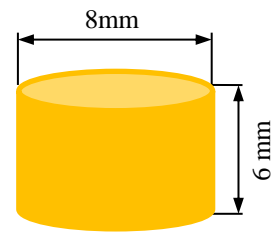


Fig. 3:32- Schematic of Specimen

4- Block-on-Ring Sliding Tests

4.1- Introduction

This testing was conducted to examine the wear resistance of Nylon 12, Nylon 66, Nylon 66a, Epoxy Glass and Phenolic Resin Bonded Fabric materials caused by a wheel sliding over an end post (see Table 3.1 (5)). Sliding wear tests were conducted on a Block-on-Ring rig (see Section 3.2.1) in dry and wet test conditions at three sliding speeds and three applied loads as described in 3.5.1. Table 4:1 summarizes the test conditions.

Table 4:1- Test Conditions.

| Sliding Speeds (m/sec) | Applied Loads (N) | |
|---------------------------|-------------------|----------|
| | Dry Test | Wet Test |
| 1.5 | 10 | 10 |
| | 30 | 30 |
| | 50 | 50 |
| 3.3 | 10 | 10 |
| | 30 | 30 |
| | 50 | 50 |
| 7.2 | 10 | 10 |
| | 30 | 30 |
| | 50 | 50 |

All tests were conducted at ambient temperature and humidity.

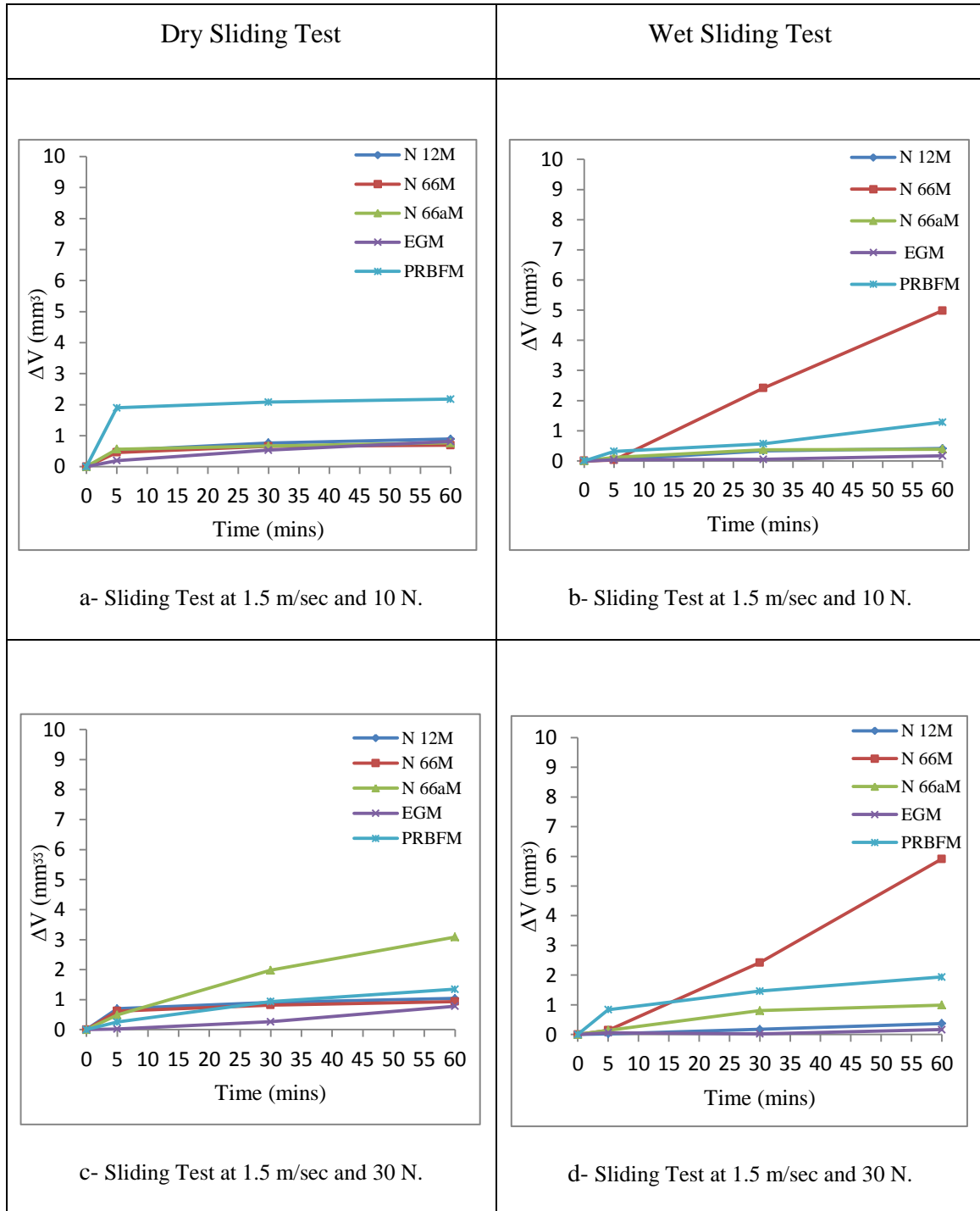
4.2- Results

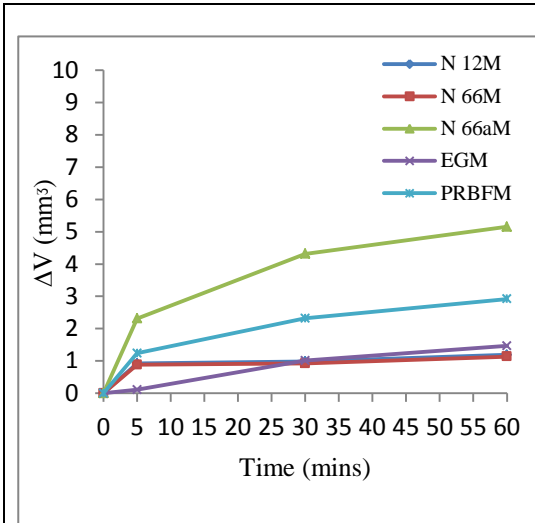
The experiments were repeated three times and the average wear rate has been taken.

4.2.1- Volume Loss Data

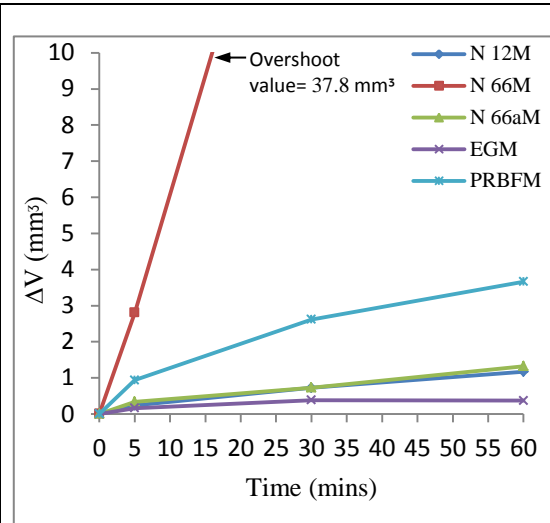
The volume loss data obtained from experimental work for the studied end post materials (Phenolic Resin Bonded Fabric Material PRBFM, Epoxy Glass Material EGM, Nylon 66 Material N66M, Nylon 66a Material N66aM and Nylon 12 Material N12M) using sliding velocities of 1.5 m/sec., 3.3 m/sec., and 7.2 m/sec. and three different loads of 10 N, 30 N, and 50 N are shown in Figure 4:1. These figures show the relationship between volume loss and time of the studied end post materials in dry and wet tests condition at different

values of sliding velocities and loads as indicated in the figures. It can be seen from the figures that value of sliding velocity has an expected effect on the volume loss of the studied end post materials at different applied loads. (V_{ij} = the volume loss from specimens; $i=1,2,\dots,5$ and $j=1,2,\dots,9$).

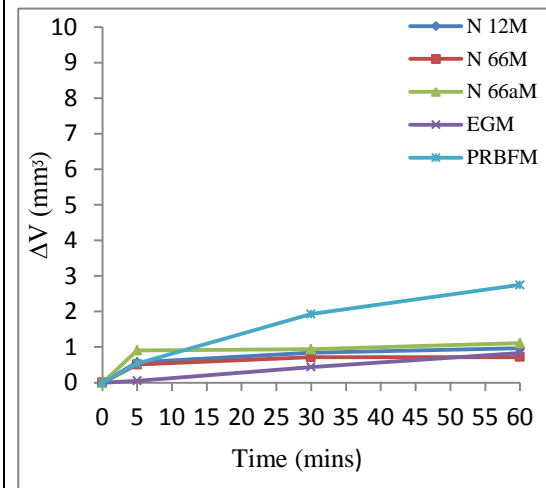




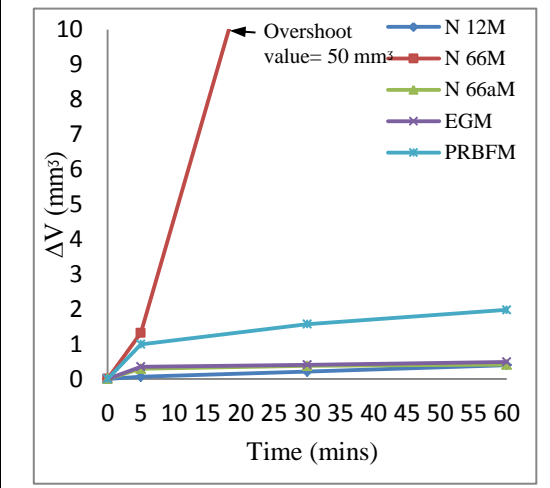
e- Sliding Test at 1.5 m/sec and 50 N.



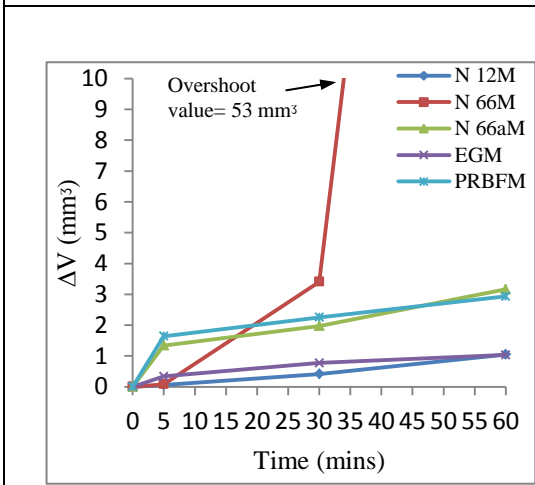
f- Sliding Test at 1.5 m/sec and 50 N.



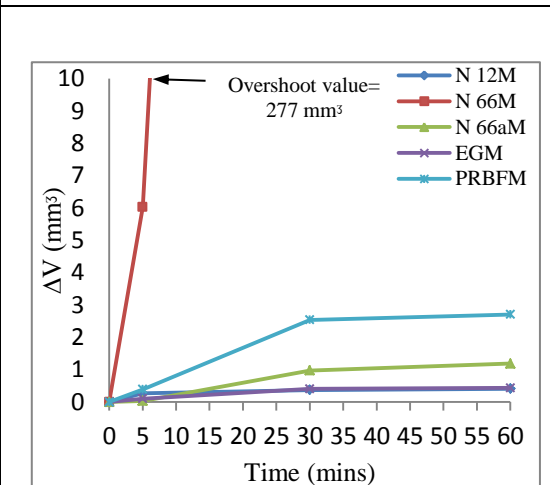
g- Sliding Test at 3.3 m/sec and 10 N.



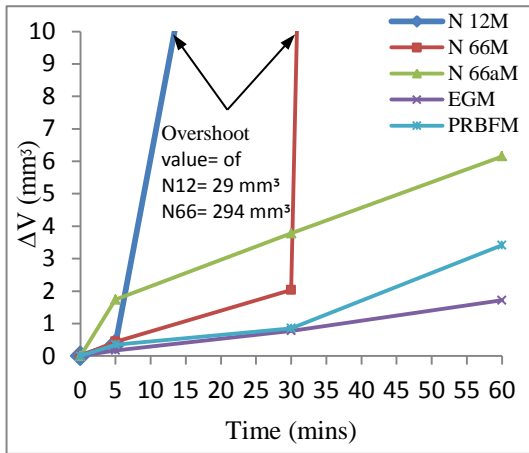
h- Sliding Test at 3.3 m/sec and 10 N.



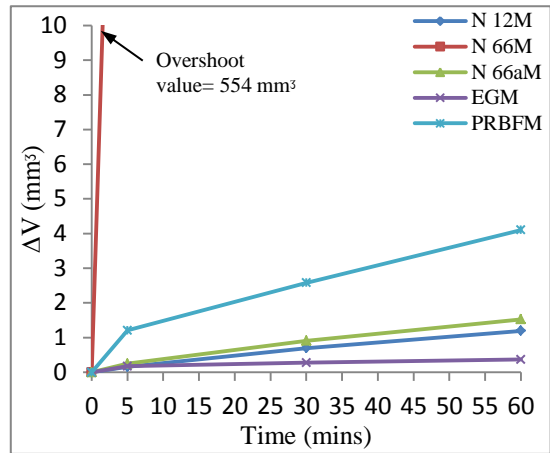
i- Sliding Test at 3.3 m/sec and 30 N.



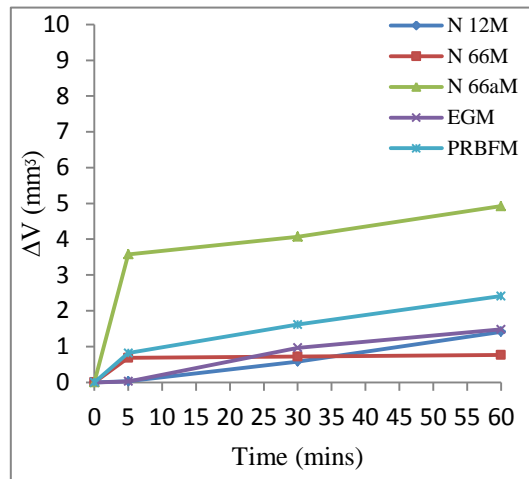
j- Sliding Test at 3.3 m/sec and 30 N.



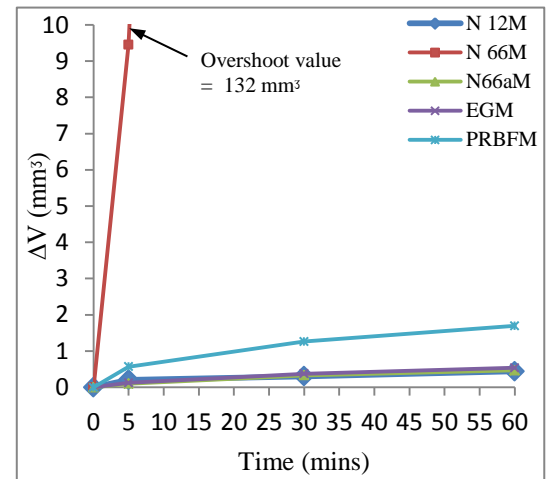
k- Sliding Test at 3.3 m/sec and 50 N.



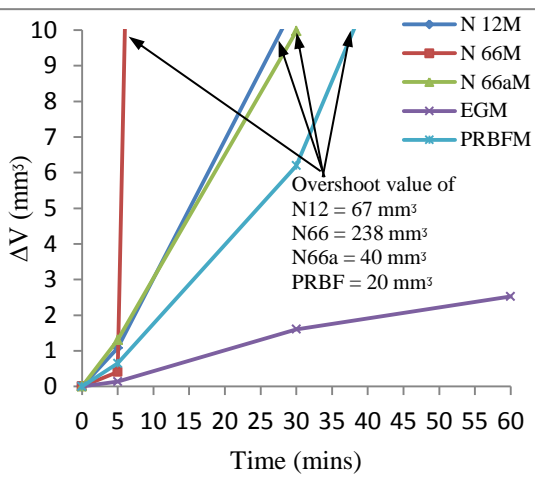
l- Sliding Test at 3.3 m/sec and 50 N.



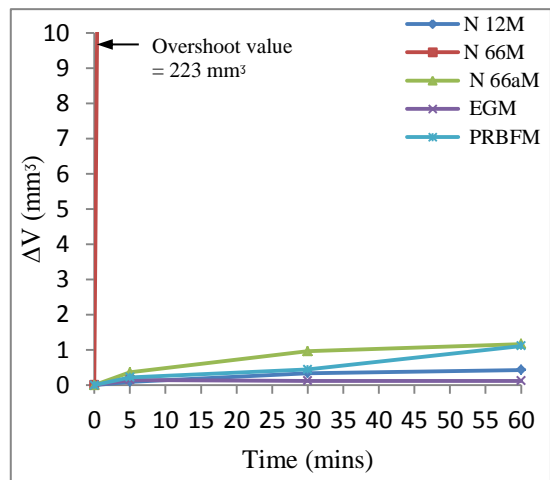
m- Sliding Test at 7.2 m/sec and 10 N.



n- Sliding Test at 7.2 m/sec and 10 N.



o- Sliding Test at 7.2 m/sec and 30 N.



p- Sliding Test at 7.2 m/sec and 30 N.

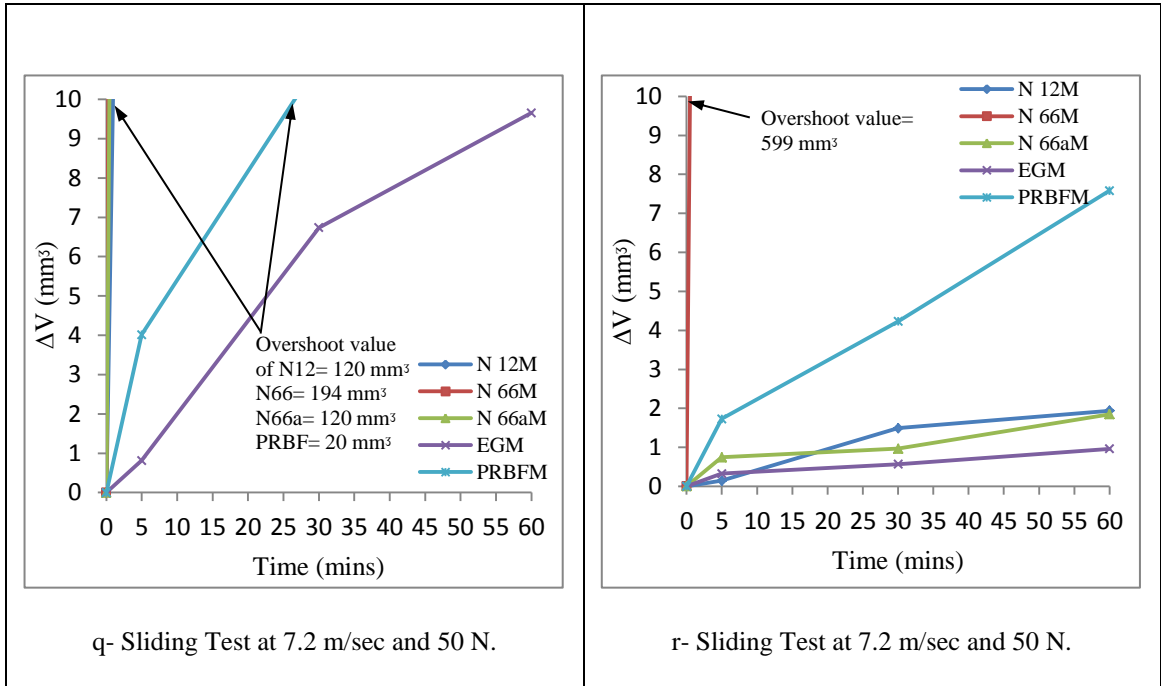


Fig. 4:1- Volume Loss of End Post Materials in Dry and Wet Sliding Tests.

4.2.2- Specimens Wear Resistance

Figures 4:2 to 4:4 summarise the volume loss of Nylon 12, Nylon 66, Nylon 66a, Epoxy Glass and Phenolic Risen Bonded Fabric materials in dry and wet conditions at sliding speeds of 1.5 m/sec, 3.3 m/sec and 7.2 m/sec and applied loads of 10 N, 30 N and 50 N.

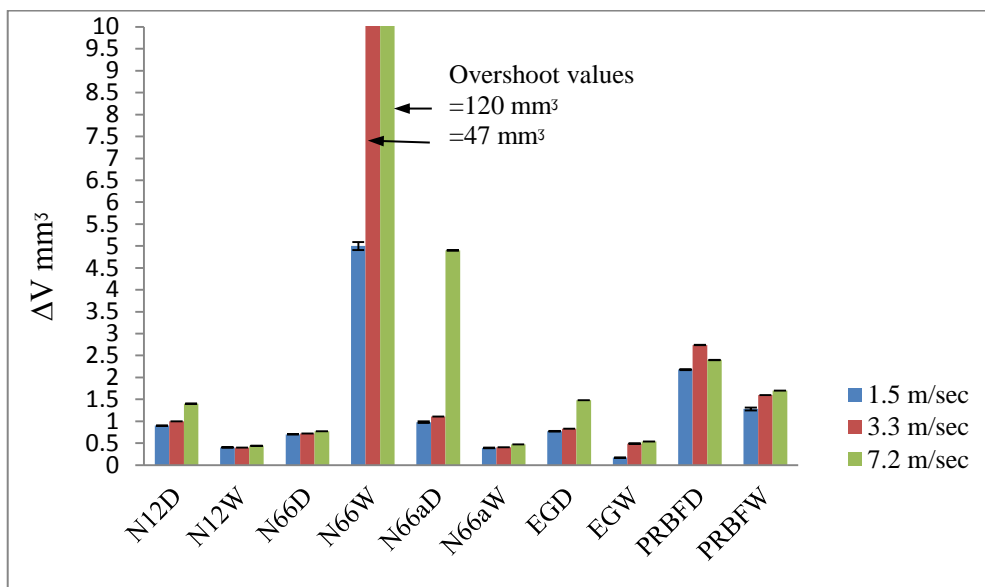


Fig. 4:2- Sliding Tests for All End Post Materials in Dry and Wet Test Conditions at an Applied Load of 10 N and Sliding Speeds of 1.5 m/sec, 3.3 m/sec and 7.2 m/sec.

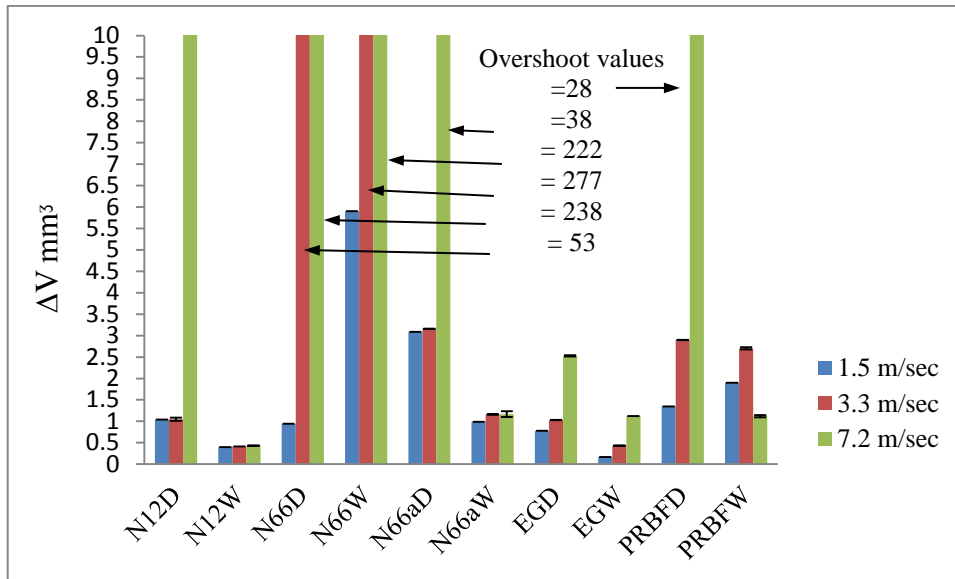


Fig. 4:3- Sliding Tests for All End Post Materials in Dry and Wet Test Conditions at an Applied Load of 30 N and Sliding Speeds of 1.5 m/sec, 3.3 m/sec and 7.2 m/sec.

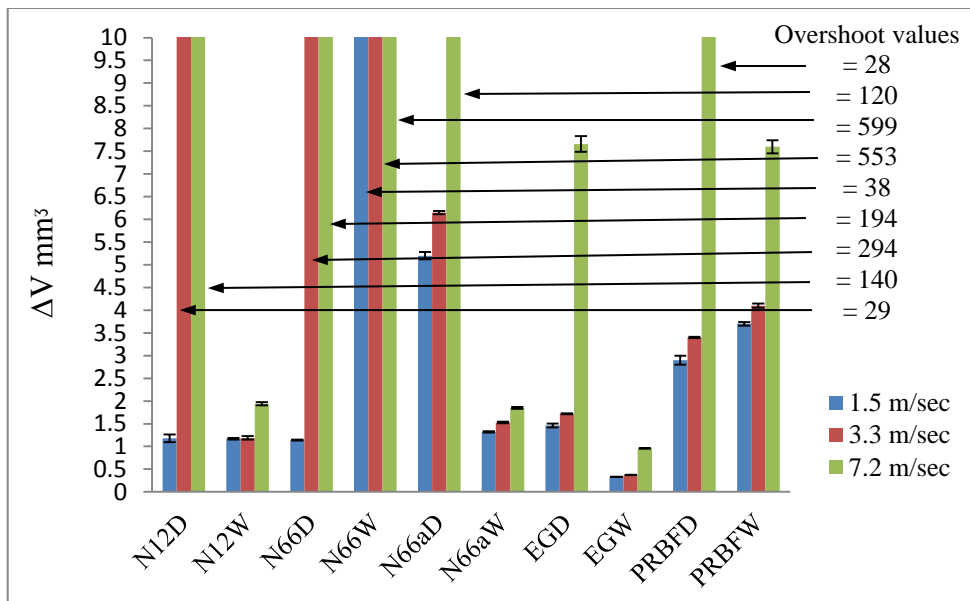


Fig. 4:4- Sliding Tests for All End Post Materials in Dry and Wet Test Conditions at an Applied Load of 50 N and Sliding Speeds of 1.5 m/sec, 3.3 m/sec and 7.2 m/sec.

In the case of low sliding speed (1.5 m/sec) and low applied load (10 N) in dry test conditions, N66 and EG Materials were more wear resistant than N12, N66a and PRBF materials respectively (see Figure 4:2).

While in the wet test condition, EG material is more wear resistant followed by N12 and N66a, PRBF and N66 materials respectively (see Figure 4:2).

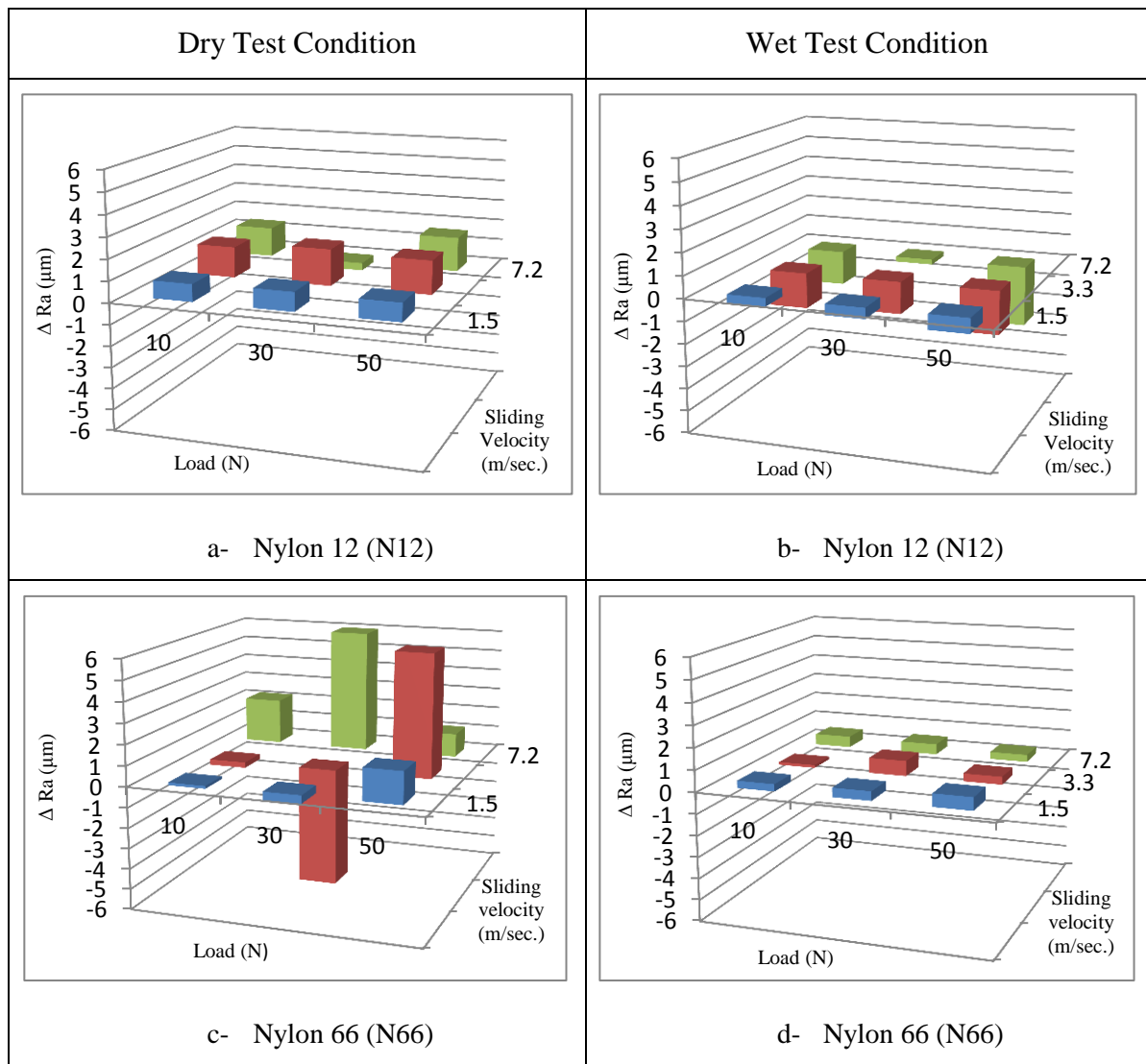
In the case of low sliding speed (1.5 m/sec) and medium load (30 N) and dry test conditions, material EG has more wear resistance than materials N66, N12, PRBF, and N66a as shown in Figure 4:3. Whilst in the wet test conditions, material EG has a higher wear resistance than N12, N66a, PRBF and N66 (see Figure 4:3). Moreover in the case of low speed (1.5 m/sec) and high applied load (50 N) and dry test conditions, the wear resistance of N12 and N66 materials was approximately equal and more than the wear resistance of the other specimens then followed by EG material then PRBF material and finally specimen N66a as seen in Figure 4:4. But in the case of the wet test conditions, the N66 is less wear resistant and then the PRBF, N66a, N12 and EG materials (see Figure 4:4). N66 has the highest wear resistance at the medium sliding velocity (3.3 m/sec) and low load (10 N) and dry conditions than materials EG, N12, N66a and PRBF respectively (see Figure 4:2). While in the wet test condition N12 has stronger wear resistance and then EG, N66a, PRBF and N66 as illustrated in Figure 4:2. In the case of the dry conditions and medium sliding velocity (3.3 m/sec) and medium force (30 N) end post EG has more wear resistance in this case followed by end post materials N12, PRBF, N66a and N66 (see Figure 4:3). Whilst the EG is more wear resistant in the case of the wet test than N12, N66a, PRBF and N66 respectively (see Figure 4:3). In the case of medium sliding speed (3.3 m/sec) and high load (50 N) and dry test condition as shown in Figure 4:4 the wear resistance of EG was the highest then PRBF, N66a, N12 and the lowest was end post material N66. But in the case of the wet tests, as seen in Figure 4:4, EG has a higher wear resistance than N12, N66a, PRBF and N66. However, in the case of the dry test and high sliding speed (7.2 m/sec) and low applied force (10N), as can be seen in Figure 4:2, N66 has the higher wear resistance in this case, followed by materials N12 and EG, PRBF and N66a respectively. While N12 was the highest wear resistance in the wet test condition, as shown in Figure 4:2, followed by N66a, EG, PRBF and N66. In the case of high sliding speed (7.2 m/sec) and medium applied load (30 N) EG material is more wear resistant than N12, PRBF, N66a, and N66 (see Figure 4:3). But in the wet test, N12 has a higher wear resistance than EG and PRBF, N66a and N66 (see Figure 4:3). The EG has the highest wear resistance, in the both test conditions then materials PRBF, N66a, N12, and N66 in the dry test condition and N66a, N12, PRBF and N66 in the wet test condition.

4.2.3- Specimens Surface Roughness

Figure 4:5 shows the surface roughness changes (ΔR_a) of the end post Materials of N12, N66, N66a, EG and PRBF after dry and wet sliding wear tests.

$$\Delta R_a = R_{a0} - R_{a1} \quad (12)$$

where, R_{a0} = specimen surface roughness before the test, and R_{a1} = specimen surface roughness after the test.



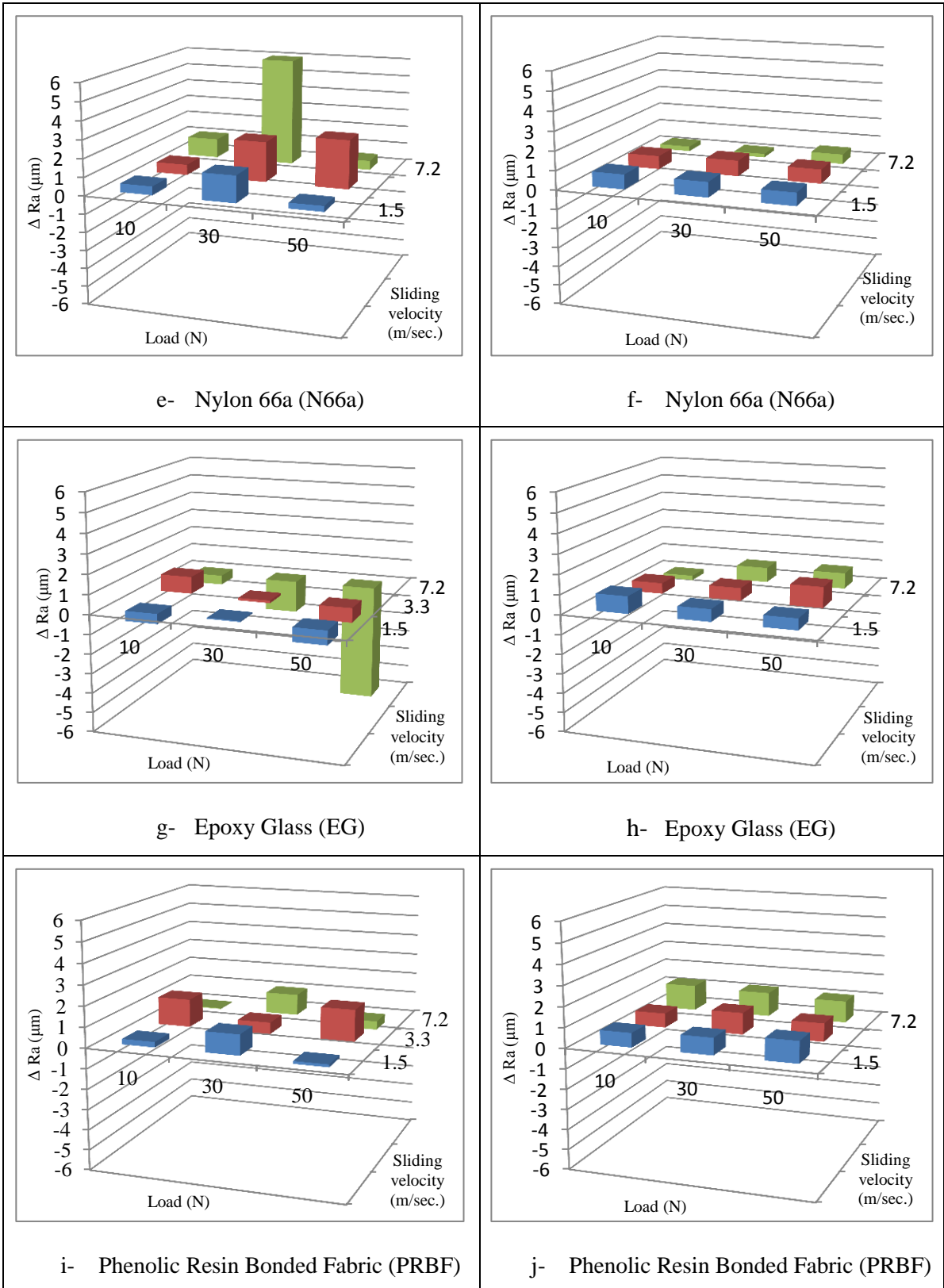


Fig. 4:5- Surface Roughness (R_a) Changes of End Post Materials Under study after Dry and Wet Sliding wear Tests.

4.2.4- Specimens Friction Coefficient

Figures 4:6 to 4:10 show the coefficients of friction for the five studied end post materials at the same sliding velocities used in the dry sliding wear experiments (1.5 m/sec, 3.3 m/sec, and 7.2 m/sec), which correspond to rotating velocities of 568 rpm, 1261 rpm, and 2764 respectively and also at the same applied loads.

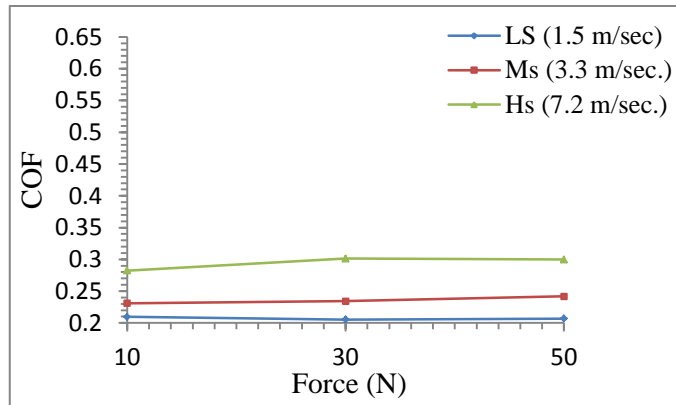


Fig. 4:6- Coefficient of Friction of (N12) at Sliding Velocities of 1.5 m/sec, 3.3 m/sec, and 7.2 m/sec and Applied Loads of 10 N, 30 N, 50 N.

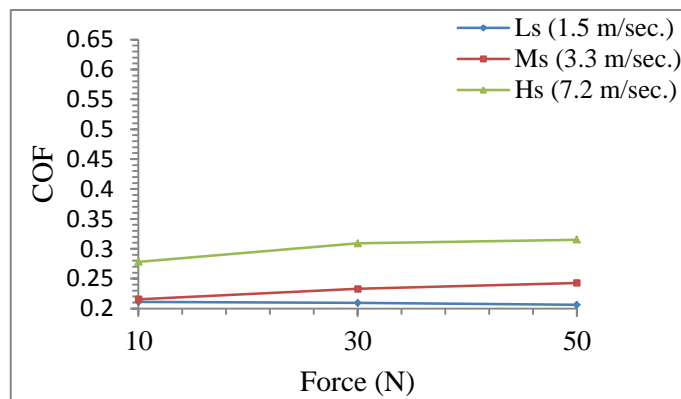


Fig. 4:7- Coefficient of Friction of (N66) at Sliding Velocities of 1.5 m/sec, 3.3 m/sec, and 7.2 m/sec and Applied Loads of 10 N, 30 N, 50 N.

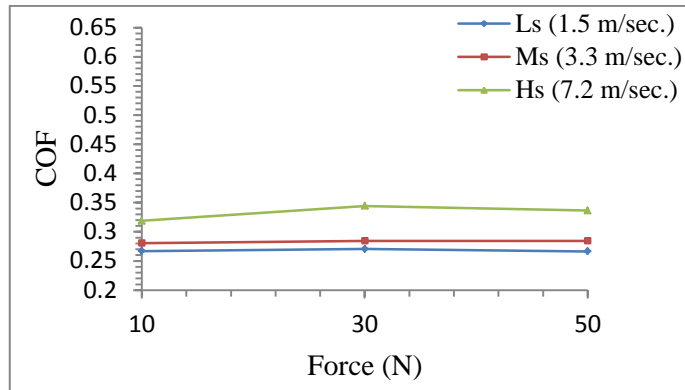


Fig. 4:8- Coefficient of Friction of (N66a) at Sliding Velocities of 1.5 m/sec, 3.3 m/sec, and 7.2 m/sec and Applied Loads of 10 N, 30 N, 50 N.

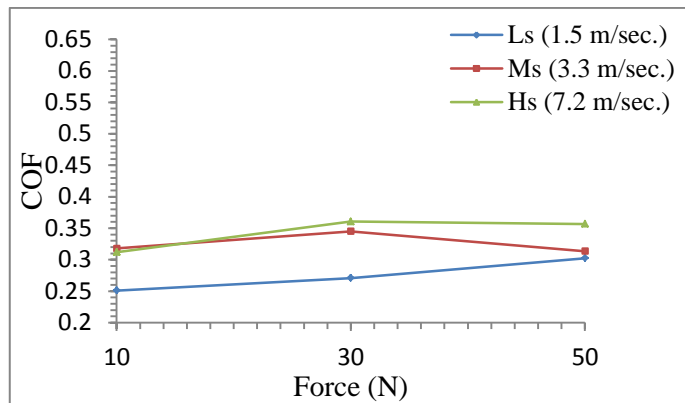


Fig. 4:9- Coefficient of Friction of (EG) at Sliding Velocities of 1.5 m/sec, 3.3 m/sec, and 7.2 m/sec and Applied Loads of 10 N, 30 N, 50 N.

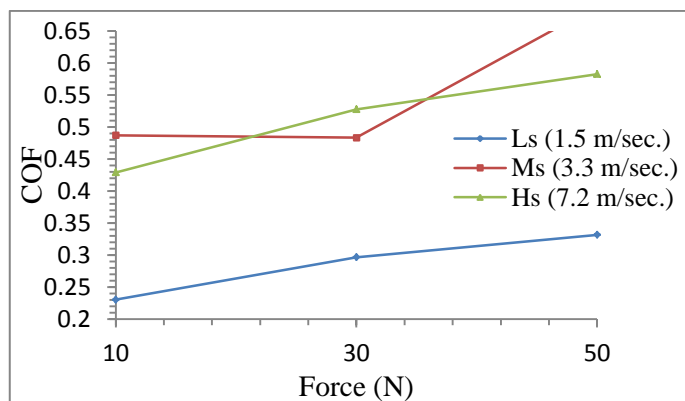


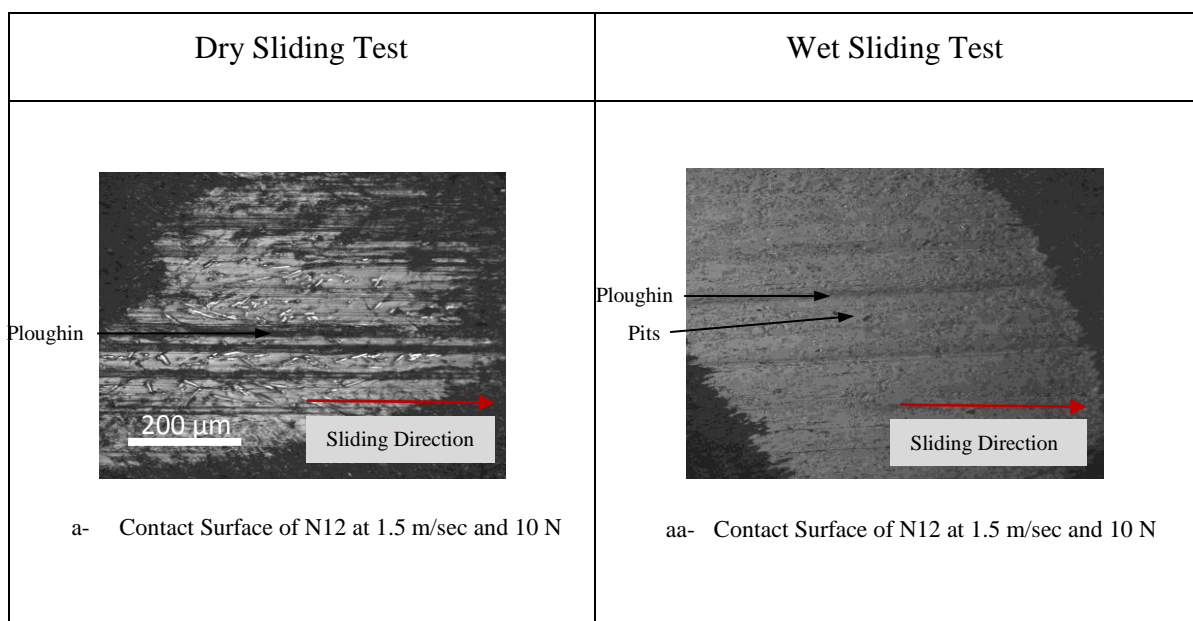
Fig. 4:10- Coefficient of Friction of (PRBF) at Sliding Velocities of 1.5 m/sec, 3.3 m/sec, and 7.2 m/sec and Applied Loads of 10 N, 30 N, 50 N.

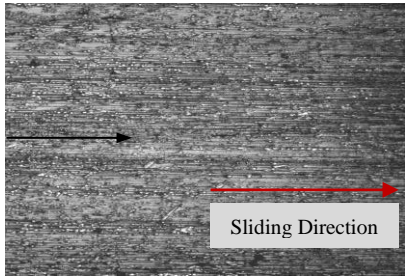
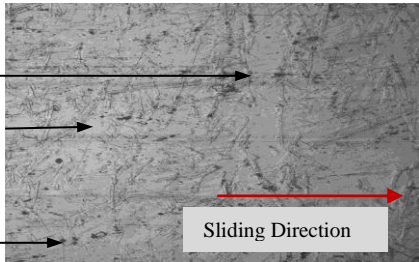
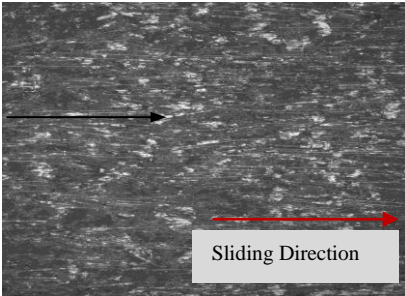
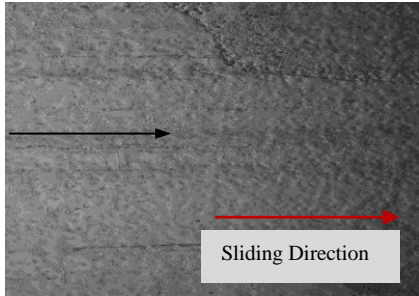
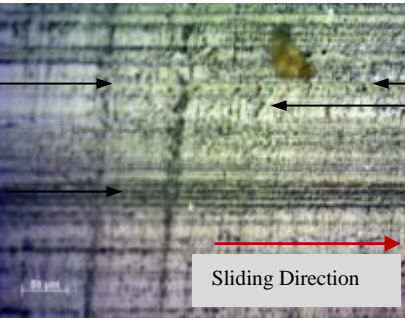
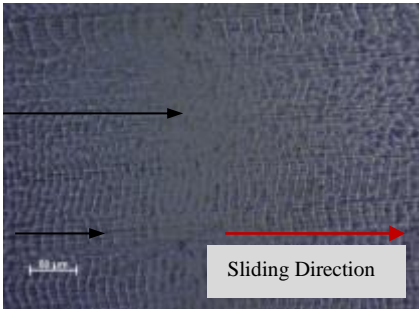
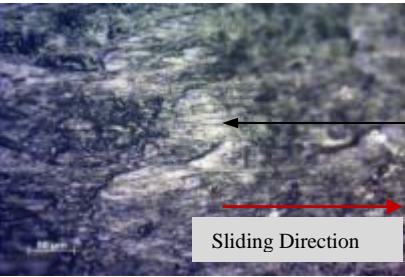
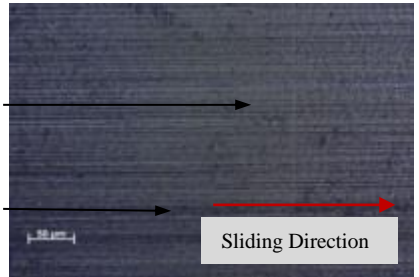
As shown in Figures 4:6 to 4:10, the coefficient of friction tests for all end post materials under study (thermoplastic materials N12, N66, and N66a and thermosetting materials EG and PRBF) started with a running-in period followed by steady-state period in some test cases or an increase or and decrease.

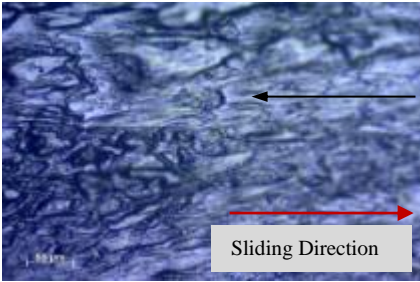
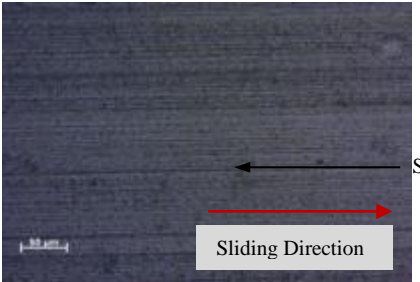

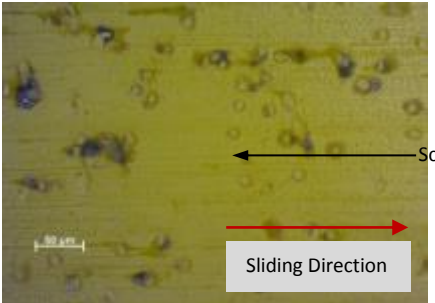
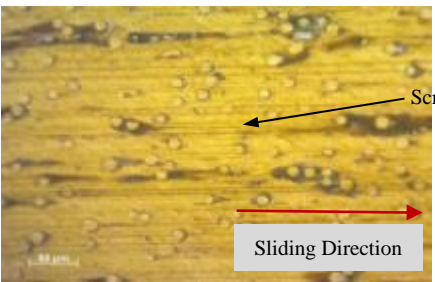
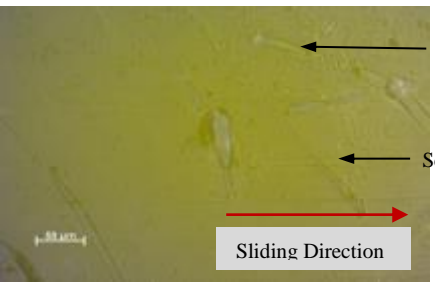

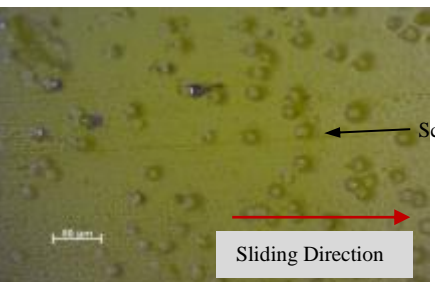
In the case of thermoplastic materials, it is believed that at the beginning of the tests, tips were formed on the surface on specimens. But with the steady-state periods, the tips disappeared and wear debris covered the contact surfaces and reduced values of friction coefficient. While with the decrease periods, the contact temperature became high which led to melting of these materials and lower values of coefficient of friction. However, in case of thermosetting materials, it is believed that with the running-in periods, it is due to nature of surface of these materials. Whilst with the steady-state period or decreased period, the fibres have broken and became powder on the surface which led to lower coefficient of friction values. But with the increased periods the contact temperature grew which led to higher values of friction coefficient. These results are in agreement with the results obtained by Unal [50] and Wang [51, 98].

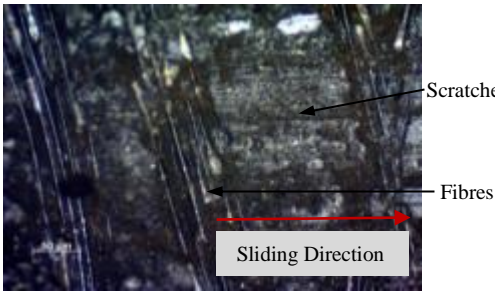

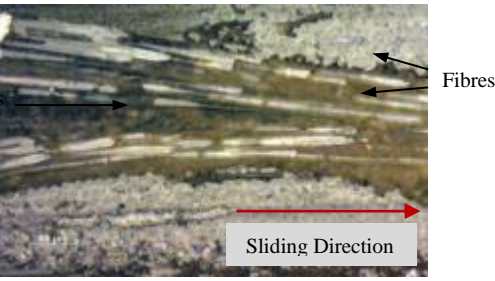
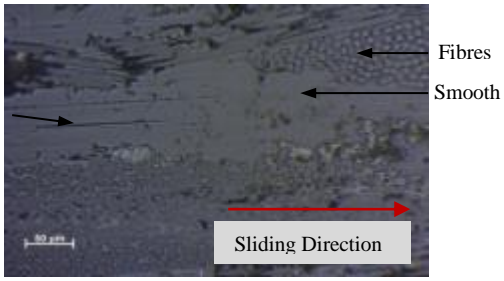
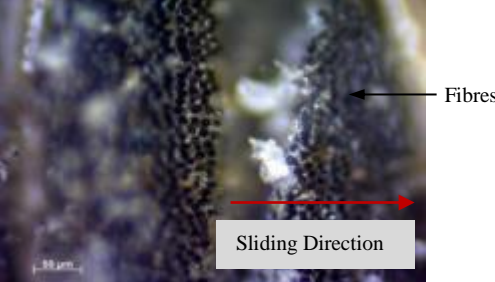

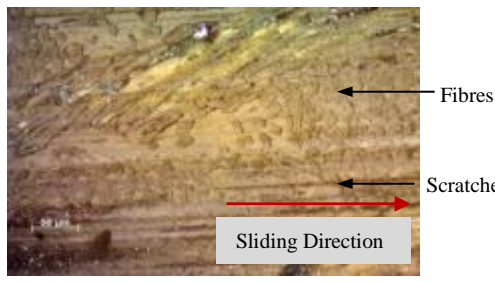
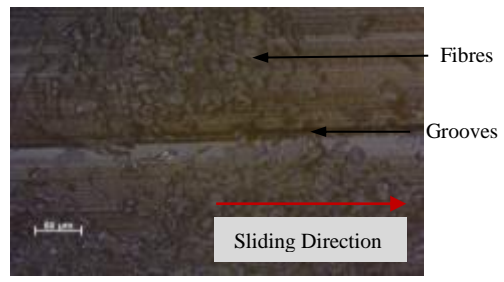
4.2.5- Worn Contact Surfaces of Specimens

Figure 4:11 shows the worn contact surface for each specimen due sliding and thermal wear after the dry and sliding wear tests (for more images see Appendix B). Images scale bar (0.1 mm= 200 μ m)



| | |
|---|--|
|  <p>Ploughing →</p> <p>Sliding Direction →</p> <p>b- Contact Surface of N12 at 3.3 m/sec and 30 N</p> |  <p>Smooth →</p> <p>Ploughing →</p> <p>Pits →</p> <p>Sliding Direction →</p> <p>bb- Contact Surface of N12 at 3.3 m/sec and 30 N</p> |
|  <p>Smearing →</p> <p>Sliding Direction →</p> <p>c- Contact Surface of N12 at 7.2 m/sec and 50 N</p> |  <p>Ploughing →</p> <p>Sliding Direction →</p> <p>cc- Contact Surface of N12 at 7.2 m/sec and 50 N</p> |
|  <p>Waves →</p> <p>Scratches →</p> <p>Pits →</p> <p>Cracks →</p> <p>Sliding Direction →</p> <p>d- Contact Surface of N66 at 1.5 m/sec and 10 N</p> |  <p>Smearing →</p> <p>Scratches →</p> <p>Sliding Direction →</p> <p>dd- Contact Surface of N66 at 1.5 m/sec and 10 N</p> |
|  <p>Smeared →</p> <p>Sliding Direction →</p> <p>e- Contact Surface of N66 at 3.3 m/sec and 30 N</p> |  <p>Smearing →</p> <p>Scratches →</p> <p>Sliding Direction →</p> <p>ee- Contact Surface of N66 at 3.3 m/sec and 30 N</p> |

| | |
|---|---|
|  <p>f- Contact Surface of N66 at 7.2 m/sec and 30 N</p> |  <p>ff- Contact Surface of N66 at 7.2 m/sec and 30 N</p> |
|  <p>h- Contact Surface of N66a at 1.5 m/sec and 10 N</p> |  <p>hh- Contact Surface of N66a at 1.5 m/sec and 10 N</p> |
|  <p>k- Contact Surface of N66a at 3.3 m/sec and 30 N</p> |  <p>kk- Contact Surface of N66a at 3.3 m/sec and 30 N</p> |
|  <p>l- Contact Surface of N66a at 7.2 m/sec and 50 N</p> |  <p>ll- Contact Surface of N66a at 7.2 m/sec and 50 N</p> |

| | |
|---|---|
|  <p>m- Contact Surface of EG at 1.5 m/sec and 10 N</p> |  <p>mm- Contact Surface of EG at 1.5 m/sec and 10 N</p> |
|  <p>n- Contact Surface of EG at 3.3 m/sec and 30 N</p> |  <p>nn- Contact Surface of EG at 3.3 m/sec and 30 N</p> |
|  <p>o- Contact Surface of EG at 7.2 m/sec and 50 N</p> |  <p>oo- Contact Surface of EG at 7.2 m/sec and 50 N</p> |
|  <p>p- Contact Surface of PRBF at 1.5 m/sec and 10 N</p> |  <p>pp- Contact Surface of PRBF at 1.5 m/sec and 10 N</p> |

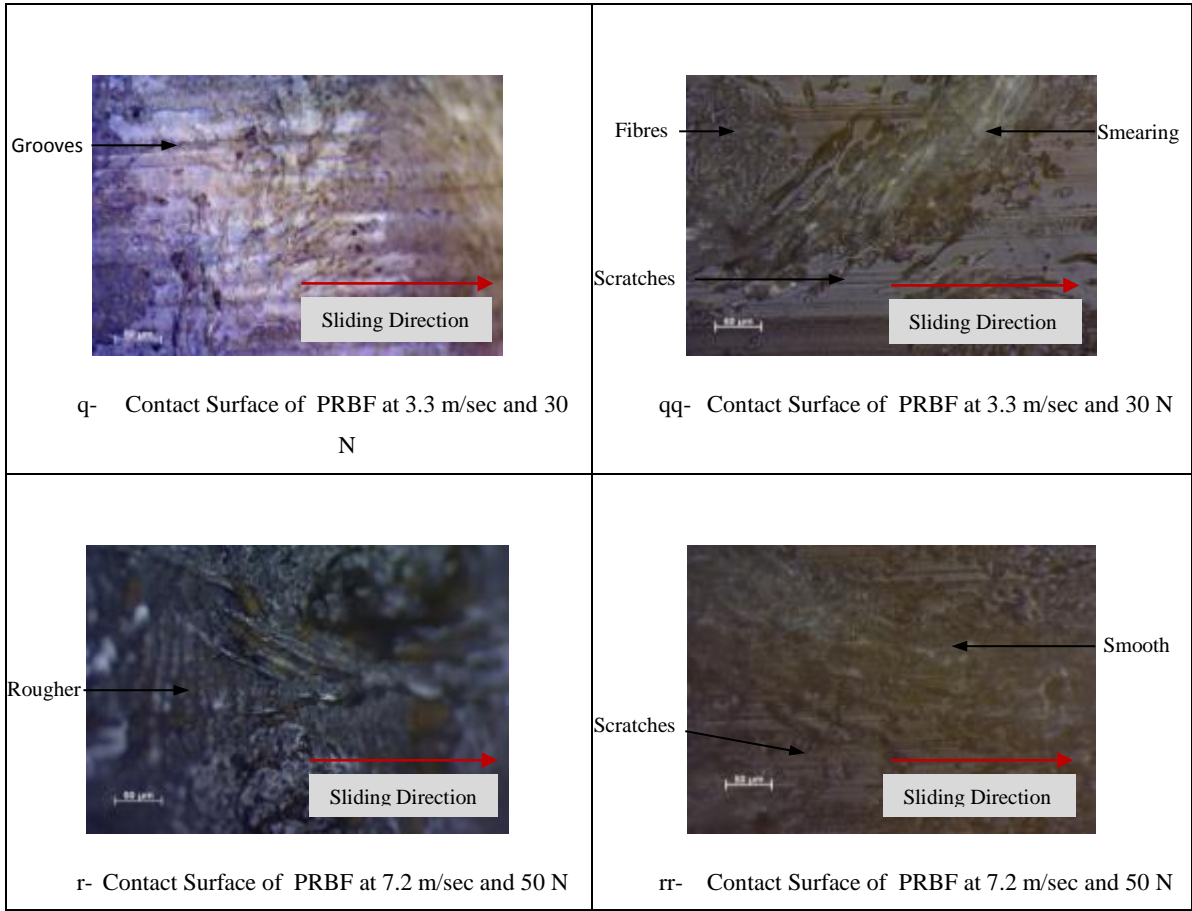


Fig. 4:11- Contact Surface of End Post Material in Both Dry and Wet Test Conditions.

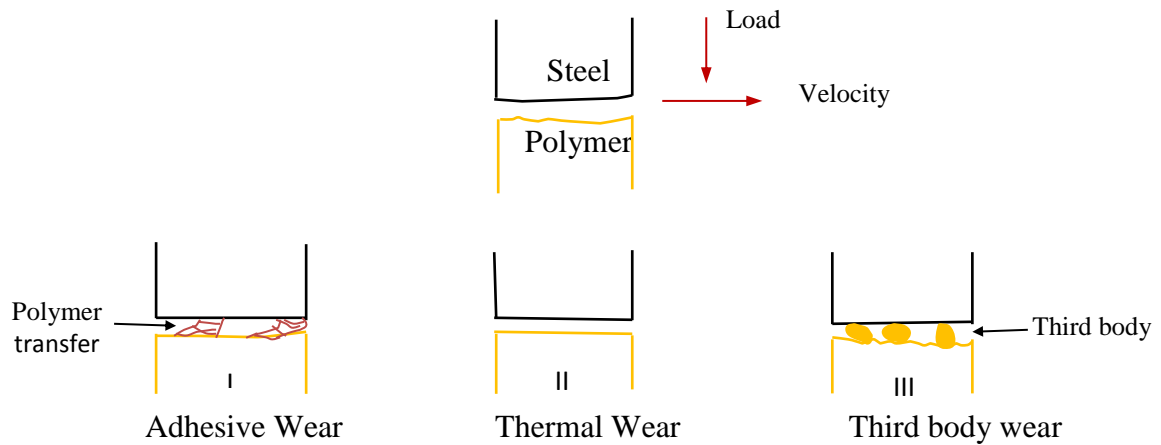


Fig. 4:12- Schematic Diagram of Wear Mechanism.

In the case of dry sliding a low sliding speed (1.5 m/sec), and low load (10 N) and medium sliding speed (3.3 m/sec) and medium load (30 N), the wear mechanism for materials N12,

N66, N66a, EG, and PRBF was adhesive wear (see Figures 4:11 and 4:12 I). While the wear mechanism for materials N12, N66, and N66a in the case of high sliding speed and high load was melt wear (see Figure 4:12 II). Whereas the wear mechanism for materials EG, and PRBF in the same test case was third-body abrasive wear (see Figure 4:12 III). Moreover, the wear mechanism for materials N12, N66a, EG, and PRBF in wet tests condition was adhesive wear and third body wear (wear debris generated, which appears in the form of third-body particles between contacting surfaces). But the wear mechanism for material M66 was probably chemical wear (the material dissolved in water and the evidence for this was: the water pool through and after the test was seen to be cloudy, the material transferred to steel disc and around the test rig powder was seen as the water dried and hardness of the material was reduced in wet condition).

4.3- Discussion

As can be seen from the previous sections, the wear resistance and mechanisms for the studied materials over a time of sixty minutes at sliding velocities of 1.5 m/sec, 3.3 m/sec, and 7.2 m/sec and applied loads of 10 N, 30 N, and 50 N in both dry and wet tests condition are demonstrated.

The end post materials under study were classified as thermoplastic and thermosetting materials according to melt temperature test in Section 3.3.1. N12, N66 and N66a were classified as thermoplastic materials, while EG and PRBF were classified as thermosetting materials.

4.3.1- Thermoplastic Materials

4.3.1.1- Nylon 12 Material (N12)

In the beginning of test there was a small effect of test parameters of sliding speed of 1.5 m/sec., 3.3 m/se. and 7.2 m/sec. and applied load of 10 N on the material wear resistance as shown in Figures 4:1 a, g and m. This was reflected in the amount of material loss during the test period of 60 minutes. The rubbing surface was partly smooth (see Figure 4:5 a). Pits and ploughing parallel to the sliding direction were observed (see Figure 4:11 a). As shown in Figure 4:1 c and I, the material wear resistance was influenced slightly on increasing sliding speed from 1.5 m/sec to 3.3 m/sec at an applied load of 30 N. The wear surface was partly smoothed as shown in Figure 4:5 a and pits and scratches were observed on the surface (see Figure 4:11 b). It is clear from the results as can be observed in Figure

4:1 o, the material wear resistance decreased massively in the case of a sliding velocity of 7.2 m/sec at constant load of 30 N. The contact surface was coarse (see Figure 4:5 a) due probably to adhesive wear and characterised by pits and scratches parallel to the orientation of sliding. Moreover, the wear resistance of the material was affected gradually as sliding velocities increased from 1.5 m/sec to 3.3 m/sec at an applied load of 50 N (see Figures 4:1 e and k). The worn surface was partly smoothed (see Figure 4:5 a). While there was a large effect of increased sliding velocity to 7.2 m/sec, specifically at the applied load of 50 N where the material was melted (see Figure 4:13 A) due to the increase of friction between the steel ring and N12 block (see Figures 4:1 q) that led to an increase in contact temperature (to over the material melting point). The contact surface smeared as shown in Figure 4:11 c.

On the other hand there was a significant effect of using water as a lubricant in wet tests on wear resistance of material where contact temperature was reduced during the test which led to a reduction in the amount of material loss as shown in Figures 4:1 b, d, f, h, j, l, n, p and r. The rubbing surface was partly rough (see Figure 4:5 b) and characterised by Pits, and ploughing parallel to the sliding direction (see Figures 4:11 aa, bb and cc).

4.3.1.2- Nylon 66 Material (N66)

Figures 4:1 a, g and m show that there was a slight effect on wear resistance of increasing sliding velocity from 1.5 m/sec to 7.2 m/sec at an applied load of 10 N. The rubbing surface became smooth as shown in Figure 4:5 c and pits, cracks, waves and scratches parallel to the sliding direction appeared across the contact surface (see Figure 4:11 d).

In Figures 4:1 c, i and o, it is possible to observe that there was a significant effect of increasing sliding speed from 1.5 m/sec to 7.2 m/sec at a load of 30 N. The wear surface in the case of a sliding speed of 3.3 m/sec and a force of 30 N was coarse (see Figure 4:5 c) due probably to adhesive wear. However in the case of a sliding speed of 7.2 m/sec and a load of 30 N, the appearance of contact surface as shown in Figure 4:11 e was partly smoothed (see Figure 4:5 c) due to thermal wear (see Figure 4:13 b).

Figure 4:1 e, k and q shows that the material wear resistance was affected considerably when the sliding speed rose from 1.5 m/sec to 7.2 m/sec at a load of 50 N. This was reflected in amount of material loss during the test period. The contact surface became

partly smooth (see Figure 4:5 c) because contact temperature increased and material melted as shown in Figures 4:13 B and 4:4 f.

In contrast, in the case of wet tests, as can be seen from Figures 4:1 b, d, f, h, j, l, n, p and r, the material wear resistance was significantly affected compared with dry tests. Water would reduce contact temperature, which would reduce the material wear, but it actually increased. This is thought to have happened because:

- i) Material became weak and the strength reduced, that led to an increase in volume loss compared with dry condition. This in agreement with the results displayed by Wang [51].
- ii) The absorption of water by the Nylon 66 material led to reduced material hardness from 230.39 in dry case to 131.27 in wet case (see Section 3.5.1.2). This result in an agreement with Jacobs results [99].

There was significant transfer of polymer to the steel ring and the water became very cloudy. The rubbing surface was smoothed (see Figure 4:5 d) and was characterised by smears in the case of a sliding speed of 1.5 m/sec and a load of 10 N (see Figure 4:8 dd). However, Figure 4:11 ee shows the worn surface of the specimen at a velocity of 3.3 m/sec and a load of 30 N. Scratches were observed on the surface. Whilst in the case of a velocity of 7.2 m/sec and a load of 50 N, the contact surface appearance was partly smoothed as shown in Figure 4:5 d and is characterized by scratches parallel to the sliding orientation (see Figure 4:11 ff).

4.3.1.3- Nylon 66a Material (N66a)

As shown in Figures 4:1 a, g and m, there was a slight influence on wear of sliding speed increase from 1.5 m/sec to 3.3 m/sec at a load of 10 N. The worn surface was partly smoothed, as seen in Figure 4:5 e, and scratches existed on the surface parallel to the orientation of sliding (see Figure 4:11 h). In the case of a sliding speed of 7.2 m/sec and a load of 10 N, the material wear resistance was lower than that in the previous cases. The rubbing surface became smooth as shown in Figure 4:5 e.

In Figures 4:1 c, i and o the material wear resistance decreased gradually. The main source of wear damage appears to be scratches as shown in Figure 4:11

k and the worn surface was smoothed as seen in Figure 4:5 e. Whilst the rubbing surface in the case of a speed of 7.2 m/sec and a force of 30 N was rough as shown in Figure 4:5 e. This was due to adhesive wear.

Figures 4:1 e, k and q shows that, material wear resistance was affected considerably when sliding velocity increased from 1.5 m/sec to 7.2 m/sec at an applied load of 50 N and the wear surface was smooth (see Figure 4:5 e). No marks were formed on the wear surface in the case of a sliding velocity of 7.2 m/sec and a load 50 N (see Figure 4:11 l), but the wear surface was smooth, this was due to thermal wear as shown in Figure 4:13 C.

In contrast, in the case of wet tests condition, as can be observed in Figures 4:1 b, d, f, h, j, l, n, p and r, there was a positive effect of water on material wear resistance, this appears in the amount of material loss through the tests compared with dry tests condition. This is because the water acted as a lubricant and reduced contact temperature which led to a rise the material wear resistance and increased material service life. The rubbing surface was more smoothed as shown in Figure 4:5 f, cracks were observed and scratches existed on the surface parallel to the orientation of sliding (see Figures 4:11 hh, kk and ll).

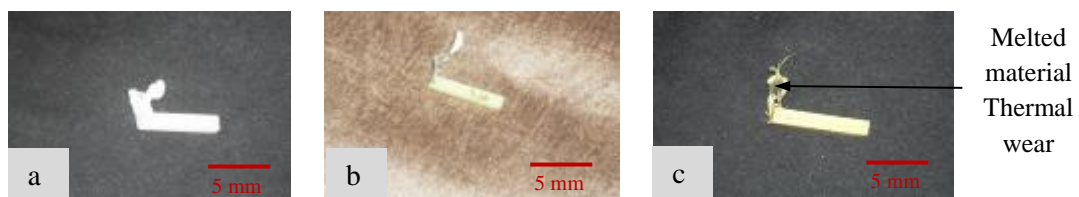


Fig. 4:13- Photos of Melted Materials of (a) Nylon 12, (b) Nylon 66 and (c) Nylon 66a.

4.3.2- Thermosetting Materials

4.3.2.1- Epoxy Glass Material (EG)

Figures 4:1 a, g and m show that the material wear resistance reduced gradually due to increased sliding speed from 1.5 m/sec to 7.2 m/sec at an applied load of 10 N. The worn contact surface was partly rough (see Figure 4:5 g) and fibres and scratches were observed (see Figure 4:11 m).

In Figures 4:1 c, i and o, the material wear resistance gradually decreased due to an increase of sliding velocity from 1.5m/sec to 7.2 m/sec at a load of 30 N. Figure 4:11 n shows the worn contact surface of the specimen after the test. The contacting surface was coarse (see Figure 4:5 g). Fibres and scratches were observed on the wear surface.

Figures 4:1 e, k and q show that, the wear resistance of the material reduced significantly when the sliding speed rose from 1.5 m/sec to 7.2 m/sec at a load of 50 N. The wear surface was more roughened as shown in Figure 4:5 g and there was a severe deterioration of fibre surface due to the increase in temperature (see Figure 4:11 o). In wet test conditions, it is possible to observe that from Figure 4:1 b, d, f, h, j, l, n, p and r the material wear resistance was better than that in dry test conditions. This occurred due to a reduction of contact temperature and a lubricating effect during the tests. The worn surface became smooth (see Figure 4:5 h), and the major source of wear damage was fibres exposed and scratch marks parallel to sliding direction as seen in Figures 4:11 mm, nn and oo.

4.3.2.2- Phenolic Resin Bonded Fabric Material (PRBF)

In Figures 4:1 a, g and m, the material wear resistance was influenced slightly in the case of sliding speeds of 1.5 m/sec, 3.3 m/sec and 7.2 m/sec at a constant applied force of 10 N. The rubbing surface was partly smooth (see Figure 4:5 i). Scratches were formed on the surface (see Figure 4:11 p). The wear resistance of end post materials decreased gradually when sliding speed rose from 1.5 m/sec to 3.3 m/sec at a constant load of 30 N as shown in Figures 4:1 c and i. The worn surface became partly rough as seen in Figure 4:5 i due to a rise in temperature and groove marks are observed on the surface (see Figure 4:11 q). While the wear resistance of end post material decreased greatly when sliding speed rose to 7.2 m/sec at an applied load of 30 N as shown in Figure 4:1 o. The worn contact surface was partly rough (see Figure 4:5 i). Finally as can be seen in Figures 4:1 e, k and q, the material wear resistance decreased slightly in the case of sliding velocity 1.5 m/sec and 3.3 m/sec and at constant load 50 N. The tested surface was partly smooth as seen in Figure 4:5 i. However, the wear resistance of material rose considerably in the case of high sliding speed 7.2 m/sec and constant applied load of 50 N. A rough structure in the matrix can be seen on the worn surface (see Figures 4:5 i and 4:11 r). This is a result of increased temperature.

However, in the case of wet test conditions, the material wear resistance rose significantly as can be observed in Figures 4:1 b, d, f, h, j, l, n, p and r. The worn surfaces became smooth as shown in Figure 4:5 j, the major source of wear damage becomes clear to be

fibre, smears and scratch marks parallel to the sliding direction (see Figures 4:11 pp, qq and rr).

4.4- Summary

The Epoxy glass material has more wear resistance than the phenolic risen bonded fabric material, Nylon 12 material and Nylon 66 and Nylon 66a materials in the dry test condition. The dominant failure mode was third-body abrasive wear for Epoxy Glass and Phenolic Risen Bonded Fabric materials and adhesive wear and melting wear for Nylon 12, Nylon 66 and Nylon 66a as well as chemical wear for Nylon 66 in the case of wet test conditions. The Epoxy Glass material has higher wear resistance in the wet test condition followed by Nylon 12, Nylon 66a and Phenolic Resin Bonded Fabric materials. The wear mechanism was third-body abrasion for Epoxy Glass and Phenolic Resin Bonded Fabric material and third-body abrasion and adhesive wear for Nylon 66a and Nylon 12 materials and chemical wear for Nylon 66 Material. All thermoplastic materials melted when sliding speeds and applied loads increased in the case of dry test condition. The wear resistance of thermoplastic materials was improved in wet tests except for Nylon 66. The thermosetting materials did not melt in all test conditions. The Epoxy glass material has the highest wear resistance.

5- Impact Tests

5.1- Introduction

These tests were carried out to examine which material from Nylon 12, Nylon 66, Nylon 66a, EG and PRBF has more resistance to impact wear caused by the impact of train's wheels (see Table 3:1 (4)). A Pneumatic Ball-on-Plate Impact rig was used to achieve this test (see Section 3.2.3). The test was implemented in both dry and wet conditions, and at three forces and three cycle numbers (see Table 5:1) as described in Section 3.5.4. The test conditions are summarised in Table 5:1.

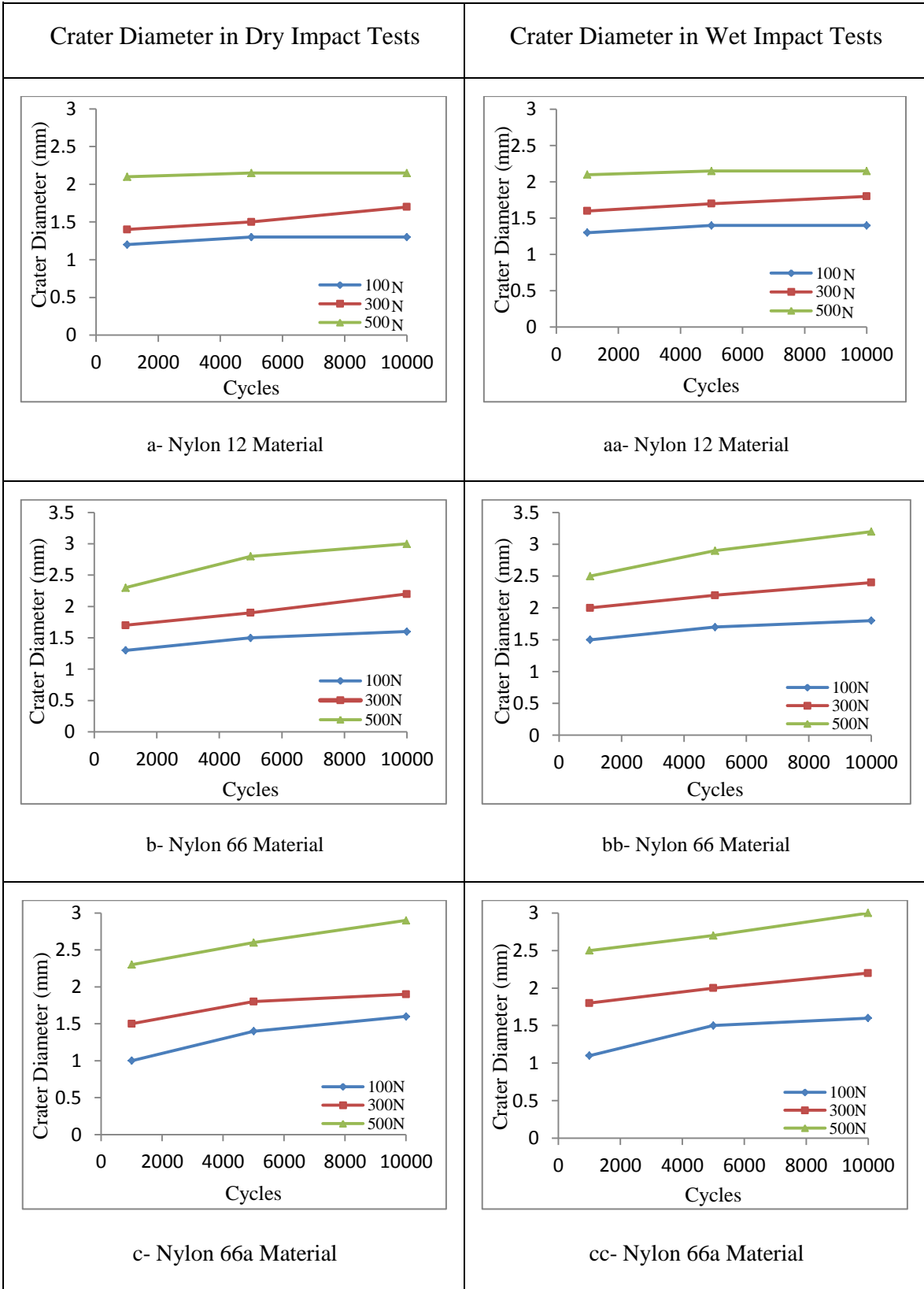
Table 5:1- Test Conditions.

| Force (N) | Number of Cycles | |
|-----------|------------------|----------|
| | Dry Test | Wet Test |
| 100 | 1000 | 1000 |
| | 5000 | 5000 |
| | 10,000 | 10,000 |
| 300 | 1000 | 1000 |
| | 5000 | 5000 |
| | 10,000 | 10,000 |
| 500 | 1000 | 1000 |
| | 5000 | 5000 |
| | 10,000 | 10,000 |

5.2- Results

5.2.1- Crater Dimensions

The data collected from experimental work for the studied end post materials of Nylon 12 material (N12), Nylon 66 material (N66), Nylon 66a material (N66a), Epoxy Glass material (EG) and Phenolic Resin Bonded Fabric material (PRBF) using 1000 cycles, 5000 cycles, and 10000 cycles in dry (D) and wet (W) test conditions are shown in Figures 5:1 to 5:8. Figures 5:1 to 5:4 summarise the crater diameter data and Figures 5:5 to 5:8 summarise the crater depth data. The tests were conducted three times and the average was employed in data analysis.



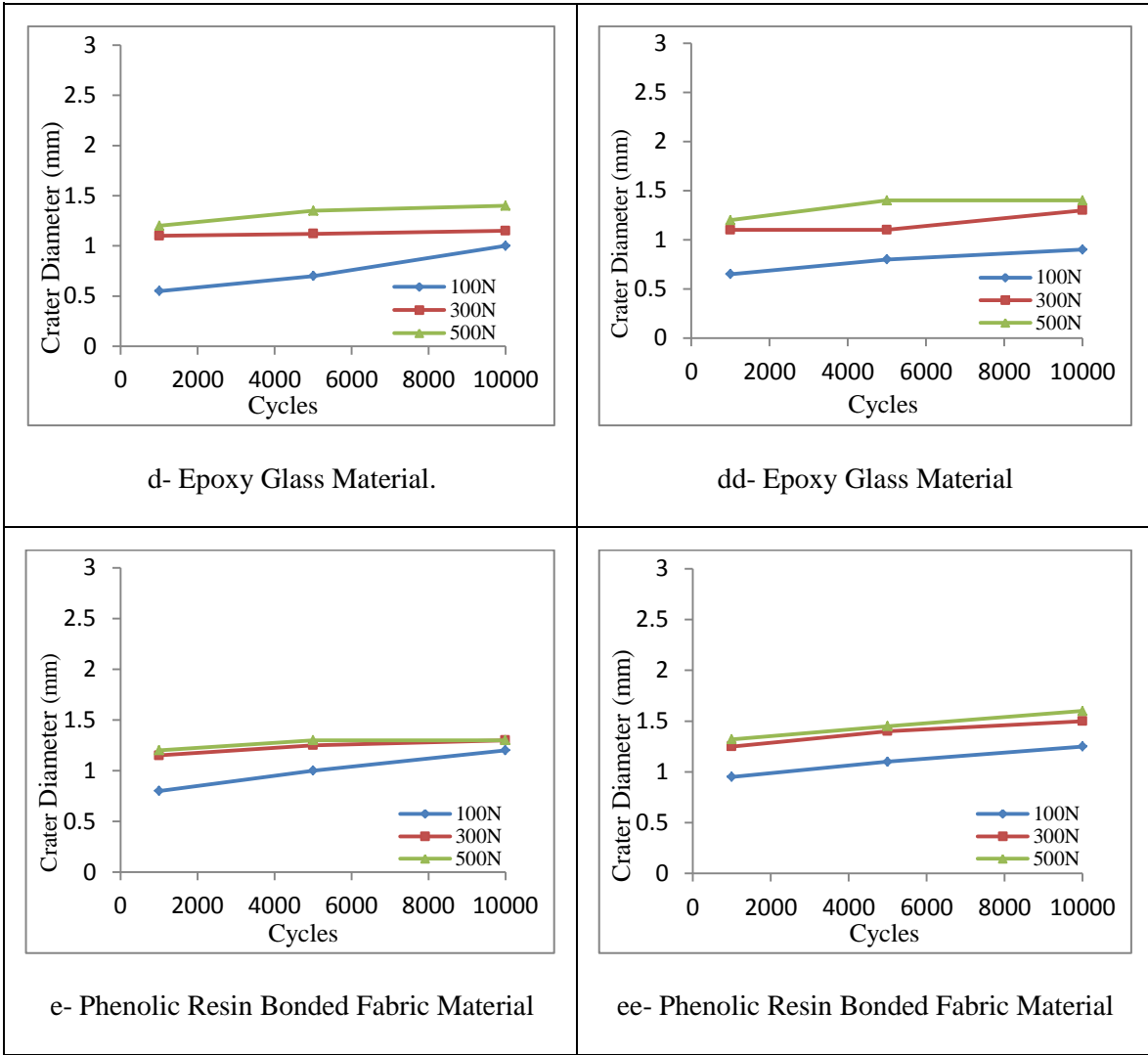


Figure 5:1- Crater Diameter of End Post Materials in Dry and Wet Impact Tests.

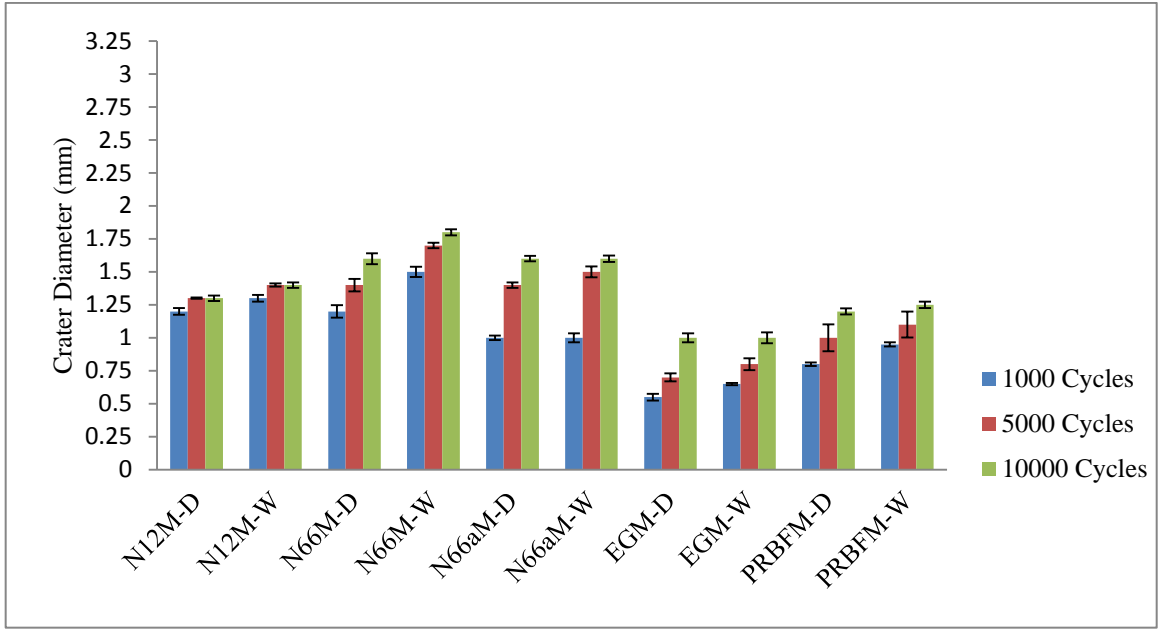


Fig. 5:2- Impact Test for All End Post Materials in Dry and Wet Conditions at an Applied Load of 100 N and 1000 Cycles, 5000 Cycles and 10,000 Cycles.

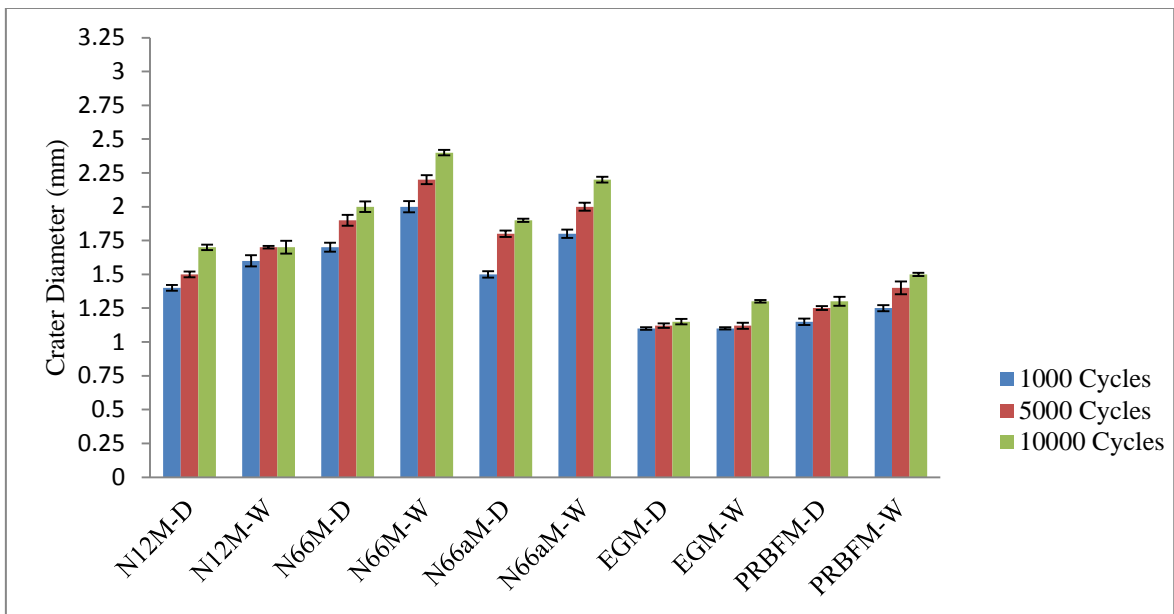


Fig. 5:3- Impact Test for All End Post Materials in Dry and Wet Conditions at an Applied Load of 300 N and 1000 Cycles, 5000 Cycles and 10,000 Cycles.

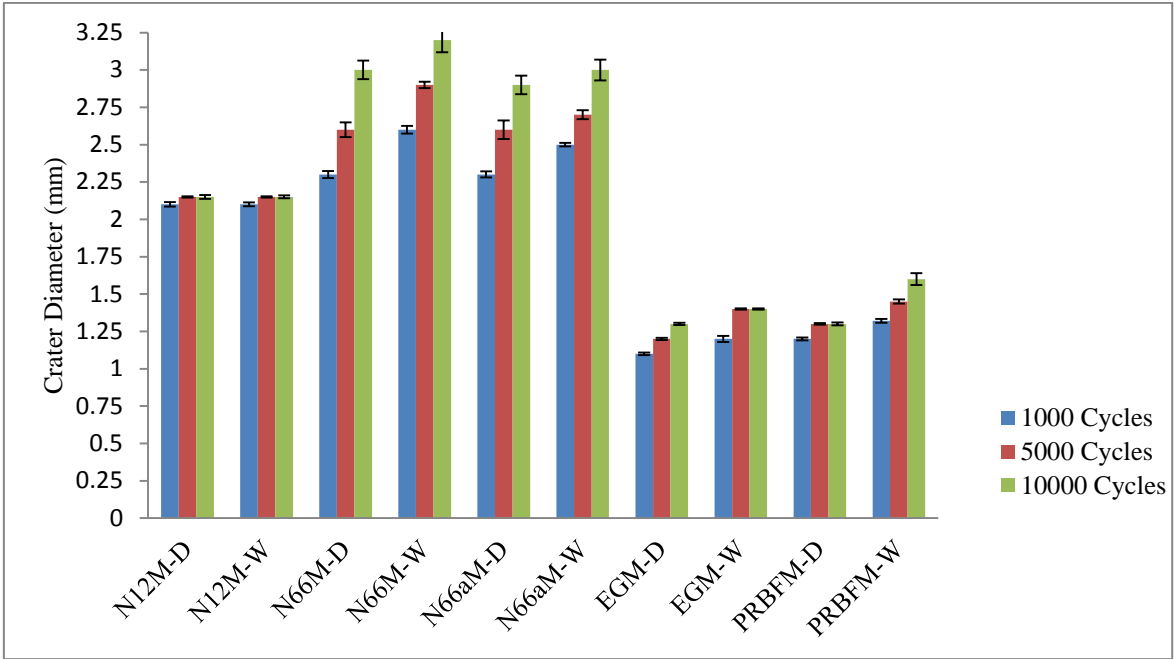
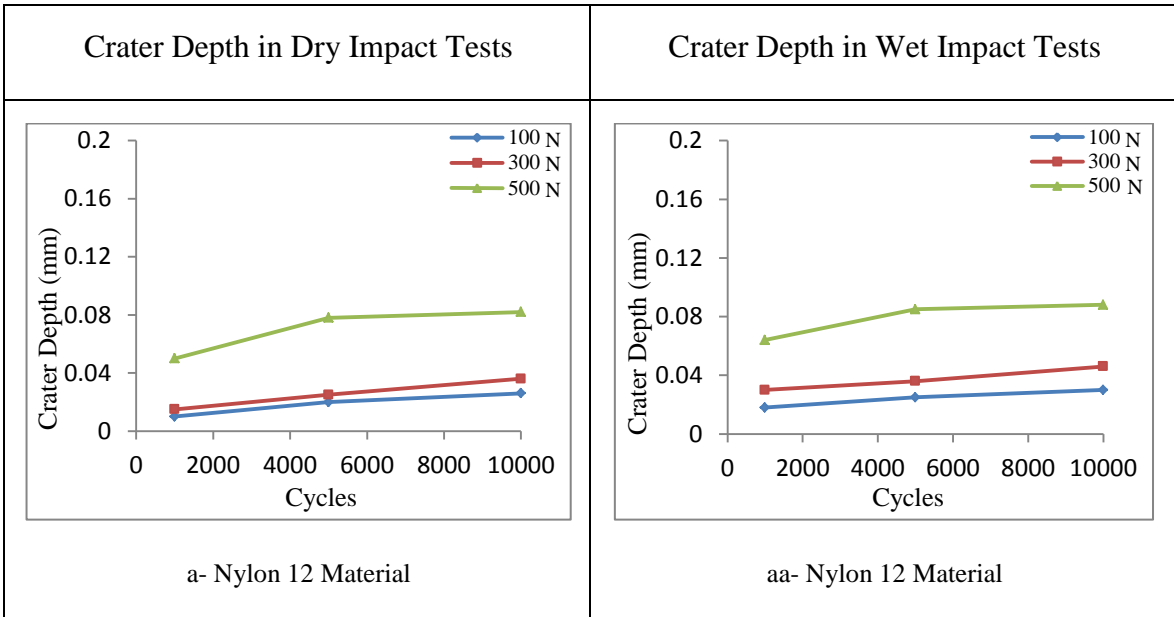
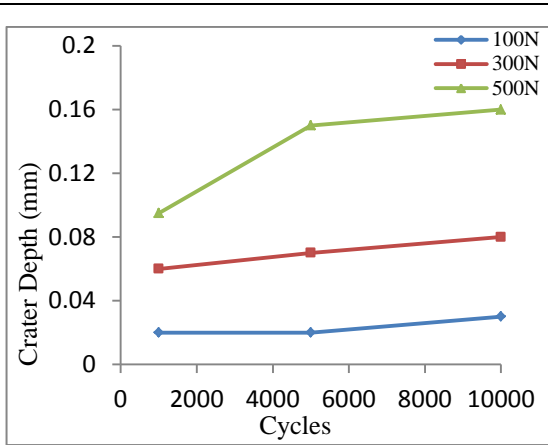
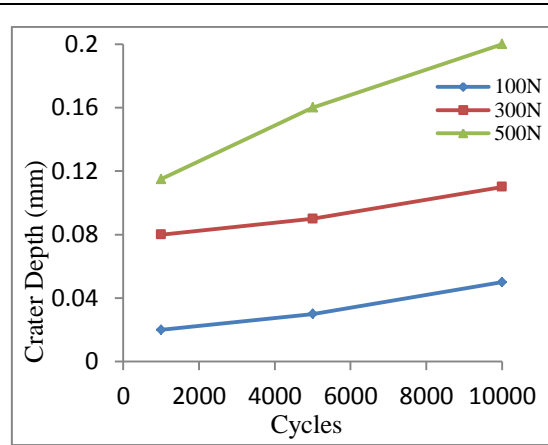


Fig. 5:4- Impact Test for All End Post Materials in Dry and Wet Conditions at an Applied Load of 500 N and 1000 Cycles, 5000 Cycles and 10,000 Cycles.

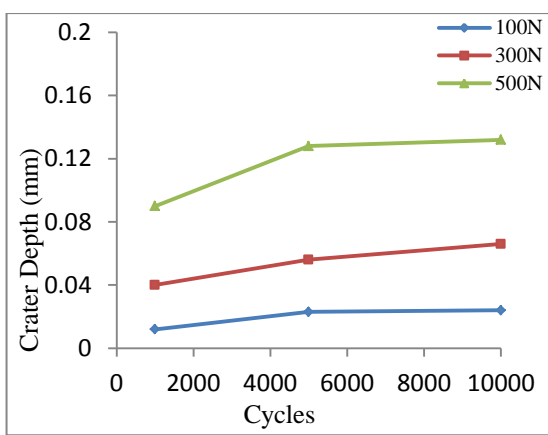




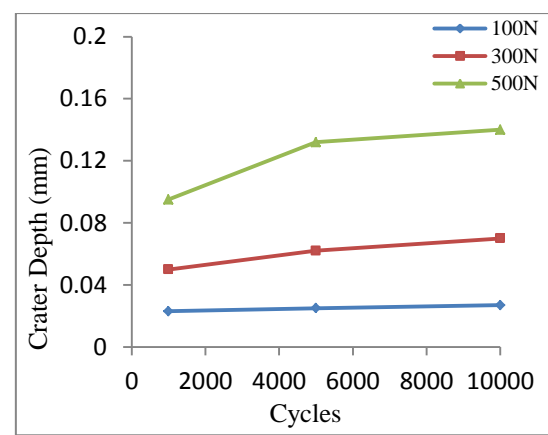
b- Nylon 66 Material



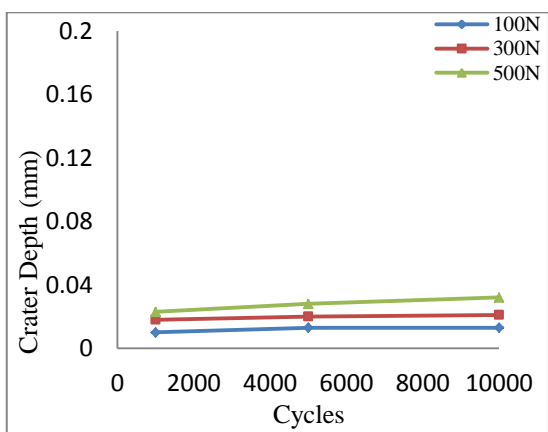
bb- Nylon 66 Material



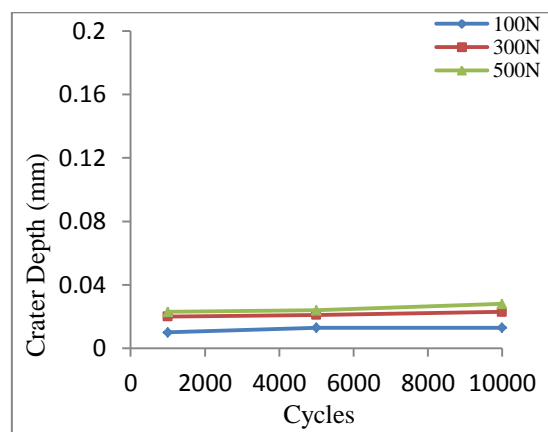
c- Nylon 66a Material



cc- Nylon 66a Material



d- Epoxy Glass Material.



dd- Epoxy Glass Material.

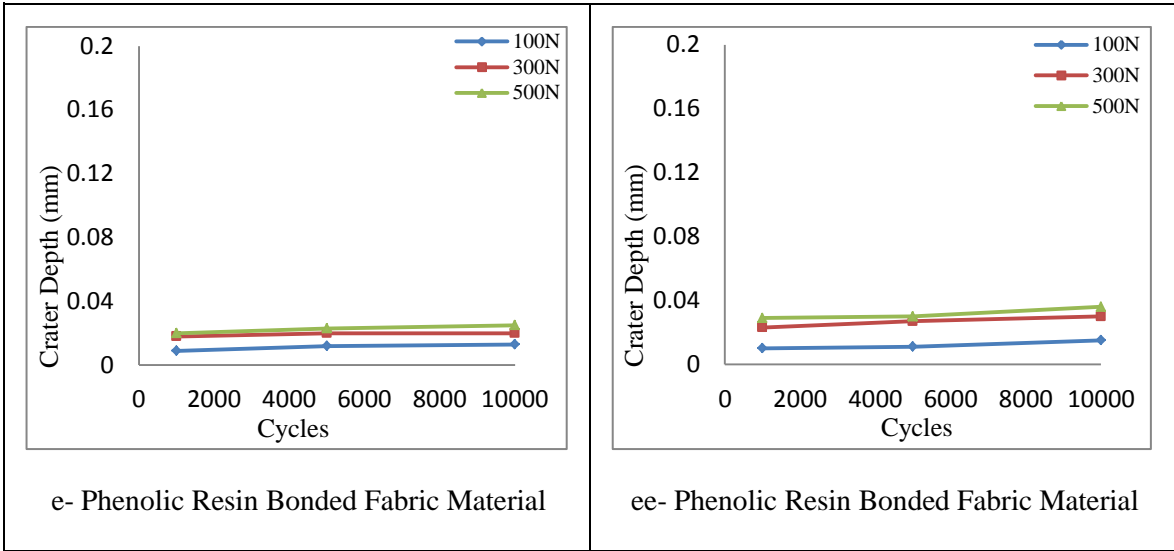


Figure 5:5- Crater Depth of End Post Materials in Dry and Wet Impact Tests.

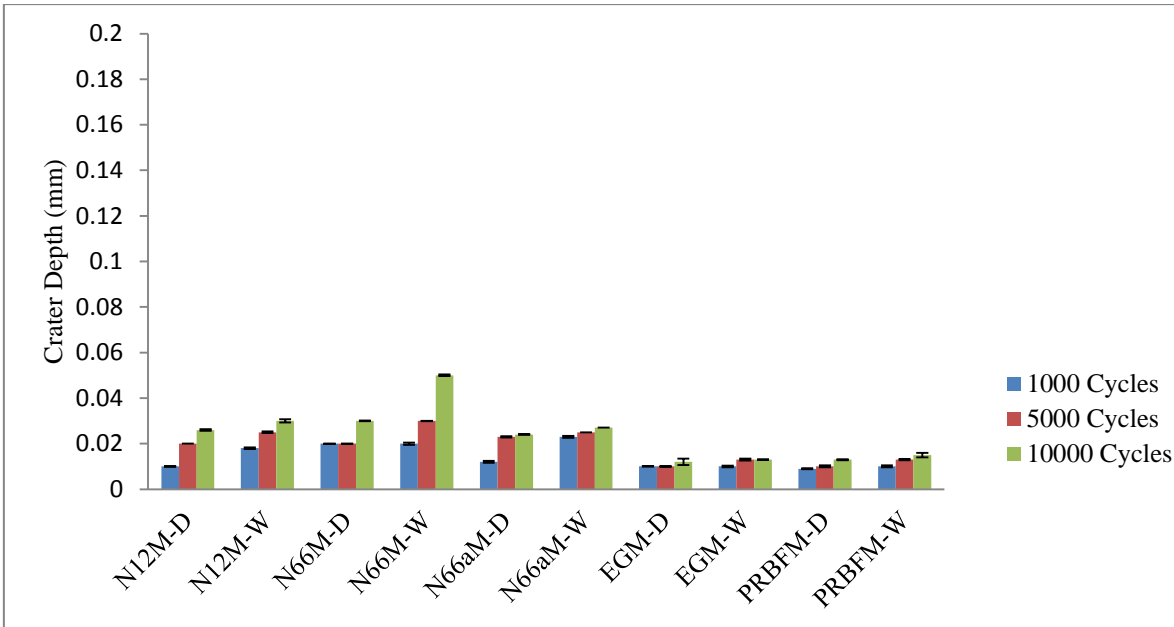


Figure 5:6- Impact Test for All End Post Materials in Dry and Wet Conditions at an Applied Load of 100 N and 1000 cycles, 5000 cycles and 10,000 cycles.

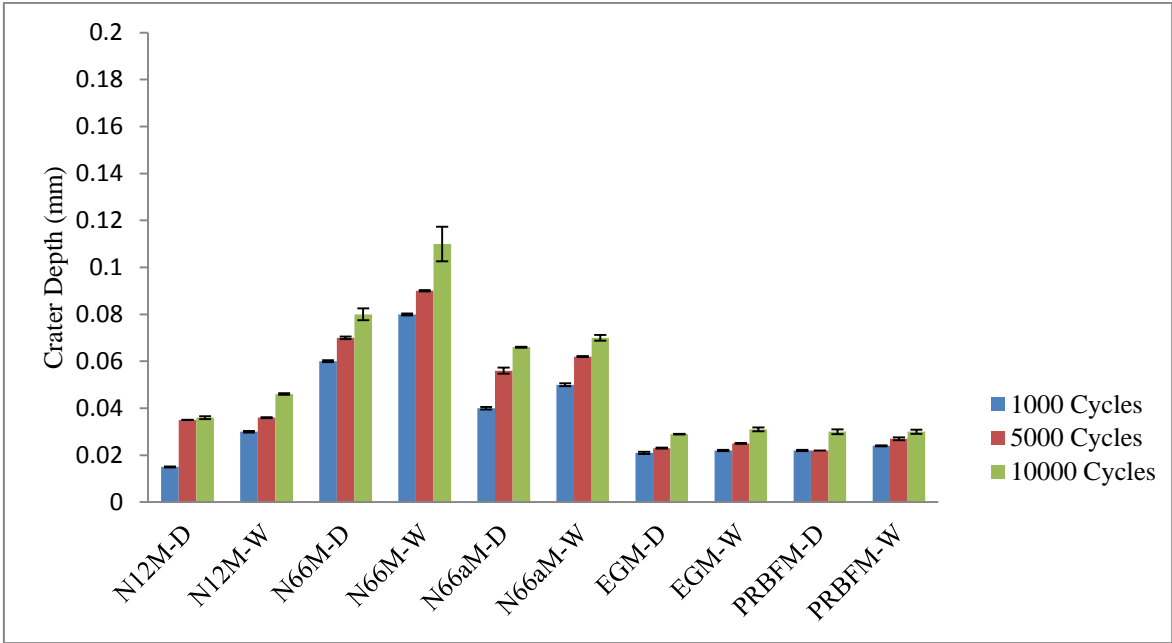


Figure 5:7- Impact Test for All End Post Materials in Dry and Wet Conditions at an Applied Load of 300 N and 1000 cycles, 5000 cycles and 10,000 cycles.

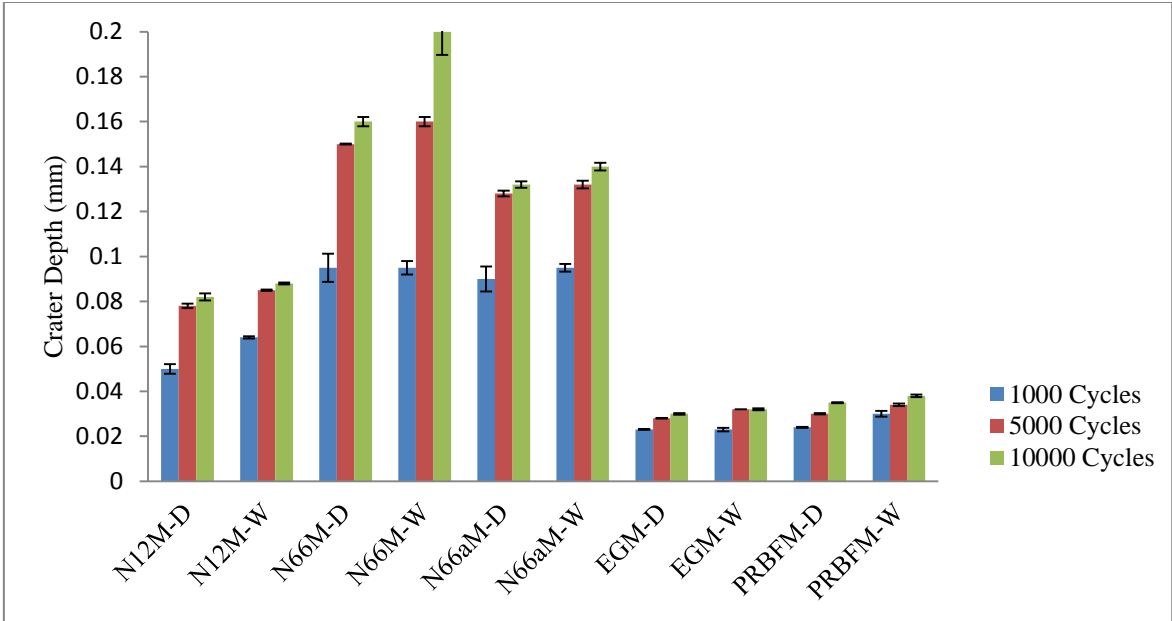


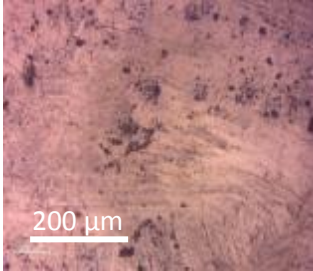
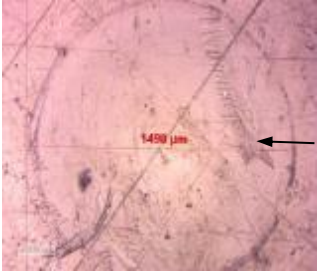
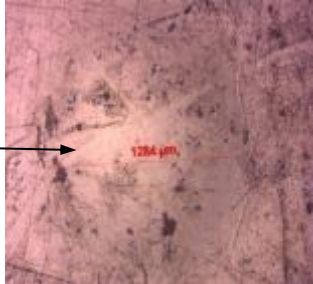
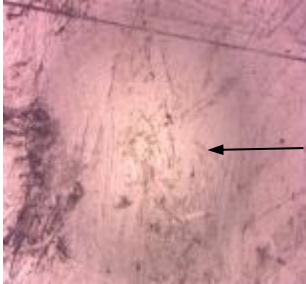
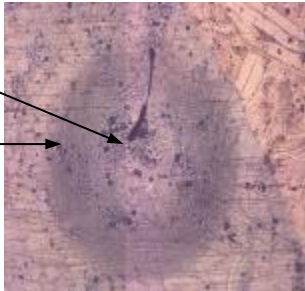
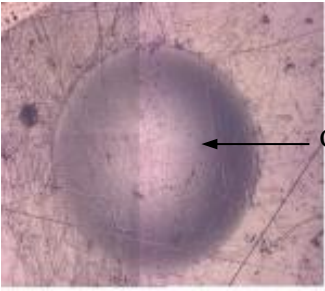
Figure 5:8- Impact Test for All End Post Materials in Dry and Wet Conditions at an Applied Load of 500 N and 1000 cycles, 5000 cycles and 10,000 cycles.

Crater depth and diameter were measured by microscope and profilometer as discussed in Section 3.5.4. These show how much the materials were damaged under the effect of test conditions. As illustrated in Figures 5.1 to 5.8, the crater diameter and depth grow with the

same trend with cycles for each material. Wear/material displacement was higher for Nylon than composite type materials.

5.2.2- Wear Images

Figures 5:9 to 5:11 show the damaged contact surfaces for Nylon 66, Epoxy Glass and Phenolic Resin Bonded Fabric specimens caused by impact wear after the tests (for more images see Appendix B). For all images the scale bar was 10 mm = 200 μ m.

| | Images of Wear in Dry Tests Condition | Images of Wear in Wet Tests Condition |
|------------------------|--|--|
| 100N and 1000 Cycles |  <p style="text-align: center;">a</p> |  <p style="text-align: center;">aa</p> |
| 100N and 10,000 Cycles |  <p style="text-align: center;">b</p> |  <p style="text-align: center;">bb</p> |
| 300N and 1000 Cycles |  <p style="text-align: center;">c</p> |  <p style="text-align: center;">cc</p> |

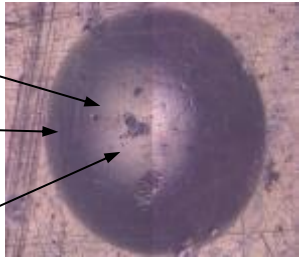
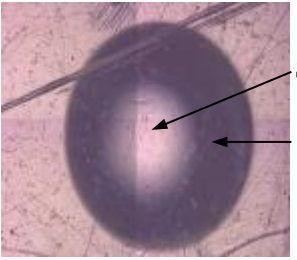
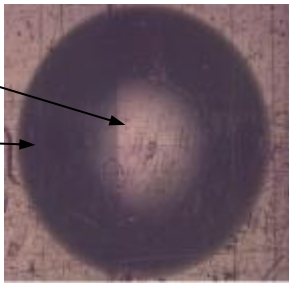
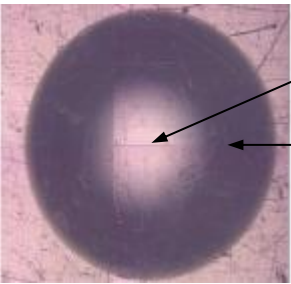
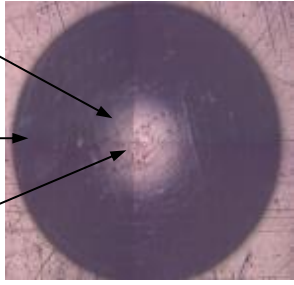
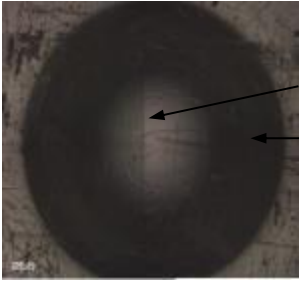
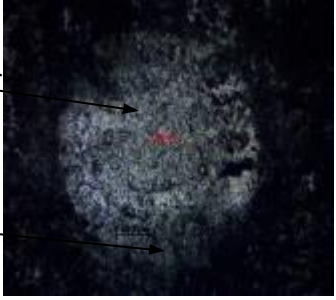
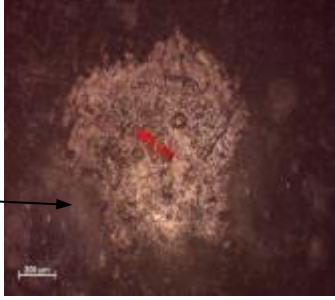
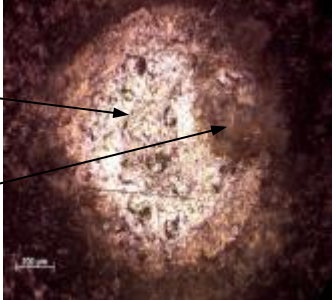
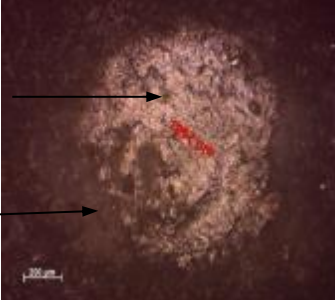
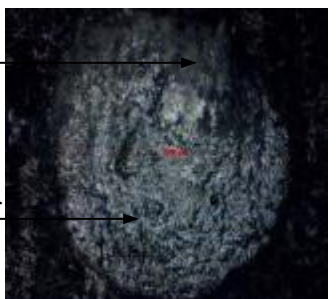

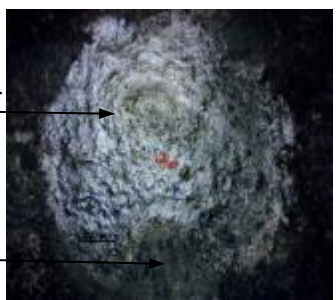
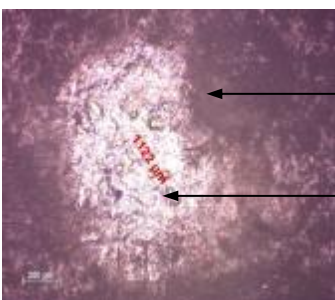
| | | |
|------------------------|--|---|
| 300N and 10,000 Cycles |  <p>Pits Crater Smoother</p> <p>d</p> |  <p>Smoother Crater</p> <p>dd</p> |
| 500N and 1000 Cycles |  <p>Smoother Crater</p> <p>e</p> |  <p>Smoother Crater</p> <p>ee</p> |
| 500N and 10,000 Cycles |  <p>Smoother Crater Pits</p> <p>f</p> |  <p>Smoother Crater</p> <p>ff</p> |

Figure 5:9- Wear Images of Nylon 66 Material at Forces of 100 N, 300 N and 500 N and 1000 Cycles and 10,000 Cycles in both Dry and Wet Conditions.

| | Images of Wear in Dry Test Condition | Images of Wear in Wet Test Condition |
|------------------------|--|--|
| 100N and 1000 Cycles |  <p>a</p> |  <p>aa</p> |
| 100N and 10,000 Cycles |  <p>b</p> |  <p>bb</p> |
| 300N and 1000 Cycles |  <p>c</p> |  <p>cc</p> |
| 300N and 10,000 Cycles |  <p>d</p> |  <p>dd</p> |

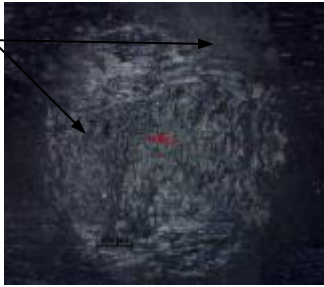
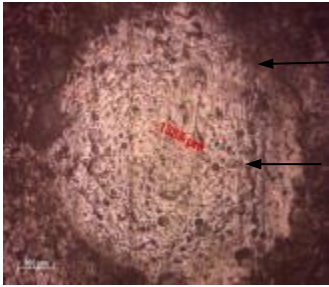
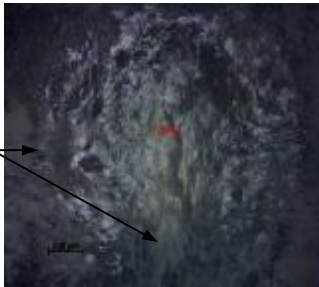
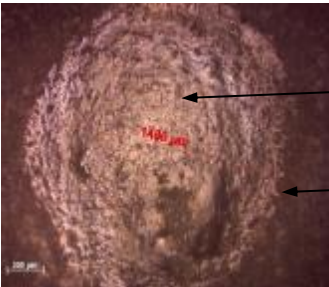



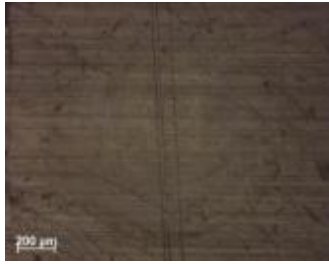


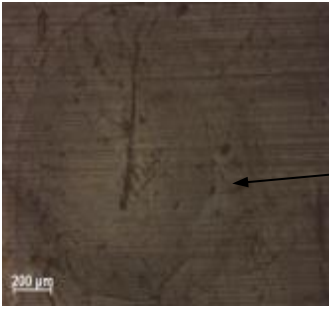
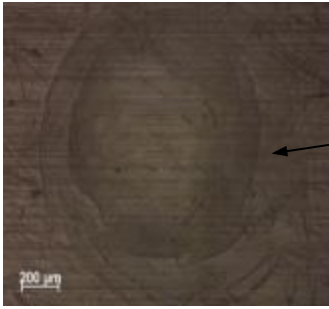
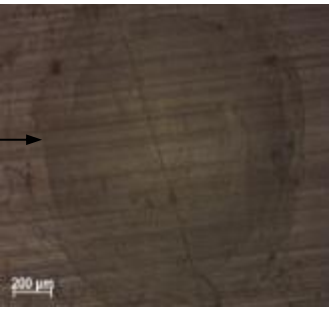
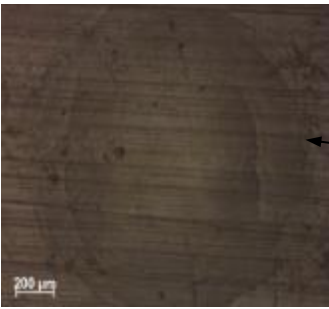
| | | |
|------------------------|--|--|
| 500N and 1000 Cycles |  <p data-bbox="327 271 411 293">Powder</p> <p data-bbox="579 568 595 591">e</p> |  <p data-bbox="1310 293 1394 315">Powder</p> <p data-bbox="1294 394 1378 416">Smoother</p> <p data-bbox="1114 568 1145 591">ee</p> |
| 500N and 10,000 Cycles |  <p data-bbox="327 779 411 801">Powder</p> <p data-bbox="579 972 595 994">f</p> |  <p data-bbox="1294 723 1378 745">Smoother</p> <p data-bbox="1294 824 1378 846">Powder</p> <p data-bbox="1114 972 1145 994">ff</p> |

Figure 5:10- Wear Images of Epoxy Glass Material at Forces of 100 N,300 N and 500 N and 1000 Cycles and 10,000 Cycles in both Dry and Wet Conditions.

| | Images of Wear in Dry Test Condition | Images of Wear in Wet Test Condition |
|----------------------|--|--|
| 100N and 1000 Cycles |  <p data-bbox="579 1738 595 1760">a</p> |  <p data-bbox="1114 1738 1145 1760">aa</p> |

| | | |
|------------------------|--|--|
| 100N and 10,000 Cycles |  <p data-bbox="582 544 603 573">b</p> |  <p data-bbox="1114 544 1150 573">bb</p> |
| 300N and 1000 Cycles |  <p data-bbox="582 954 603 983">c</p> |  <p data-bbox="1114 954 1150 983">cc</p> |
| 300N and 10,000 Cycles |  <p data-bbox="582 1373 603 1402">d</p> |  <p data-bbox="1114 1373 1150 1402">dd</p> |
| 500N and 1000 Cycles |  <p data-bbox="582 1798 603 1827">e</p> |  <p data-bbox="1114 1798 1150 1827">ee</p> |

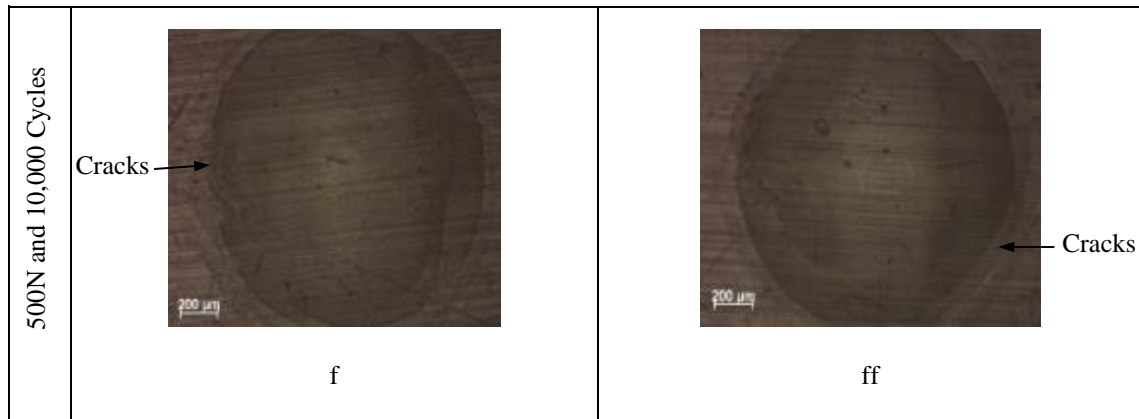


Figure 5:11- Wear Images of Phenolic Resin Bonded Fabric Material at Forces of 100 N, 300 N and 500 N and 1000 Cycles and 10,000 Cycles in both Dry and Wet Conditions.

5.3- Discussion

As shown from the previous figures, the wear resistance of the studied end post materials in dry and wet test conditions at applied forces of 100N, 300N and 500N and number of cycles of 1000 cycles, 5000 cycles and 10,000 cycles are demonstrated.

5.3.1- Thermoplastic Materials

5.3.1.1- Nylon 12 Material

Figures 5:1 a and aa and 5:5 a and aa show that, the crater diameter of specimens in dry and wet conditions did not change much with cycles, but the depth did increase though. There was not a big difference in crater size between wet and dry tests. Nylon 12 material has the lowest crater size of all Nylon materials (see Figures 5:2 to 5:4 and 5:6 to 5:8).

5.3.1.2- Nylon 66 Material

In Figures 5:1 b and 5:5 b through the tests, there was a significant growth in crater depth and width with cycles and loads. In Figures 5:1 bb and 5:5 bb, crater size was significantly larger in the wet condition than the dry condition (as with sliding tests the material softened therefore making it less resistant to impact). In Figures 5:2 to 5:4 and 5:6 to 5:8, it possible to observe that the crater depth and width were larger than the crater depth and width of all other materials. The contact surface of the material experienced compression/deformation as shown in Figures 5:9 and 5:12.

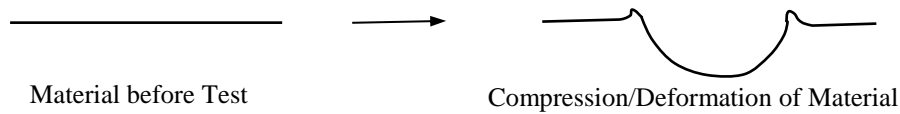


Fig. 5:12- Schematic of N 66 Material Wear Mechanisms.

5.3.1.3- Nylon 66a Material

In Figures 5:1 c and cc and 5:5 c and cc, it can be seen that, the behaviour of material was very similar to Nylon 66, but damage was a bit lower and the material displacement/compression in wet tests was slightly higher than the material displacement/compression in dry conditions. The failures observed here are happening to the end post in reality as mentioned in Section 1.7.2 and seen in Figure 1:25.

5.3.2- Thermosetting Materials

5.3.2.1- Epoxy Glass Material

Crater depth and width grew from the beginning of the test to 5000 cycles, but not much more up to 10,000 cycles. The crater diameter grew with increased load, but depth stayed constant with load. The crater size was not affected by water (see Figures 5:1 d and dd and 5:5 d and dd). The crater size was lower than all other materials (see Figures 5:2 to 5:4 and 5:6 to 5:8). As can be seen in Figures 5:10 and 5:13 the craters had a smoother internal surface and powder was seen in and around the crater.

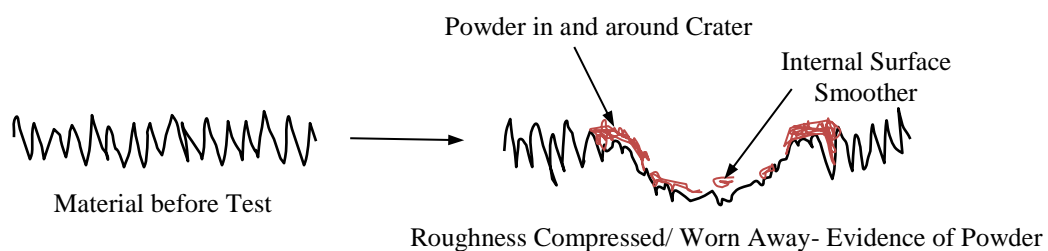


Fig. 5:13- Schematic of EG Material Wear Mechanisms.

5.3.2.2- Phenolic Resin Bonded Fabric Material

As can be seen in Figures 5:1 e and 5:5 e, crater width grew with increased number of cycles, but depth did not grow. The crater depth and width increased when load increased from 100 N to 300 N, but at 500 N it was no higher. The crater size of specimens in wet tests was approximately the same as those in dry condition. In Figures 5:2 to 5:4 and 5:6 to

5:8, the craters size of PRBF material were higher than the craters size of the EG material, but lower than all the Nylon materials. As can be observed in Figures 5:11 and 5:14, the damage mechanism was material displacement/compression (layers of material compressed with impact and cracks around the crater edges). Cracks and displacement that were observed in this test are one of the common failures which occur frequently to the end post in railway networks as mentioned in section 1.7.2 and seen in Figure 1:25. The cracks were only evident above 300 N and then only after 5000 cycles.

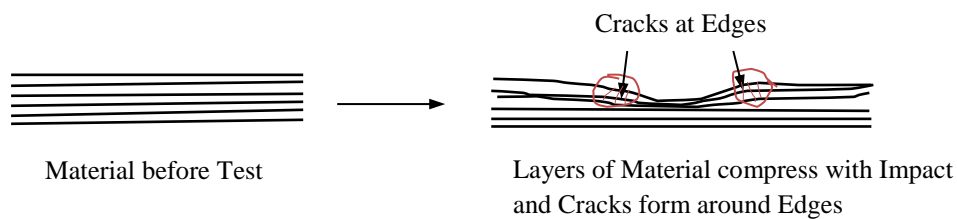


Fig. 5:14- Schematic of PRBF Material Wear Mechanisms.

5.4- Summary

From experimental results, two states of impact wear of end post materials under study were observed. The first state relates primarily to material displacement/compression and no material loss with cracks formed around edges of PRBF material (see Figures 5:12 and 5:14) and a second state, which results in material loss where the surface became smoother and powder appeared. This is in agreement with Bayer [68].

Crater sizes of all materials were affected by cycles and loads. The crater depths and widths of N 12, N 66 and N 66a materials were affected by water, but the crater dimensions of EG and PRBF materials was not affected by water. In the case of dry test conditions, the end post material of Epoxy Glass has higher impact wear resistance, followed by Phenolic Resin Bonded Fabric, Nylon 12 and Nylon 66a and Nylon 66 materials. The dominant failure mode in this test was compression with no material loss for thermoplastic materials and deformation with material loss for Epoxy Glass material and compression with cracks around crater edge for Phenolic Resin Bonded Fabric material. The End post material of Epoxy Glass has more impact failure resistance in wet test conditions followed by Phenolic Resin Bonded Fabric, Nylon 66a and Nylon 66 materials respectively. The Nylon 12 material has the highest material displacement/compression

resistance in the “thermoplastic” materials group and the Epoxy Glass material has the highest wear resistance in the “thermosetting” materials group. But the Epoxy Glass material has the greatest wear resistance of all end post thermoplastic and thermosetting materials under study.

6- Lipping Tests

6.1- Introduction

Tests have been conducted to determine the appropriate width of end post materials, which prevents contact between adjacent rails when metal flow occurs and is appropriate to protect the end post materials from excess loads and operating conditions (see Table 3:1 (3 and 5)). The work was divided into two separate tests as mentioned in Section 3.5.2:

- The first test was a 100% sliding ratio lipping test (see Section 3.5.2.1). This test was implemented on the Block-on-Ring rig (see Section 3.2.1) at sliding speeds of 7.2 m/sec., under a constant load of 50 N and during a period of 60 minutes. The end post width was 1 mm.
- The second test was a partial slip ratio (1%) lipping test (see Section 3.5.2.2). This test was carried out on a twin-disc machine (see Section 3.2.2) at a rotating speed of 400 rpm. Table 6:1 summarizes the test conditions.

Table 6:1- Partial Slip Ratio 1% Lipping Test Conditions.

| Disc No. | End Post Width (mm) | Contact Pressure (MPa) | Slip % | No. of Cycles |
|----------|---------------------|------------------------|--------|---------------|
| R1 | 0.5 and 1 | 900 | 1 | 2000 |
| R2 | 0.5 and 1 | 900 | 1 | 20,000 |
| R3 | 0.5 and 1 | 1500 | 1 | 2000 |

The tests were implemented at room temperature and humidity.

6.2- Specimens

6.2.1- 100% Slip

The samples under study in the 100% slip tests were steel block (rail material) and epoxy glass end post material against railways wheel steel. The rail steel block was machined into a 5mm x 5mm x 32mm section and arranged like an actual joint, as shown in Figure 3:17. A section of epoxy glass material was cut from an actual end post into a 1mm x 5mm x 32mm piece and arranged between the steel blocks like the actual joint (see Figure 3:17).

6.2.2- Partial Slip

The specimens tested in the partial slip tests were three rail steel discs (R1, R2, and R3) and epoxy glass end post material; each disc was machined with 3 slots, 0.5mm x 10mm x 3mm, and 3 slots, 1mm x 10mm x 3mm and filled with a section of epoxy glass material cut from an actual end post (see Figures 3:18 and 6:1).

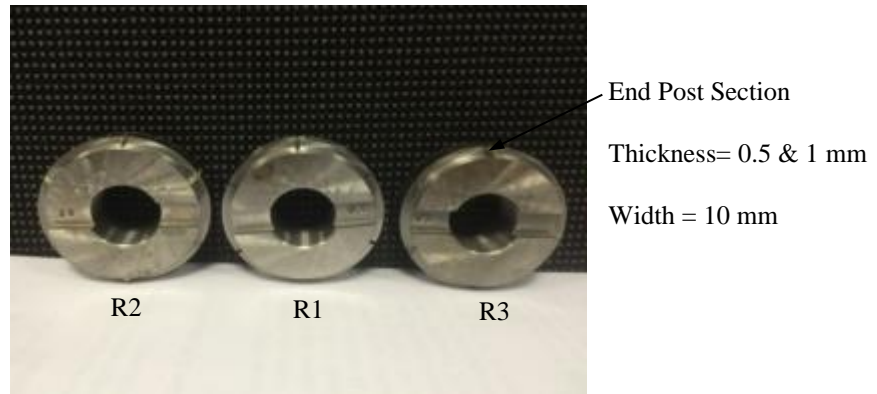


Fig. 6:1- Rail Steel Disc and Epoxy Glass End Post Materials (R1, R2 and R3).

The discs shown in Figure 6:1 were tested in the following conditions:

- R1: 900 MPa and 2000 Cycles
- R2: 900 MPa and 20,000 Cycles
- R3: 1500 MPa and 2000 Cycles

6.3- Results

6.3.1- 100% Slip Ratio Lipping Test

Metal flow length data obtained from the 100% Slip Ratio Lipping tests is shown in Figures 6:2-6:4. All tests were repeated two and three times then compared together

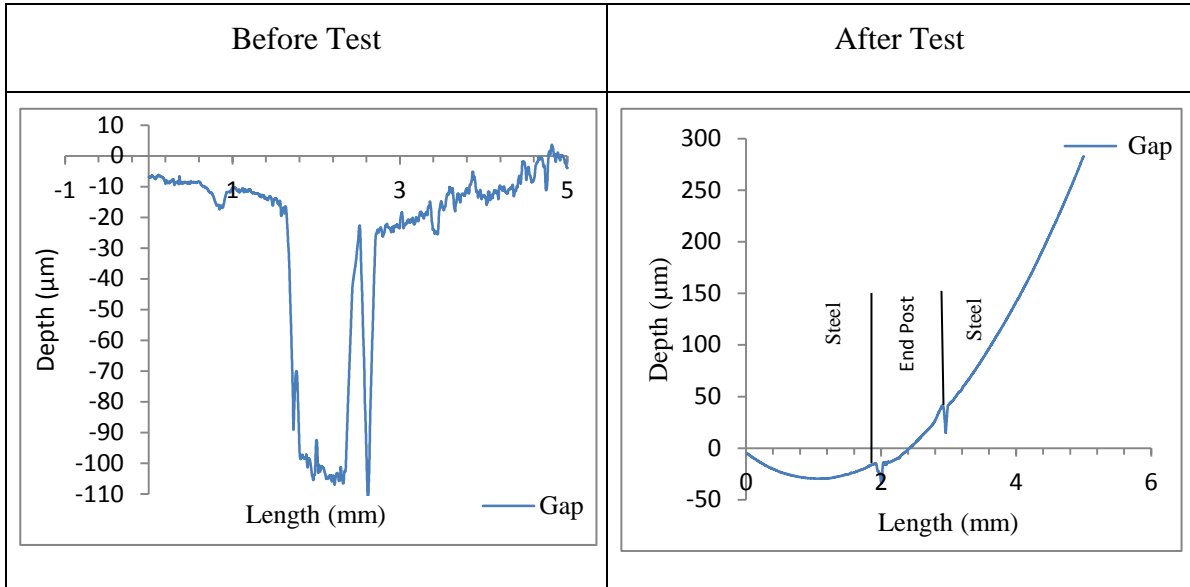


Fig. 6:2- End Post Thickness before and after the Test.

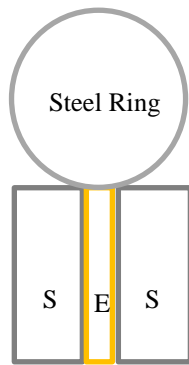


Fig. 6:3- Schematic Gap before Test

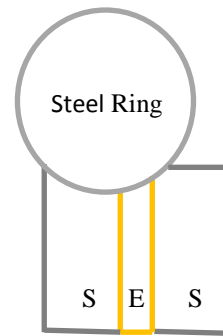


Fig. 6:4- Schematic Gap after Test

6.3.2- 100% Slip Ratio Lipping Test Images

The 100% slip ratio lipping tests images obtained from experimental work to determine appropriate width of end post materials are shown in Figure 6:5. The image scale bar was (10 mm = 100 µm).



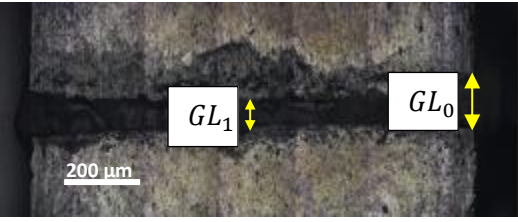
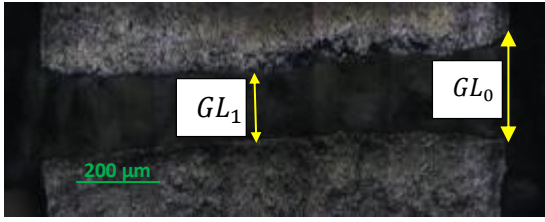
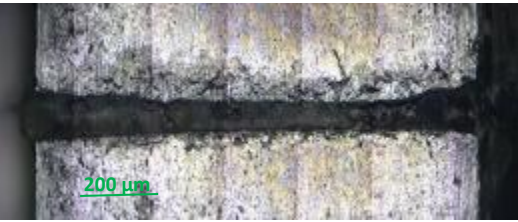

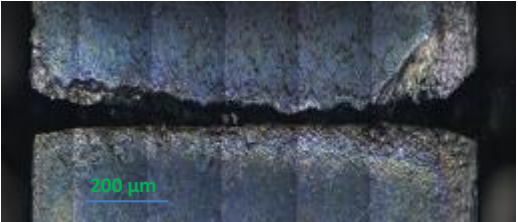
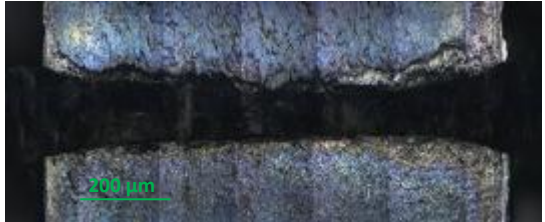
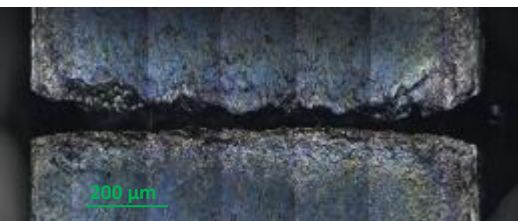

Fig. 6:5- Length of Gap Image after the Test.

6.3.3- Partial Slip Ratio (1%) Lipping Test

Metal flow length data obtained from the partial slip ratio (1%) lipping tests to determine appropriate thickness of end post materials are shown in Figures 6:6 and 6:7. Figure 6:6 illustrate deformation occurred during the test and Figures 6:6 and 6:7 show the metal flow and deformation.

6.3.4- Partial Slip Ratio (1%) Lipping Test Images

The metal flow and deformation images collected from the partial slip ratio of 1% lipping tests are displayed in Figure 6:6. All images scale bar was (0.1 mm = 200 μm).

| | End Post Material Width of 0.5 mm | End Post Material Width of 1 mm |
|--------------------------------|---|--|
| 900 MPa and 2000 Cycles (R1) |  |  |
| |  |  |
| 900 MPa and 20,000 Cycles (R3) |  |  |
| |  |  |

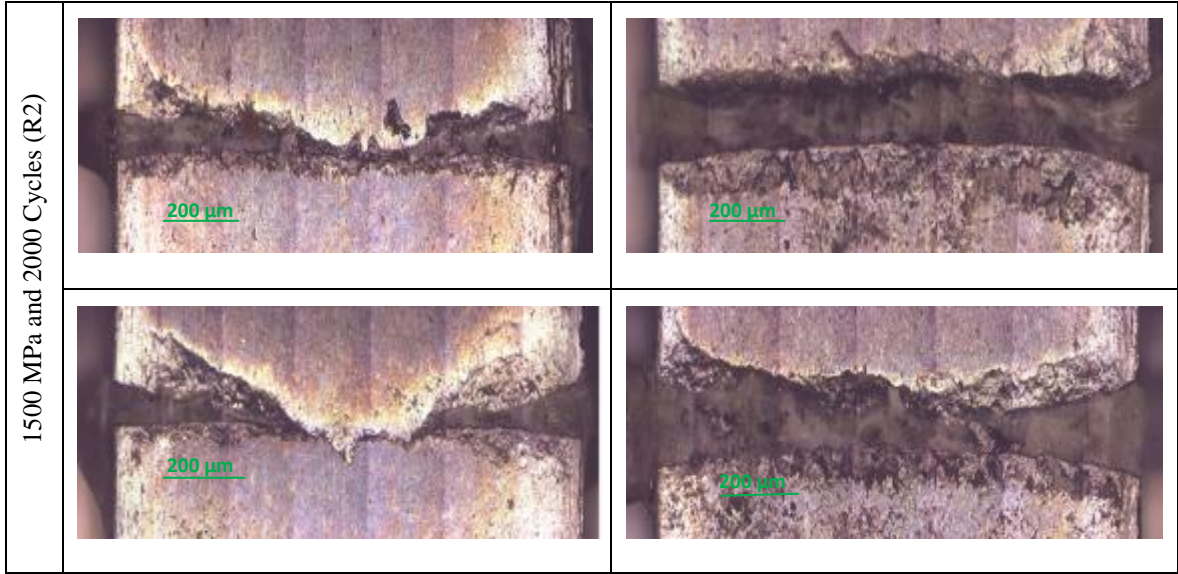


Fig. 6:6- Gaps Length Images after the Test.

Figure 6:7 summaries the average length of metal flow at all test conditions. The average length has been calculated from images in Figure 6:6.

Example calculation of (Figure 6:6):

$$\text{Average Metal Flow Length } MFL = \frac{MFL_2 + MFL_4 + MFL_6}{3} \quad (13)$$

where, $MFL_1 = GL_0 - GL_1$

$MFL_3 = GL_0 - GL_3$

$MFL_5 = GL_0 - GL_5$

MFL_1, MFL_3 and MFL_5 = Metal Flow Length of Gap 1, 3 and 5

GL_0 = Gap length before the test

GL_1, GL_3 and GL_5 = Gap Length 1, Gap Length 3 and Gap Length 5 after the test.

The average length of metal flow (MFL) was calculated by equation (13).

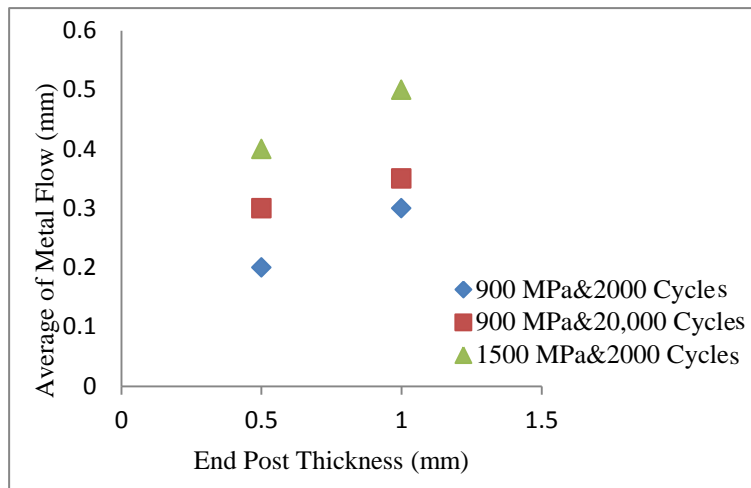


Fig. 6:7. Average Length of Lip (mm).

6.4- Discussion

As can be seen from the Figures 6:5 and 6:8 to 6:10 plastic deformation and metal flow appeared in the 100% slip test and the partial slip (1%) test.

6.4.1- 100% Sliding Slip Test

Figures 6:2 and 6:5 shows that, there was a significant effect on the gap size at a sliding speed of 7.2 m/sec and applied load of 50 N, where the steel edges were flattened, wore and lipped. This is due to the 100% slip.

6.4.2- Partial Slip (1%) Test

6.4.2.1- End Post Width of 0.5 mm

In Figures 6:6 and 6:7, it is possible to see that the steel flows over the end post becoming flattened, battered and lipped. This is caused by high cyclic loads and partial slip. The deformation and gap size were changed with contact pressure and cycles and metal flow (see Figure 6:7). This type of failure commonly occurs in reality in railway networks as mentioned in Section 1.7.2 and shown in Figures 1:21, 1:24 and 1:25. In the case of a contact pressure of 900 MPa and 2000 cycles, as can be seen in Figure 6:8, the damage was severe battering and slight metal flow (see Figure 6:7). While the damage in disc R2 in the case of a contact pressure of 900 MPa and 20,000 cycles was significant flattening, battering and steel flow (see Figures 6:6 and 6:7). Moreover, the plastic deformation in the

case of contact pressure of 1500 MPa and number of cycle of 2000 cycles on R3 led to flattening and severe steel flow (see Figures 6:6-6:8)

6.4.2.2- End Post Width of 1 mm

As can be seen In Figures 6:6, testing led to edges over the end post being flattened, battered and to steel flow occurring. These happened due to cyclic loads and high impact force because the gap between adjoining steel rails was excessive. The damage in the test on R1 was flattening, battering (see Figure 6:6) and steel flow as shown in Figure 6:7, but the failure observed on R2 after the test was a significant flattening, battering (see Figure 6:6) and plastic flow (see Figure 6:7). Whilst in case of contact pressure of 1500 MPa and 2000 cycles for disc specimen R3, as can be observed in Figures 6:6 and 6:9, was a severe flattening and battering and steel flow over the end post (see Figures 6:6 and 6:9). The average length of metal flow in the case of end post thickness of 0.5 mm was approximately 0.44 mm at contact pressure of 1500 MPa and 2000 cycles, but in one case the metal flow length was approximately 0.54 mm in the same test condition. In the case of the end post thickness of 1 mm the average metal flow length was approximately 0.54 mm. So 0.54 mm was the highest length of metal flow in this test and this is equivalent to 6 mm in a real joint. In this case, the small gap size led to contact between adjacent rails when metal flow occurred as shown in Figures 6:8 and 6:9 in case of 1500 MPa and 2000 cycles, that will cause the passage of electric current from one rail to the other rail, and the large gap size led to an increase in impact force which affects insulated joints (joint bars, bolts and isolation) and rail edges. The end post thickness of 6 mm is therefore not ideal to use. This result validated the output of Wu et al. [100].



Fig. 6:8- R3 Specimen Imitating Rail Head Deformation over the Insulating End Post (0.5 mm)



Fig.6:9- R3 Specimen Imitating Rail Head Deformation over the Insulating End Post (1 mm)

6.5- Summary

There was a significant growth in deformation and metal flow with increasing contact pressure and cycles in both cases on end post widths of 0.5 mm and 1 mm as shown in Figures 6:6 and 6:7. There was a difference in metal flow in the case of a 1 mm end post width to a 0.5 mm end post width under the same test conditions (see Figure 6:6). This was probably due to the increase of impact force when the gap size increases.

7- Rolling/Sliding Tests

7.1- Introduction

Testing was carried out to evaluate the performance of Nylon 12, Nylon 66, Nylon 66a, Epoxy glass and phenolic risen bonded fabric materials in a rolling/sliding test (see Table 3:1 (3)). The tests were carried out on a twin-disc machine (see Section 3.2.2) in dry and wet conditions. Table 7:1 summarises the test conditions.

Table 7:1- Rolling/Sliding Test Conditions.

| Rotation Velocity (rpm) | Dry and Wet Test Conditions | | |
|----------------------------|-----------------------------|----------------------|---------------|
| | Slip Ratio 1% | Contact Pressure MPa | No. of Cycles |
| 400 | 1 | 200 | 12,000 |

7.2- Specimens

The disc specimens were cut out from real end posts of Nylon 12, Nylon 66, Nylon 66a, Epoxy Glass and phenolic Resin Bonded Fabric materials and wheel steel sections. The disc specimens had a diameter of 46 mm and a contact width of 10 mm and contact surface roughness of 1 micron (see Figure 7:1).

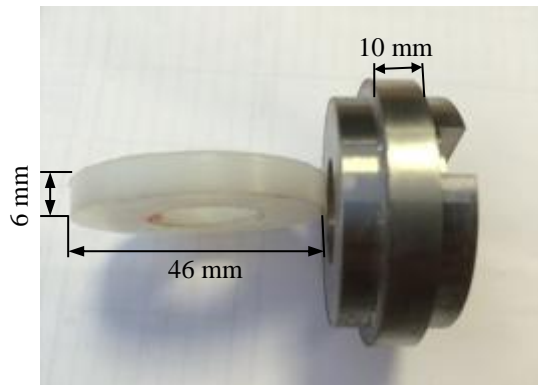


Fig. 7:1- Disc Specimens of End Post and Steel Wheel

7.3- Results

7.3.1- Worn Surface Images

Figure 7:2 shows the damaged contact surfaces for Nylon 12, Nylon 66, Nylon 66a, Epoxy Glass and Phenolic Resin Bonded Fabric specimens.

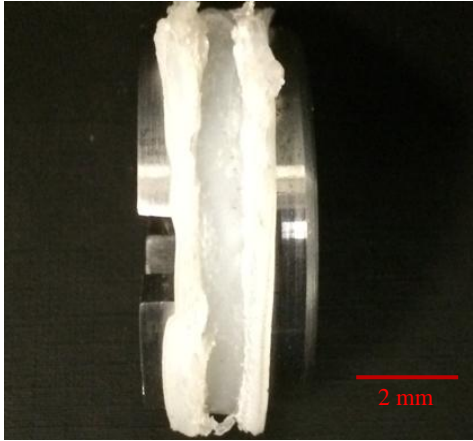
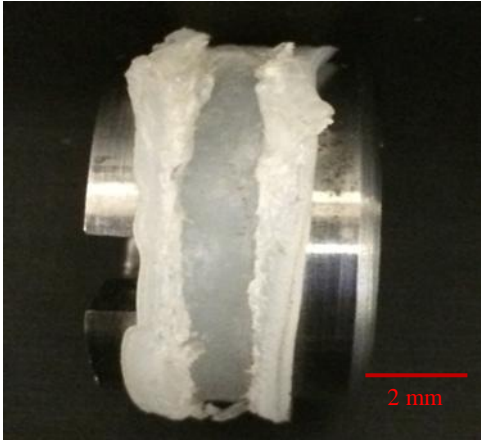
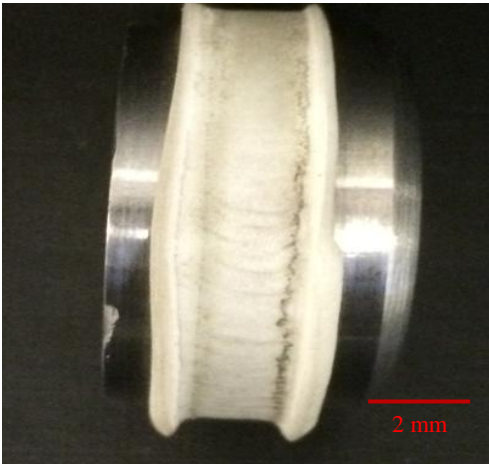
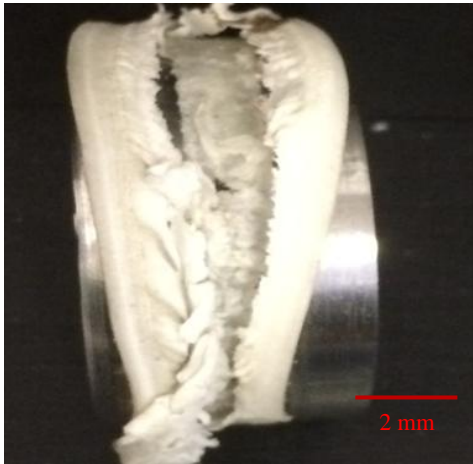
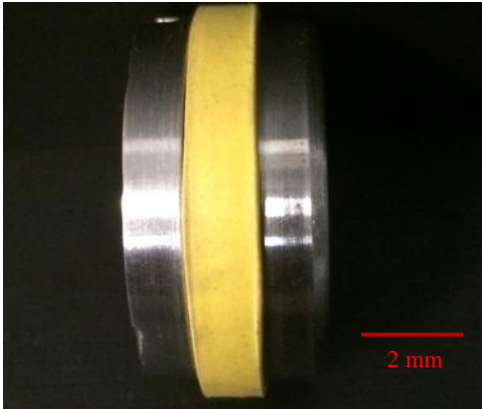
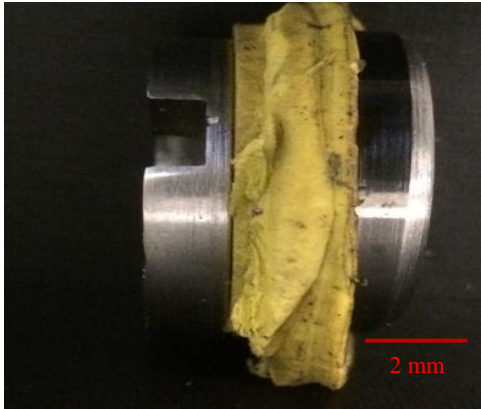
| | Dry Test | Wet Test |
|------------------|--|--|
| Nylon 12 (N12) |  <p>A photograph showing a cross-section of a white, fibrous material (Nylon 12) between two metal rollers. The material appears relatively intact but has some fraying at the edges. A red scale bar labeled "2 mm" is located in the bottom right corner.</p> |  <p>A photograph showing a cross-section of a white, fibrous material (Nylon 12) between two metal rollers after a wet test. The material is significantly more frayed and disintegrated compared to the dry test. A red scale bar labeled "2 mm" is located in the bottom right corner.</p> |
| Nylon 66 (N66) |  <p>A photograph showing a cross-section of a white, fibrous material (Nylon 66) between two metal rollers. The material shows some internal layering and fraying. A red scale bar labeled "2 mm" is located in the bottom right corner.</p> |  <p>A photograph showing a cross-section of a white, fibrous material (Nylon 66) between two metal rollers after a wet test. The material is heavily frayed and disintegrated. A red scale bar labeled "2 mm" is located in the bottom right corner.</p> |
| Nylon 66a (N66a) |  <p>A photograph showing a cross-section of a yellow, fibrous material (Nylon 66a) between two metal rollers. The material appears relatively intact. A red scale bar labeled "2 mm" is located in the bottom right corner.</p> |  <p>A photograph showing a cross-section of a yellow, fibrous material (Nylon 66a) between two metal rollers after a wet test. The material is heavily frayed and disintegrated. A red scale bar labeled "2 mm" is located in the bottom right corner.</p> |



Fig. 7:2- Specimens Tested Surface Images of Nylon 12, Nylon 66, Nylon 66a, Epoxy Glass and Phenolic Resin Bonded Fabric Materials.

7.4- Discussion

The twin-disc test was employed to examine resistance of five end post materials of Nylon 12, Nylon 66, Nylon 66a, Epoxy Glass and Phenolic Resin Bonded Fabric materials for wear caused by rotating/sliding contact. This test provides a simulation of the rolling/sliding contact. The results obtained from the tests displayed the material wear resistance and wear mechanisms.

7.4.1- Thermoplastic Materials

The thermoplastic materials are the end post materials of Nylon 12 material, Nylon 66 material and Nylon 66a material.

7.4.1.1- Nylon 12, 66, and 66a Materials

Figure 7:2 shows that the Nylon 12, 66 and 66a end post material completely failed. The specimen in this case was subjected to rolling and sliding and it is thought that the failure was largely due to thermal effects induced by the high contact pressure used and the friction from the partial slip. The specimen disc deformation and material moved towards side of contact. In reality the end post would be constrained by rail material on either side. Water application still led to high wear, but reduction in temperature would have been countered by hardness reduction.

7.4.2- Thermosetting Materials

The thermosetting materials are the end post materials of Epoxy Glass material and Phenolic Resin Bonded Fabric material.

7.4.2.1- Epoxy Glass Material

Figure 7:2 shows that there was surface damage on the specimen disc of Epoxy Glass material. This occurred as a result of rolling contact with high contact pressure. However, in wet test condition as shown in Figure 7:2, the wear mechanism was similar to that in dry test condition.

7.4.2.2- Phenolic Resin Bonded Fabric Material

In Figure 7:2, it is possible to observe severe wear of Phenolic Resin Bonded Fabric disc in dry and wet test conditions. This was due to the rolling contact and high contact pressure. Material moved to the sides of contact and particles of the material transferred to steel wheel disc. This occurred as a result of partial slip and high contact pressure (yielding).

7.5- Summary

From the previous results, there was a severe failure of end post materials specimens of Nylon 12, Nylon 66, Nylon 66a and Phenolic Resin Bonded Fabric. The materials failed rapidly. The wear included removal of material (ring shape) from discs. The Epoxy Glass material disc was better than the other materials. The common way to calculate the rolling/sliding contact wear is mass loss or diameter change, but in this study the wear caused by rolling/sliding contact was very clear and no calculation of mass loss was needed. This severe failure that occurred to the materials under study may be due to high

contact pressure and the fact the specimens were free without support unlike the end post in reality which has support from the rail ends.

The test should be improved in the future to simulate reality better. That is by putting the end post materials in a groove that manufactured in the centre of steel disc to provide support for the end post.

8- Static Compression Test

Dipping of rail ends occurs due to wheel loads when they passing over the area of an insulated rail joints (IRJ). This action has an effect on the end post. As the rails dip the gap between the rail ends closes and the top of the end post is compressed. The exact distance can be estimated. The maximum allowable length of dipping of a rail is 3 mm [101]. The assumptions in this case were; the rail dipping occurred for one cycle and bending was in a straight line. By using the Pythagorean Theorem:

Maximum penetration of rail edge in end post $x = 0.01125 \text{ mm}$.

$$\tan \theta = \frac{x}{3}$$

(14)

$$\theta = 0.2148$$

$$0.00375 \times 3 = x$$

$$x = 0.01125 \text{ mm}$$

$$y = 3.00185 \text{ mm}$$

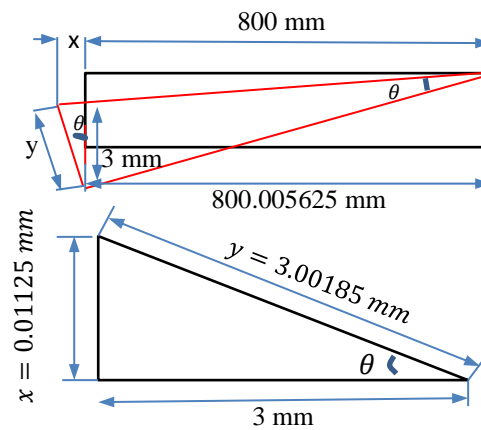


Fig. 8:1- Rail End Bending

8.1- Introduction

Testing was carried to evaluate the performance of end post materials of Nylon 12, Nylon 66, Epoxy Glass and Phenolic Resin Bonded Fabric materials in a static load compression test (see Table 3:1 (2 and 6)) to evaluate the effect of compression due to rail extending and dipping. The test was carried out on a Tiniuse Olsen-H25kN hydraulic test machine (see Section 3.2.5). The specimens were compressed between two steel plates (see Figure 8:2) at rate of the machine of 0.5 mm/min and a pre-load of 100 N. For composite materials in tension, a rate of 1mm/min is standard [102, 103]. Due to the small size of the samples, the rate was lowered so that the strain rate in the material was not too high. The pre-load of 100N was chosen by observing the sample. At around 100N the surfaces of the samples appeared to be flat against the metal plates, meaning that the experiment could start without any slack in the system.

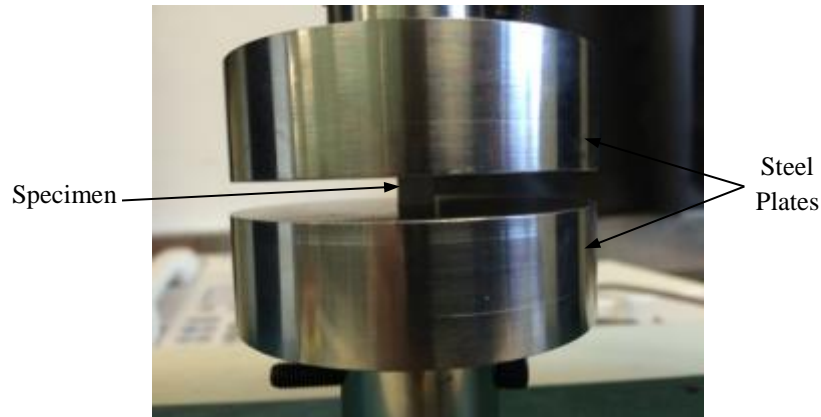


Fig. 8:2- Static Compression Test Set-up.

8.2- Specimens

For each end post material of Nylon 12, Nylon 66, Epoxy Glass and Phenolic Risen Bonded

Fabric materials, three cylindrical specimens were cut out from real end posts, 8 mm in diameter and 6 mm in thick (see Figures 3:27 and 8:3). The specimen size was selected to be suitable for the test machine, where the maximum load of the machine is 25 kN. The output from an finite element model indicated the compressive stress at the top of the end post during bending is about 300 MPa [104]. The suitable area of the specimens related to the stress from the FE model is calculated as follows:

$$\sigma = \frac{F}{A_0} [N/mm^2] \quad (15)$$

where σ = Stress,

F = force (N)

A_0 = original area (mm^2)

A_0 in this test = πr^2

$$300 = \frac{25000}{A_0}$$

$$A_0 = \frac{25000}{300} = 83 \text{ mm}^2$$

Maximum $D \cong 10$ mm

where D is the specimen diameter.

Each test was conducted three times under the same test condition of strain rate, pre-load and environmental condition (i.e temperature and humidity). The damage of material (displacement or rupture) was measured by put the specimens under a certain force and the machine measure a the displacement against the force. The results obtained from experimental work showed that test repeatability was very good.



Fig. 8:3- End Post Materials Specimens (1) PRBF, (2) EG, (3) N12, and (4) N66 Materials.

8.3- Results

8.3.1- Failure Behaviour

The results obtained from experimental work for the end post materials of Nylon 12, Nylon 66, Nylon 66a, Epoxy Glass and Phenolic Resin Bonded Fabric materials using a displacement rate of 0.5 mm/min and pre-load of 100 N are shown in Figures 8:4 to 8:7. Figures 8:4-8:7 summarise the relationship between force and material displacement. Each figure is divided into two or three regions, elastic deformation and plastic deformation (see Figures 8:4 and 8:5), elastic deformation and rupture (see Figure 8:6) and elastic deformation, plastic deformation and fracture (see Figure 8:7).

8.3.1.1- Stress Strain Curves Analysis

The strain for each case was calculated from the following formula:

$$\varepsilon = \frac{\Delta L}{L_0} [mm/mm] \quad (16)$$

where ε = Strain,

$\Delta L = L_1 + L_0$ (displacement)

L_0 = original length (mm),

L_1 = final length (mm),

$L_0 = 6 \text{ mm}$

The stress was calculated from the equation (14)

A_0 in this test = $\pi r^2 = \pi \times 4^2 = 50.24 \text{ mm}^2$

The point where the graph stops being linear is its proportional limit or elastic limit and it is the boundary between the elastic region and plastic region.

Yield strength is the stress amount at the yield point. It is used as a measure of material resistance to permanent deformation. It was calculated by plotting a straight line which is parallel to the young modulus line at 0.2% offset.

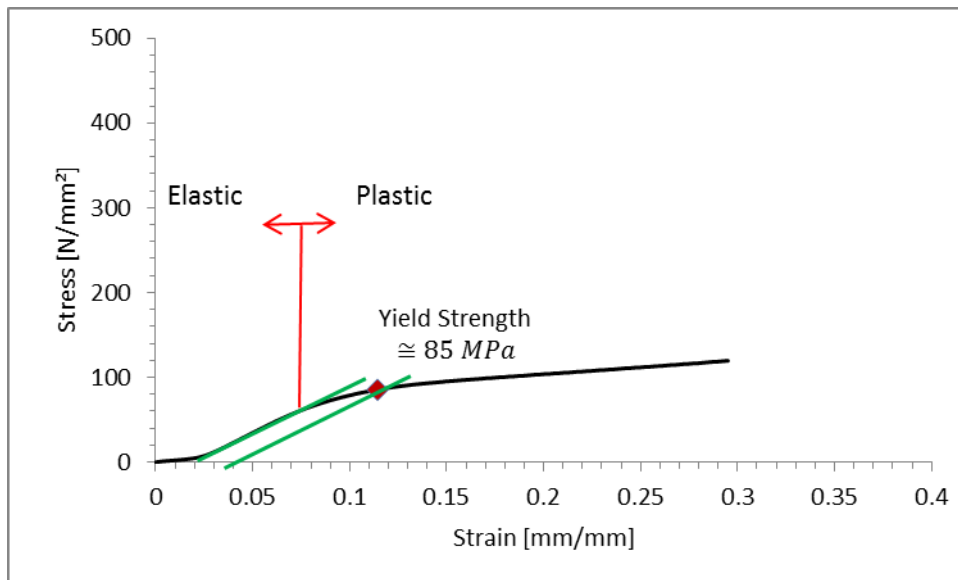


Fig. 8:4- Nylon 12 Stress vs Strain.

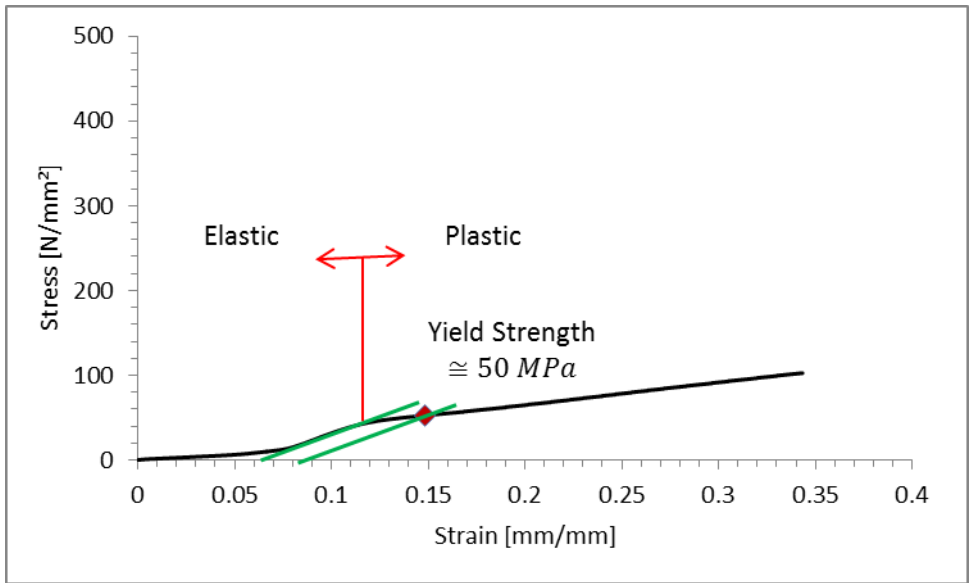


Fig. 8:5- Nylon 66 Stress vs Strain.

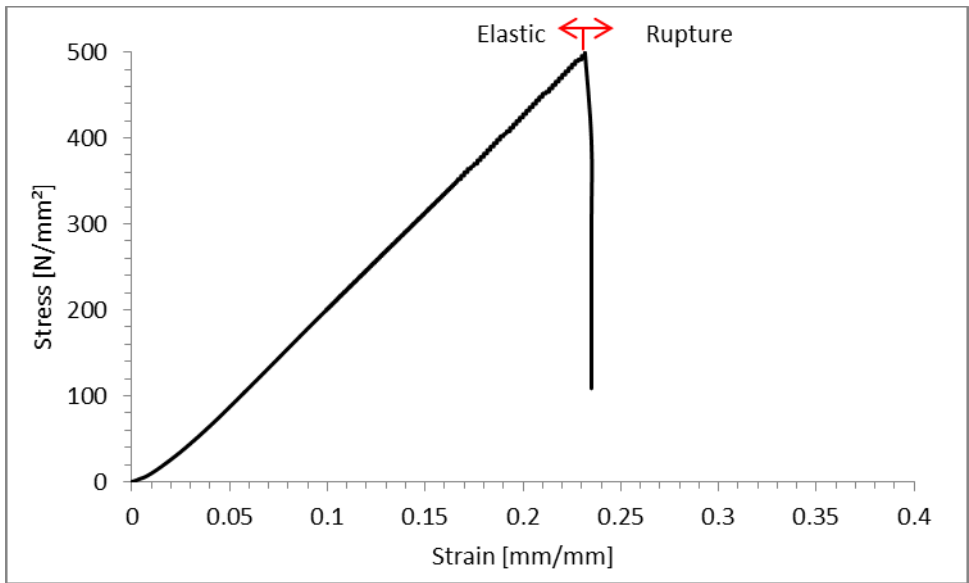


Fig. 8:6- Epoxy Glass Stress vs Strain.

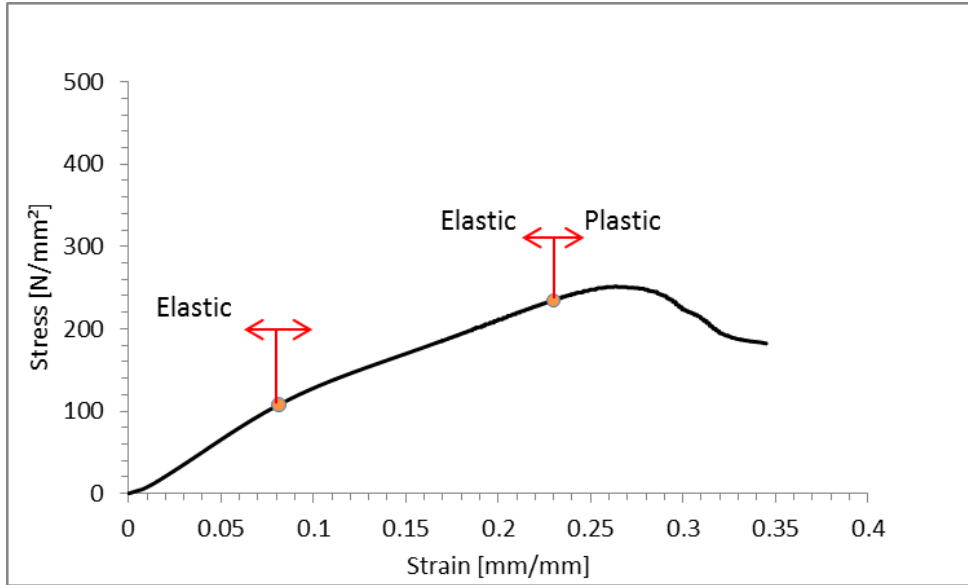


Fig. 8:7- Phenolic Resin Bonded Fabric Stress vs Strain.

Figures 8:8 - 8:17 show the material damage after the tests (i.e; elastic deformation, plastic deformation and fracture).

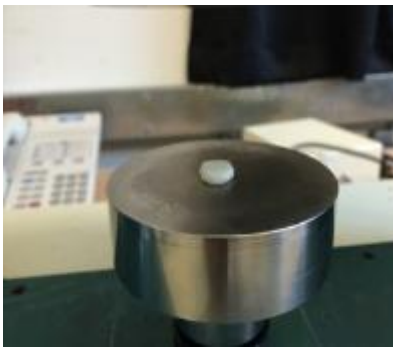


Fig. 8:8- Nylon 12 Material Specimen after Test.

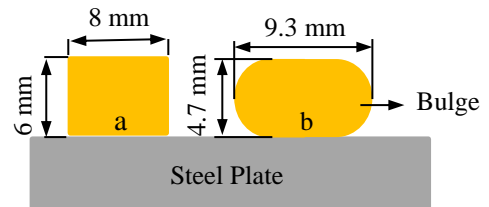


Fig. 8:9- Schematic Diagram of Nylon 12 (a) before Test (b) after Test.



Fig. 8:10- Nylon 66 Material Specimen after Test.

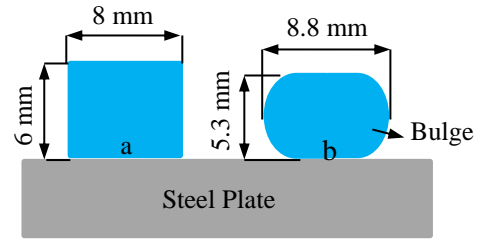


Fig. 8:11- Schematic Diagram of Nylon 66 (a) before Test (b) after Test.

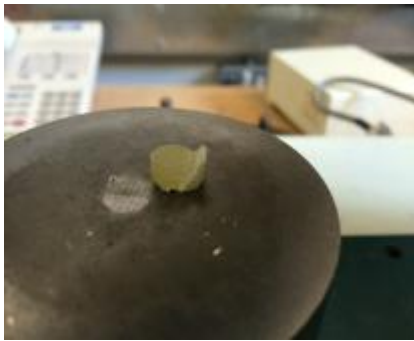


Fig. 8:12- Epoxy Glass Material Specimen after Test.

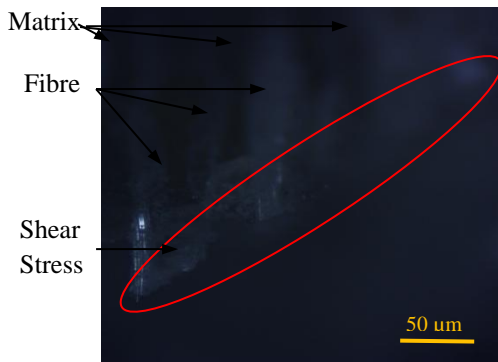
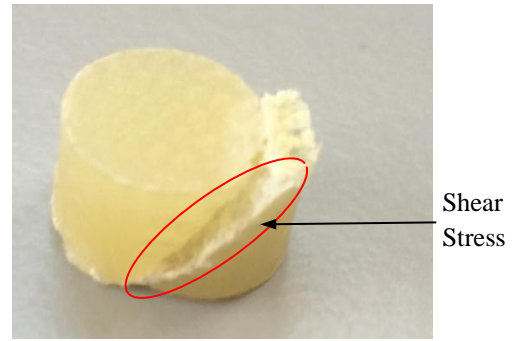


Fig. 8:13- Epoxy Glass Specimen Fracture Surface Image

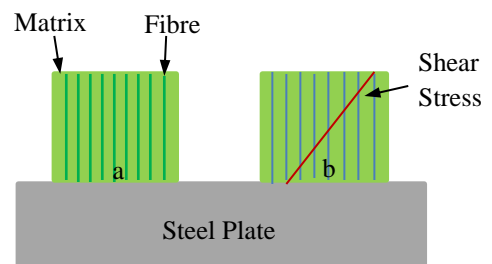


Fig. 8:14- Schematic Diagram of Epoxy Glass (a) before Test (b) after Test.

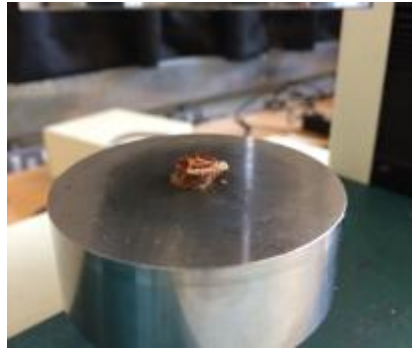


Fig. 8:15- Phenolic Resin Bonded Fabric Material Specimen after Test.

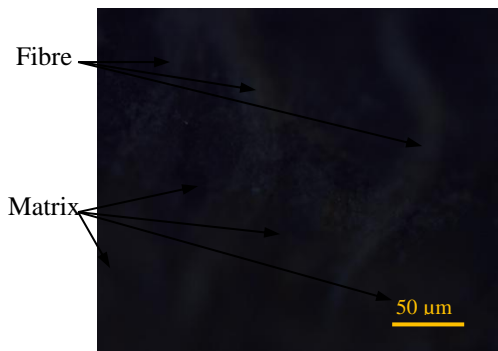


Fig. 8:16- Phenolic Resin Bonded Fabric Specimen Fracture Surface Image.

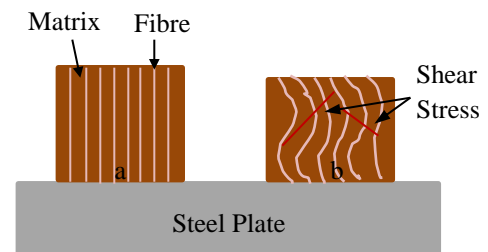


Fig. 8:17- Schematic Diagram of Phenolic Resin Bonded Fabric (a) before Test (b) after Test.

8.4- Discussion

8.4.1- Thermoplastic Materials

The end post materials that are classified as thermoplastic materials in this test were Nylon 12 material and Nylon 66 material.

8.4.1.1- Nylon 12

Figure 8:4 shows the failure map of the Nylon 12 material when compressed between two steel plates by the test machine at pre-load of 100 N and machine rate of 0.5 mm/min. The figure shows two regions. The first region is elastic failure and the second plastic. Within the elastic regime, the material returns to its original shape and dimensions once the load is no longer applied. While the plastic deformation means that the material does not return. Nylon 12 material has a large range of plastic failure as shown in Figure 8:4. The compressive stress results in permanent deformation causing the specimens to become

compressed and expand outwards (see Figures 8:8 and 8:9 a and b). The yield strength of the material as shown in Figure 8:4 is 85 MPa. The Nylon material will bear forces till yield without plastic failure (plastic deformation or rupture). This damage is common in real end posts as mentioned in section 1.7.2 and shown in Figure 1:25.

8.4.1.2- Nylon 66

As can be seen in Figure 8:5, the failure of the specimen due to compressive load was divided into two ranges, a plastic deformation range and plastic failure range. The Nylon 66 material bears a maximum value of compressive stress of 55 MPa (yield strength) without permanent failure. This value is in an agreement with previous values [105]. As shown in Figure 8:5, once the compressive stress exceeded the yield strength, the material started to plastically deform. The compressive stress caused plastic deformation for the specimen and the specimen became shorter and bulged at the sides (see Figures 8:10 and 8:11 a and b). This damage is common in real sites as mentioned in section 1.7.2 and shown in Figure 1:25.

8.4.2- Thermosetting Materials

The end post materials of Epoxy Glass material and Phenolic Resin Bonded Fabric material were classified as thermosetting materials according to melting point test in section 3.3.1.

8.4.2.1- Epoxy Glass

In Figure 8:6 it is possible to observe that the Epoxy Glass material specimen did not show any permanent deformation. The specimen failed while the deformation still in the elastic range. The material failed at an inclined level oriented at angle of approximately 45° to the direction of loading that indicated a shear failure of fibres and matrix (see Figures 8:12 to 8:14). This is in an agreement with Boll [59]. This type of failure occurs when “fibre volume fractions are very high and fibres are very well aligned to direction of loading” [106].

8.4.2.2- Phenolic Resin Bonded Fabric

Figure 8:7 shows the stress-strain curve of compressed specimen of Phenolic Resin Bonded Fabric material. The curve showed two elastic deformation ranges, a plastic deformation range and a rupture region. This happened probably due to weak bonding

between fibres and the matrix. The compressive failure in this case, depicted in Figures 8:15 to 8:17, was a shear buckling mode. This is in an agreement with results obtained by Jelf and Fleck [60] and Budiansky [107].

8.5- Summary

The thermoplastic materials were strong materials, but not strong enough to bear the loads. All thermoplastic material specimens have attained a barrel shape. The Epoxy Glass has the best resistance to static compression followed by Phenolic Resin Bonded Fabric material, Nylon 12 material and Nylon 66 material respectively. The dominant damage mode in this test was elastic deformation then rupture for Epoxy Glass and elastic deformation and plastic deformation then rupture for Phenolic Resin Bonded Fabric material, while the failure dominant mode for thermoplastic materials was elastic deformation followed by plastic deformation. The thermosetting materials were stronger than the thermoplastic materials. They did not bulge. The relationship between fibres and matrix adhesion in the Phenolic Resin Bonded Fabric material was poor. Epoxy Glass material has a linear elastic deformation and failed while in the elastic regime, the other good thing is low deflection at a high force keeping rails a part. Epoxy Glass material has higher resistance of static compressive load.

9- Conclusions and Recommendations

9.1- Conclusions

In this chapter an outline of the obtained results and findings from the experimental works implemented on this study are displayed. It gives a brief summary of all experiments carried out on the studied end post materials of Nylon 12 (N12), Nylon 66 (N66), Nylon 66a (N66a), Epoxy Glass (EG) and Phenolic Resin Bonded Fabric (PRBF) material to develop and improve the performance of insulated rail Joints (IRJs). Recommendations are made on the optimum end post material that can be used to improve the performance of insulated rail joints (IRJs).

9.1.1- Block-on-Ring Sliding Wear Tests

As mentioned in Table 3:1 100% sliding wear was one of the damage mechanisms in the wheel/rail-end post contact which has a direct effect on an end post. Tests were carried out in dry and wet conditions as presented in Section 3.5.1 and Chapter 4. The Block-on-Ring rig was used to achieve this test as illustrated in Section 3.2.1.

9.1.1.1- Dry Test Condition

The results showed clearly that:

1. Surface wear due to sliding depends on the sliding velocity, load, and sliding distance.
2. An increase of sliding speed, load, and sliding distance led to increased coefficient of friction which led to a rise in contact temperature that caused the melting of thermoplastic end post materials.
3. Thermosetting materials of Epoxy Glass and Phenolic Resin Bonded Fabric do not melt.
4. All thermoplastic and thermosetting end post materials under study are affected significantly in the case of high speed and heavy load.

9.1.1.2- Wet Test Condition

The data obtained showed that:

1. The wear resistance of all thermoplastic and thermosetting materials was improved except Nylon 66 where the use of water has led to softening and far greater wear.

The thermosetting material of Epoxy Glass exhibited the best wear performance and can be considered as a very good tribo-material between the materials used in this study in this condition.

9.1.2- Impact Tests

The second wear mechanism that has a significant effect on the end post, as explained in contact scenario wheel/rail-end post in Table 3:1, is impact wear. These tests were performed in dry and wet conditions as described in Section 3.5.4 and Chapter 5. Pneumatic Ball-on-Plate apparatus was employed to carry out this test as presented in Section 3.2.3.

The experimental data showed that:

1. Crater size caused by impact force depends on load and number of cycles
2. The crater size of thermoplastic materials was affected positively (less wear) by water in wet test conditions.
3. The crater size of Nylon 66 material was affected by water negatively (more wear) in wet test conditions as with sliding tests the material softened therefore making it less resistant to impact.
4. The thermosetting materials of Epoxy Glass and Phenolic Resin Bonded Fabric materials were not affected by water in wet tests.
5. The mechanism of impact wear of the thermoplastic materials of Nylon 12, Nylon 66 and Nylon 66a and thermosetting materials of Phenolic Resin Bonded Fabric was displacement/compression and with materials loss.
6. The mechanism of impact wear of thermosetting material of Epoxy Glass was material loss which results in the contact surface became smoother and powder appearing on the material surface.
7. The Nylon 12 material has highest material displacement/compression resistance in the thermoplastic materials group.
8. The Epoxy Glass material has the highest wear resistance in the thermosetting materials group.

9.1.3- Lipping Tests

The lipping phenomenon has a big effect on the end post as shown in the contact scenario wheel/rail-end post in Table 3:1. The Block-on-Ring rig and Twin-Disc machine were used

for these tests (see Sections 3.2.1 and 3.2.2). The tests were conducted in dry conditions as demonstrated in Section 3.5.2 and Chapter 6.

9.1.3.1- 100% Slip Ratio Lipping Test

The 100% sliding has a significant effect on the end post width and as a result the steel edges were flattened, wore and lipped.

9.1.3.2- Partial Slip Ratio (1%) Lipping Test

1. The bulk deformation of metal grew significantly with contact pressure and cycles.
2. The highest metal flow length in the tests was 0.54 mm in the case of a contact pressure of 1500 MPa and 2000 cycles for both end post thickness of 0.5 mm and 1 mm and this is equivalent to 6 mm in real site.
3. The metal flow size in the case of an end post width of 1 mm was larger than the metal flow size in case of end post width of 0.5 mm. This occurred due to increases in impact forces.

9.1.4- Rolling/Sliding Contact Wear Tests

The Rolling/Sliding contact has a major effect on the end post as mentioned in Table 3:1. A Twin-Disc machine has been employed to carry out the test in dry and wet conditions (see Section 3.5.3 and Chapter 7).

The test results displayed that:

1. The effect of contact pressure was very severe on the thermoplastic materials of Nylon 12, Nylon 66, Nylon 66a and the thermosetting material of Phenolic resin bonded fabric material which led to the specimens completely failing in early stage.
2. The Epoxy Glass material was less affected by the load used.
3. The impact of rolling and partial sliding contact was significant in all studied end post materials.
4. There was no positive affect of using water in wet test on all Thermoplastic and thermosetting materials.

9.1.5- Static Compression Tests

The final damage effect on the thermoplastic and the thermosetting end post materials as described in Table 3:1 is a static compression load. These tests were carried out as

explained in Section 3.5.5 and Chapter 8. A Tinius Olsen H-25kN hydraulic test machine was used to perform this test as presented in Section 3.2.4.

The experimental works results showed that:

1. The thermoplastic materials of Nylon 12 and Nylon 66 and the thermosetting materials of Phenolic Resin Bonded Fabric have two damage modes (plastic deformation and plastic deformation)
2. The Nylon 12 material and Nylon 66 material have a large region of plastic deformation, with Nylon 12 being a larger.
3. The thermoplastic materials of Nylon 12 and Nylon 66a barrelled.
4. The Phenolic Resin Bonded fabric material has a shear buckling compressive failure mode. The material has elastic deformation range first then plastic deformation and finally rupture.
5. The compressive failure of Phenolic Resin Bonded fabric material showed that the adhesion between matrix and fibres was poor.
6. The Epoxy Glass material has elastic deformation range then fails, with no plastic deformation.
7. The Nylon 12 material has the highest resistance of compressive load in the thermoplastic materials group.
8. The Epoxy Glass material has the higher resistance of a static compressive load in all thermoplastic and thermosetting end post materials groups under study.

The Nylon 12 material (N12) has the highest wear/displacement resistance in the thermoplastic materials group. But the Epoxy Glass material (EG) has a higher wear resistance in the thermoplastic and thermosetting materials groups. So the Epoxy Glass material is the best tribo-material in this study. It is recommended using this as an end post material to contribute to the development and improve the performance of insulated rail joints (IRJs). The end post thickness of 6 mm is not recommended because it can be affected by lipping more than thicker end posts although the thicker end post causes greater impact damage to the rails.

From the results obtained in this experimental study, which were conducted on the five most commonly used materials in railway track as end posts, it can be seen that, thermoplastic materials of (N 12, N 66, N 66a) do not bear excessive loads that they are

exposed to in service as a component of an insulated rail joint (IRJ). In addition, these materials melt at severe working conditions when contact temperature is increased. Also elastic and plastic deformation is took place which led to increased rail bending, resulting in contact between the adjacent rails ends. Also plastic deformation led to end post bulging from the sides and the top which led to the end post cracking and coming out the gap. In contrast the thermosetting materials of (EG and PRBF) did not melt at all. The PRBF material do not bear severe working conditions, resulting in weight loss, permanent deformation and cracking. While the EG material shows high wear resistance and no deformation occurred. This makes it a good support for rails and reduces bending. This result validated the result of Mandal [23].

9.2- Recommendations for Future Work

The rolling/sliding tests should be conducted in future work using procedures that simulate reality better. This could be by making a groove in the centre of rail steel disc and placing the end post materials in it. These will act as rails and joint bars and provide a good support for the end posts which will give good results. Test should be conducted at dry and wet conditions at certain test parameters of contact pressure, rotation speed and slip ratio. The test will carried out at 400 rpm and slip ratio of 1%. Applied load will be calculated by Hertz theory to produce 200 MPa contact pressure.

References

1. Freight Transport Associated. Available from: www.fta.co.uk/export/sites/fta/_galleries/downloads/rail_freight/importance_of_rail_freight_0408pdf.
2. Lewis, M., *Railways in the Greek and Roman World*, University of Hull. p. 8-19.
3. Hylton, S., 2007, *The Grand Experiment: The Birth of the Railway Age 1820 - 1845*, Ian Allan Publishing. p. 288.
4. Kriechbaum and Reinhard, 2004, *Die große Reise auf den Berg*. der Tagespost (in German).
5. Marshall, J., 1979, *Guinness Book of Rail Facts and Feats*. Guinness World Records Limited.
6. Skempton, A., 2002, *A Biographical Dictionary of Civil Engineers in Great Britain and Ireland*. Thomas Publish in Behalf of Civil Engineering, Thomas Telford Ltd, 1 Heron Quay , London. p. 59-60.
7. Elephant, S., 2001, *Early Railways*, in *First International Railway* , London: Newcomen Society. p. 360.
8. Mundrey, J., 2010, *Railway Track Engineering.*, Tata McGraw Hill Education Private Limited, New Delhi.
9. Railway. Available from: <http://www.railway-technical/finance.shtml>.
10. Daniels, L.E., 2008, *Track Maintenance Costs on Rail Transit Properties*. Oaks, CA.
11. Protec Rail Group, Sheffield, UK.
12. Railway Group Standards, R.P., 1998, *Track Standards Manual - Section 2: Rails*. Safety & Standards Directorate, Railtrack PLC, : Euston Square, London NW1 2EE. p. 38.
13. bbrail.co.uk. *Rail section*. Available from: <http://www.bbrail.co.uk/Products-and-Services/Track/Rail-sections>.
14. AREMA. *Practical Guide to Railway Engineering, Viewed January*, Available from: https://www.arema.org/eseries/scriptcontent/custom/e_arema/Practical_Guide/PGChapter3.pdf, 2009.
15. Tong, D., 1968, *Rail Road Track*, Beijing.
16. Lim, W., 2004, *Mechanics of Railway Ballast Behaviour*, University of Nottingham: Nottingham, UK.
17. Dahlberg, T., 2006, *Track Issues*, in *Handbook of Railway Vehicle Dynamics*. Taylor & Francis Group, LLC. p. 143-179.

18. Alibaba.com. Available from: http://www.alibaba.com/product-detail/rail-fish-plate-joint-bar_346878550.html.
19. AREMA. *Canadian National Railway. Track Maintainers Course*, Available from: https://www.arena.org/publications/pgre/Practical_Guide/PGChapter3.pdf, viewed August. 2003.
20. Charlton, Z., 2007, *Innovative Design Concepts for Insulated Joints*, in *Mechanical Engineering*. Virginia Polytechnic Institute and State University: Blacksburg, Virginia. p. 232.
21. Cope, G., 1993, *British Rail Way Track; Design, Construction, and Maintenance*. Barnsly: Permanent Way
22. Zong, N., Wexler, D. and Dhanasekar, M., 2013, *Structural and Material Characterisation of Insulated Rail Joints*. *Electronic Journal of Structural Engineering*, 13(1): p. 75-87.
23. Mandal, N. and Dhanasekar, M., 2012, *A Sensitivity Analysis of End Post Materials of Insulated Rail Joints Sing Finite Element Analysis* in *9th International Conference on Contact Mechanics and Wear of Rail/Wheel System*. Chengdu, china. p. 509-515.
24. Mandal, N. and Peach, B., 2010, *An Engineering Analysis of Insulated Rail Joints: A General Perspective*. *International Journal of Engineering Science and Technology*, 2(8): p. 3964-3988.
25. Pang, T., 2007, *Studies on Wheel/Rail Contact – Impact Forces at nsulated Rail Joints*. Central Queensland University: Australia.
26. RAILFOTO. *Insulated Rail Fishplate Joint*. Available from: <http://railfoto.fotopic.net/p15613474.html>, 2006.
27. Davis, D. and Akhtar, M., 2005, *Improving The Performance of Bonded Insulated Joints*. *Railway Track and Structures*, 101(1): p. 14-17.
28. LBFOSTER. *Rail Products, viewed January*. Available from: <http://www.lbfoster.com/content.aspx?id=1452>, 2009.
29. Ayasse, J. and Chollet, H., 2006, *Wheel – Rail Contact*, in *Handbook of Railway Vehicle Dynamics*. 2006, Taylor & Francis Group, LLC. p. 85-120.
30. Marshall, M., Lewis, R., Dwyer-Joyce, R. Demilly, F. and Flament, Y., 2011, *Ultrasonic Measurement of Railway Wheel Hub–Axle Press-Fit Contact Pressures*. *Proceedings of the Institution of Mechanical Engineers, Part F: Journal of Rail and Rapid Transit*, 225(3): p. 287-298.
31. Jeong, D., 2001, *Progress in Rail Integrity Research, Final Report, Dot/Fra/Ord-01/18, Volpe National Transportation System Centre*. Massachusetts, USA.

32. Akhtar, M. and Davis, D., 2008, *Preliminary Results of Prototype Insulated Joint Tests at the Facility for Accelerated Service Testing*. Federal Railroad Administration: U.S. Department Of Transportation. p. RR08-11.
33. Chen, Y., 2003, *The Effect of Proximity of a Rail End in Elastic-Plastic Contact cv between a Wheel and a Rail*. Proceedings of the Institution of Mechanical Engineers, Part F: Journal of Rail and Rapid Transit, 217(3): p. 189-201.
34. Mayville, A. and Hilton, P., 1984, *Fracture Mechanics Analysis of a Rail-End Bolt Hole Crack*. Theoretical and Applied Fracture Mechanics, 1, p. 51-60.
35. Dhanasekar, M., Pang, T., and Marks, I., 2007-a, *Wheel Impact at Insulated Rail Joints*, Proceedings of the 9th International Railway Engineering Conference, London, UK.
36. Dhanasekar, M., Pang, T., Ashman, T. and Marks I., 2007-b, *Determination of Railhead Wheel Contact Impact through Measured Strain Signatures*, 2nd International Conference on Experimental Vibration Analysis for Civil Engineering Structure, Portugal.
37. Rathod, C., Wexler, D. Chandra, T. and Huiju Li, 2012, *Microstructural Characterisation of Railhead Damage in Insulated Rail Joints*. Material science, 906-709: p. 2937-2942.
38. Koro, K., Abe, K., Ishida, M. and Suzuki, T., 2004, *Timoshenko Beam Finite Element for Vehicle—Track Vibration Analysis and its Application to Jointed Railway Track*. Proceedings of the Institution of Mechanical Engineers, Part F: Journal of Rail and Rapid Transit, 218(2): p. 159-172.
39. Kataoka, H., Abe, N., Wakatsuki, O. and Oikawa, Y., 1997, *A dynamic Stress Analysis of Joint Rail Using Finite Beam Element Model*. Proceeding of the 14th Japan National Symposium on Boundary Element Method, Japanese.
40. Busquet, M., Baillet, L., Bordreuil, C. and Berthier, Y., 2005, *3D Finite Element Investigation on the Plastic Flows of Rolling Contacts—Correlation with Railhead Microstructural Observations*. Wear, 258(7-8): p. 1071-1080.
41. Wen, Z., Jin, X. and Zhang, W., 2005, *Contact-Impact Stress Analysis of Rail Joint Region Using the Dynamic Finite Element Method*. Wear, 258(7-8): p. 1301-1309.
42. Chen, Yung-Chuan and Chen, Li-Wen, 2006, *Effects of Insulated Rail Joint on the Wheel/Rail Contact Stresses under the Condition of Partial Slip*. Wear, 260(11-12): p. 1267-1273.
43. Kabo, E., Nielsen, J.C.O. and Ekberg, A., 2006, *Prediction of Dynamic Train-Track Interaction and Subsequent Material Deterioration in Presence of Insulated Rail Joints*. Vehicle System Dynamics, 44: p. 718-729.
44. Mandal, N. and Peach, B., 2009, *3D Stress Analysis of Insulated Rail Joints*, 9th International Heavy Haul Conference, Shanghai, China.

45. Sandstrom, J., Kabo, E., Nissen, A., Jansson, F., Ekberg, A. and Lunden, R., 2012, *Deterioration of Insulated Rail Joints-A three-Year Field Study*, 9th International Conference on Contact Mechanics and Wear of Rail/Wheel System. Chengdu, China. p. 301-308.
46. Holmberg, K. and Wickstrgm, G., 1987, *Friction and Wear Tests of Polymers*. Wear, 1987. 115: p. 95-105.
47. Clarke, C. and Allen, C., 1991, *The Water Lubricated, Sliding Wear Behaviour of Polymeric Materials Against Steel*. Tribology International, 24(2): p. 109-118.
48. Mens, J and Gee, A., 1991, *Friction and Wear Behaviour of 18 Polymers in Contact with Steel in Environments of Air and Water*. Wear, 149: p. 255-268.
49. Bellow, D. and Viswanath, N., 1993, *An Analysis of the Wear of Polymers*. Wear, 162-164, Part B: p. 1048-1053.
50. Unal, H., Sen, U. and Mimaroglu, A., 2004, *Dry Sliding Wear Characteristics of some Industrial Polymers Against Steel Counterface*. Tribology International, 37(9): p. 727-732.
51. Wang, J. and Gu, M., 2004, *Wear Properties and Mechanisms of Nylon and Carbon-Fibre-Reinforced Nylon in Dry and Wet Conditions*. Journal of Applied Polymer Science, 93(2): p. 789-795.
52. Basavarajappa, S., Arun, K. and Davim, J, 2009, *Effect of Filler Materials on Dry Sliding Wear Behaviour of Polymer Matrix Composites – A Taguchi Approach*. Minerals & Materials Characterization & Engineering, 8(5): p. 379-391.
53. Bayer, R., Engel, P. and Sacher, E., 1975, *Impact Wear Phenomena in Thin Polymer Films*. Wear, 32(2): p. 181-194.
54. Bayer, R., 1986, *Impact Wear of Elastomers*. Wear, 112(2): p. 105-120.
55. Kukureka, S., Hookeb, C., Raob, M., Liaob, P. and Chen, Y., 1999, *The Effect of Fibre Reinforcement on the Friction and Wear of Polyamide 66 under Dry Rolling–Sliding Contact*. Tribology International, 32(2): P. 107–116.
56. Chen, Y., Modi, O., Mhay, A., Chrysanthou, A. and O'Sullivan, J., 2003, *The Effect of Different Metallic Counterface Materials and Different Surface Treatments on the Wear and Friction of Polyamide 66 And Its Composite in Rolling–Sliding Contact*. Wear, 255(1-6): p. 714-721.
57. Avanzini, A., Donzella, G., Mazzu, A. and Petrogallic, C., 2013, *Wear and Rolling Contact Fatigue of PEEK and PEEK Composites*. Tribology International, 57: p. 22-30.
58. Hoskins, T., Dearn, K., Chen, Y. and KuKureka, S., 2014, *The Wear of PEEK in Rolling–Sliding Contact–Simulation of Polymer Gear Applications*. Wear, 309(1): p. 35-42.

59. Boll, D., Jensen, R., Corder, L. and Bascom, W., 1990, *Compression Behaviour of Single Carbon Filaments Embedded in an Epoxy Polymer*. Journal of composite materials, 24(2): p. 208-219.
60. Jelf, P. and Fleck, N., 1992, *Compression Failure Mechanisms in Unidirectional Composites*. Journal of Composite Materials, 26(18): p. 2706-2726.
61. Chen, W. and Zhou, W., 1998, *Constitutive Behaviour of Epon 828/T-403 at Various Strain Rates*. Mechanics of Time-Dependent Materials, 2(2): p. 103-111.
62. Roslan, A., Zaidi, M., and Pasricha, M., 2001, *Compressive Properties of Carbon Fibre Reinforced Plastic (CFRP) at Low Strain Rate*. Pertanika Journal of Science & Technology, 9(2): p. 219-227.
63. Brown, K., Brooks, R. and Warrior, N., 2010, *The Static and High Strain Rate Behaviour of a Commingled E-Glass/Polypropylene Woven Fabric Composite*. Composites Science and Technology, 70(2): p. 272-283.
64. ASTM, *Standard Test Method for Ranking Resistance of Material to Sliding Wear Using Block-on-Ring Wear Test*. 2010.
65. Kennedy, D. and Hashmi, M., 1998, *Methods of Wear Testing for Advanced Surface Coatings and Bulk Materials*. Material Processing Technology, 77: p. 246-253.
66. Ruff, A., 1989, *Comparison of Standard Test Methods for Non-Lubricated Sliding Wear*. Wear, 134: p. 49 - 57.
67. Veenhuizen, P. and Steinbuch, I., 2006, *The Application of a CVT in a Two Disc Test Machine*. Eindhoven University of Technology Department of Mechanical Engineering Section Control Systems Technology: Eindhoven.
68. Wright, N. and Kukureka, N. 2011, *Wear Testing and Measurement Techniques for Polymer Composite Gears*, 13th International Wear of Materials Conference. Vancouver.
69. Gordon, H. and Kukureka, S., 2009, *The Wear and Friction of Polyamide 46 and Polyamide 46/Aramid-Fibre Composites in Sliding–Rolling Contact*. Wear, 267(1-4): p. 669-678.
70. Aldajah, S., Fenske, G., Ajayi, L., Kumar, S., Reed, C., Xu, Z. and DiMelfi, R., 2005, *Laser Glazing of Rails WBB/IWS Tests (CNRC-Ottawa)*.
71. Lewis, R., Braghin, F., Ward, A., Bruni, S., Dwyer-Joyce, R., Bel Knani, K., and Bologna, P., 2003, *Integrating Dynamics and Wear Modelling to Predict Railway Wheel Profile Evolution*, 6th International Conference on Contact Mechanics and Wear of Rail/Wheel Systems (CM2003) Gothenburg, Sweden. p. 7-16.
72. Lewis, R., Dwyer-Joyce, R. and Lewis, J., 2003, *Wheel/Rail Contact Isolation Due to Track Contamination*, 6th International Conference on Contact Mechanics and Wear of Rail/Wheel Systems (CM2003). Gothenburg, Sweden.

73. Vasic G., Franklin, F. and Kapoor, A., 2003, *New Rail Materials and Coatings*. the University of Sheffield: Sheffield, UK.
74. Bejnon, J. and Beynon, J., 1991, *The Early Detection of Rolling-Sliding Contact Fatigue Cracks*. *Wear*, 144: p. 103-116.
75. Fletcher, D. and Beynon, J., 2000, *Development of a Machine for Closely Controlled Rolling Contact Fatigue and Wear Testing*. *Journal of Testing and Evaluation*, 28(4): p. 267-275.
76. Jarvis, A., 2013, *Overview and Operating Guidelines to Pneumatic Ball on Plate Impact Tester*. Sheffield University: Department of Material Science & Engineering Research Centre in Surface Engineering. p. 5.
77. Knotek, O., Bosserhoff, B. and Schrey, A., 1992, *A New Technique for Testing the Impact Load of Thin Films: The Coating Impact Test*. *Surface anti Coatings Technology*, 54/55: p. 102-107.
78. Bouzakis, K., Michailidis, N., Lontos, A., Siganos, A., Hadjiyiannis, S. and Giannopoulos, G., 2001, *Coating Dynamic Cohesion, Adhesion and Creep Properties Characterization through the Impact Tester*. *Z. Metallkd*, 92(10): p. 1180– 1185.
79. Bouzakis, K., Vidakis, N. and David, K., 1999, *The Concept of an Advanced Impact Tester Supported by Evaluation Software for the Fatigue Strength Characterization of Hard Layered Media*. *Thin Solid Films*, 355-356: p. 322-329.
80. Bouzakis, K., Michailidis, N., Haydjiyiannis, S., Efstathiou, K., Pavlidoub, E., Erkense, G. Rambadt, S. and Wirthc, I., 2001, *Improvement of PVD Coated Inserts Cutting Performance, Through Appropriate Mechanical Treatments of Substrate and Coating Surface*. *Surface and Coatings Technology*, 146-147: p. 443–450.
81. Lugscheider, E., Knotek, O., Wolff, C. and Brawulf, S., 1999, *Structure and Properties of PVD-Coatings by Means of Impact Tester*. *Surface and Coatings Technology*, 116-119: p. 141-146.
82. Voevodin, A., Bantle, R. and Matthews, A., 1995, *Dynamic Impact Wear of TiCxNy and Ti-DLC Composite Coatings*. *Wear*, 185: p. 151-157.
83. Bantle, R. and Matthews, A., 1995, *Investigation into the Impact Wear Behaviour of Ceramic Coatings* *Surface and Coatings Technoiog*, 1995. 74-75: p. 857-868.
84. Bouzakis, K. and Siganos, A., 2004, *Fracture Initiation Mechanisms of Thin Hard Coatings During the Impact Test*. *Surface and Coatings Technology*, 185(2-3): p. 150-159.
85. Bruno, M., Miola, M., Bretcanu, O., Vitale-Brovarone, C., Laviano, F. and Verne, E., 2014, *Composite Bone Cements Loaded with a Bioactive and Ferrimagnetic Glass-Ceramic. Part I: Morphological, Mechanical and Calorimetric Characterization*. *Journal of Biomaterials Applications*, p. 08-85.

86. Doyle, B., Corbett, T., Cloonan, A., O'Donnell, M., Walsh, M., Vorp, A. and McGloughlin, T., 2009, *Experimental Modelling of Aortic Aneurysms: Novel Applications of Silicone Rubbers*. *Medical engineering & physics*, 31(8): p. 1002-1012.
87. Doyle, B., Corbett, T., Cloonan, A., O'Donnell, M., Walsh, M., Vorp, D. and McGloughlin, T., 2009, *An Experimental and Numerical Comparison of the Rupture Locations of an Abdominal Aortic Aneurysm*. *Journal of Endovascular Therapy*, 16(3): p. 322-335.
88. Tinius Oslen. Available from: <http://www.tiniusolsen.com/material-testing-groups/testing-Elastomers-calc.html>.
89. PAR. Available from: www.par.group.co.uk.
90. Insulation., L., *Techniacal Properties*.
91. Insulations, L., *Material Data Sheet Epoxy GlassSheet FR4*.
92. Insulations, L., *Technical Data Sheet SRBF F2*.
93. Pyris Software for Windows, 1999.
94. Xu, B. and Jiang, Y., 2002, *Elastic-Plastic Finite Element Analysis of Partial Slip Rolling Contact*. *Journal of Tribology*, 124(1): p. 20-26.
95. Dwyer-Joyce, R., 1997, *Tribological Design Data Part 3: Contact Mechanics*, U.o.S.o.b. of; and T.T.G.o.T.I.o.M. Engineers, Editors.
96. Sandström, J. and Ekberg, A., 2009 , *Numerical Study of the Mechanical Deterioration of Insulated Rail Joints*. *Proceedings of the Institution of Mechanical Engineers, Part F: Journal of Rail and Rapid Transit*, 223(3): p. 265-273.
97. Gallardo-Hernandez, E. and Lewis, R., 2008, *Twin Disc Assessment of Wheel/Rail Adhesion*. *Wear*, 265(9): p. 1309-1316.
98. Wang, Y. and Li, J., 1999, *Sliding Wear Behaviour and Mechanism of Ultra-High Molecular Weight Polyethylene*. *Material Science Engineering*, A266: p. 60-155.
99. Jacobs, O., Jaskulka, R., Yang, F. and Wu, W., 2004, *Sliding Wear of Epoxy Compounds Against Different Counterparts under Dry and Aqueous Conditions*. *Wear*, 256(1-2): p. 9-15.
100. Wu, C., Zefeng, W., Xuesong, J. and Wanming, Z., 2007, *Dynamic Stress Analysis of Rail Joint with Height Difference Defect Using Finite Element Method*. *Engineering Failure Analysis*, 14(8): p. 1488-1499.
101. Network, R., *Insulated Rail Joints*.
102. Kennedy, D. and Hashmi, M., 1998, *Methods of Wear Testing for Advanced Surface Coatings and Bulk Materials*. *Journal of Materials Processing Technology*, 77(1): p. 246-253.

103. Tarfaoui, M., Choukri, S. and Neme, A., 2010, *Effect of Fibre Orientation on Mechanical Properties of the Laminated Polymer Composites Subjected to Out-of-Plane High Strain Rate Compressive Loadings*. Science and Technology, 68(2): p.1-8.
104. Beagles, A., Beaty, P., Fletcher, D. and Lewis, R., 2015, *Insulated Rail Joint Enhancement: Testing and Analysis*, Proceedings of the IMechE Railway Division Stephenson Conference, London.
105. MatWeb. *Compressive Strength Testing of Plastics*. Available from: <http://www.matweb.com/reference/compressivestrength.aspx>.
106. Alif, N. and Carlsson, L., 1997, *Failure Mechanisms Of Woven Carbon And Glass Composites*. ASTM Special Technical publication, 1285: p. 471-493.
107. Budiansky, B. and Fleck, N., 1993, *Compressive failure of fibre composites*. Journal of the Mechanics and Physics of Solids, 41(1): p. 183-211.

Published Works

- 1- Elshukri, A., Fathi and Lewis, Roger, An Experimental Investigation and Improvement of Insulated Rail Joints (IRJs). Proceeding of the 14th International Conference on Tribology, May 2015, Belgrade, Serbia.

Abstract: In this study the impact of sliding speed, applied load and period of time on the wear resistance of end post materials of Nylon 12 (N12), Nylon 66 (N66), Nylon 66a (N66a), Epoxy Glass (EG) and Phenolic Resin Bonded Fibre materials were investigated. Wear tests were implemented in dry and wet conditions on a Block-on-Ring apparatus. The tests were carried out at different sliding speeds of 1.5 m/sec., 3.3 m/sec., and 7.2 m/sec., applied loads of 10 N, 30 N, and 50 N, and three periods of time 5 min., 30 min. and 60 min. The obtained results in dry condition tests showed that the wear resistance of nylon and fibre materials used in this study decreases with the increase in applied load and sliding speed due to increase in contact temperature. But the impact of these increases in sliding speed and applied load was less on the wear resistance of fibre materials. Unexpected results were that in wet test condition for nylon66 materials where the wear resistance was less compared with the same material in a dry test.

- 2- Elshukri, A., Fathi and Lewis Roger, An Experimental Investigation and Improvement of Insulated Rail Joints (IRJs). 1st International Conference on Tribology, 2015, Istanbul, Turkey.

Abstract: In this work the effect of impact on end post material was assessed using a Pneumatic Ball-on-Plate Impact rig in dry and wet conditions. The influence of impact forces and number of cycles on the wear resistance of Nylon 12, Nylon 66, Nylon 66a, Epoxy Glass and Phenolic Resin Bonded Fibre materials were tested. Two states of impact wear were observed. The first state relates primarily to material displacement and deformation with cracks formed around edges and second state, which results in material loss where the surface became smoother and powder appeared.

Appendix A

T γ Calculations

Nylon 66 Material (N 66)

Modulus of Elasticity = 3100 MPa

Poisson's Ratio = 0.4

Steel Poisson's Ratio = 0.3

Steel Modulus of Elasticity = 200000 MPa

$$a = \sqrt{(4 \times P \times R / (\pi \times E))}$$

$$1/E = ((1 - \nu_1^2)/E_1) + ((1 - \nu_2^2)/E_2)$$

E = 3629.53 MPa

a (10 N) = 0.12138 mm, a (20 N) = 0.21024 mm, and a (50 N) = 0.2714 mm

Contact area (10 N) = 1.2138 mm²

Contact area (30 N) = 2.1024 mm²

Contact area (50 N) = 2.7142 mm²

Whole contact area = 25 mm²

T γ /A = (fn x μ x slip%) / contact area

$$= (10 \times 0.211 \times 1) / 25 = 0.0844$$

$$= (10 \times 0.278 \times 1) / 25 = 0.1112$$

$$= (10 \times 0.211 \times 1) / 1.2138 = 1.7384$$

$$= (10 \times 0.278 \times 1) / 1.2138 = 2.2903$$

$$= (30 \times 0.2092 \times 1) / 25 = 0.25116$$

$$= (30 \times 0.309 \times 1) / 25 = 0.3708$$

$$= (30 \times 0.2093 \times 1) / 2.1024 = 2.9866$$

$$= (30 \times 0.309 \times 1) / 2.1024 = 4.4092$$

$$= (50 \times 0.2061 \times 1) / 25 = 0.4122$$

$$= (50 \times 0.315 \times 1) / 25 = 0.630$$

$$= (50 \times 0.2061 \times 1) / 2.7142 = 3.7967$$

$$= (50 \times 0.315 \times 1) / 2.7142 = 5.8028$$

Nylon 66a Material (N 66a)

$$T\gamma/A = (f_n \times \mu \times \text{slip}\%) / \text{contact area}$$

$$= (10 \times 0.2668 \times 1) / 25 = 0.10672$$

$$= (10 \times 0.3188 \times 1) / 25 = 0.1275$$

$$= (10 \times 0.2668 \times 1) / 1.2138 = 2.1980$$

$$= (10 \times 0.3188 \times 1) / 1.2138 = 2.6263$$

$$= (30 \times 0.2706 \times 1) / 25 = 0.3247$$

$$= (30 \times 0.3444 \times 1) / 25 = 0.41328$$

$$= (30 \times 0.2706 \times 1) / 2.1024 = 3.8613$$

$$= (30 \times 0.3444 \times 1) / 2.1024 = 4.9143$$

$$= (50 \times 0.2706 \times 1) / 25 = 0.533$$

$$= (50 \times 0.3444 \times 1) / 25 = 0.6726$$

$$= (50 \times 0.2706 \times 1) / 2.7142 = 5.9093$$

$$= (50 \times 0.3444 \times 1) / 2.7142 = 6.1952$$

Desired Contact Pressure Disc Contact Calculations in Rolling/Sliding Test s

| | | |
|------------------|----------|-------------|
| Nylon Materials: | T (m) | 0.006 |
| | P0 (MPa) | 2.00E+02 |
| | Load kN | 2.385951277 |
| | Load N/m | 397658.5461 |
| | D1 (m) | 0.047 |
| | D2 (m) | 0.045 |
| | Ri | 0.011494565 |

| | | |
|----------------------|----------|-------------|
| | E1 | 2.1E+11 |
| | E2 | 3.10E+09 |
| | n1 | 0.3 |
| | n2 | 0.4 |
| | E* | 3632386830 |
| | b (m) | 0.001265786 |
| | P0 (MPa) | 200 |
| | 2b(mm) | 2.531572931 |
| Composite Materials: | T (m) | 0.006 |
| | P0 (MPa) | 200 |
| | Load kN | 1.671228263 |
| | Load N/m | 278538.0439 |
| | D1 (m) | 0.047 |
| | D2 (m) | 0.045 |
| | Ri | 0.011494565 |
| | E1 | 2.1E+11 |
| | E2 | 2.40E+09 |
| | n1 | 0.3 |
| | n2 | 0.74 |
| | E* | 5185825411 |
| | b (m) | 0.000886614 |
| | P0 (MPa) | 200 |
| | 2b(mm) | 1.773228261 |

Appendix B

Microscopic Photocopies for Unworn and Worn Contact Surfaces of Specimens in Sliding Wear Test:

1- Nylon 12 Material (N12)

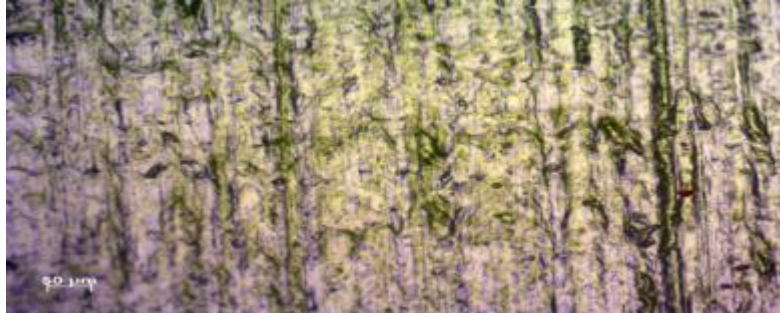


Fig.1- Contact Surface before Test.

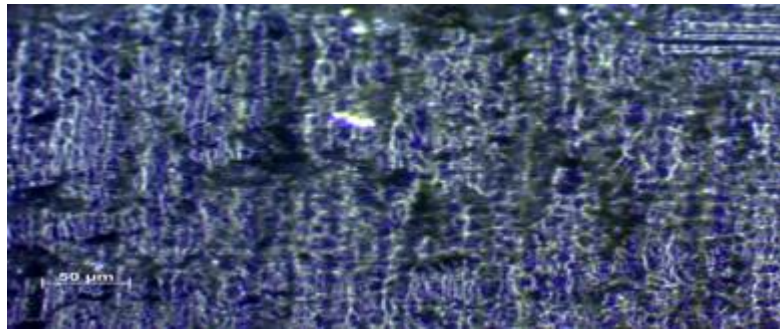


Fig. 2- Contact Surface after 05 Minutes at 1.5 m/sec and 10 N Test.

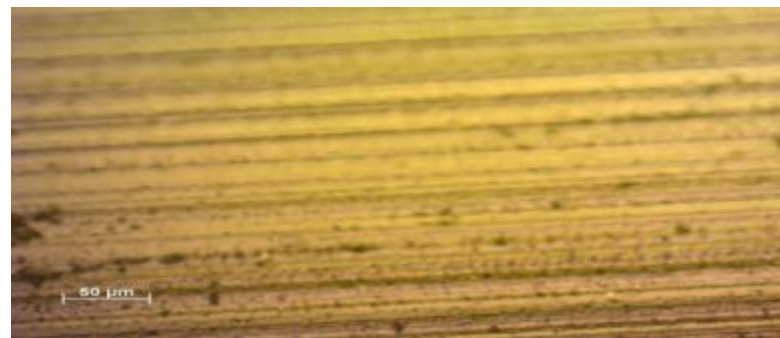


Fig. 3- Contact Surface after 30 Minutes at 1.5 m/sec and 10 N Test.

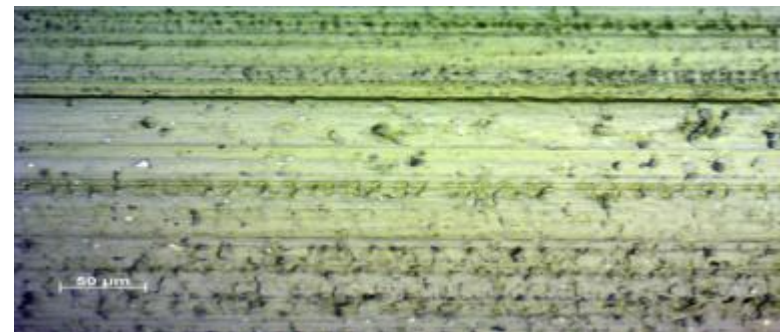


Fig. 4- Contact Surface after 60 Minutes at 1.5 m/sec and 10 N Test.

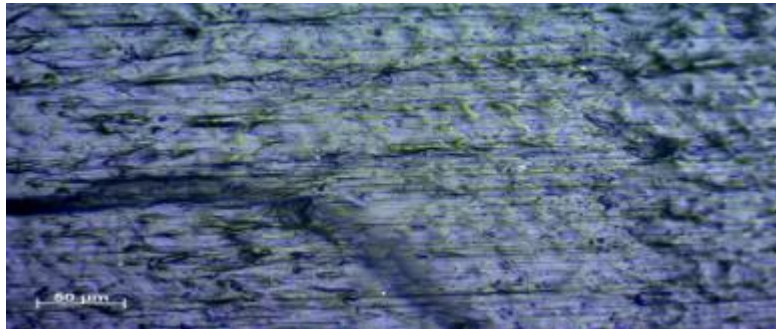


Fig. 5- Contact Surface before Test.



Fig. 6- Contact Surface after 05 Minutes at 1.5 m/sec and 30 N Test.

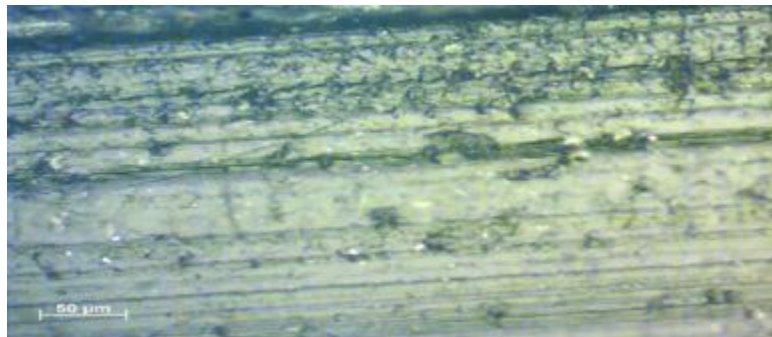


Fig. 7- Contact Surface after 30 Minutes at 1.5 m/sec and 30 N Test.



Fig. 8- Contact Surface after 60 Minutes at 1.5 M/sec and 30 N Test.



Fig. 9- Contact Surface before Test.

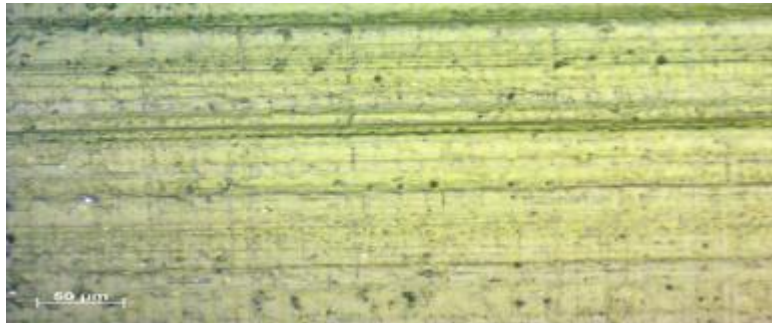


Fig. 10- Contact Surface after 05 Minutes at 1.5 m/sec and 50 N Test.

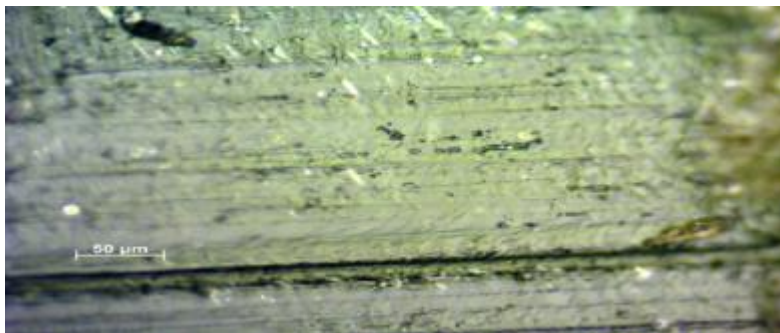


Fig. 11- Contact Surface after 30 Minutes at 1.5 m/sec and 10 N Test.

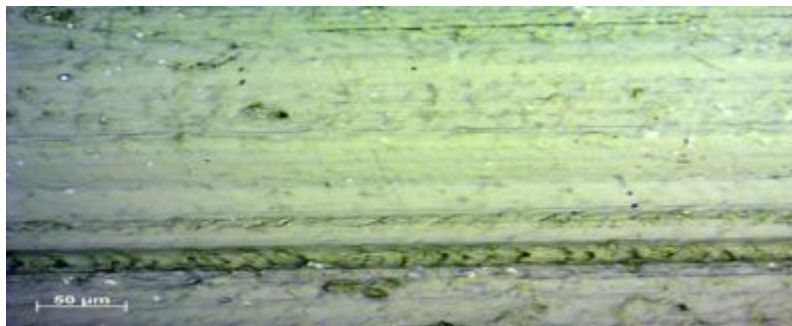


Fig. 12- Contact Surface 60 Minutes at 1.5 m/sec and 50 N Test.

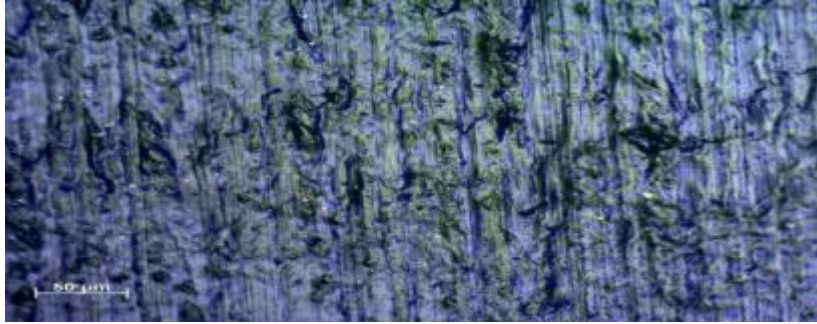


Fig. 13- Contact Surface before Test.

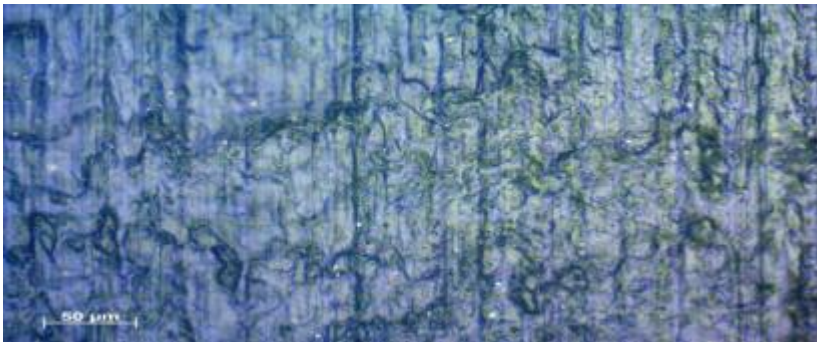


Fig. 14- Contact Surface after 05 Minutes at 3.3 m/sec and 10 N Test.

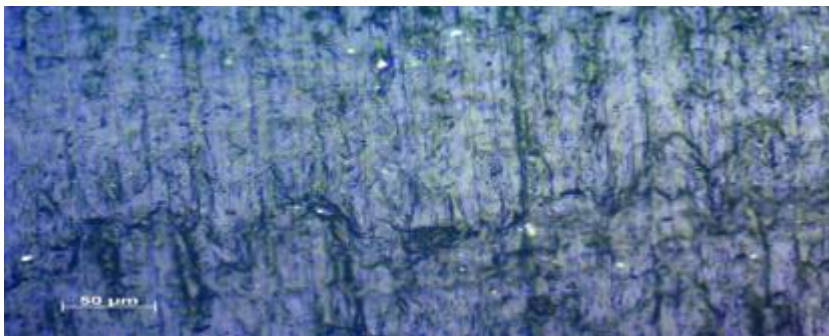


Fig. 15- Contact Surface after 30 Minutes at 3.3 m/sec and 10 N Test.

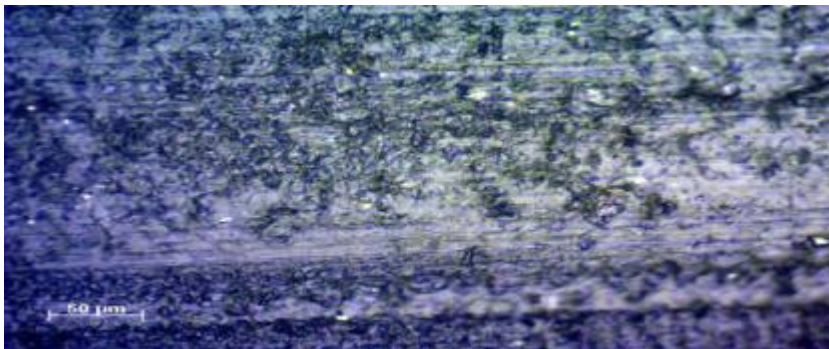


Fig. 16- Contact Surface after 60 Minutes at 3.3 m/sec and 10 N Test.

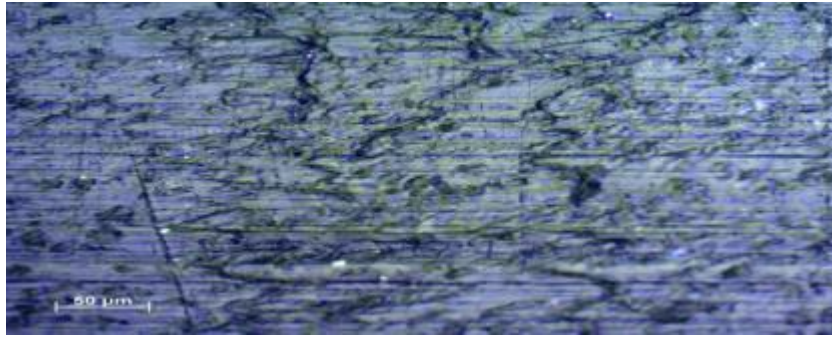


Fig. 17- Contact Surface before Test.

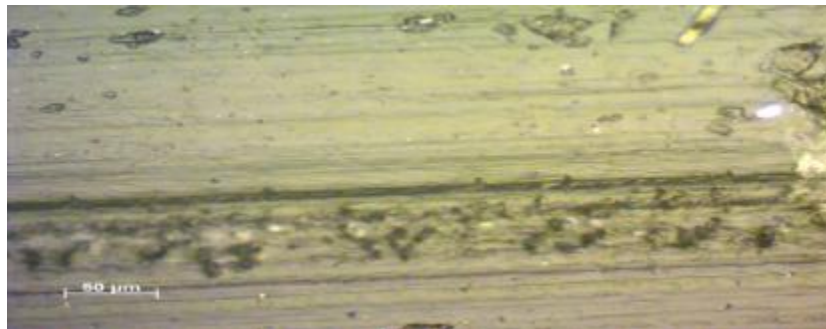


Fig. 18- Contact Surface after 05 Minutes at 3.3 m/sec and 30 N Test.

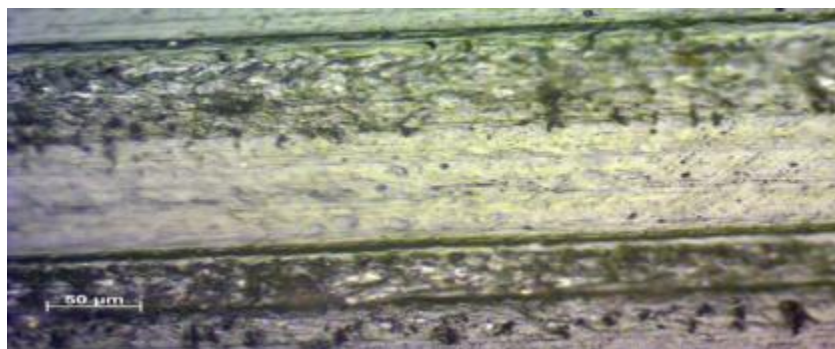


Fig. 19- Contact Surface after 30 Minutes at 3.3 m/sec and 30 N Test.

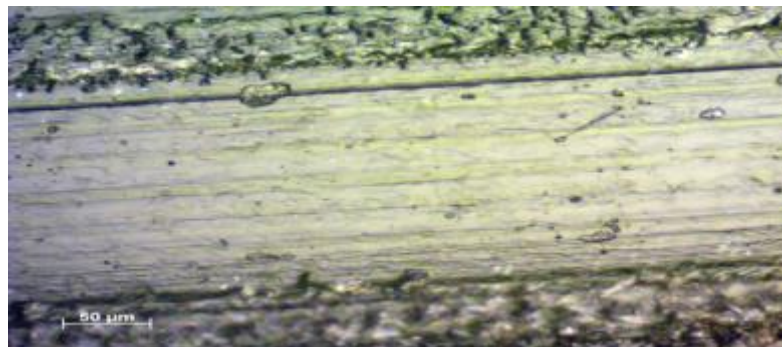


Fig. 20- Contact Surface after 60 Minutes at 3.3 m/sec and 30 N Test.

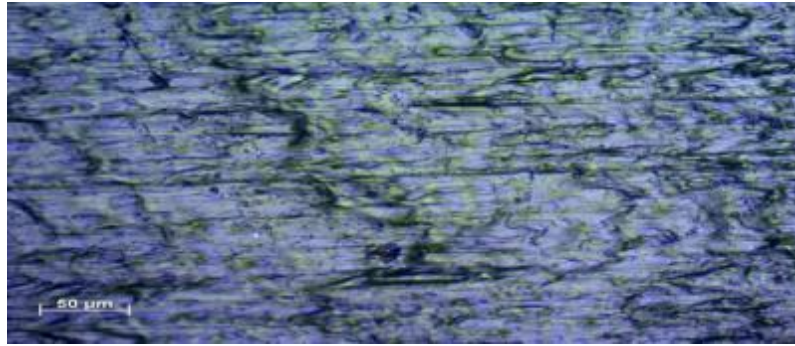


Fig. 21- Contact Surface before Test



Fig. 22- Contact Surface after 05 Minutes at 3.3 m/sec and 50 N Test.

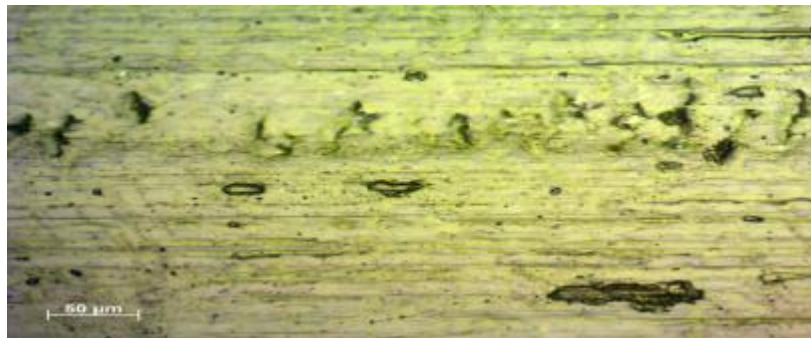


Fig. 23- Contact Surface after 30 Minutes at 3.3 m/sec and 50 N Test.



Fig. 24- Contact Surface after 60 Minutes at 3.3 m/sec and 50 N Test.

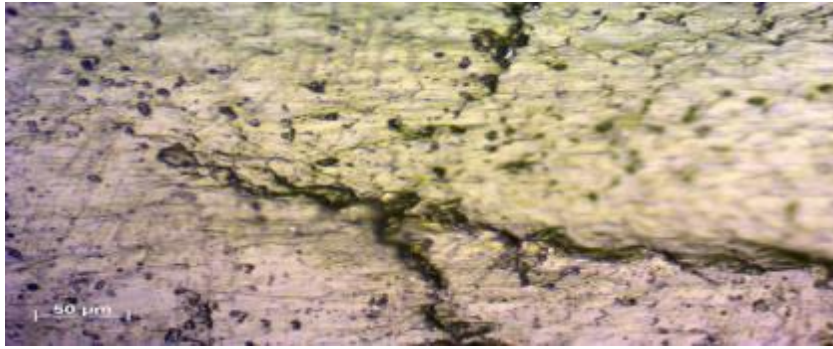


Fig. 25- Contact Surface before Test.

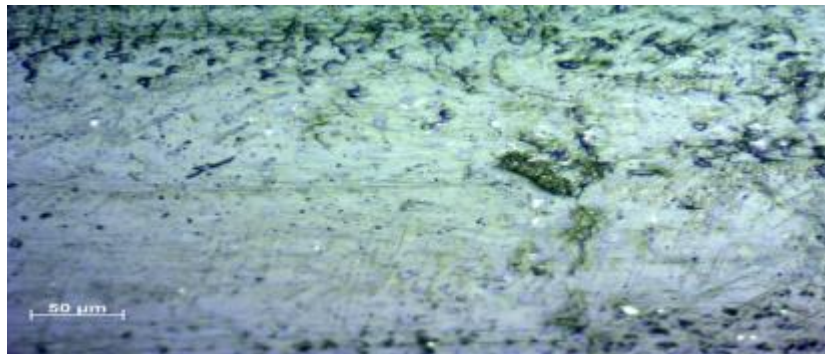


Fig. 4:26- Contact Surface after 05 Minutes at 7.2 m/sec and 10 N Test.

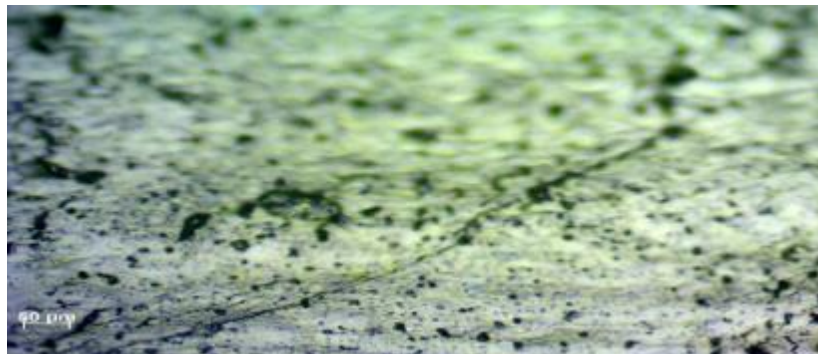


Fig. 27- Contact Surface after 30 Minutes at 7.2 m/sec and 10 N Test.

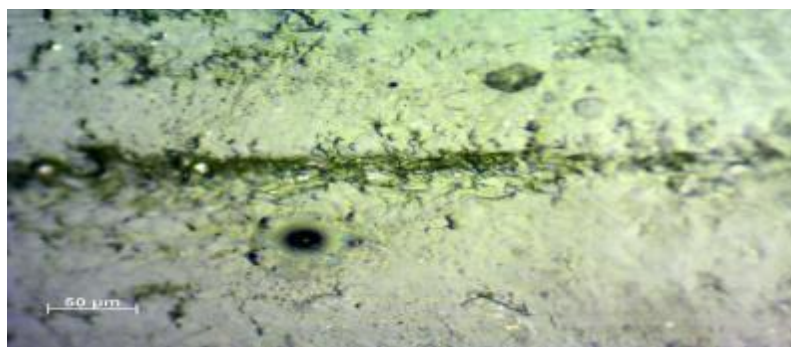


Fig. 28- Contact Surface after 60 Minutes at 7.2 m/sec and 10 Test.

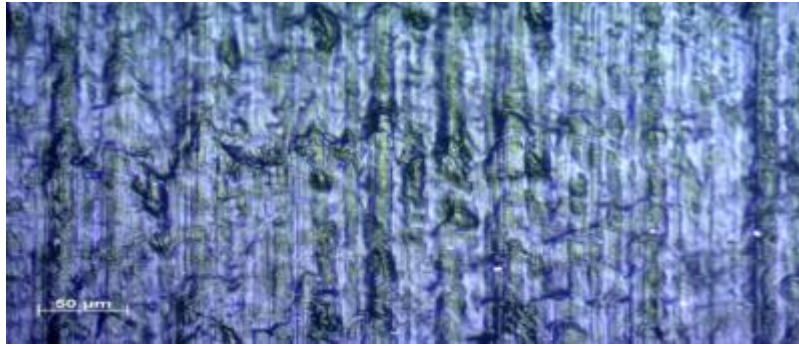


Fig. 29- Contact Surface before Test.



Fig. 30- Contact Surface after 05 Minutes at 7.2 m/sec and 30 N Test.

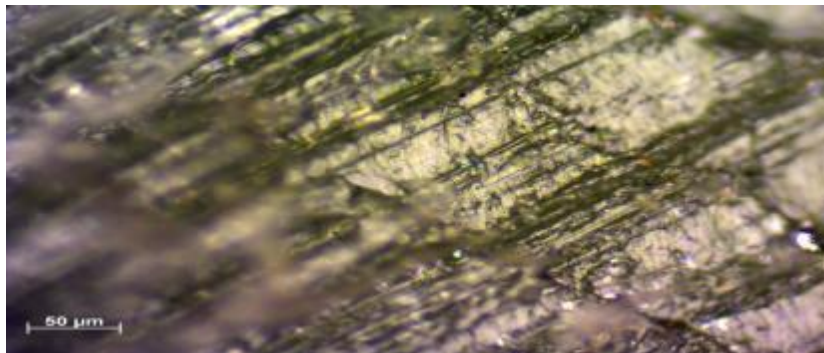


Fig. 31- Contact Surface before Test.

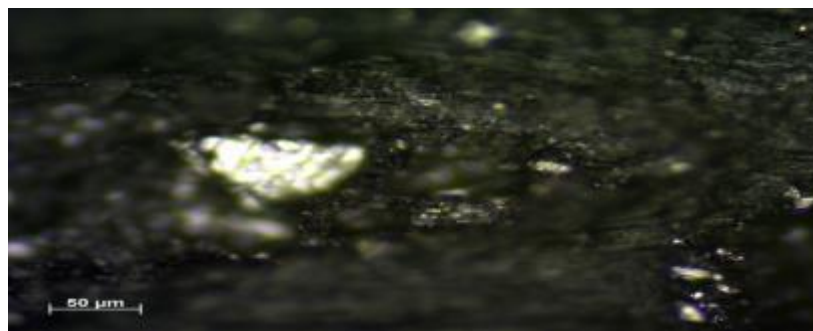


Fig. 32- Contact Surface after 05 Minutes at 7.2 m/sec and 50 N Test.

2- Nylon 66 Material (N 66)

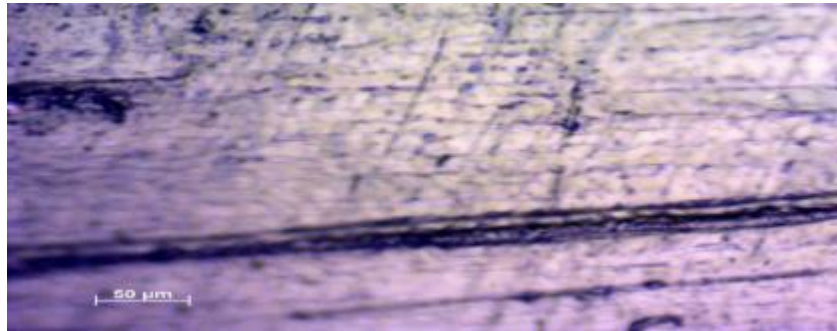


Fig. 33- Contact Surface before Test.

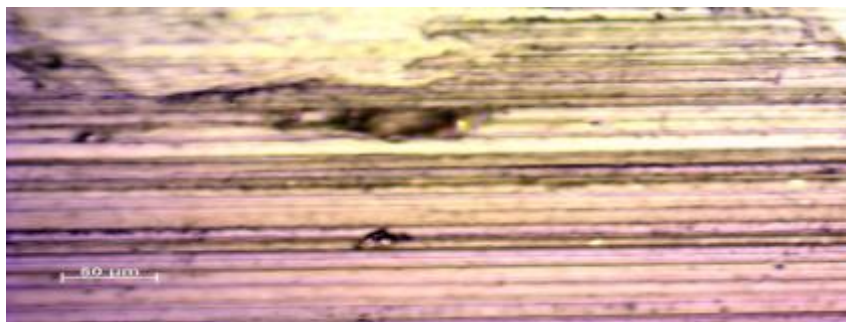


Fig. 34- Contact Surface after 05 Minutes at 1.5 m/sec and 10 N Test.

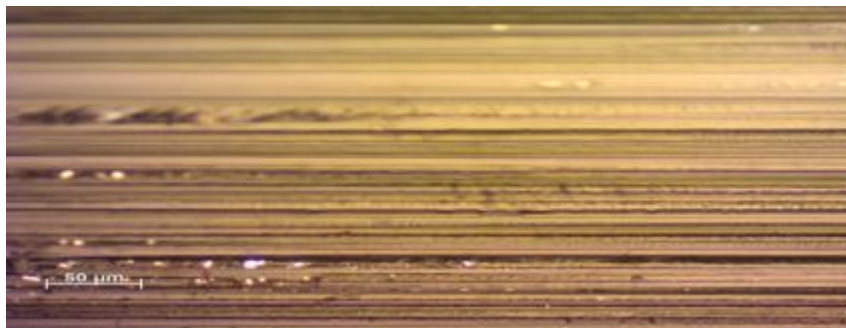


Fig. 35- Contact Surface after 30 Minutes at 1.5 m/sec and 10 N Test.

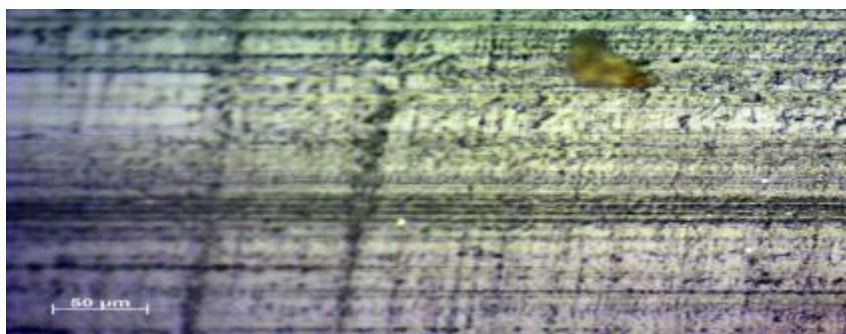


Fig. 36- Contact Surface after 60 Minutes at 1.5 m/sec and 10 N Test.

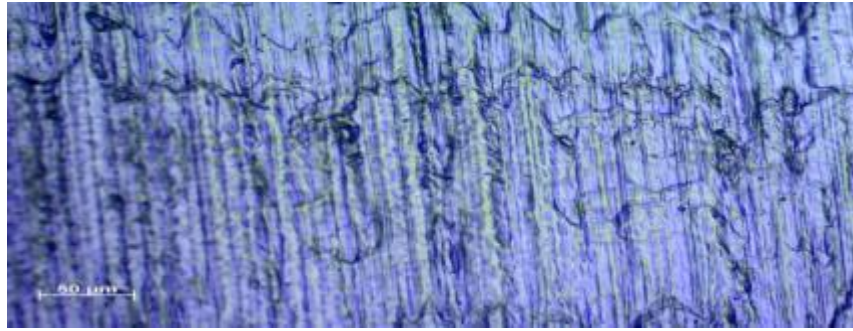


Fig. 37- Contact Surface before Test.

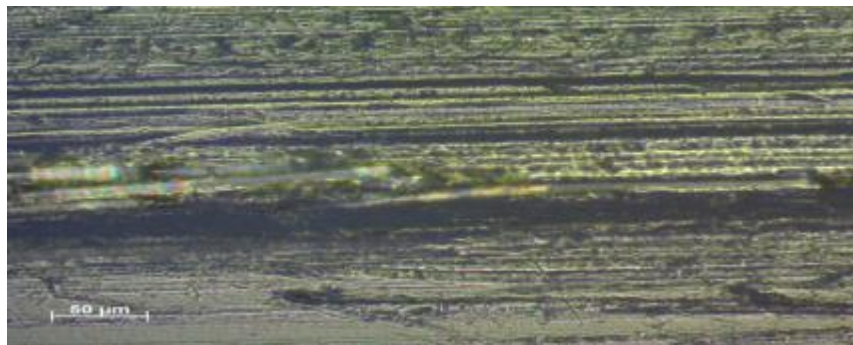


Fig. 38- Contact Surface after 05 Minutes at 1.5 m/sec and 30 N Test.

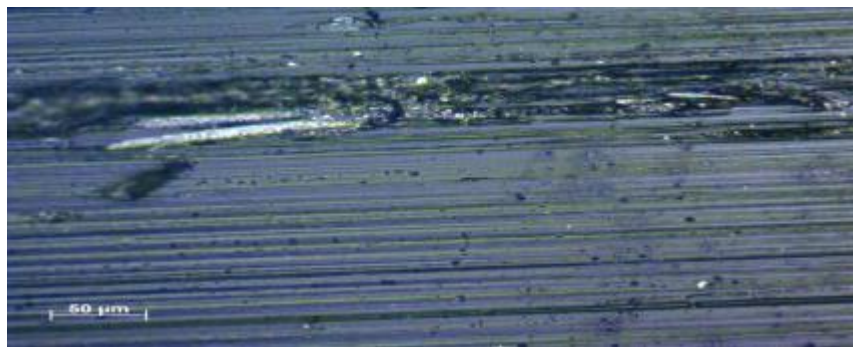


Fig. 39- Contact Surface after 30 Minutes at 1.5 m/sec and 30 N Test.

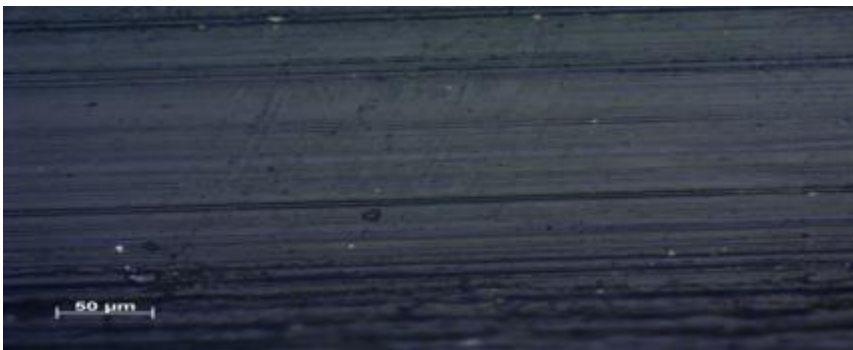


Fig. 40- Contact Surface after 60 Minutes at 1.5 m/sec and 30 N Test.

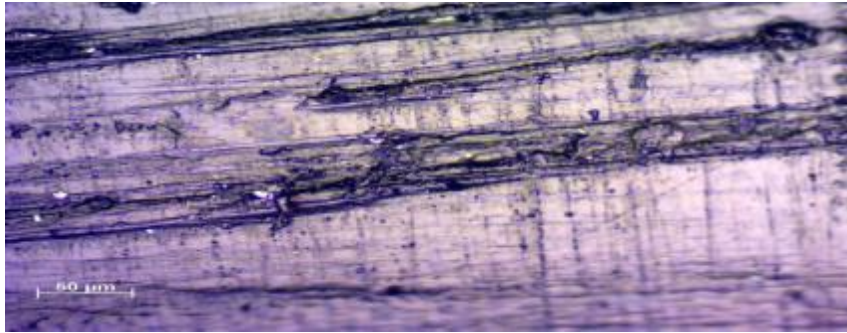


Fig. 41- Contact Surface before Test.

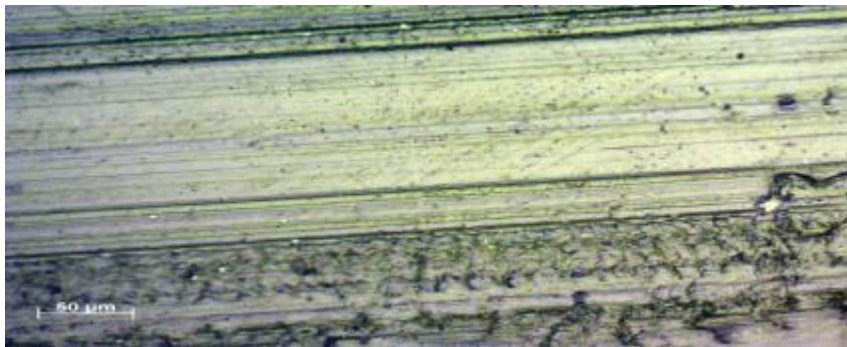


Fig. 42- Contact Surface after 05 Minutes at 1.5 m/sec and 50 N Test.

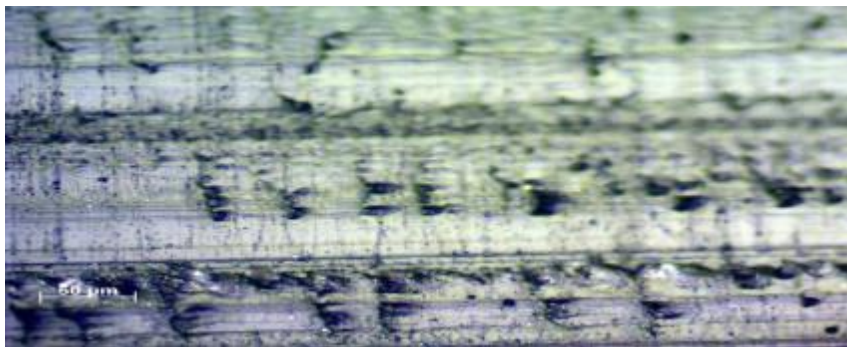


Fig. 43- Contact Surface after 30 Minutes at 1.5 m/sec and 50 N Test.



Fig. 44- Contact Surface after 60 Minutes at 1.5 m/sec and 50 N Test.

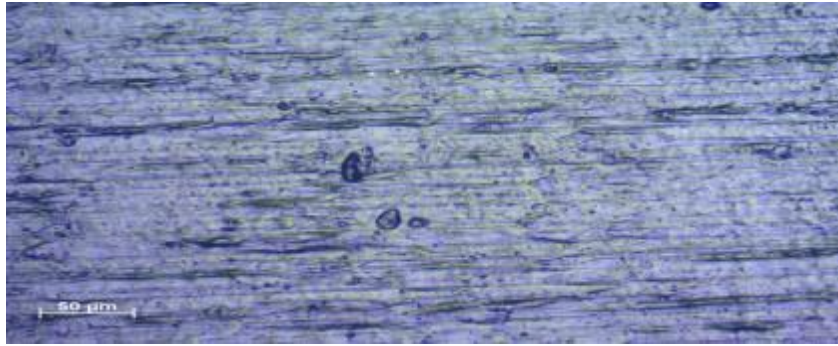


Fig. 45- Contact Surface before Test.

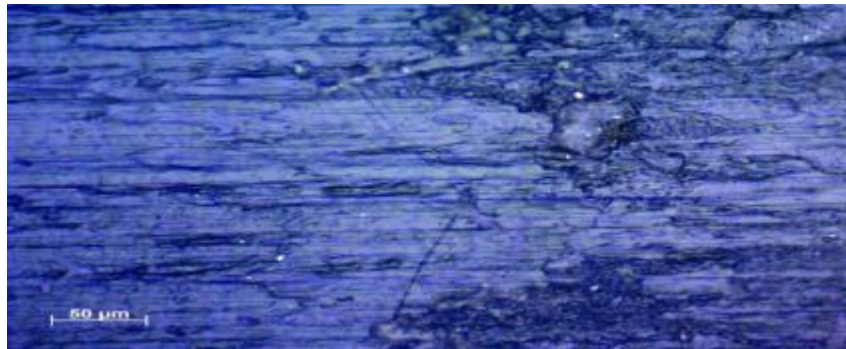


Fig. 46- Contact Surface after 05 Minutes at 3.3 m/sec and 10 N Test.

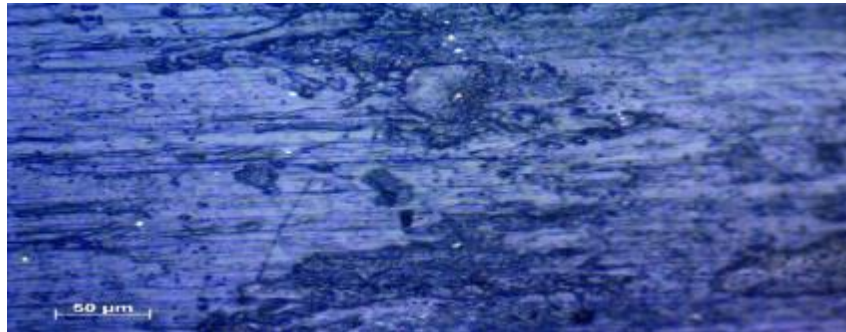


Fig. 47- Contact Surface after 30 Minutes at 3.3 m/sec and 10 N Test.

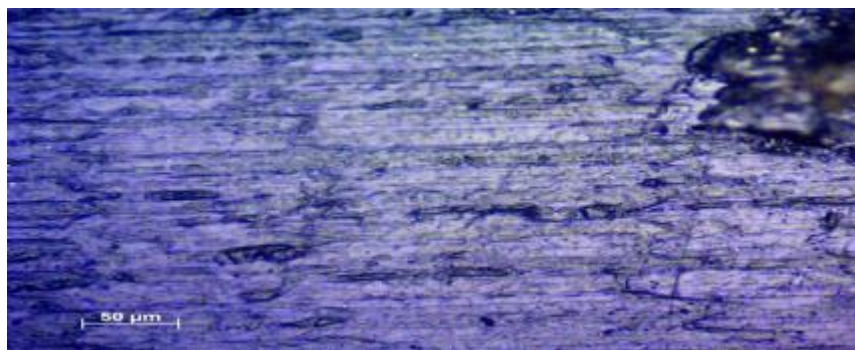


Fig. 48- Contact Surface after 60 Minutes at 3.3 m/sec and 10 N Test.

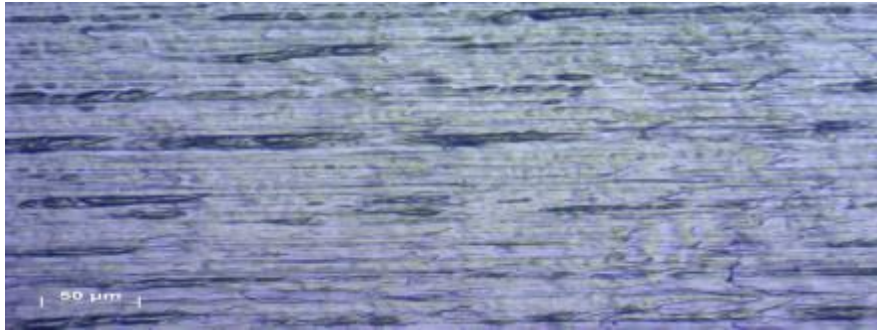


Fig. 49- Contact Surface before Test.

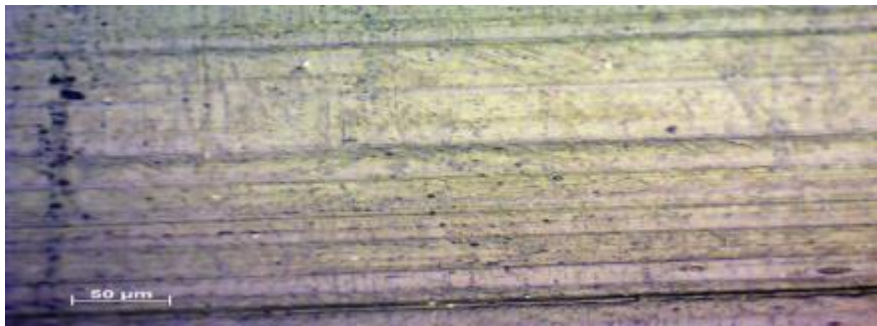


Fig. 50- Contact Surface after 05 Minutes at 3.3 m/sec and 30 N Test.

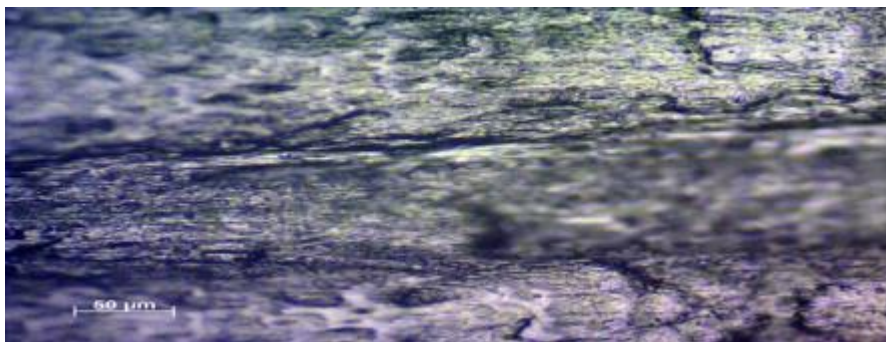


Fig. 51- Contact Surface after 30 Minutes at 3.3 m/sec and 30 N Test.



Fig. 52- Contact Surface after 60 Minutes at 3.3 m/sec and 30 N Test.

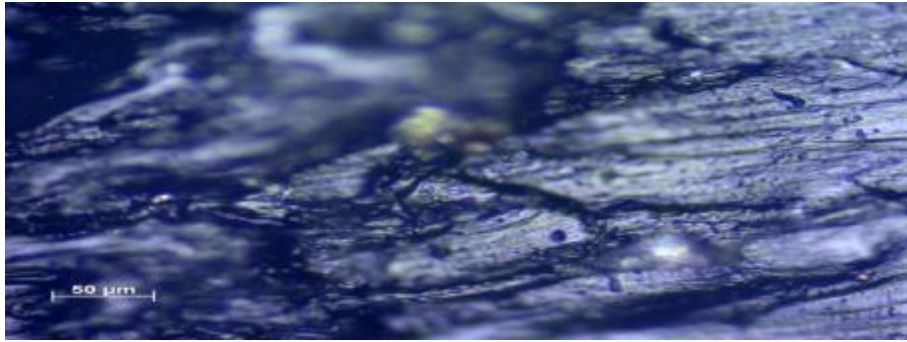


Fig. 53- Contact Surface before Test.

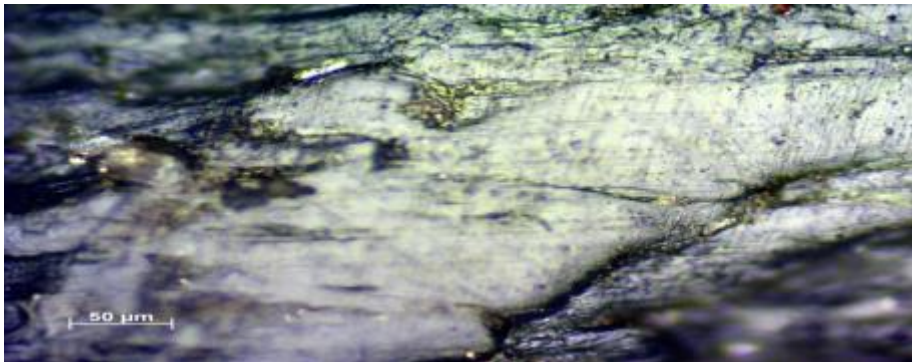


Fig. 54- Contact Surface after 05 Minutes at 3.3 m/sec and 50 N Test.

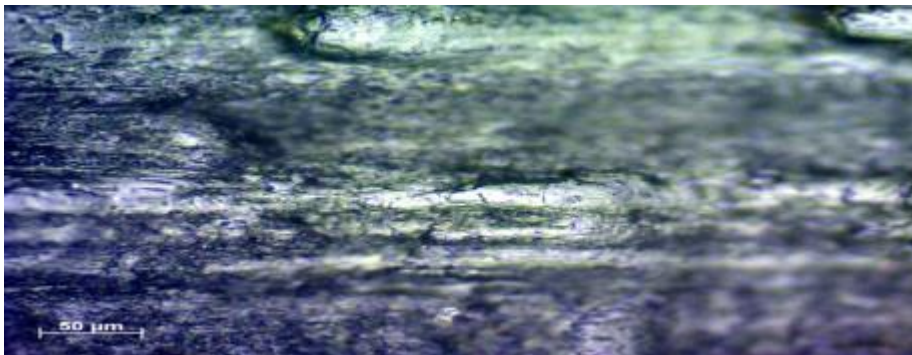


Fig. 55- Contact Surface after 30 Minutes at 3.3 m/sec and 50 N Test.

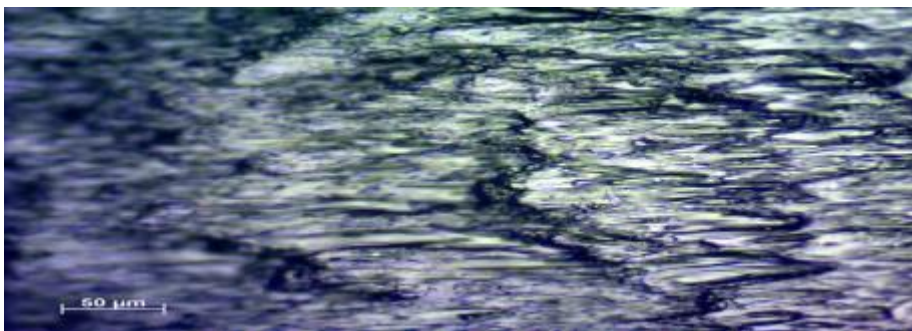


Fig. 56- Contact Surface after 60 Minutes at 3.3 m/sec and 50 N Test.

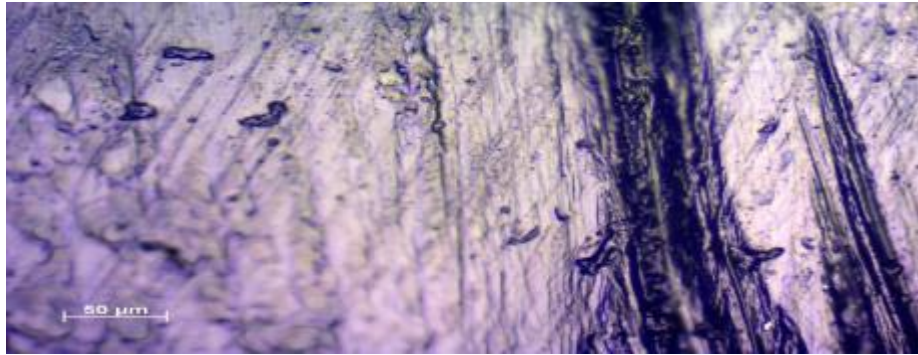


Fig. 57- Contact Surface before Test.

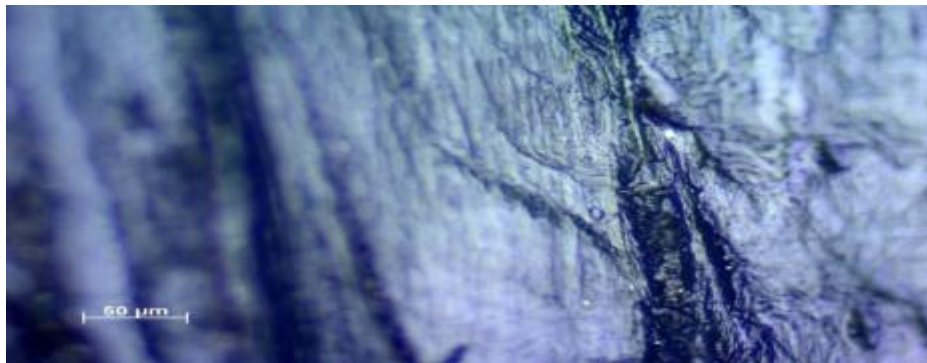


Fig. 58- Contact Surface after 05 Minutes at 7.2 m/sec and 10 N Test.

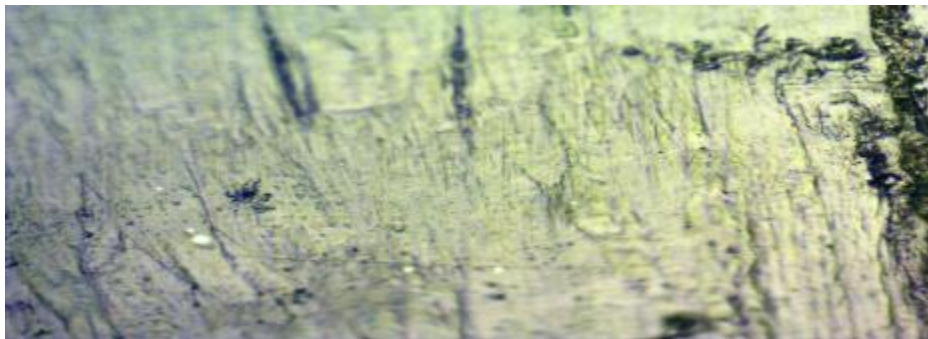


Fig. 59- Contact Surface after 30 Minutes at 7.2 m/sec and 10 N Test.

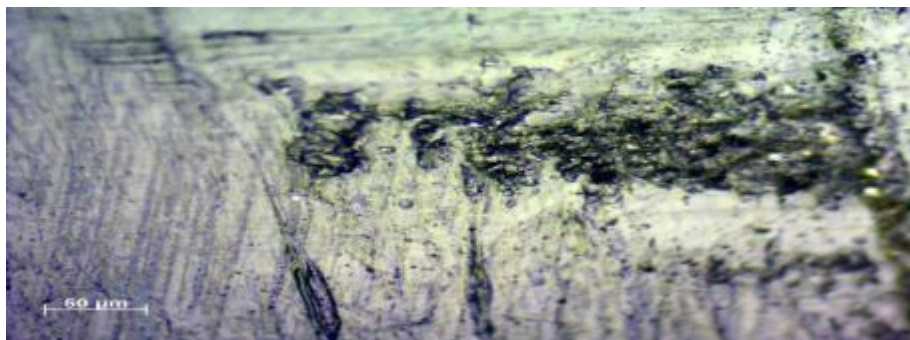


Fig. 60- Contact Surface after 60 Minutes at 7.2 m/sec and 10 N Test.

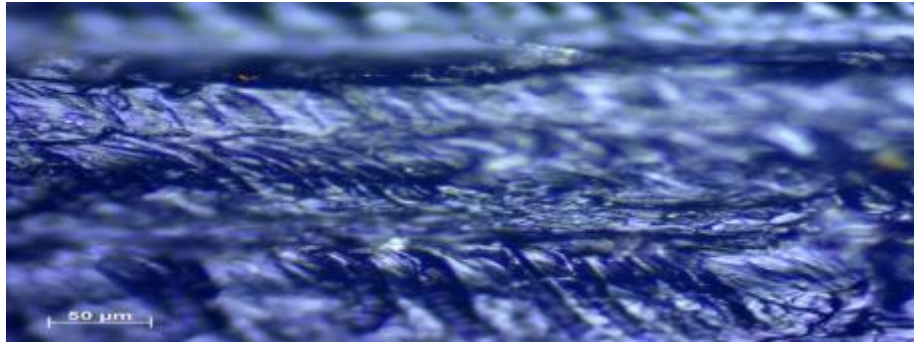


Fig. 61- Contact Surface before Test.

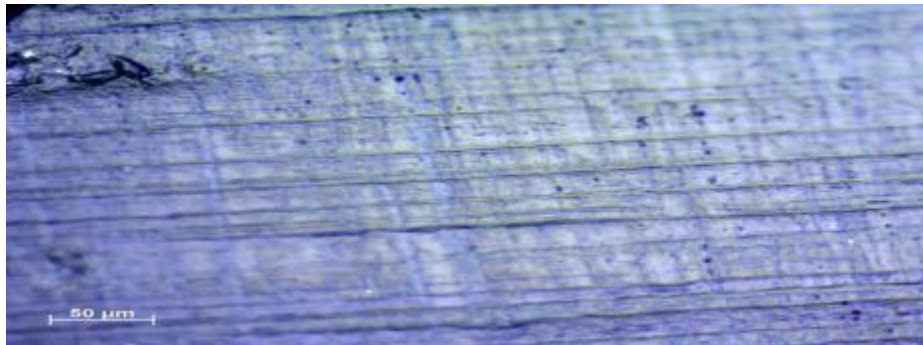


Fig. 62- Contact Surface after 05 Minutes at 7.2 m/sec and 30 N Test.

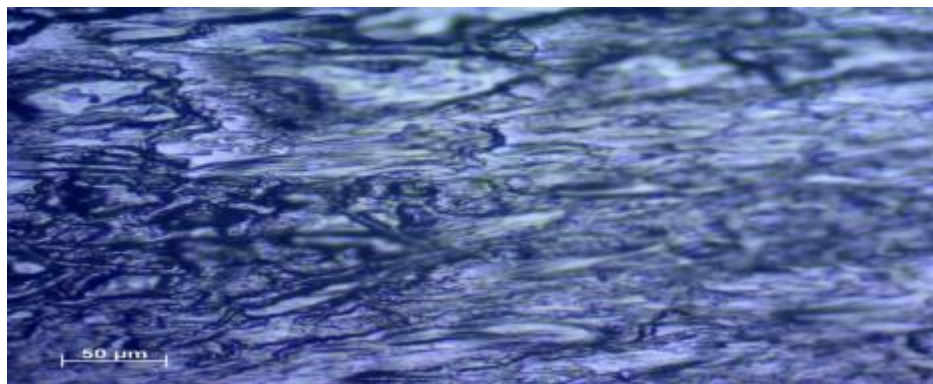


Fig. 63- Contact Surface after 30 Minutes at 7.2 m/sec and 30 N Test.

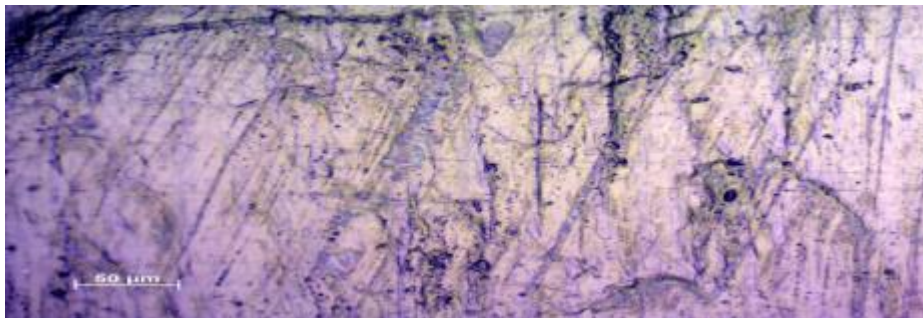


Fig. 64- Contact Surface before Test



Fig. 65- Contact Surface after 05 Minutes at 7.2 m/sec and 50 N Test.

3- Nylon 66a Material (N 66a)



Fig. 66- Contact Surface before Test.



Fig. 67- Contact Surface after 05 Minutes at 1.5 m/sec and 10 N Test.

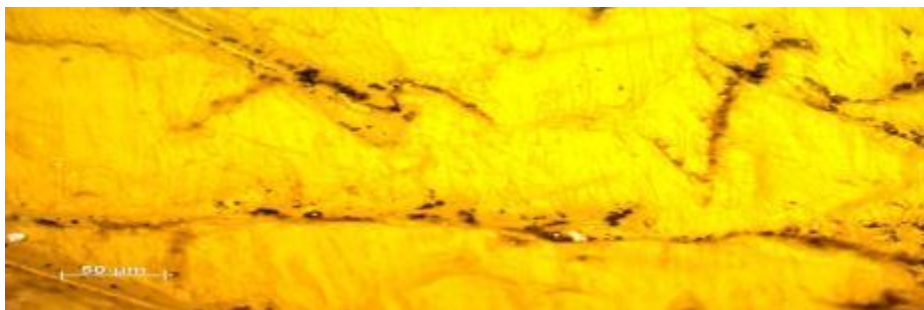


Fig. 68- Contact Surface after 30 Minutes at 1.5 m/sec and 10 N Test.



Fig. 69- Contact Surface after 60 Minutes at 1.5 m/sec and 10 N Test.



Fig. 70- Contact Surface before Test.

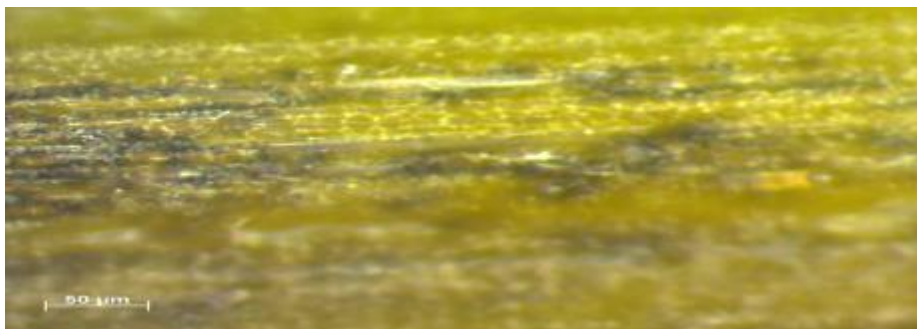


Fig. 71- Contact Surface after 05 Minutes at 1.5 m/sec and 30 Test.

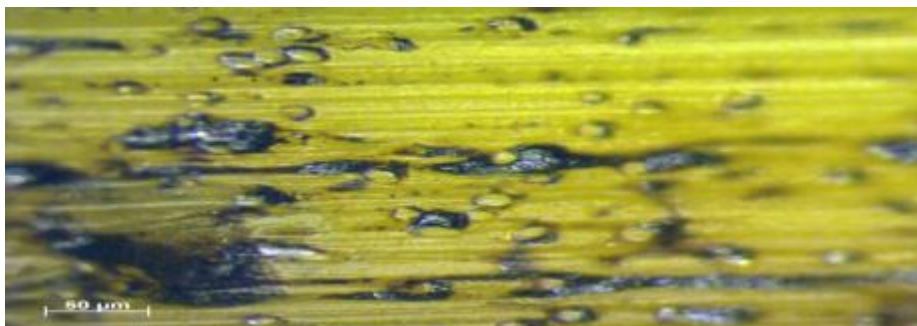


Fig. 72- Contact Surface after 30 Minutes at 1.5 m/sec and 30 N Test.

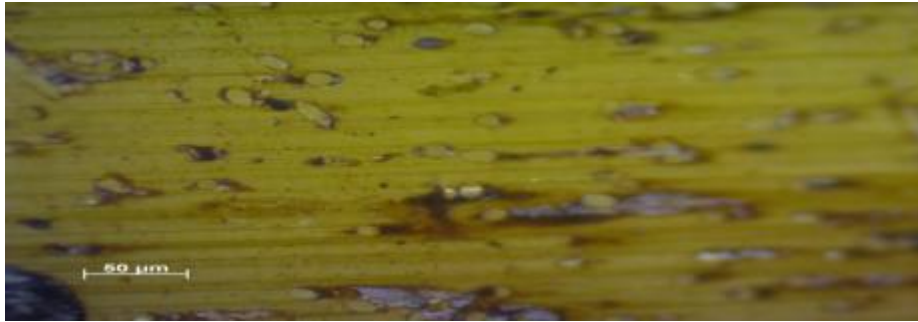


Fig. 73- Contact Surface after 60 Minutes at 1.5 m/sec and 30 N Test.



Fig. 74- Contact Surface before Test.

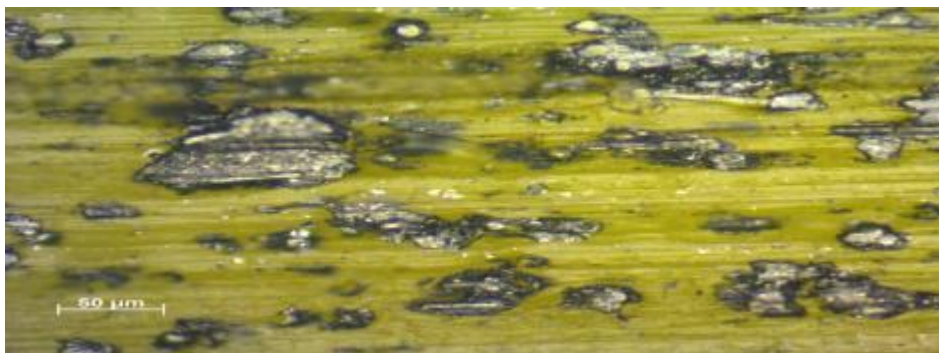


Fig. 75- Contact Surface after 05 Minutes at 1.5 m/sec and 50 Test.

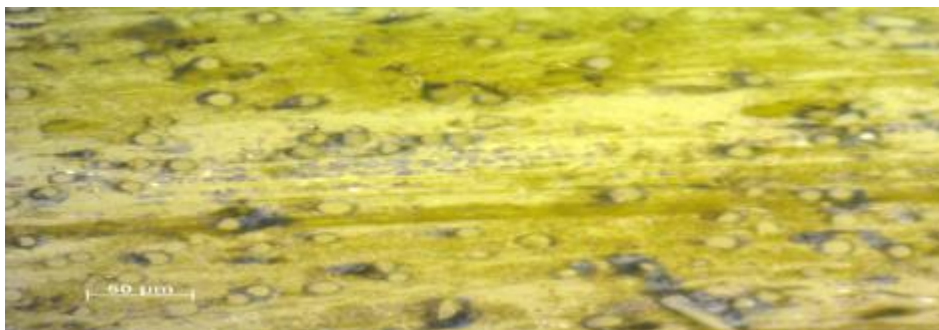


Fig. 76- Contact Surface after 30 Minutes at 1.5 m/sec and 50 Test.

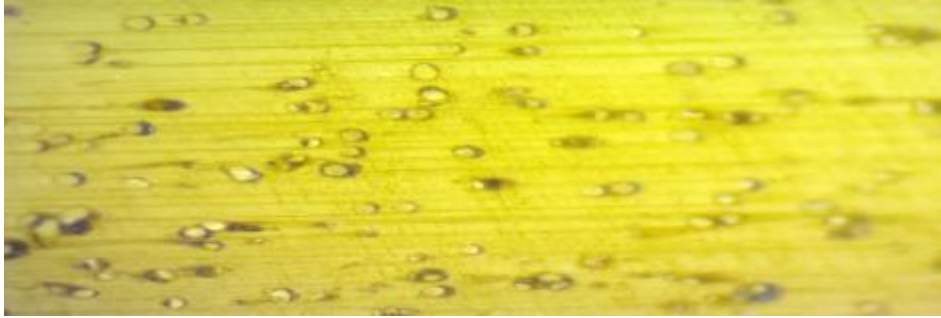


Fig. 77- Contact Surface after 60 Minutes at 1.5 m/sec and 50 N Test.



Fig. 78- Contact Surface before Test.

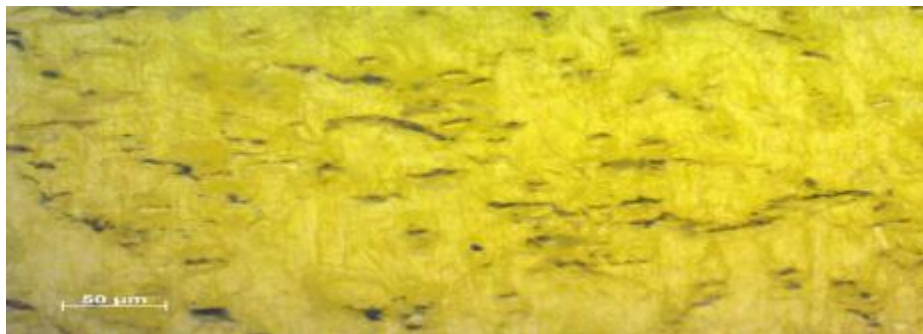


Fig. 79- Contact Surface after 05 Minutes at 3.3 m/sec and 10 N Test.

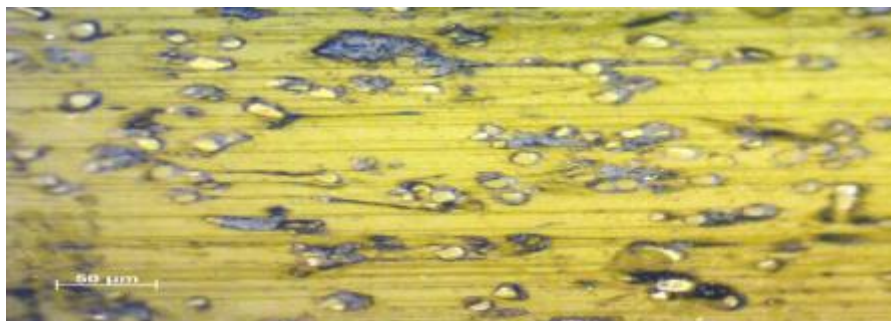


Fig. 80- Contact Surface after 30 Minutes at 3.3 m/sec and 10 N Test.

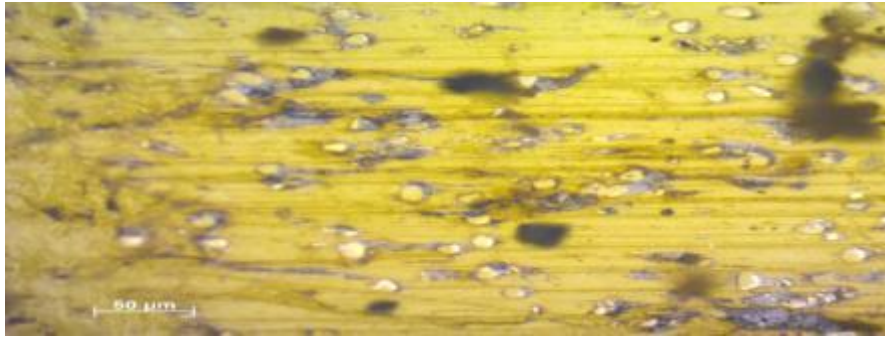


Fig. 81- Contact Surface after 60 Minutes at 3.3 m/sec and 10 Test.



Fig. 82- Contact Surface before Test.



Fig. 83- Contact Surface after 05 Minutes at 3.3 m/sec and 30 N Test.

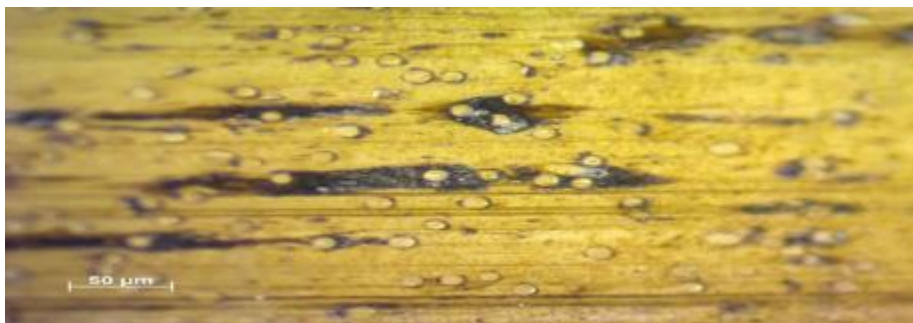


Fig. 84- Contact Surface after 30 Minutes at 3.3 m/sec and 30 N Test.

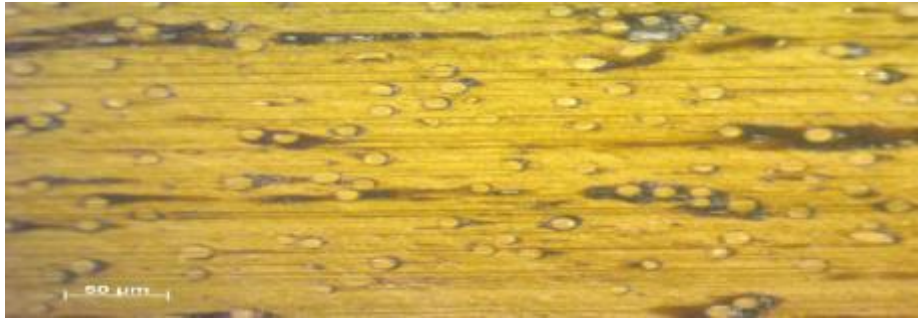


Fig. 85- Contact Surface after 60 Minutes at 3.3 m/sec and 30 N Test.



Fig. 86- Contact Surface before Test.

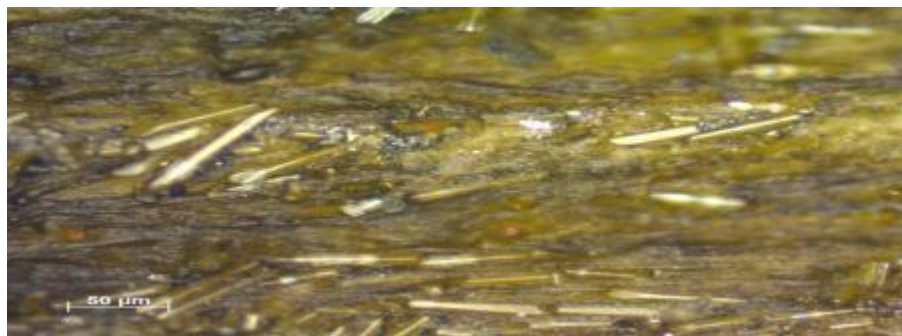


Fig. 87- Contact Surface after 05 Minutes at 3.3 m/sec and 50 N Test.



Fig. 88- Contact Surface after 30 Minutes at 3.3 m/sec and 50 N Test.

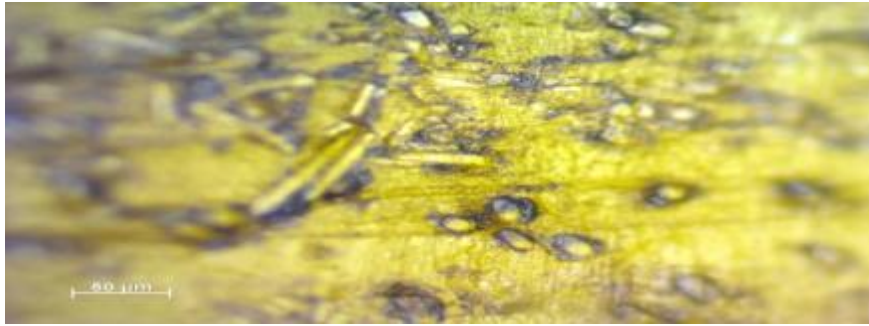


Fig. 89- Contact Surface after 60 Minutes at 3.3 m/sec and 50 N Test.



Fig. 90- Contact Surface before Test.

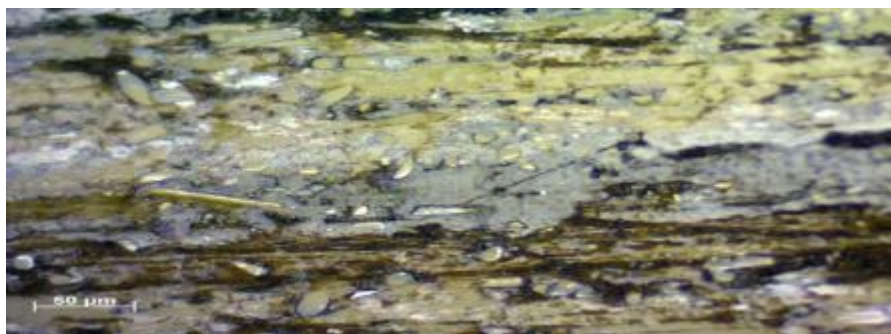


Fig. 91- Contact Surface after 05 Minutes at 7.2 m/sec and 10 N Test.

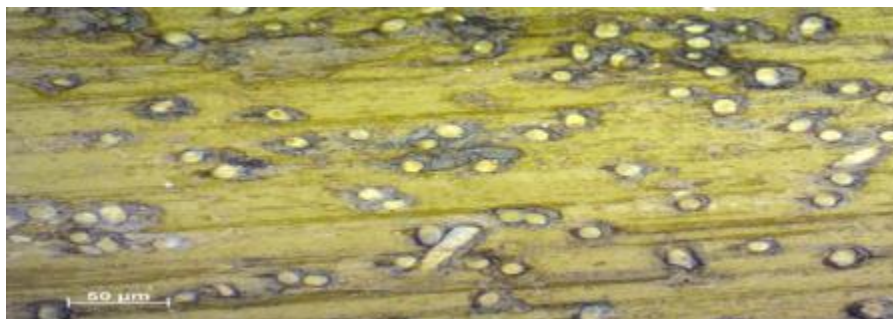


Fig. 92- Contact Surface after 30 Minutes at 7.2 m/sec and 10 N Test.

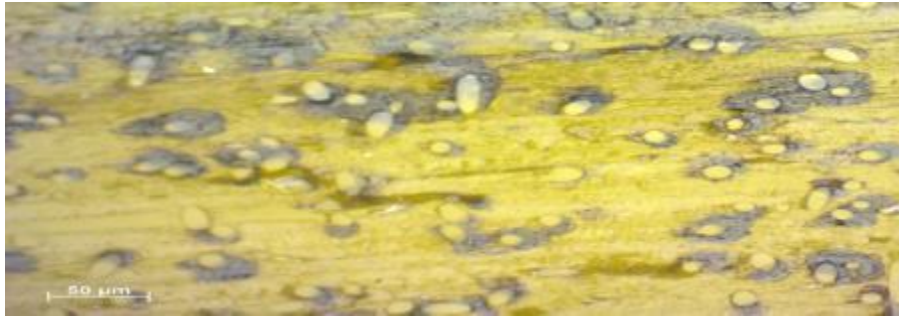


Fig. 93- Contact Surface after 60 Minutes at 7.2 m/sec and 10 N Test.



Fig. 94- Contact Surface before Test.

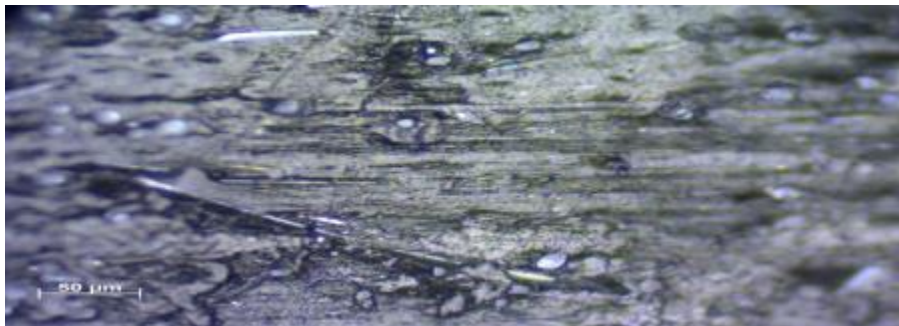


Fig. 95- Contact Surface after 05 Minutes at 7.2 m/sec and 30 N Test.



Fig. 96- Contact Surface after 30 Minutes at 7.2 m/sec and 30 N Test.

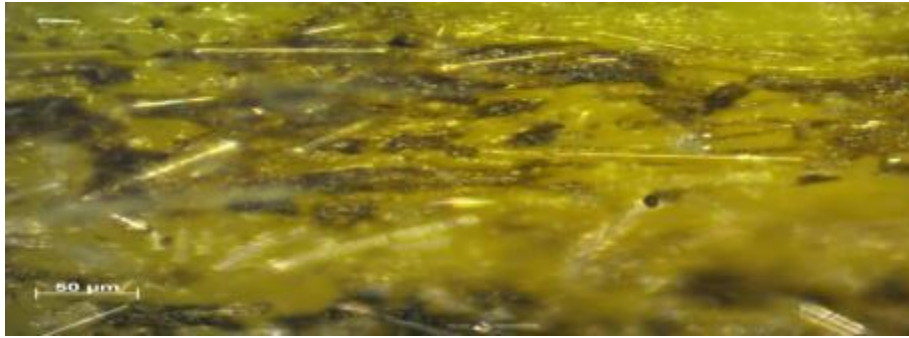


Fig. 97- Contact Surface after 60 Minutes at 7.2 m/sec and 30 N Test.



Fig. 98- Contact Surface before Test.



Fig. 99- Contact Surface after 05 Minutes at 7.2 m/sec and 50 N Test.

4- Epoxy Glass Material (EG)

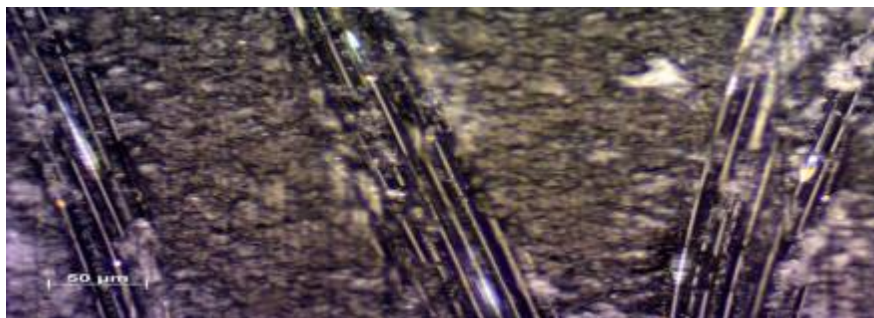


Fig. 100- Contact Surface before Test.

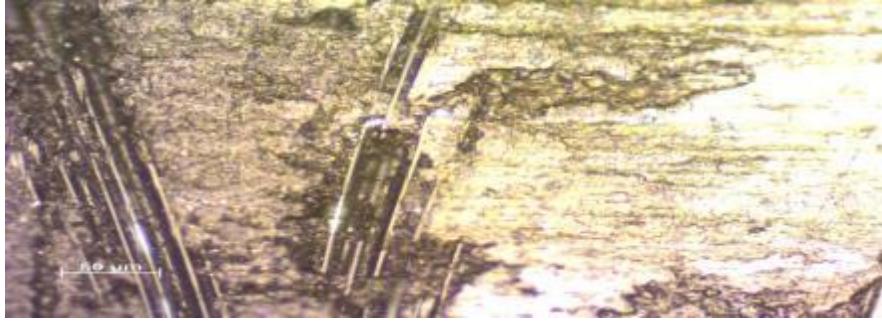


Fig. 101- Contact Surface after 05 Minutes at 1.5 m/sec and 10 N Test.

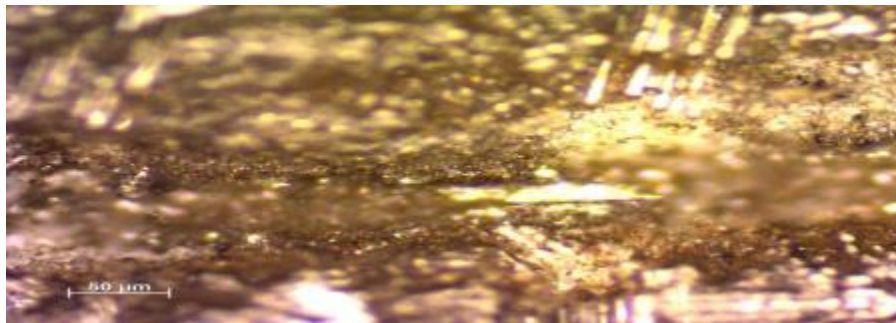


Fig. 102- Contact Surface after 30 Minutes at 1.5 m/sec and 10 N Test.

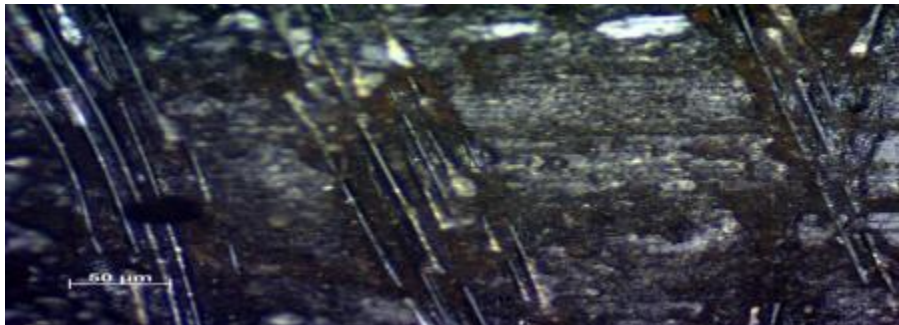


Fig. 103- Contact Surface after 60 Minutes at 1.5 m/sec and 10 N Test.

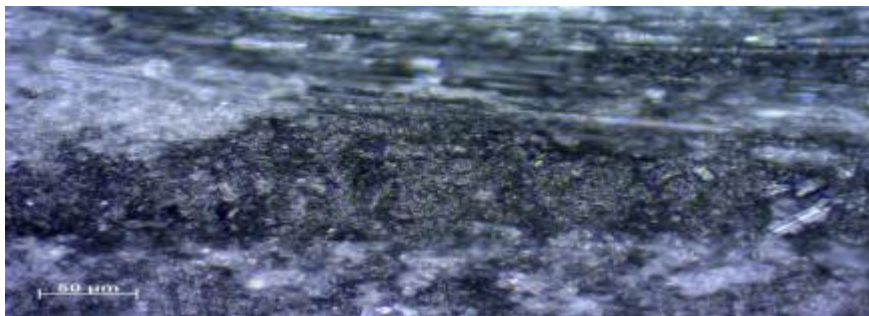


Fig. 104- Contact Surface before Test.

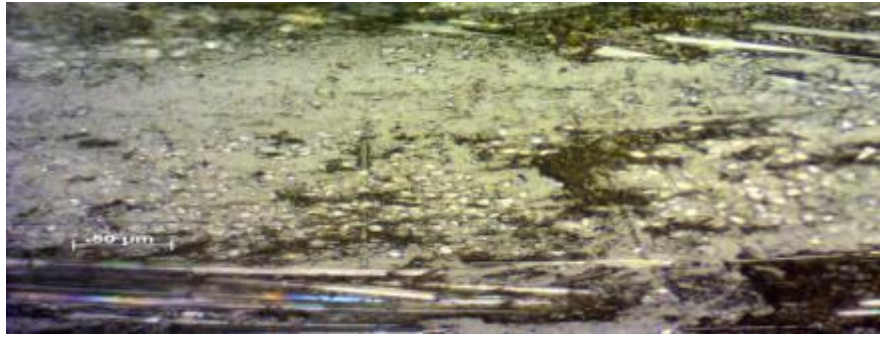


Fig. 105- Contact Surface after 05 Minutes at 1.5 m/sec and 30 N Test.

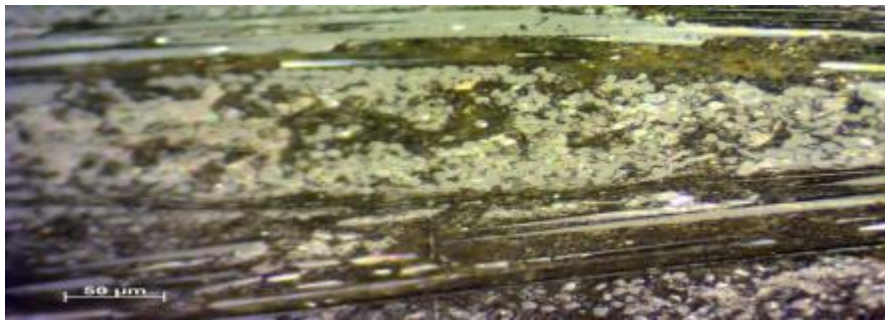


Fig. 106- Contact Surface after 30 Minutes at 1.5 m/sec and 30 N Test.

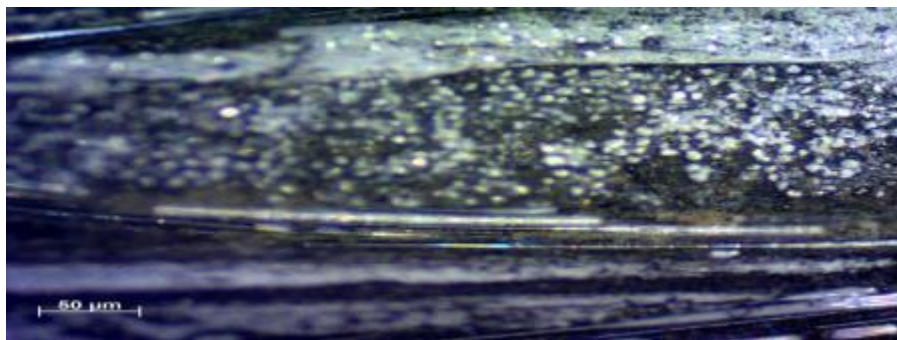


Fig. 107- Contact Surface after 60 Minutes at 1.5 m/sec and 30 N Test.

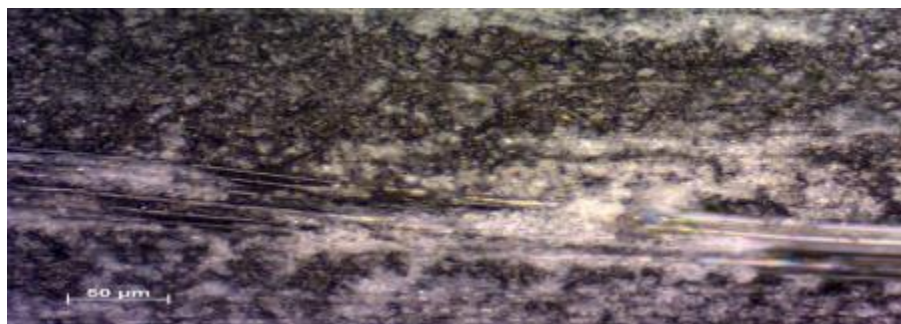


Fig. 108- Contact Surface before Test.

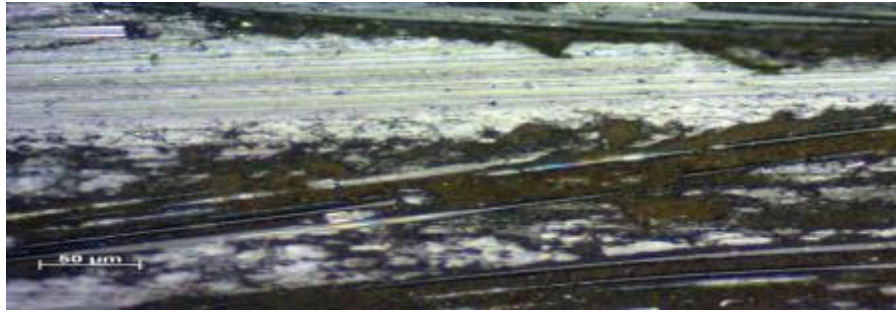


Fig. 109- Contact Surface after 05 Minutes at 1.5 m/sec and 50 N Test.



Fig. 110- Contact Surface after 30 Minutes at 1.5 m/sec and 50 N Test.

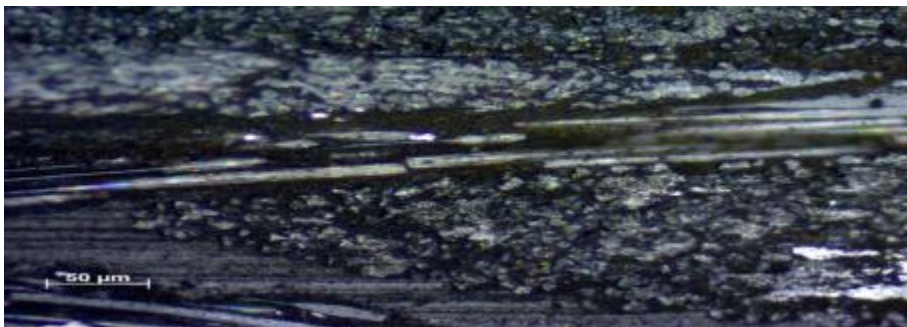


Fig. 111- Contact Surface after 60 Minutes at 1.5 m/sec and 50 N Test.

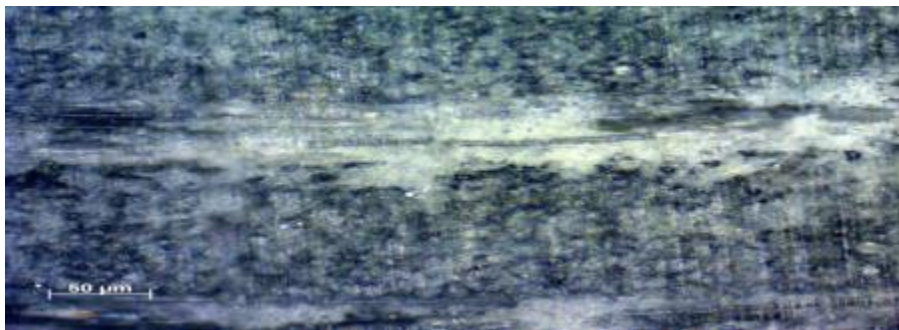


Fig. 112- Contact Surface before Test.

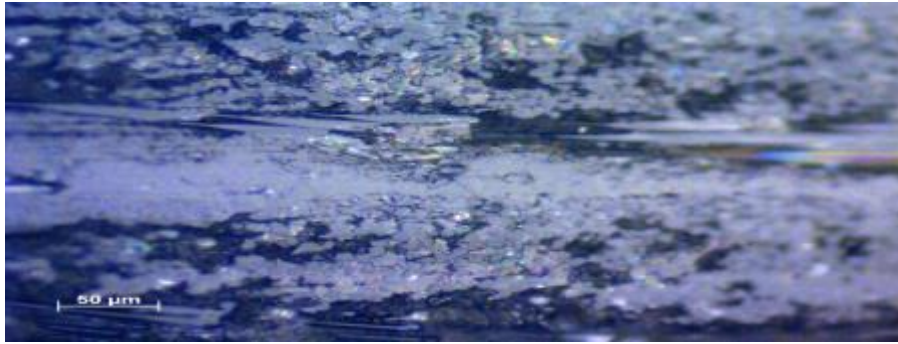


Fig. 113- Contact Surface after 05 Minutes at 3.3 m/sec and 10 N Test.

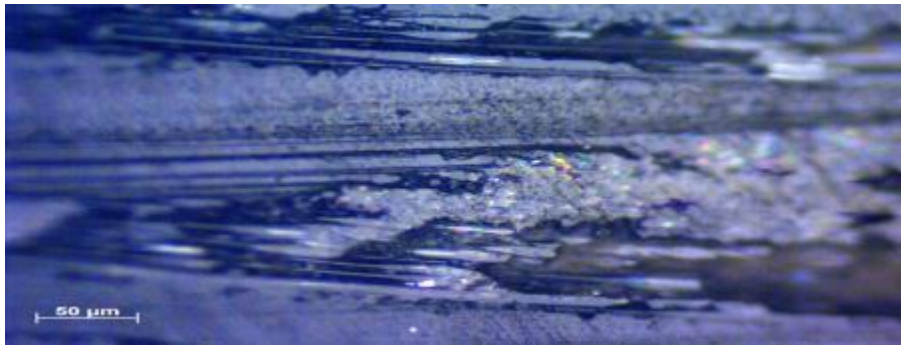


Fig. 114- Contact Surface after 30 Minutes at 3.3 m/sec and 10 N Test.

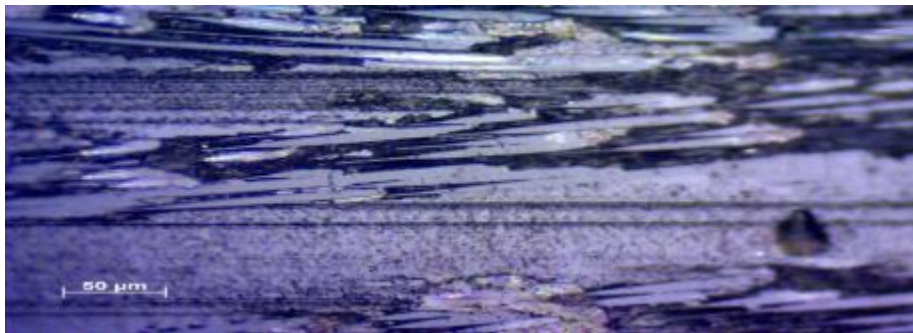


Fig. 115- Contact Surface after 60 Minutes at 3.3 m/sec and 10 N Test.

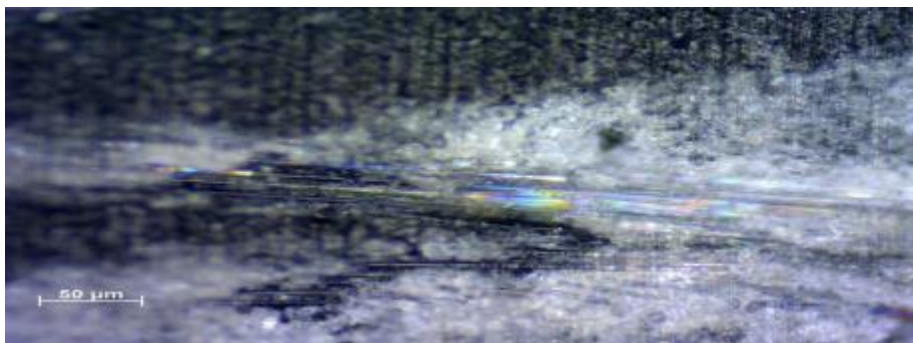


Fig. 116- Contact Surface before Test.

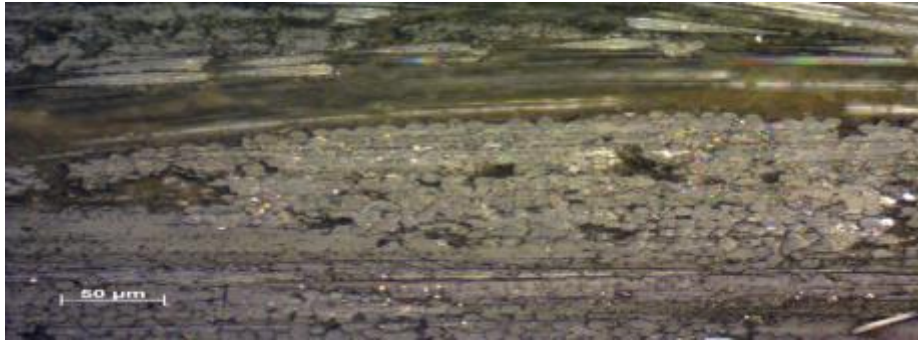


Fig. 117- Contact Surface after 05 Minutes at 3.3 m/sec and 30 N Test.

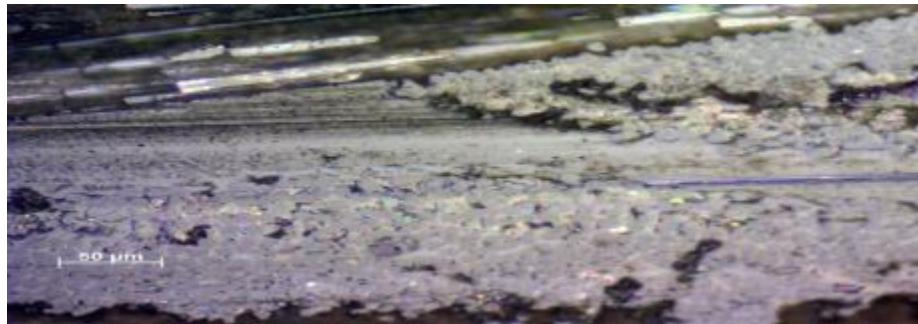


Fig. 118- Contact Surface after 30 Minutes at 3.3 m/sec and 30 N Test.

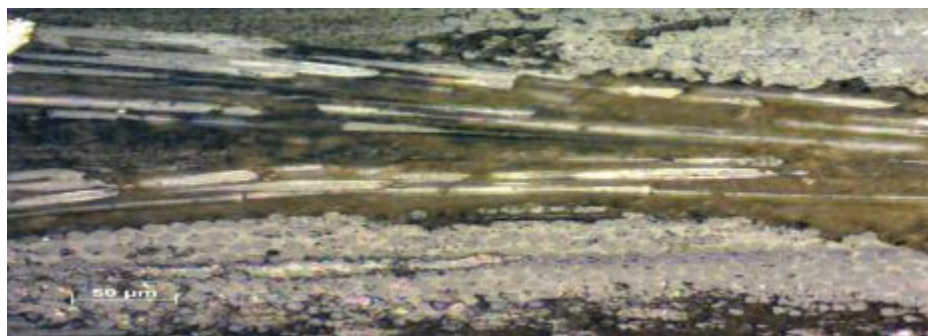


Fig. 119- Contact Surface after 60 Minutes at 3.3 m/sec and 30 N Test.

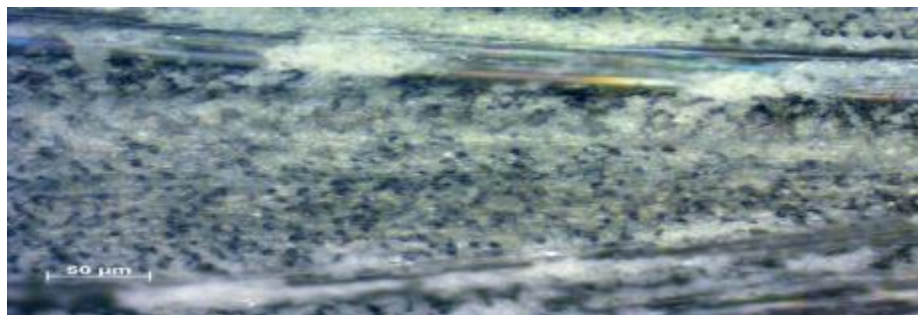


Fig120- Contact Surface before Test.

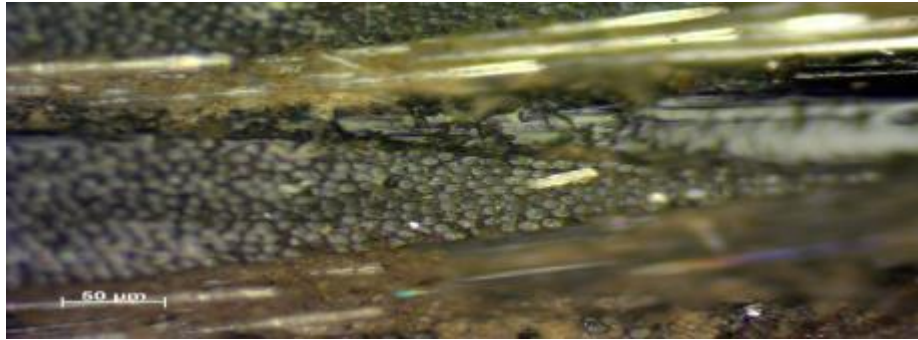


Fig. 121- Contact Surface after 05 Minutes at 3.3 m/sec and 50 N Test.

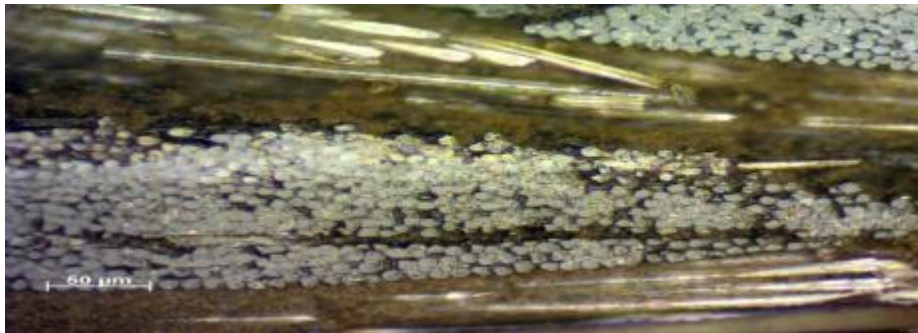


Fig. 122- Contact Surface after 30 Minutes at 3.3 m/sec and 50 N Test.

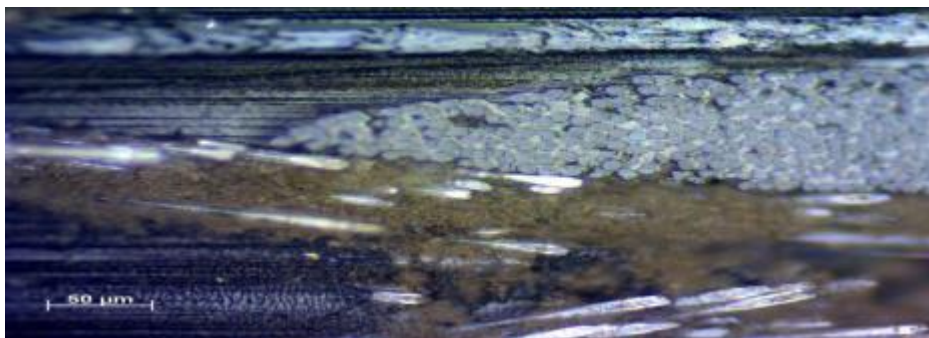


Fig. 123- Contact Surface after 60 Minutes at 3.3 m/sec and 50 N Test.

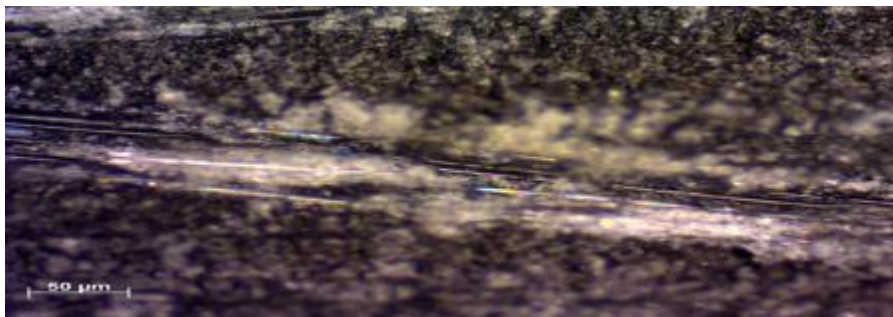


Fig. 124- Contact Surface before Test.

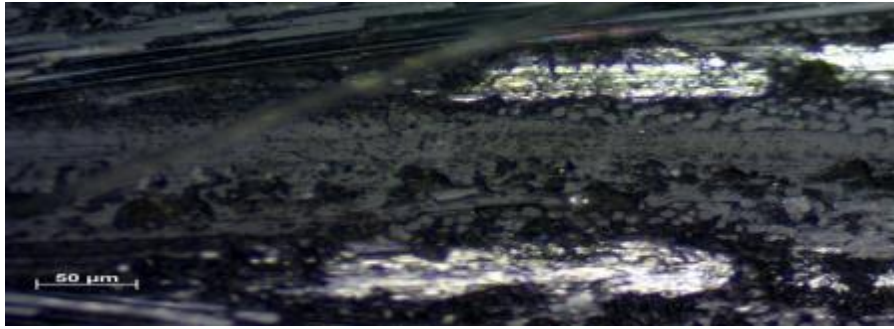


Fig. 125- Contact Surface after 05 Minutes at 7.2 m/sec and 10 N Test.

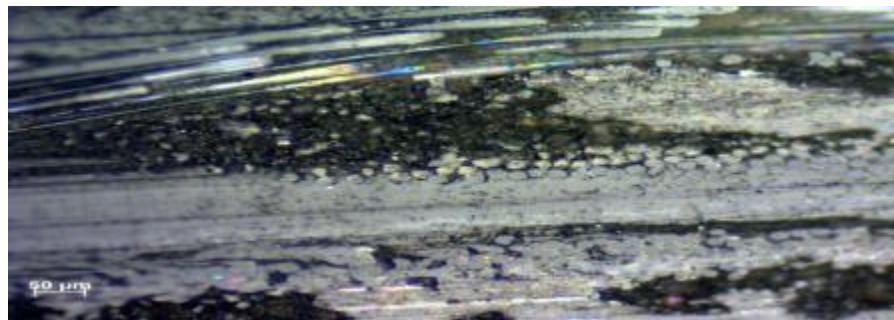


Fig. 126- Contact Surface after 30 Minutes at 7.2 m/sec and 10 N Test.

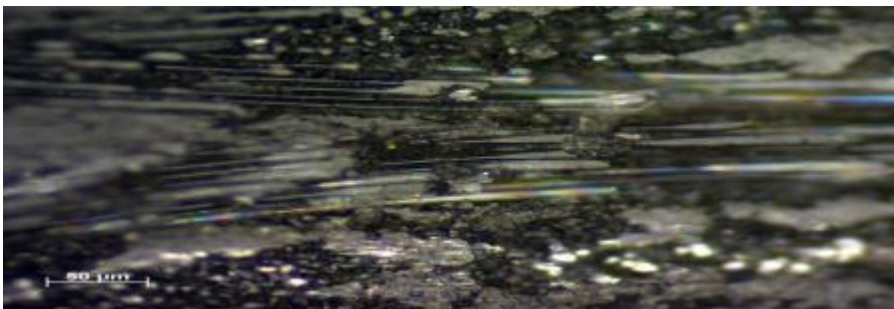


Fig. 127- Contact Surface after 60 Minutes at 7.2 m/sec and 10 N Test.

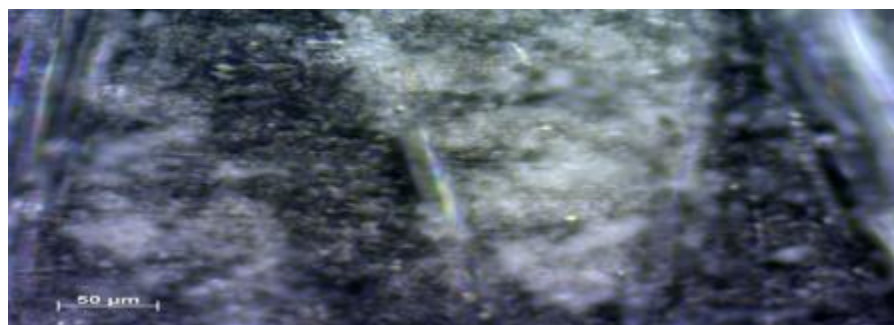


Fig. 128- Contact Surface before Test.

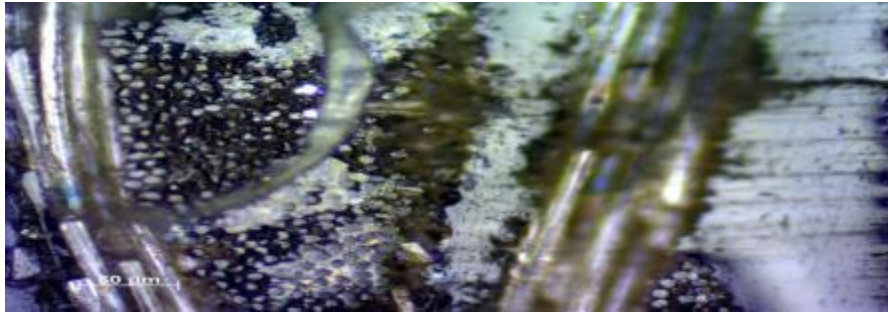


Fig. 129- Contact Surface after 05 Minutes at 7.2 m/sec and 30 N Test.

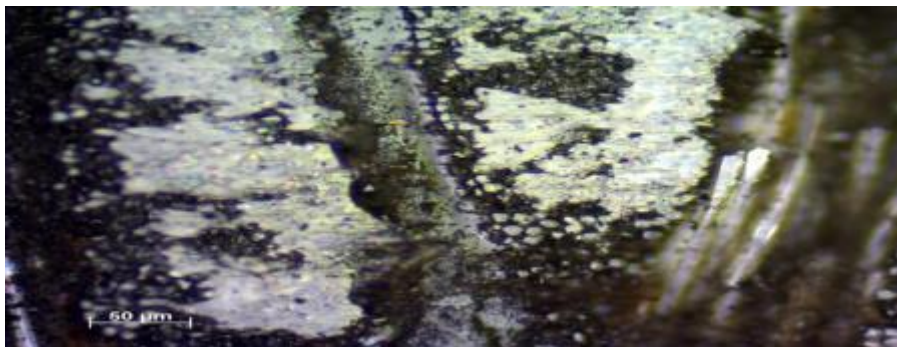


Fig. 130- Contact Surface after 30 Minutes at 7.2 m/sec and 30 N Test.



Fig. 131- Contact Surface after 60 Minutes at 7.2 m/sec and 30 N Test.

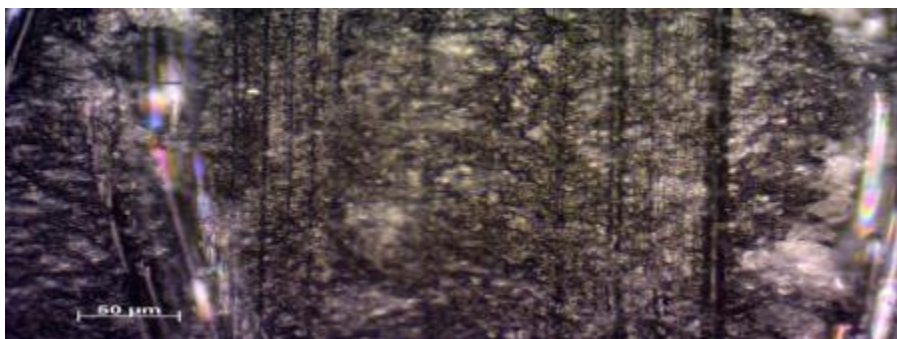


Fig. 132- Contact Surface before Test.

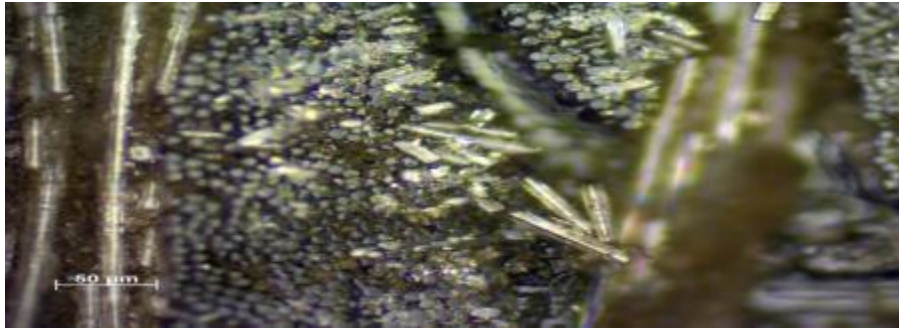


Fig. 133- Contact Surface after 05 Minutes at 7.2 m/sec and 50 N Test.

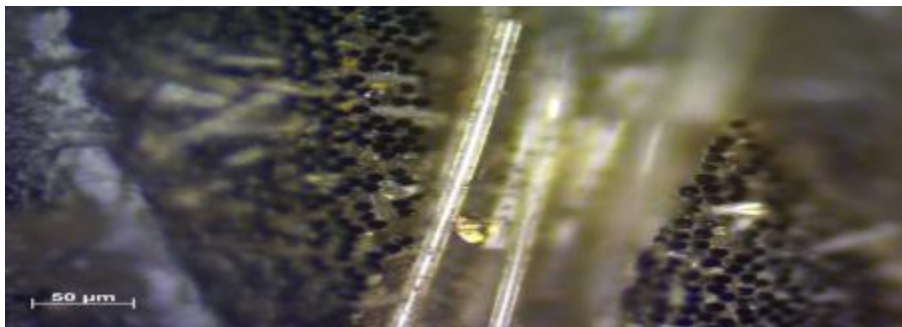


Fig. 134- Contact Surface after 30 Minutes at 7.2 m/sec and 50 N Test.

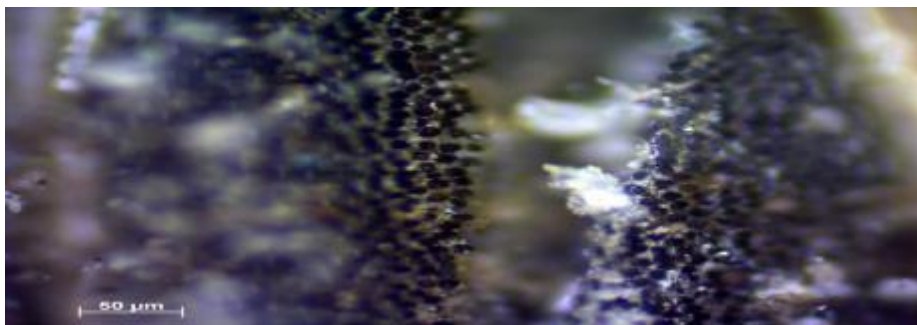


Fig. 135- Contact Surface after 60 Minutes at 7.2 m/sec and 50 N Test.

5- Phenolic Resin Bonded Fabric Material (PRBF)

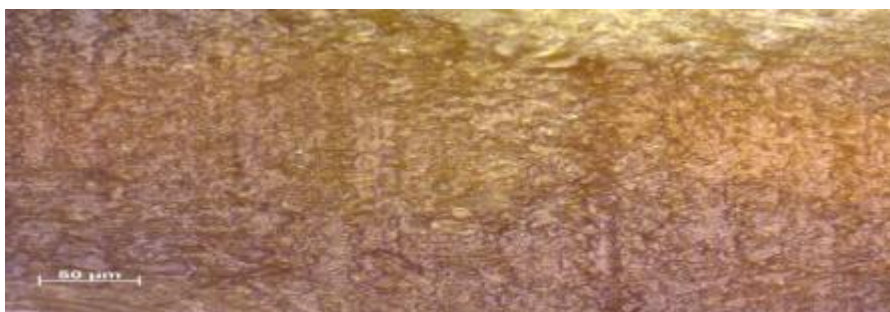


Fig. 136- Contact Surface before Test.

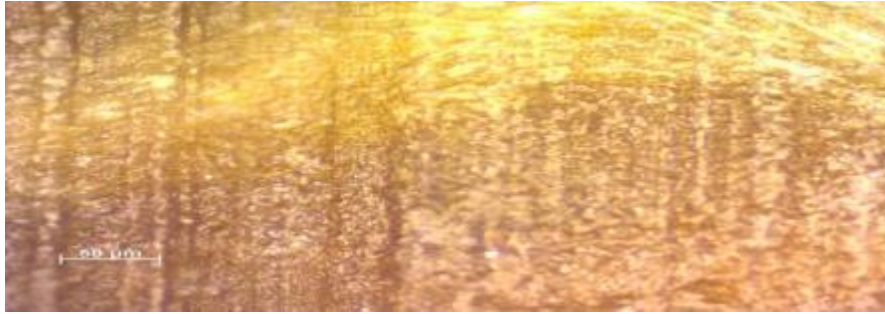


Fig. 137- Contact Surface after 05 Minutes at 1.5 m/sec and 10 N Test.



Fig. 138- Contact Surface after 30 Minutes at 1.5 m/sec and 10 N Test.

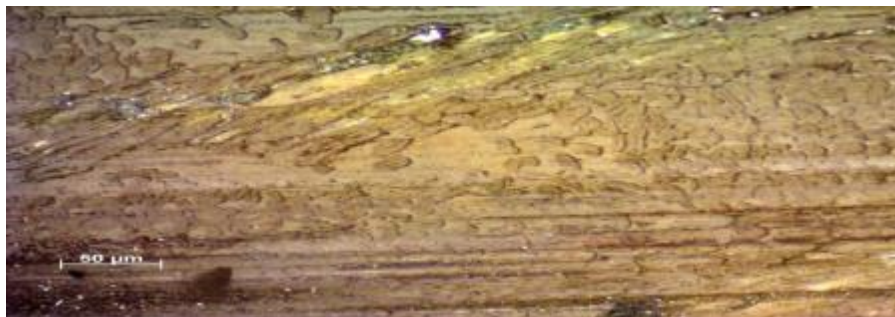


Fig. 139- Contact Surface after 60 Minutes at 1.5 m/sec and 10 N Test.

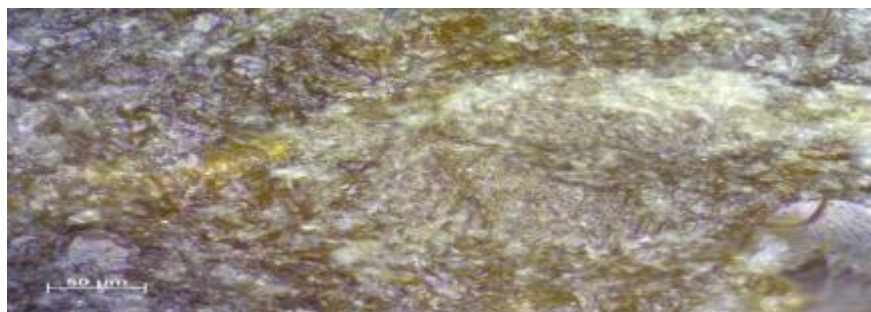


Fig. 140- Contact Surface before Test.

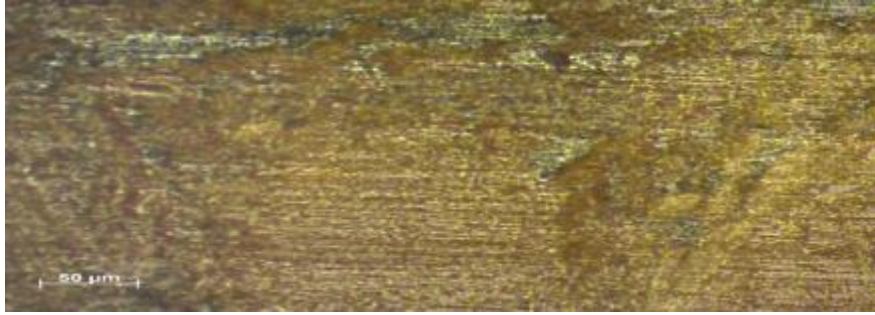


Fig. 141- Contact Surface after 05 Minutes at 1.5 m/sec and 30 N Test.

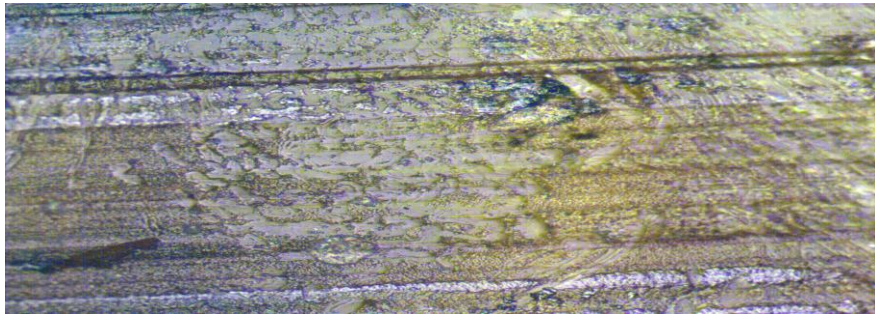


Fig. 142- Contact Surface after 30 Minutes at 1.5 m/sec and 30 N Test.



Fig. 143- Contact Surface after 60 Minutes at 1.5 m/sec and 30 N Test.

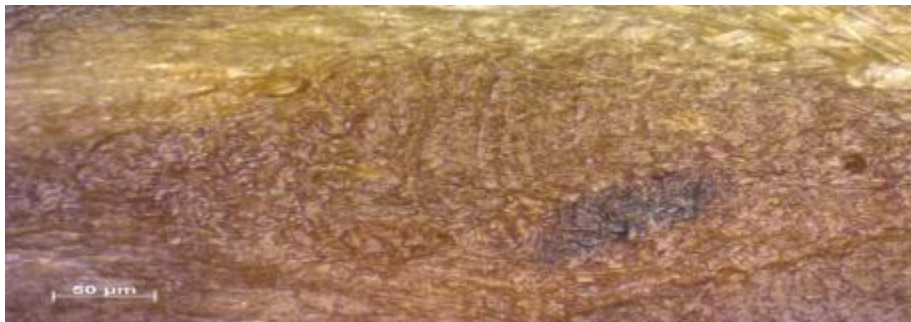


Fig. 144- Contact Surface before Test.



Fig. 145- Contact Surface after 05 Minutes at 1.5 m/sec and 50 N of Test.

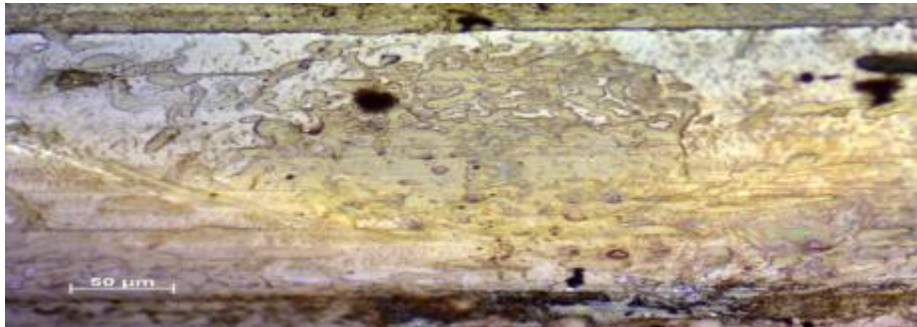


Fig. 146- Contact Surface after 30 Minutes at 1.5 m/sec and 50 N Test.



Fig. 147- Contact Surface after 60 Minutes at 1.5 m/sec and 50 N Test.

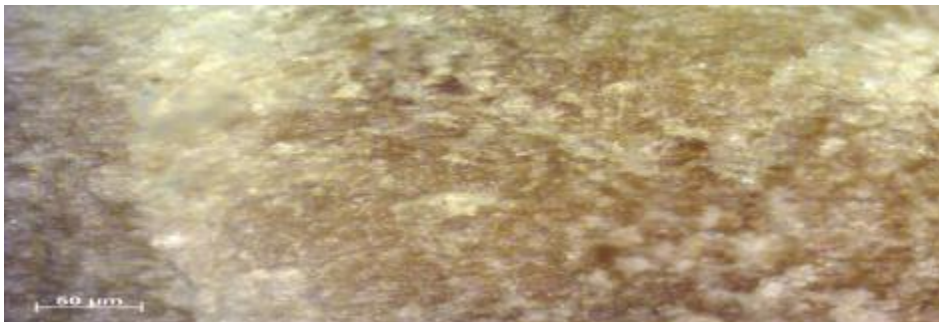


Fig. 148- Contact Surface before Test.

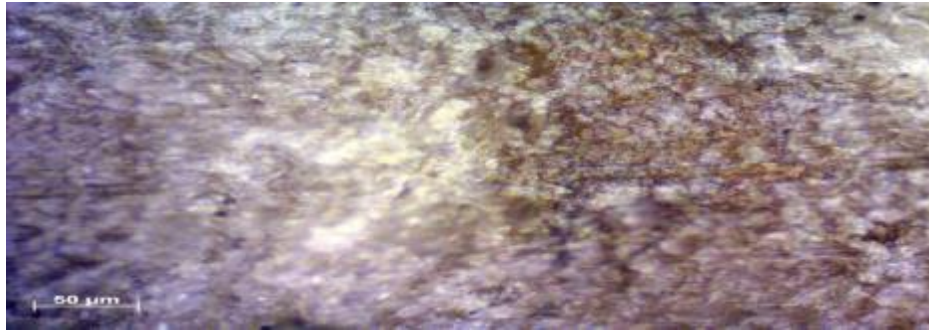


Fig. 149- Contact Surface after 05 Minutes at 3.3 m/sec and 10 N Test.

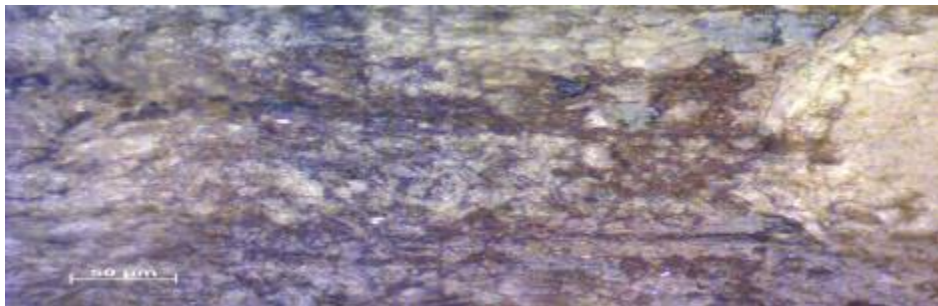


Fig. 150- Contact Surface after 30 Minutes at 3.3 m/sec and 10 N Test.



Fig. 151- Contact Surface after 60 Minutes at 3.3 m/sec and 10 N Test.

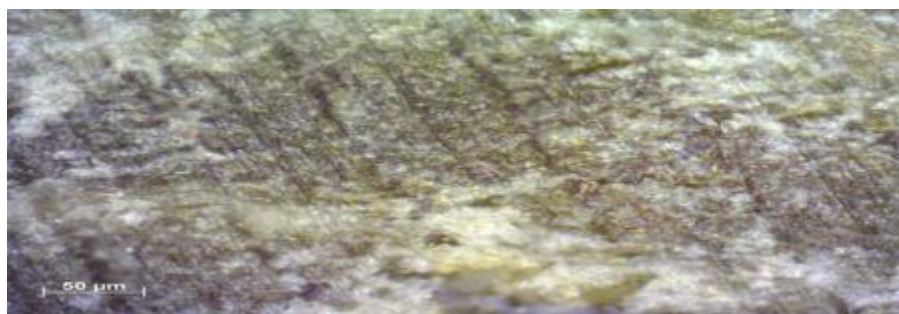


Fig. 152- Contact Surface before Test.

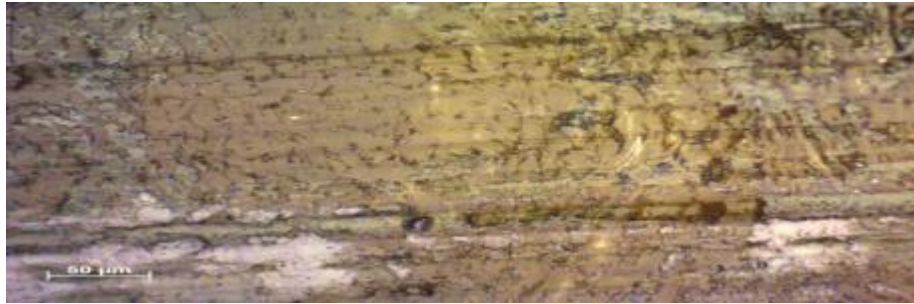


Fig. 153- Contact Surface after 05 Minutes at 3.3 m/sec and 30 N Test.



Fig. 154- Contact Surface after 30 Minutes at 3.3 m/sec and 30 N Test.

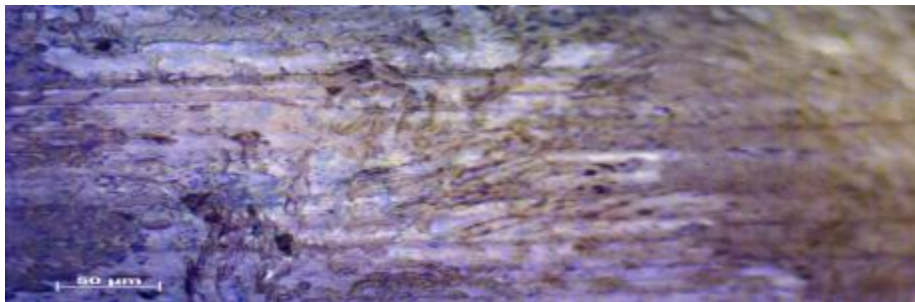


Fig. 155- Contact Surface after 60 Minutes at 3.3 m/sec and 30 N Test.

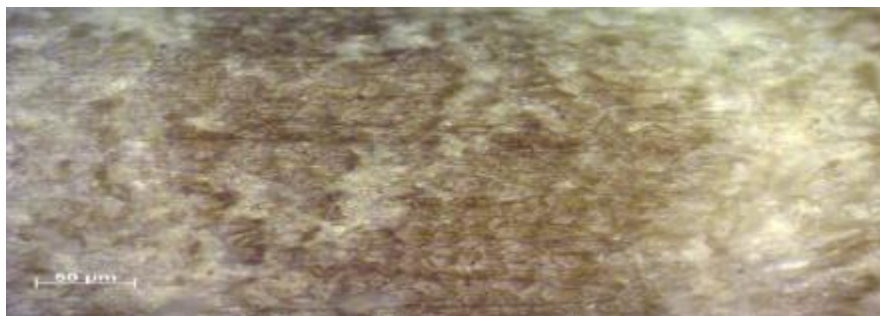


Fig. 156- Contact Surface before Test.

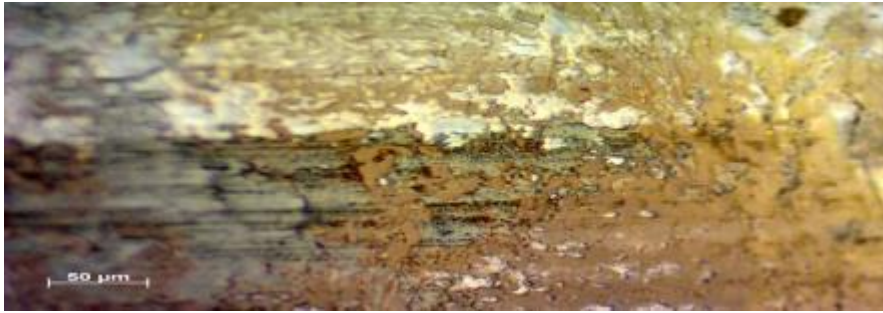


Fig. 157- Contact Surface after 05 Minutes at 3.3 m/sec and 50 N Test.



Fig. 158- Contact Surface after 30 Minutes at 3.3 m/sec and 50 N Test.



Fig. 159- Contact Surface after 60 Minutes at 3.3 m/sec and 50 N Test.



Fig. 160- Contact Surface before Test.

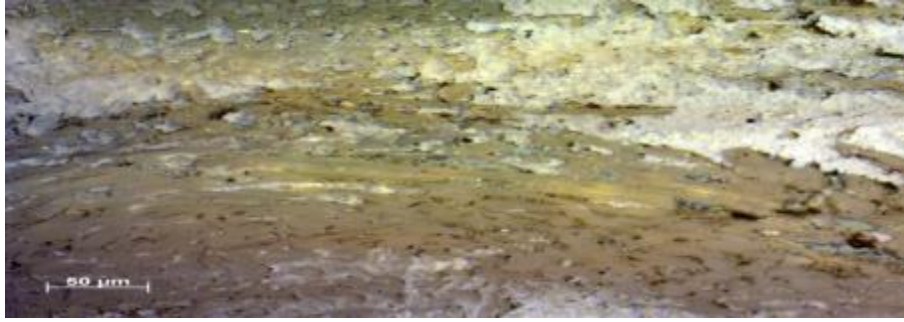


Fig. 161- Contact Surface after 05 Minutes at 7.2 m/sec and 10 N Test.

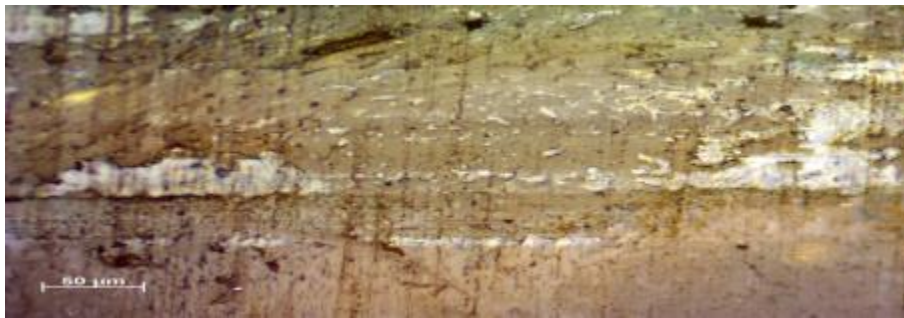


Fig. 162- Contact Surface after 30 Minutes at 7.2 m/sec and 10 N Test.



Fig. 163- Contact Surface after 60 Minutes at 7.2 m/sec and 10 N Test.

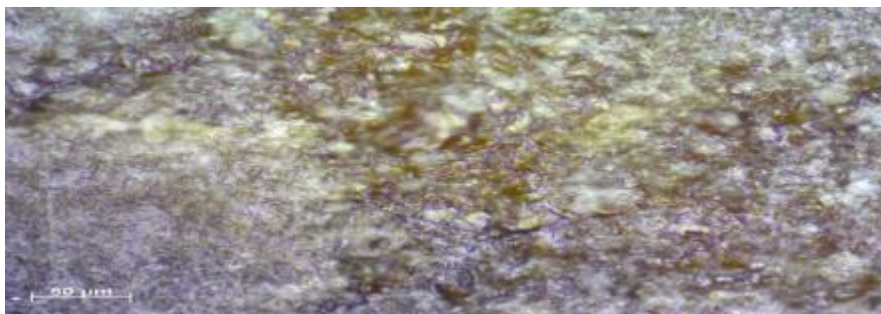


Fig. 164- Contact Surface before Test.

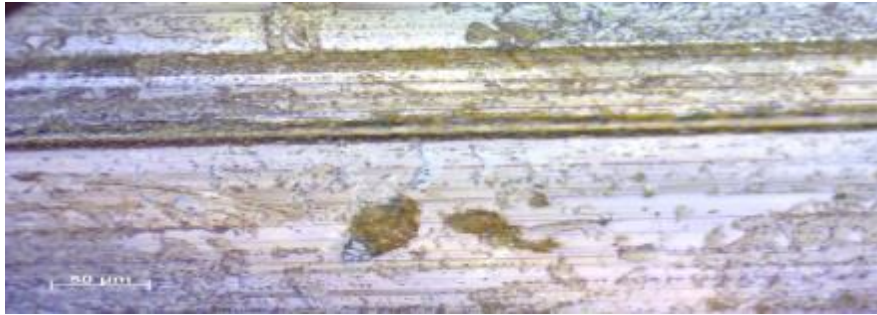


Fig. 165- Contact Surface after 05 Minutes at 7.2 m/sec and 30 N Test.

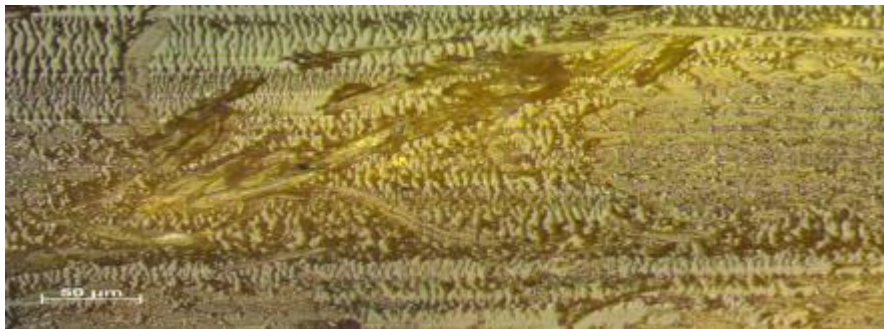


Fig. 166- Contact Surface after 30 Minutes at 7.2 m/sec and 30 N Test.

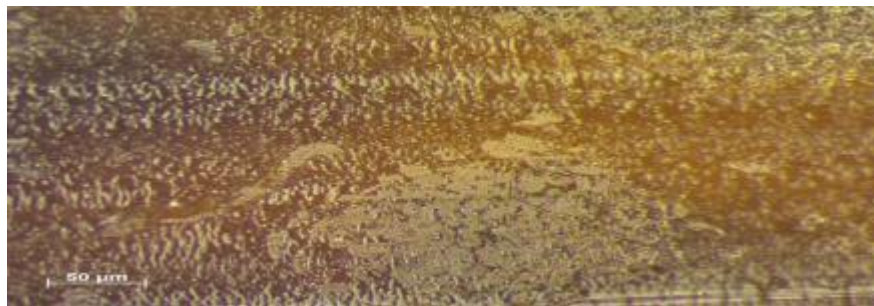


Fig. 167- Contact Surface after 60 Minutes at 7.2 m/sec and 30 N Test.



Fig168- Contact Surface before Test.

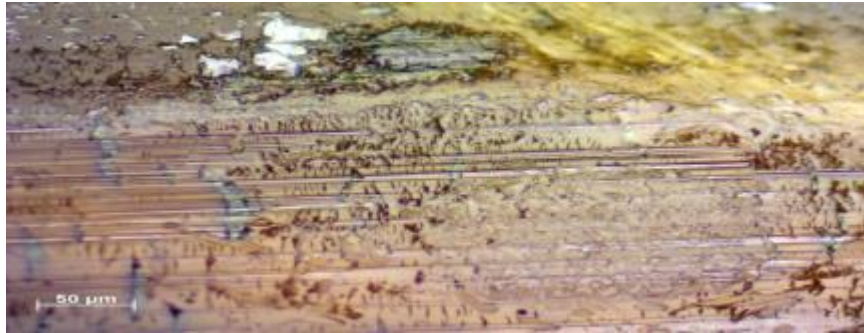


Fig. 169- Contact Surface after 05 Minutes at 7.2 m/sec and 50 N Test.



Fig. 170- Contact Surface after 30 Minutes at 7.2 m/sec and 50 N Test.

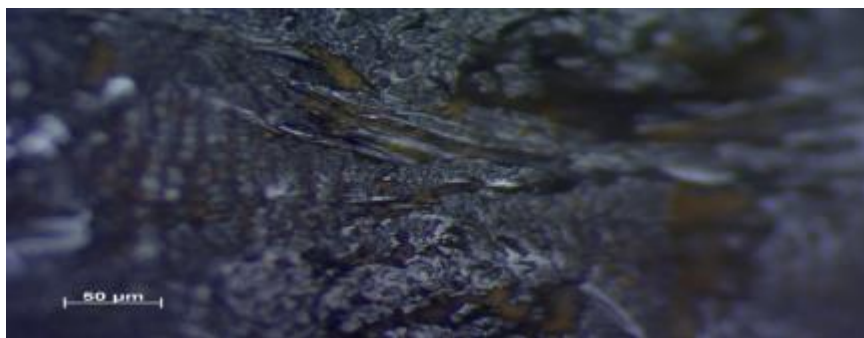


Fig. 171- Contact Surface after 60 Minutes at 7.2 m/sec and 50 N Test.

Block-On-Ring 100% Slip Lipping Test Images





Table 1- Images of Tested Surfaces of Nylon 66 Material Specimens in both Dry and Wet Conditions:

| | | |
|---|---|---|
|  |  |  <p>Nylon 66 material dry impact test at</p> |
|---|---|---|









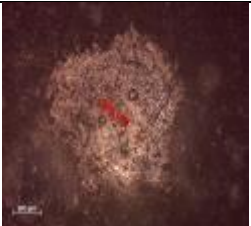
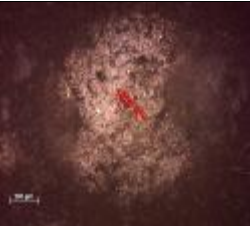


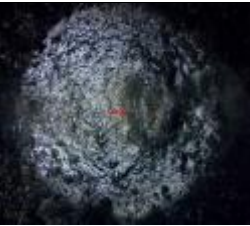
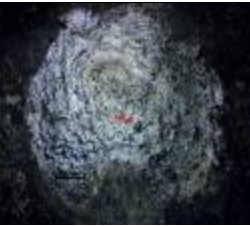

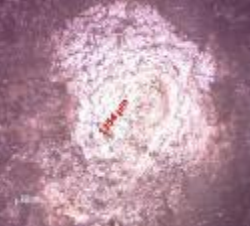

| | | |
|--|--|---|
| <p>Nylon 66 material dry impact test at 100 N & 1000 Cycle</p> | <p>Nylon 66 material dry impact test at 100 N & 5000 Cycle</p> | <p>100 N & 10000 Cycle</p> |
|  <p>Nylon 66 material wet impact test at 100 N & 1000 Cycle</p> |  <p>Nylon 66 material wet impact test at 100 N & 5000 Cycle</p> |  <p>Nylon 66 material wet impact test at 100 N & 10000 Cycle</p> |
|  <p>Nylon 66 material dry impact test at 300 N & 1000 Cycle</p> |  <p>Nylon 66 material dry impact test at 300 N & 5000 Cycle</p> |  <p>Nylon 66 material dry impact test at 300 N & 10000 Cycle</p> |
|  <p>Nylon 66 material wet impact test at 300 N & 1000 Cycle</p> |  <p>Nylon 66 material wet impact test at 300 N & 5000 Cycle</p> |  <p>Nylon 66 material wet impact test at 300 N & 10000 Cycle</p> |
|  <p>Nylon 66 material dry impact test at 500 N & 1000 Cycle</p> |  <p>Nylon 66 material dry impact test at 500 N & 5000 Cycle</p> |  <p>Nylon 66 material dry impact test at 500 N & 10000 Cycle</p> |
|  <p>Nylon 66 material wet impact test at 500 N & 1000 Cycle</p> |  <p>Nylon 66 material wet impact test at 500 N & 5000 Cycle</p> |  <p>Nylon 66 material wet impact test at 500 N & 10000 Cycle</p> |

Table 2- Images of Tested Surfaces of Epoxy Glass Material Specimens in both Dry and Wet Conditions:

| | | |
|---|---|--|
|  <p>Epoxy glass material dry impact test at 100 N & 1000 Cycle</p> |  <p>Epoxy glass material dry impact test at 100 N & 5000 Cycle</p> |  <p>Epoxy glass material dry impact test at 100 N & 10000 Cycle</p> |
|  <p>Epoxy glass material wet impact test at 100 N & 1000 Cycle</p> |  <p>Epoxy glass material wet impact test at 100 N & 5000 Cycle</p> |  <p>Epoxy glass material wet impact test at 100 N & 10000 Cycle</p> |
|  <p>Epoxy glass material dry impact test at 300 N & 1000 Cycle</p> |  <p>Epoxy glass material dry impact test at 300 N & 5000 Cycle</p> |  <p>Epoxy glass material dry impact test at 300 N & 10000 Cycle</p> |
|  <p>Epoxy glass material wet impact test at 300 N & 1000 Cycle</p> |  <p>Epoxy glass material wet impact test at 300 N & 5000 Cycle</p> |  <p>Epoxy glass material wet impact test at 300 N & 10000 Cycle</p> |



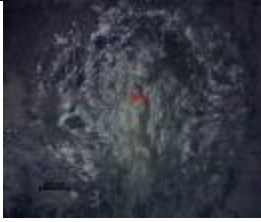

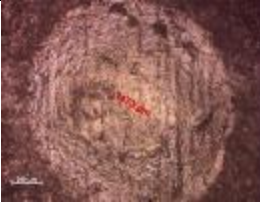

| | | |
|---|---|--|
|  <p>Epoxy glass material dry impact test at 500 N & 1000 Cycle</p> |  <p>Epoxy glass material dry impact test at 500 N & 5000 Cycle</p> |  <p>Epoxy glass material dry impact test at 500 N & 10000 Cycle</p> |
|  <p>Epoxy glass material wet impact test at 500 N & 1000 Cycle</p> |  <p>Epoxy glass material wet impact test at 500 N & 5000 Cycle</p> |  <p>Epoxy glass material wet impact test at 500 N & 10000 Cycle</p> |

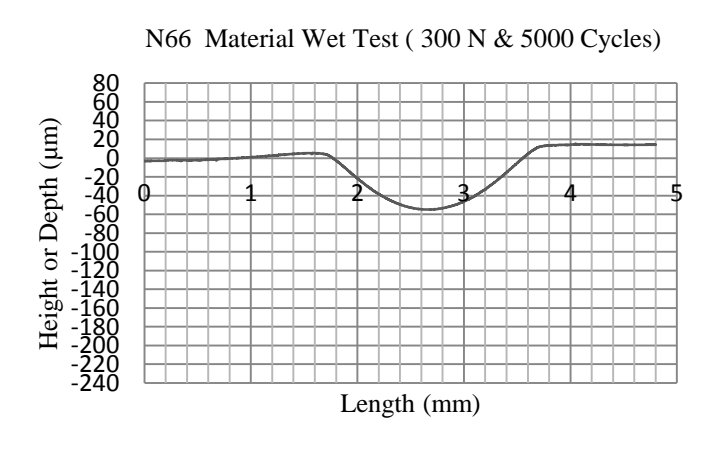
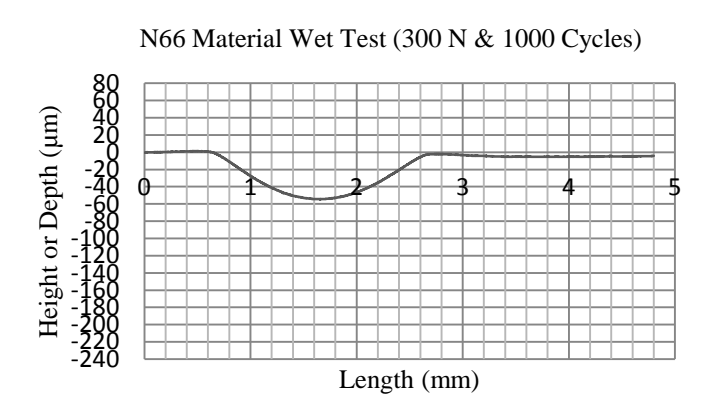
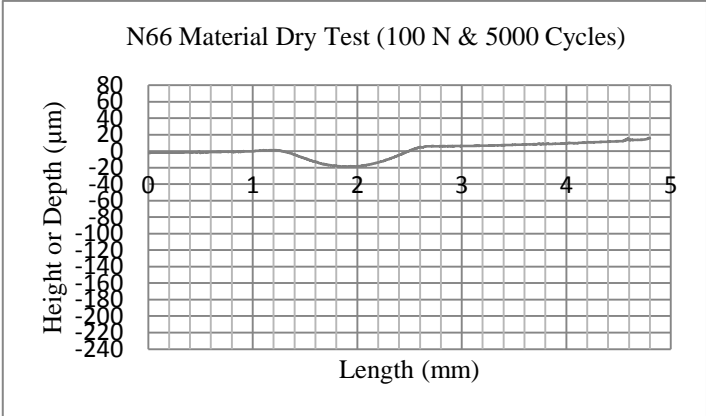
Table 3- Images of Tested Surfaces of Phenolic Resin Bonded Fabric Material Specimens in both Dry and Wet Conditions:

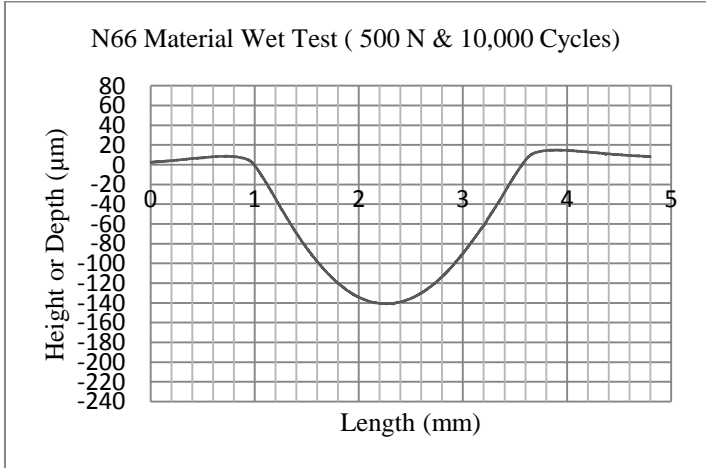
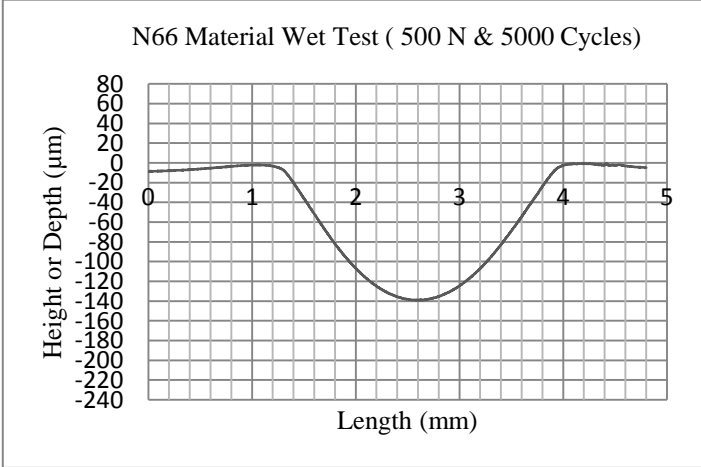
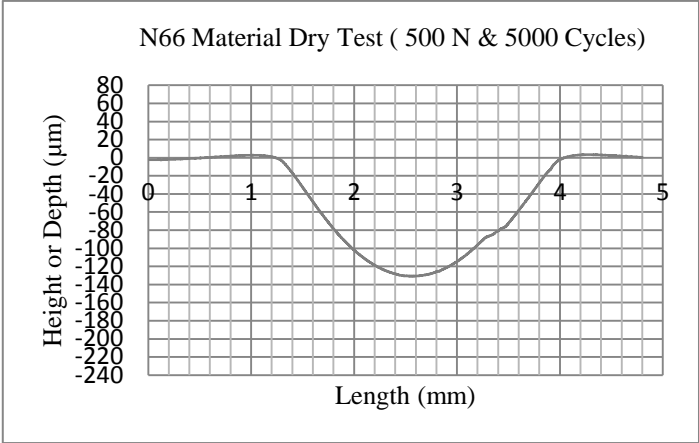
| | | |
|--|--|---|
|  <p>Phenolic resin bonded fabric material dry impact test at 100N & 1000Cycles.</p> |  <p>Phenolic resin bonded fabric material dry impact test at 100N & 5000Cycles</p> |  <p>Phenolic resin bonded fabric material dry impact test at 100N & 10000Cycles.</p> |
|  <p>Phenolic resin bonded fabric material wet impact test at 100N & 1000Cycles.</p> |  <p>Phenolic resin bonded fabric material wet impact test at 100N & 5000Cycles.</p> |  <p>Phenolic resin bonded fabric material wet impact test at 100N & 10000Cycles.</p> |
| | | |

| | | |
|--|--|---|
|  <p>Phenolic resin bonded fabric material dry impact test at 300N & 1000Cycles.</p> |  <p>Phenolic resin bonded fabric material dry impact test at 300N & 5000Cycles.</p> |  <p>Phenolic resin bonded fabric material dry impact test at 300N & 10000Cycles.</p> |
|  <p>Phenolic resin bonded fabric material wet impact test at 300N & 1000Cycles.</p> |  <p>Phenolic resin bonded fabric material Wet impact test at 300N & 5000Cycles.</p> |  <p>Phenolic resin bonded fabric material wet impact test at 300N & 10000Cycles.</p> |
|  <p>Phenolic resin bonded fabric material dry impact test at 500N & 1000Cycles.</p> |  <p>Phenolic resin bonded fabric material dry impact test at 500N & 5000Cycles</p> |  <p>Phenolic resin bonded fabric material dry impact test at 500N & 10000Cycles.</p> |
|  <p>Phenolic resin bonded fabric material Wet impact test at 500N & 1000Cycles.</p> |  <p>Phenolic resin bonded fabric material Wet impact test at 500N & 5000Cycles.</p> |  <p>Phenolic resin bonded fabric material wet impact test at 500N & 10000Cycles.</p> |

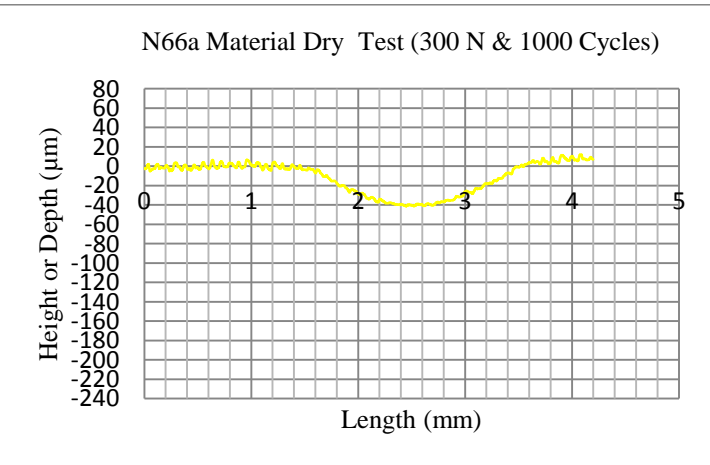
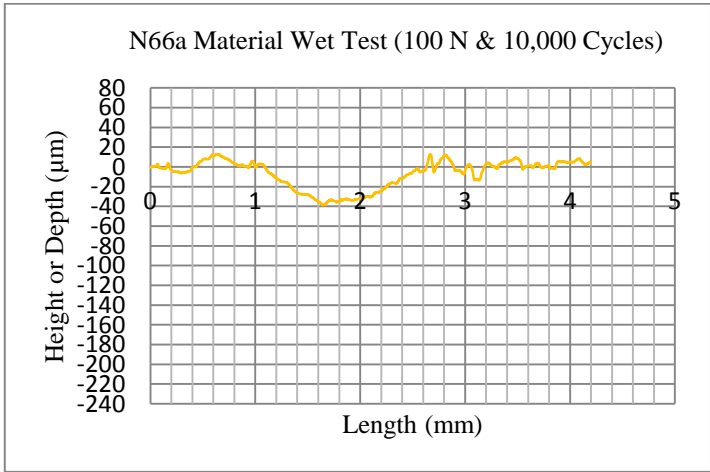
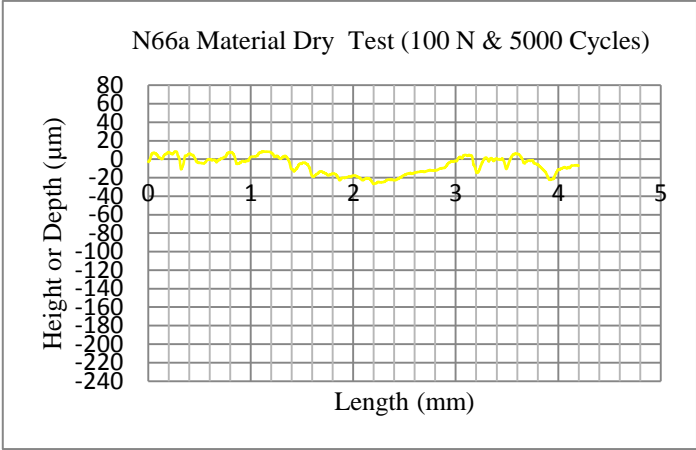
Impact Test Profilometer Graphs

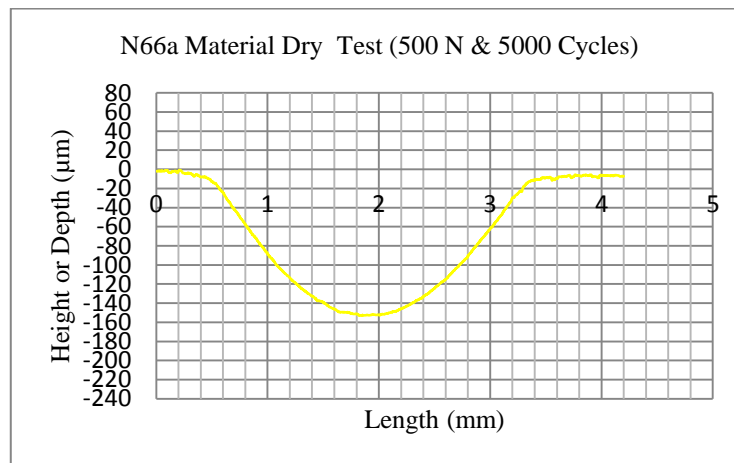
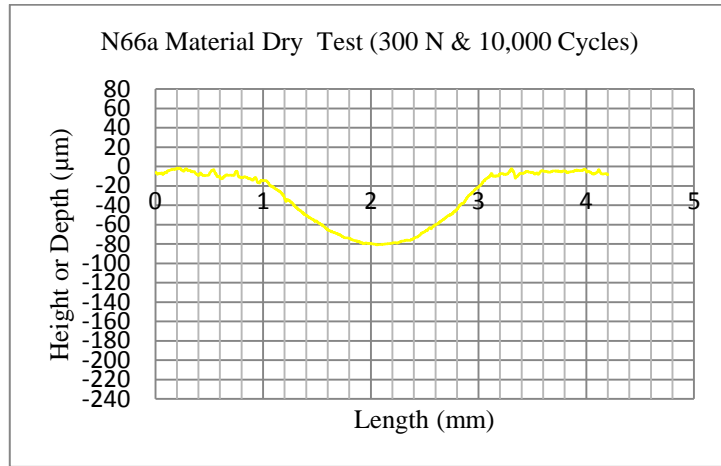
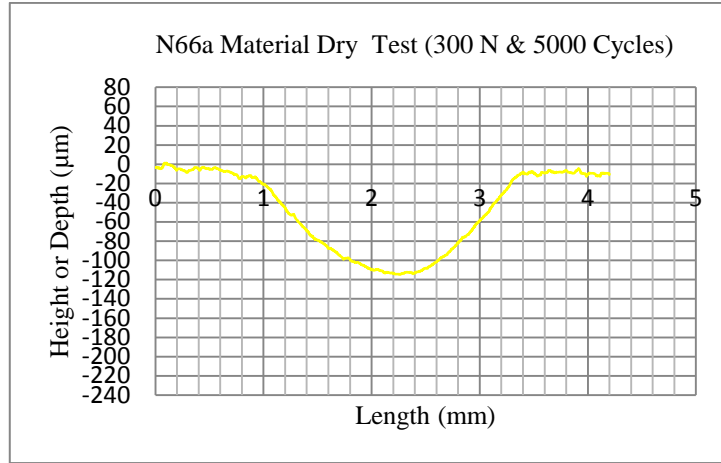
1- Nylon 66 Material (N66)

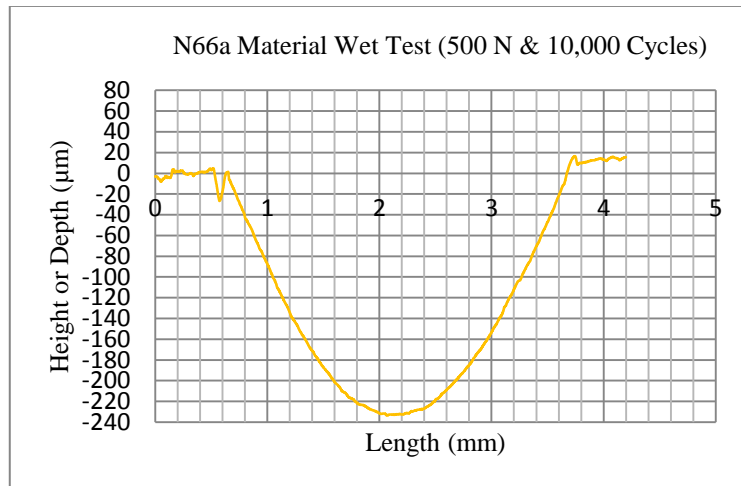
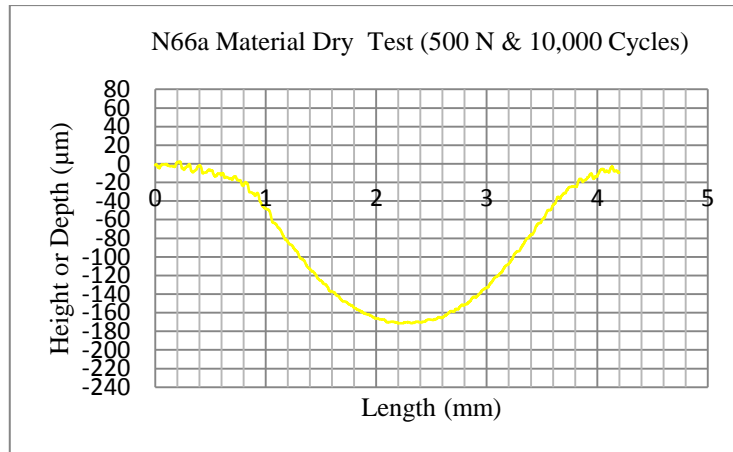




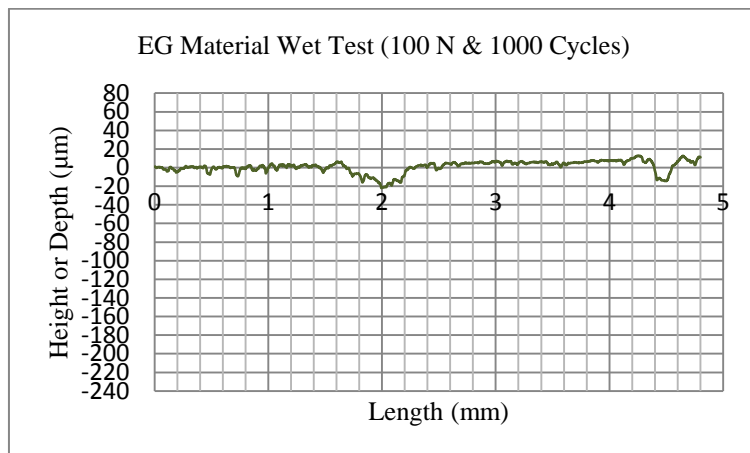
2- Nylon 66a Material

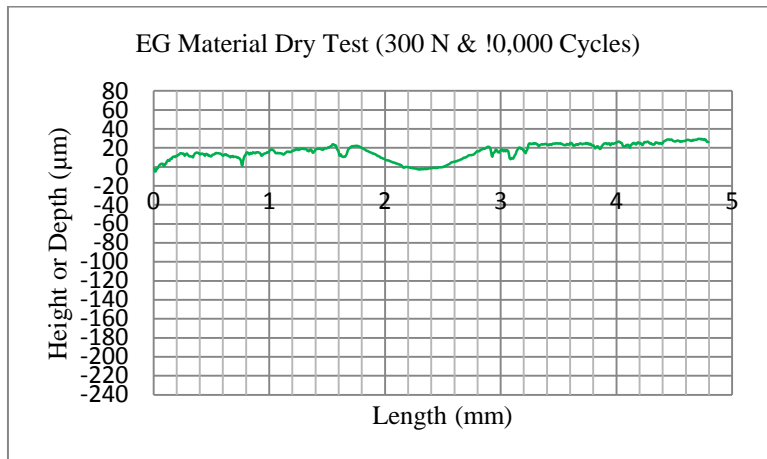
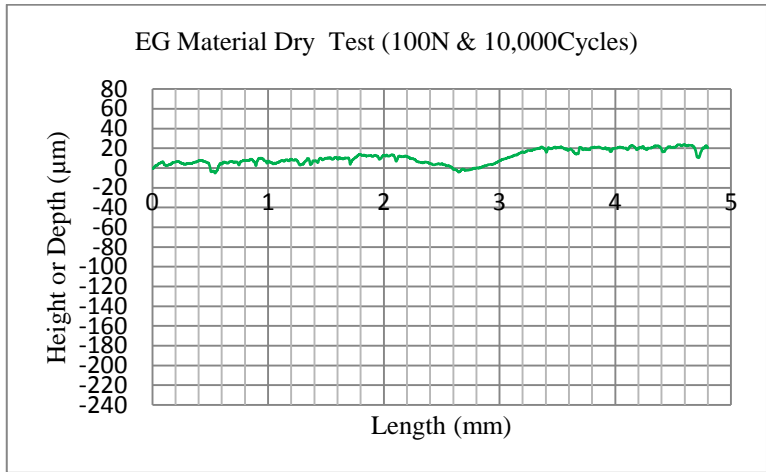
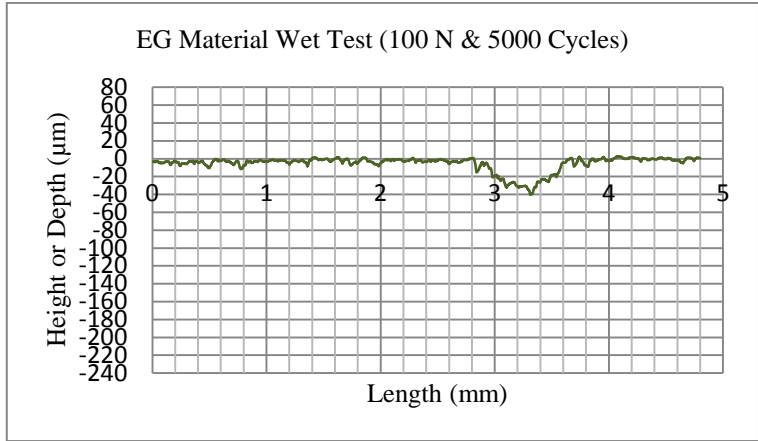


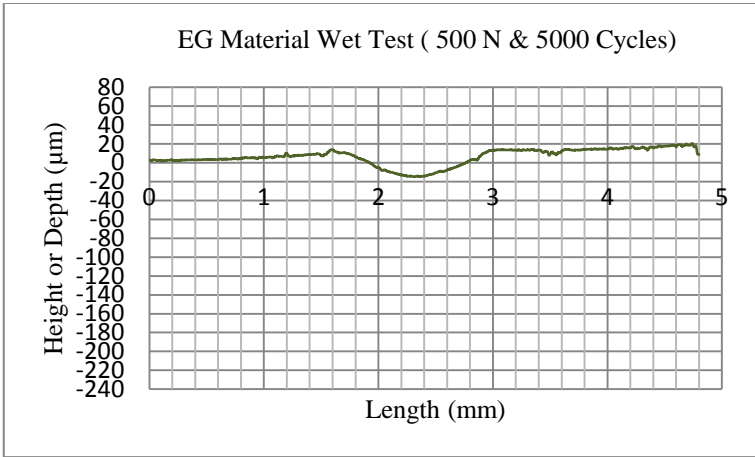
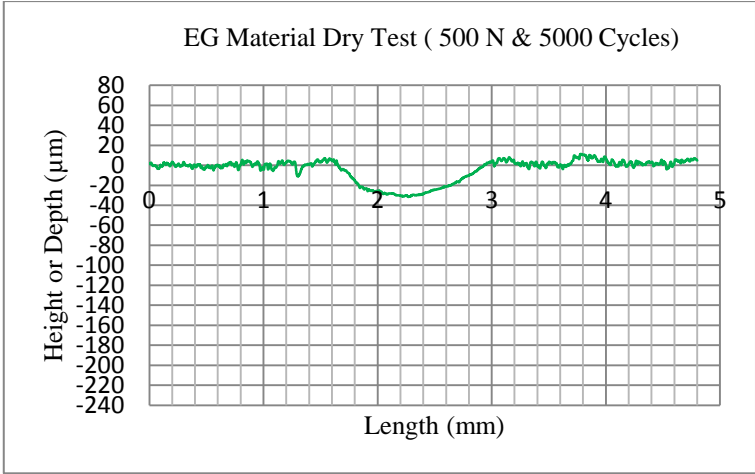




3- Epoxy Glass Material (EG)







4- Phenolic Resin Bonded Fabric Material (PRBF)

